Author:
Darch, Henry

Title:
Neural Network Activity during Visuomotor Adaptation

Neural Network Activity during Visuomotor Adaptation

Henry Thomas Darch

A dissertation submitted to the University of Bristol in accordance with the requirements for award of the degree of Doctor of Philosophy in the Faculty of Life Sciences

School of Physiology, Pharmacology and Neuroscience

University of Bristol

September 2018

Word count: - 43,029

Abstract

The vertebrate brain can rapidly adjust voluntary movements in response to errors through a process of trial-by-trial motor adaptation. There are several regions of the brain known to influence this adaptation of voluntary movements. The cerebellum is the principal area associated with adaptive movements and is thought to enable predictions of the consequences of movements. The motor cortex has been implicated in the long-term memory and maintenance of appropriate patterns of neural activity to execute accurate movements- the motor engram. The prefrontal cortex has also been implicated in the implementation of cognitive strategies and maintaining task engagement.

Evidence to-date showing each of these areas' influence on motor adaptation suggests a functional network that works together to appropriately modify motor actions in response to behavioural errors. The neural mechanisms by which these distant nodes communicate with one another are not yet understood.

The present study has investigated the neurophysiological changes that occur in the neural activity of the cerebellum (paravermal cortex), motor cortex and prefrontal cortex, as well as the level of network communication between them, during a visuomotor adaptation paradigm in both humans and cats. In both species, neural population activity (EEG in humans and local field potential activity in cats) showed a modulation of beta frequency oscillations in the primary motor cortex just prior to movement, specific to early stages of adaptation. No significant effects were observed in the cerebellar cortex and phase synchrony between the three brain areas was unchanged during adaptation.

Together, these data suggest changes in motor cortical activity related to adaptation of reaching movements but no detectable changes to functional connectivity between the distributed brain nodes involved in motor adaptation. Contrary to predictions related to updating internal models during adaptation, this suggests neural network connectivity remains similar throughout the motor learning process.

Acknowledgements

There are of course numerous people involved in the generation and execution of the studies contained within this thesis. Principally, I thank Professors Richard Apps and Iain D. Gilchrist for their supervision, ideas, guidance and support throughout these years.

Additionally, I thank Dr Nadia Cerminara and Mrs Rachel Bissett for their enduring support and daily assistance throughout the project, without which the animal study would not have been possible. I thank Dr Nina Kazanina for the use of the EEG facilities, along with Sarah Wolfsthurn, Luisa Taylor, and Diana Grunberg for the assistance with the EEG experiment.

I am indebted to all members of the Sensory and Motor Systems Group, who not only willingly assisted my work, but also put up with my demeanour during the tougher days and laughed at my jokes during the better ones.

Gratitude must also be shown to the BBSRC for the funding of my studentship and principle project costs, and the staff of the SWBio DTP for the organisation of, and opportunity for this project. Additionally, thanks to the MRC, who's funding provided support for the animal study.

Naturally, this thesis is not complete without my personal thanks and dedication to my family and friends for the steadfast love and support through these past years.

Author's Declaration

I declare that the work in this dissertation was carried out in accordance with the requirements of the University's Regulations and Code of Practice for Research Degree Programmes and that it has not been submitted for any other academic award. Except where indicated by specific reference in the text, the work is the candidate's own work. Work done in collaboration with, or with the assistance of, others, is indicated as such. Any views expressed in the dissertation are those of the author.

SIGNED: …… …….. DATE: 21/03/2019

Publications and abstracts associated with this work

Darch H., N. Cerminara, I.D. Gilchrist, R. Apps 2018. Non-invasive Stimulation of the Cerebellum in Health and Disease. *In: Transcranial Magnetic Stimulation in Neuropsychiatry*. Ed: L. Ustohal IntechOpen. ISBN: 978-1-78923-651-4

Darch H., R. Apps, I.D. Gilchrist 2018. EEG correlates of motor cortex and prefrontal activity during visuomotor adaptation. 11th FENS Forum of Neuroscience, Berlin. Abstract No. 3250

Darch H., N. Cerminara, I.D. Gilchrist, R. Apps 2017. A pilot study on the effects of cerebellar trans-cranial Direct Current Stimulation on motor network dynamics during motor adaptation in human and cat. BNA 2017, Birmingham. Poster No. P-M028

Darch H., N. Cerminara, R. Apps 2016. The effects of cerebellar trans-cranial direct current stimulation on neural network dynamics in supraspinal motor circuits during motor adaptation in cats. *Clinical Neurophysiology*. 128(3):e161 DOI: 10.1016/j.clinph.2016.10.415

Contents

List of Figures

List of Tables

Abbreviations

[early/late] Adapt. – [early/late] Adaptation trial epoch

[early/late] After. – [early/late] After-effect trial epoch

ANOVA – Analysis of Variance

ctDCS – Cerebellar transcranial direct current stimulation

EEG – Electroencephalogram

EMG - Electromyography

fMRI – Functional magnetic resonance imaging

HD-tDCS – High definition transcranial direct current stimulation

LFP – Local field potentials

M1 – Primary motor cortex

MOSAIC - Modular selection and identification for control

mPfc – Medial prefrontal cortex

Ms- Millisecond

NSP- Neural signal processor

PC – Personal computer

PI – Principle Investigator

PFC – Prefrontal cortex

PSTH – Peri-stimulus time histogram

RT – Reaction time

SD – Standard deviation

SEM – Standard error of the mean

S/s – Samples per second

tDCS – Transcranial direct current stimulation

tES – Transcranial electrical stimulation

TMS – Transcranial magnetic stimulation

TTL – Transistor-transistor logic

USB – Universal Serial Bus

VOR- Vestibulo-occular reflex

Chapter 1 – General Introduction

1.1 General introduction

A distinguishing feature of animal organisms is the ability to move and interact with their environment. Particularly evident in higher order species is the development of sophisticated motor systems that enable efficient, and accurate execution of highly complex movements, forming a rich repertoire of behaviours. The nervous systems controlling such behaviours have thus developed mechanisms to support such complex movements. Indeed, even a seemingly simple movement for a human to accomplish, such as raising an arm at the shoulder, quickly becomes an astonishing achievement of control, given the many muscles involved and the near unbounded freedom of movement of a multi-joint limb.

Movements can be broadly classified into either reflexive or voluntary movements. Reflexive movements are mainly under the control of local neural circuitry within the spinal cord, with comparatively less supraspinal (descending) control than voluntary movements. Voluntary movements on the other hand, have much greater involvement of supraspinal central nervous system circuits, and generally speaking have some level of conscious intent driving them.

Voluntary movement control is largely studied in the context of learning. In this respect, two subdivisions of 'motor learning' can be made; skill acquisition, and adaptation. Motor skill acquisition involves the ability to learn a novel movement (such as a sequence of finger tapping). Motor adaptation on the other hand maintains an established movement in the face of changes in the internal or external environment. The neural networks and mechanisms supporting these two forms of motor learning may not be identical. This thesis will focus on motor adaptation of voluntary movements.

1.2 Motor adaptation

In response to a predictable change in some feature governing a movement (such as application of a novel load force on a reaching limb), individuals can iteratively modify motor behaviours, and thus maintain previous levels of task success. A classic example is throwing a dart at a dart board **Figure 1.1**. A healthy individual can throw a dart at a target with a reasonable degree of accuracy (which improves with practice through skill acquisition). If the movement is then subjected to a perturbation – classically a set of prism glasses which shifts the visual field laterally to the right or left of the target – on their next throw, the individual will likely miss the target by a similar degree as the visual shift (i.e. the magnitude of the error depends on the extent of the perturbation). Using the visual feedback of where the previous dart had landed, the individual is able to modify their throwing pattern to reduce the error of the next throw. This cycle of incorporating previous error into the next attempt is repeated until a minimum throwing error is reached – representing the fundamental skill level of that individual. This iterative

process of motor adaptation can be thought of as a mechanism by which the brain maintains the [implicit] understanding of the input-output relationship between motor commands and their behavioural consequences, updating these sensorimotor mappings, or internal models, when prior experience indicates they are incorrect.

Once the prism glasses are removed, and the participant continues throwing, an 'equal-and-opposite' error typically occurs to which the participant 're-adapts' over a number of trials to return to their pre-prism wearing performance. This after-effect is the cardinal behavioural indicator that plastic changes have occurred in the CNS that are thought to reflect a revision of a motor memory (Fernández-Ruiz and Díaz 1999). This adaptation process is distinct from the generation of a new skill, or other learning mechanisms that may be used to correct for the perturbation.

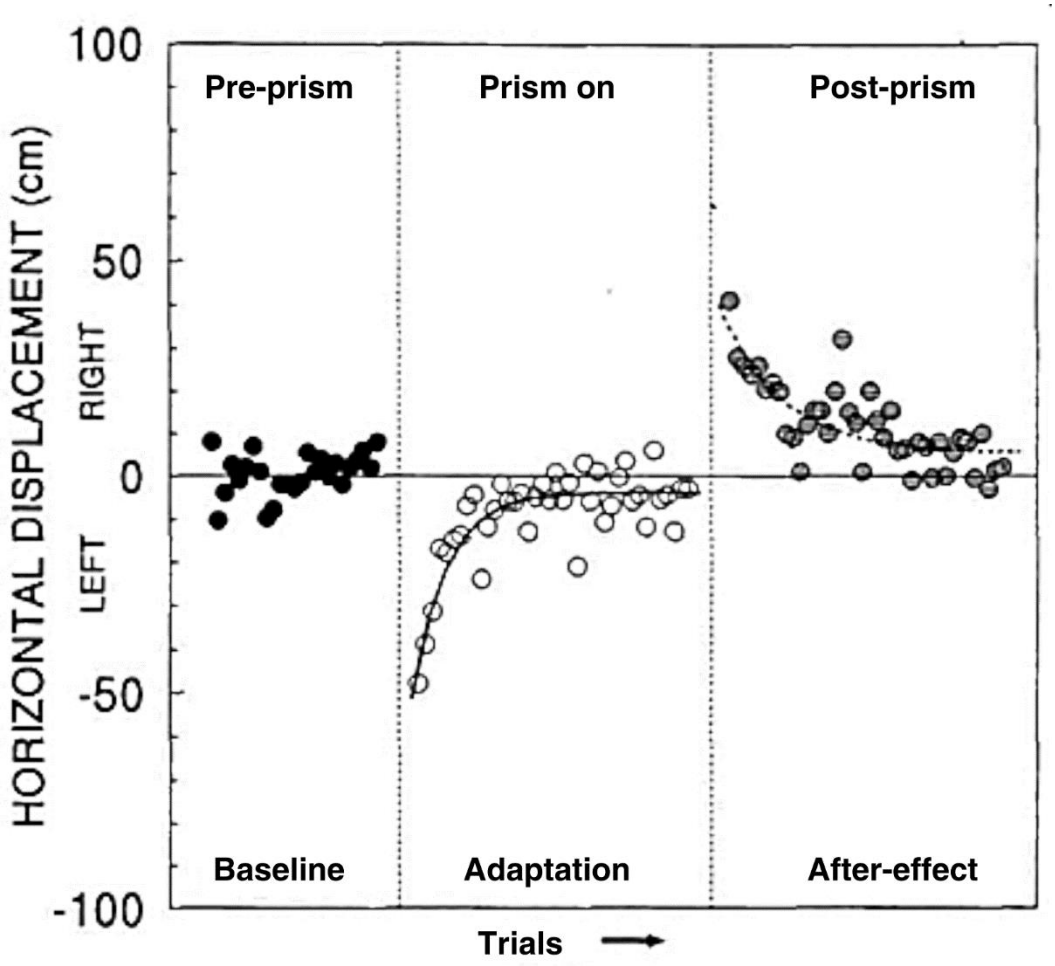

Figure 1.1. Illustration of progression of motor adaptation.
Circles represent the landing position of a thrown dart relative to a target. During Baseline (black filled circles), the participant can throw the dart close to the target. During Adaptation (while filled circles), when leftward displacing prism glasses are put on) the participant rapidly overcomes the initial lateral error until the performance plateaus. On removal of the prisms (grey filled circles), an equal and opposite after-effect is apparent. Adapted from Thach et al. 1996 with permission of Oxford University Press.

1.2.1 Savings

Although not explored in detail in this thesis, in addition to the trial-to-trial adaptation of movements that occur within the same training session, longer term improvements in performance, known as savings, also occur. Exposing human subjects to the same perturbation repeatedly over many days results in a gradual improvement in the rate of adaptation across sessions (Krakauer 2009). Investigations have shown that the mechanisms of savings are distinct from those of error-based adaptation, and are likely a result of improved action selection (Morehead et al. 2015), perhaps based on use-dependent reinforcement of the repeated movement (Huang et al. 2011).

1.2.2 Importance of adaptation

The behavioural importance of motor adaptation can be exemplified by everyday situations such as an experienced driver driving an unfamiliar car. Whilst the layout and usage of the principle controls of a modern car are highly standardised, the finer details- the weight and biting point of the clutch system, sensitivity of the brake pedal and so on- vary between cars. When the driver first begins to drive the car, they may make sharp braking actions, or jerky gear changes. It will take them a short while to 'get used' to the new dynamics of the car, re-calibrating their foot movements to establish smooth braking and gear changes. Again, after driving this car for a time, a service may be due, in which the brake-pads are replaced. Once serviced, the driver may once again experience sharp breaking during their first few miles as they get used to the new brake pads. All these events in which the driver has experienced an initial disruption in their usually smooth driving ability, and shown rapid improvement with experience, can be attributed to motor adaptation. The driver's brain has logged the unexpected change in braking performance and because this change is systematic and predictable, a change is made to the motor action sequences of subsequent braking events, gradually leading to smoother and smoother braking until the driver is back to their normal level of driving performance.

The above is an example in which the environmental conditions have changed (the way that the brakes respond to the driver's input). However, adaptation can also occur in response to internal state changes, such as adaptation to increases in muscle fatigue affecting limb dynamics.

Failure to successfully adapt to environmental/internal conditions could have significant negative consequences to an individual; in the above example, if the driver was unable to modify their braking behaviour in the new car, this could lead to a collision.

1.2.3 Studying motor adaptation

In the laboratory setting, motor adaptation is studied by applying a controlled perturbation to an individual performing a previously learned task. The perturbation is typically in the form of a

physical force (force-field adaptation), or a manipulation of the visual feedback (visuomotor adaptation). Applying a physical force to an outward reach of a participant holding a robotic manipulandum is a popular paradigm in both human and animal studies (Hunter et al. 2009; Li et al. 2001; Stockinger et al. 2014). Alternatively, split belt treadmills (that require adaptation of an individual's gait) have also been used (Morton and Bastian 2006; Kuczynski et al. 2017; Roemmich et al. 2016). Manipulations of visual feedback through either prismatic lenses that lead to a lateral shift in perceived visual field (Martin et al. 1996a; Striemer and Borza 2017; Harris 2012), or artificially changing visual feedback given on computer-based tasks (Galea et al. 2011; Jalali et al. 2017) are also highly used. The different methods used to apply the perturbation affect whether the detected error is carried by the visual system, or proprioceptive pathways, and the choice of which modality to manipulate is task dependent. Consequently, there may be differences in neural pathways underpinning these different sub-forms of adaptation, for instance the neural pathways carrying visual information are not the same as those carrying joint proprioceptive information. Nevertheless, the fundamental processes leading to adaptation are thought to be broadly the same.

1.2.4 Theory of motor adaptation

Much of the motor adaptation literature considers the theoretical neural processes supporting motor adaptation in relation to the field of robotics, with the motor system considered in terms of control theory as a feedback controller (Haruno and Wolpert 1999; Wolpert and Kawato 1998; Wolpert et al. 1998). A key feature of this theory is that the brain forms representations of expected outcomes of its actions (internal models), which are compared against the actual consequences of that action. Two general forms of internal model exist: a forward model takes the input commands and generates the expected outcome of that command. Conversely, an inverse model takes as its input the desired outcome and generates the necessary motor command(s) to achieve that outcome. In the context of biological movements, it is believed that motor commands that result in effector actions are generated through inverse models (Shadmehr and Mussa-Ivaldi 1994). In contrast, forward models are able to provide an accurate estimate of the future outcome of that command, potentially even before the motor command is executed, allowing more rapid refinement of the motor commands (if the expected outcome is not appropriate to the goal) or more seamless transitions between movements (rather than having to wait for the completion of a set of motor commands before planning the next set).The two forms of internal model are by no means mutually exclusive and, although the precise form and loci are still debated, there is reasonable evidence that the brain maintains both forms of model processes (Wolpert and Kawato 1998; Honda et al. 2018).

Regarding motor adaptation, if the motor system uses internal models to generate and execute motor behaviours, there should be a mechanism through which these internal models may be validated (compared to what occurs on execution of a given motor command) and modified accordingly if they are no longer accurate (i.e. if they do not accurately/reliably predict the external dynamics). Motor adaptation can thus be viewed as the updating of internal models (in response to predictable changes in either the environment or motor effectors) to maintain their accuracy and utility in motor control. Furthermore, a credit assignment issue exists in determining where behavioural errors stem from and so what the appropriate modifications should be (Wolpert et al. 2011).

Using internal models as a framework to describe the error-based learning mechanisms of motor adaptation, there have been some attempts to map the components of an internal model onto the neurocircuitry of the brain areas known to be responsible for motor adaptation.

1.3 Brain areas involved in motor adaptation

Over the past century of scientific research, ideas of isolated brain structures being responsible for specific behaviours are giving way to a much greater level of integrative and network control of behaviours. Described here are the proposed roles in motor adaptation of three principal brain areas, a schematic of the network is shown in **Figure 1.2**.

Although the areas detailed in the below sections are the most firmly established with motor adaptation (and form the focus of this thesis), there is evidence that they are not the sole players in this motor control network. In brief, other nodes include the basal ganglia, classically linked to reward-based learning, known to have extensive interconnections with the cerebellum - including neuroimaging data suggesting a direct projection in humans (Milardi et al. 2016) - and has also been shown to be activated during sensorimotor adaptation (reviewed in Bostan and Strick 2018). Additionally, a temporary lesion (using non-invasive magnetic stimulation) of the posterior parietal cortex has been shown to inhibit force-field adaptation (Della-Maggiore 2004). A case study on a patient with bilateral damage to the posterior parietal cortex showed a deficit in prism adaptation, in spite of a conscious awareness of the reaching errors being made (Newport et al. 2006). The authors propose that the posterior parietal cortex is a site of coordination between visual scenes and limb coordinates, enabling a translation of ocuclocentric coordinates (gaze direction) to egocentric coordinates (reach direction), a notion supported by recent data showing neurons in the posterior parietal cortex are able to encode a

variety of reference frames such as those of the eyes (looking to the target) and of the hands (moving to the target) (Bosco et al. 2016).

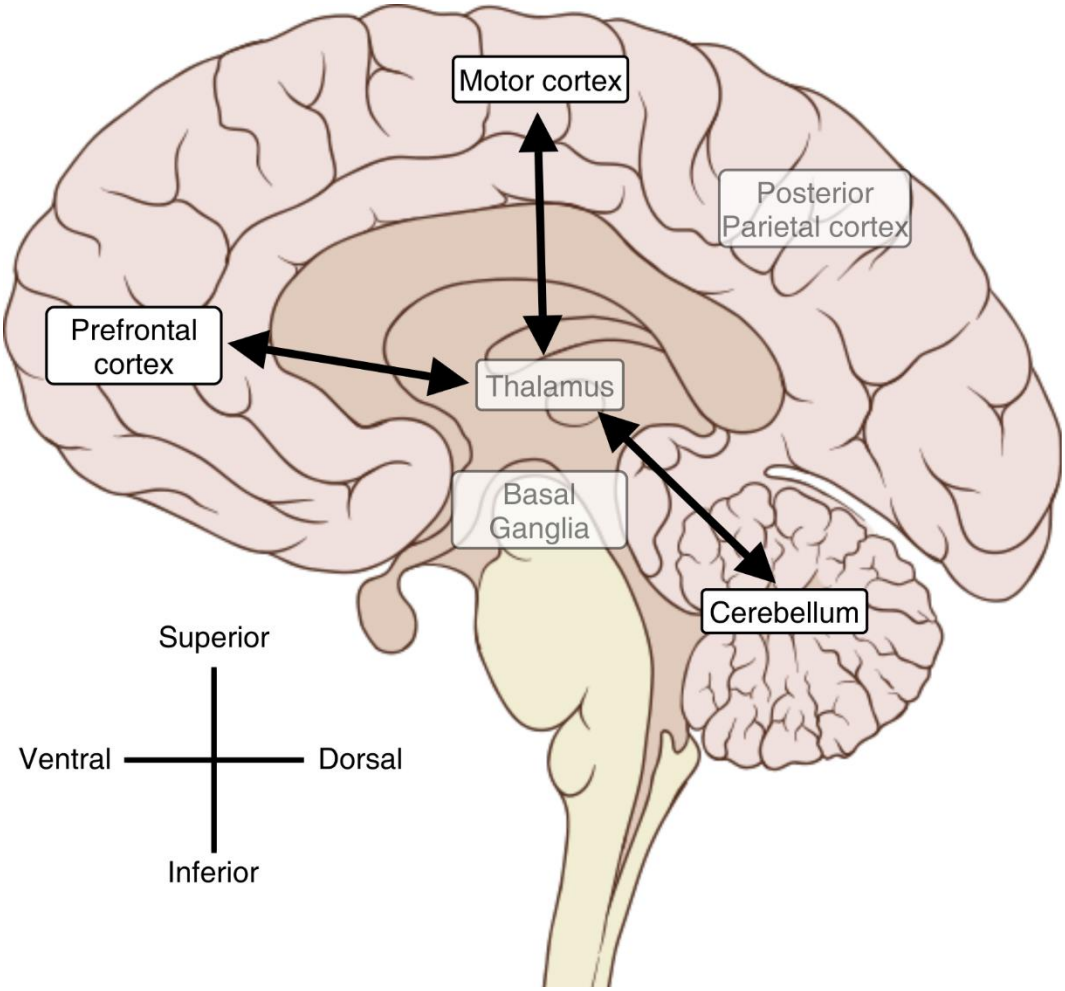

Figure 1.2 Schematic of the major motor network under consideration.
The three principle nodes under consideration in this thesis are shown as bold labels and interconnections. Other areas with evidence of a role in this network are displayed in faded labels.

1.3.1 Cerebellum

The mammalian cerebellum (Latin for 'little brain') is a distinct structure found in the hindbrain of vertebrates, containing the majority of all central nervous system neurons in mammals (Herculano-Houzel 2010).

The circuitry of the cerebellum is summarised in **Figure 1.3.** Key features relevant to this thesis include the finding that information from almost all parts of the nervous system enters the cerebellum primarily through the pontocerebellar tract in humans and other mammals (Buckner et al. 2011). This mossy fibre projection makes excitatory connections to both the cerebellar nuclei, and cerebellar cortex granule cells. In the cortex, the granule cells project and form excitatory synapses onto the dendritic arbours of the principal cortical neurons- the Purkinje cells. The Purkinje cells, the sole output of the cerebellar cortex, send inhibitory projections to the cerebellar nuclei. The cerebellar nuclei send projections out of the cerebellum to the rest of

the nervous system, including neurons in the inferior olive. The olive sends powerful excitatory climbing fibre projections to the Purkinje cells. Being the sole output of the cerebellar cortex, Purkinje cells are the principal locus of sensorimotor integration within the cerebellum (see below).

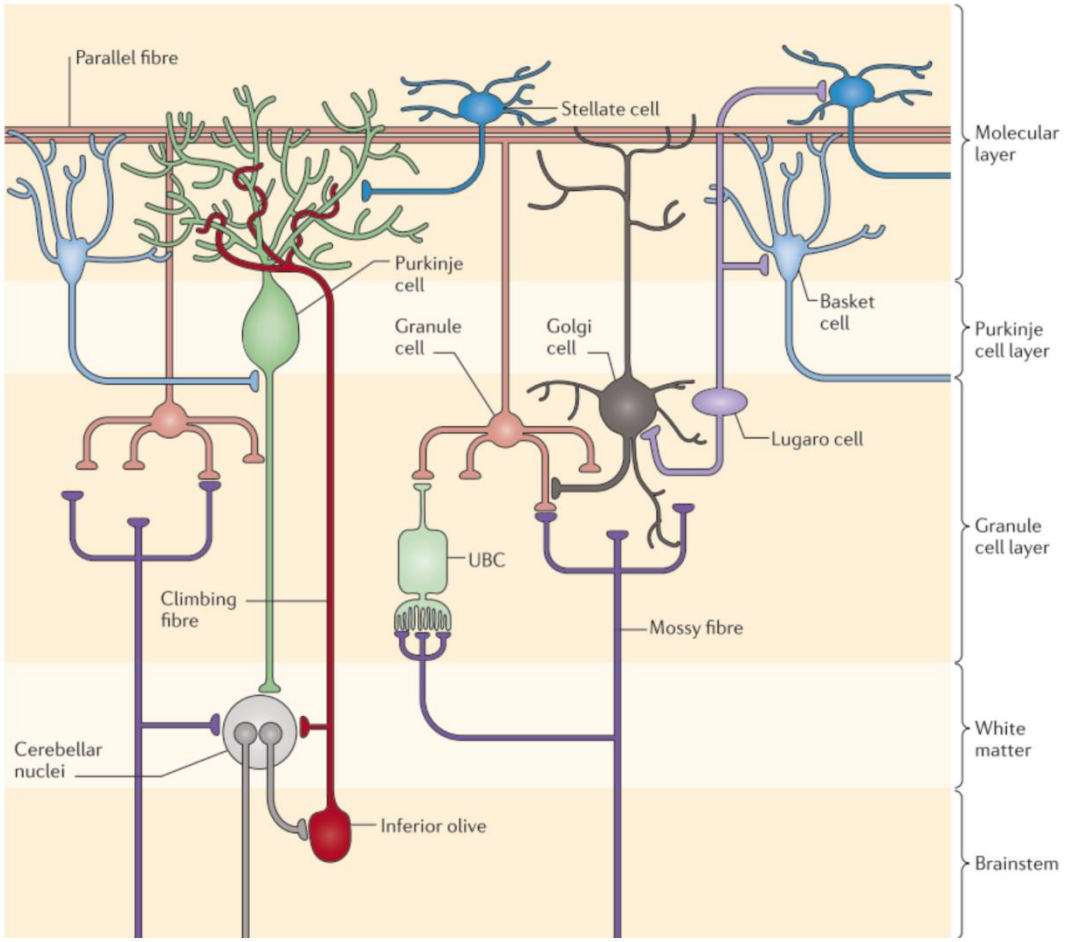

Figure 1.3 Cerebellar neuronal circuit.
Classical representation of the cerebellar cytoarchitecture. Principal neurons include granule cells, relaying the mossy fibre inputs to the Purkinje cells, the sole output of the cerebellar cortex. Purkinje cells synapse onto the cerebellar nuclei which project out of the cerebellum to the rest of the nervous system and the inferior olive, which projects back to the Purkinje cells, generating complex spikes. Multiple interneuron types also exist including Golgi, Stellate, Basket, Lugaro, and unipolar brush cells (UBC). Taken from Cerminara et al. (2015)*, reproduced with permission of Springer Nature.*

Purkinje cells can elicit two forms of spike potential; simple spikes that reflect input from the mossy fibre/granule cell inputs to the dendritic arbour, and complex spikes caused by input from climbing fibres. In the awake cat, simple spikes are usually reported as having an irregular tonic rate between 19 and 95 spikes/second with a mean discharge of 44 spikes/second (Armstrong and Rawson 1979). By contrast, complex spikes appear as an initial spike (usually similar but larger amplitude than simple spikes) followed by a variable number of [typically] smaller amplitude spikelets. Additionally, the presence of a complex spike is usually followed by a short cessation of simple spikes (Hobson and McCarley 1972; Eccles et al. 1966). In the awake cat, complex spikes have a low tonic discharge of around 1.5 spikes/second (Armstrong and Rawson

1979). As detailed below, these two forms of spiking activity have been instrumental in theories relating to error-dependent learning in the cerebellum.

The cerebellum's involvement with coordinated movements was established in the early 19th century through the observations in animals that damage to the cerebellum leads to degradation in movement control – typically an appearance of a tremor during goal-directed movements (Rolando 1809, Flourens 1822; cited in Ito 2002). Critically, this degradation in movements (dysmetria) is not the total abolition of movement, but the loss of coordination. These early findings revealed the cerebellum's role in shaping voluntary movements into coordinated actions.

The first observations made in humans followed the first World War, when soldiers with gunshot wounds damaging the cerebellum experienced deficits in voluntary movements (Holmes 1917). Holmes went on to describe the cardinal signs of cerebellar damage on voluntary movements, which are still used in the clinic today- including a slowness to start a movement and general dis-coordination (ataxia), intention tremor in movement, as well as mis-reaching and hunting of a target (dysmetria) (Holmes 1939).

Although the classic view of cerebellar function is a structure primarily concerned with motor control, a growing consensus now contends that the cerebellum also has significant involvement with non-motor (cognitive) functions such as attention and emotion (Koziol et al. 2014; Timmann and Daum 2007; Buckner 2013; Strick et al. 2009). In addition to difficulties with movement, cerebellar patients can also have deficits in executive functions such as set-shifting, working memory, abstract reasoning, as well as changes in emotional behaviours (Schmahmann and Sherman 1998).

1.3.1.1 Cerebellar function: learning and timing

Two dominant views of cerebellar function exist: Learning hypotheses are widely attributed to the work of Marr, Albus and Ito (Schutter and Maex 1996; Strata 2009). Central to these views is the proposal that the numerous parallel fibre inputs to each Purkinje cell transmit a broad range of sensorimotor information. When a behavioural error is detected (such as a mismatch between the prediction and consequence of a movement), this error is transmitted to Purkinje cells via the powerful synaptic input of climbing fibres. The coincidence of this activity with parallel fibre synaptic inputs leads to long term depression of these parallel fibre inputs, modifying Purkinje cell information processing (Ito 2000). Consequently, the cerebellar circuit is seen as a substrate of supervised learning, in which the climbing fibre serves as a teaching signal, informing the Purkinje cells of a computational error that requires changing (Knudsen 1994).

An alternative view suggests that the olivocerebellar circuit (a feedback loop between the inferior olive, cerebellar cortical neurons including Purkinje cells, and cerebellar nuclei) generates rhythmic and synchronised activity, driving timing and spatial organisation of motor sequences (Llinás 2011; Ivry et al. 2002; Avanzino et al. 2015), as well as in non-motor domains such as perceptual timing (Salman 2002; O'Reilly et al. 2008).

However both viewpoints are not mutually exclusive, with reports to-date presenting little or no data specifically precluding a dual role of the olivocerebellar system in both motor learning and in the organisation of synchronised activity (Lang et al. 2017). Overall, it is generally accepted that the neuronal circuitry of the cerebellar cortex is well suited as a site of motor learning.

1.3.1.2 Cerebellum in motor adaptation.

The cerebellum's importance in motor adaptation is firmly established, as demonstrated by the inability of patients with dysfunction or damage to the cerebellum (such as cerebellar ataxias) to adapt to controlled perturbations (Martin et al. 1996a; Tseng et al. 2007; Deuschl et al. 1996). Similar deficits occur in animals with lesions of the cerebellum (Baizer et al. 1999), and non-invasive stimulation of the human cerebellum is able to alter the time-course (rate) of adaptation (Galea et al. 2011; Herzfeld, Pastor, et al. 2014; Cantarero et al. 2015).

Linking cerebellar function to theories of motor control by internal models has been a key focus for much of the field. There is a mixture of data supporting the case that the cerebellum can act as either a forward or an inverse model. For example, recordings of Purkinje cell simple spike activity in monkeys performing a manual tracking task under varying feedback loads (a force-field adaptation task) showed that 91% of recorded neuron activity was tuned to kinematic properties of the movement (speed and arm position), but not arm dynamics (such as electromyography (EMG) activity and applied force). This is consistent with an output of a forward model predicting movement consequences of motor commands, but not an inverse dynamics model that would relate more directly to the generation of arm forces (Pasalar et al. 2006). Separately, Purkinje cell simple spiking activity has been shown to encode both predictions of, and feedback about targeting errors in a manual tracking task, consistent with updating a forward model of the behaviour (Popa et al. 2012; Popa et al. 2016). This is in addition to the behavioural error signals carried by the olivary climbing fibres and represented in the Purkinje cells as complex spikes (Streng et al. 2017).

Conversely, studies of the vestibulo-occular reflex (VOR), which stabilises gaze direction in response to head movement, have provided the best evidence for inverse-model control of movements (reviewed in Kawato 1993). For example, in an ocular tracking task performed by

monkeys, Purkinje cell simple spike activity was able to represent eye acceleration and velocity, consistent with an inverse-model of eye-movements (Shidara et al. 1993).

In light of the experimental and theoretical basis of both forms of internal model situated in the cerebellar circuitry, it has been proposed that the cerebellum may encode inverse and forward models simultaneously, possibly depending on the specific task or the sub-region of the cerebellum responsible for the task (Wolpert and Kawato 1998; Ito 2000; Wolpert et al. 1998; Haruno and Wolpert 1999). The current consensus is that the cerebellum is the principal site of these internal representations of body/environment dynamics, which require plastic changes during adaptation of movement in response to errors.

1.3.2 Motor cortex

As first demonstrated in 1870 by Fritch and Hitzig in the dog, stimulation of an area in the contralateral cerebral cortex produces movement responses on the contralateral side of the body to stimulation (reviewed in Gross 2007). Stimulation of different parts of this area also elicited twitching responses in differing muscles, suggesting a clustering of neurons controlling different body parts. These initial findings were extended to show a topographic representation of the body (Penfield's famed homunculus -Penfield and Boldrey 1937) in this 'motor cortex', located in a medial-lateral orientated strip in front of the central sulcus in primates.

The motor cortex has been studied in many species including cat (Livingston and Phillips 1957; Kobaiter-Maarrawi et al. 2011), non-human primates (Ferrier 1874) and humans. The details of studies and findings are far too numerous to include here, however significant contributions are discussed in a recent review (Ebbesen and Brecht 2017). Modern interpretations suggest that the focal areas of the motor cortex comprise collections of neurons that control coordinated groups of muscles, known as muscle synergies (reviewed in Bizzi and Cheung 2013). These muscle synergies are groups of muscles that, when evoked by stimulation of the upstream motor cortical neurons, elicit complex and behaviourally-relevant movement repertoires. For example, biphasic microstimulation of motor cortex in monkeys (at 'behaviourally relevant' timescales of 100-1000ms durations) elicit movements such as grasping of the hand, followed by retraction of the arm to the mouth, and the mouth to open (Graziano et al. 2002). Interestingly, the authors state;

> *"Stimulation of this site always drove the joints toward this final posture, regardless of the direction of movement required to reach the posture"*
> *– Graziano et al. 2002*

These results could be interpreted as evidence that the motor cortex has initiated an inverse model of the complex movement. In this case, the specific stimulation site in the motor cortex

represented the desired posture, and the brain circuity associated with this site was able to compute a solution to arrive at that posture regardless of starting position.

1.3.2.1 Motor cortex in adaptation

Like the cerebellum, the motor cortex has been implicated as a site of both forward and inverse models, although is most commonly related to inverse modelling (reviewed in Yavari et al. 2013).

In relation to motor adaptation, neuronal activity in the primary motor cortex (M1) of monkeys undertaking a force-field adaptation paradigm (pushing a manipulandum arm to a target through an applied force-field) exhibit changes in directional tuning of responses that encode the direction of compensatory forces (Gandolfo et al. 2000; Richardson et al. 2012). Further, the activity of primary motor neurons during the preparatory phase of movement whose activity is tuned to the hand direction offering the task 'solution' is increased as adaptation progresses (Paz et al. 2003).

Studies in humans have also shown that motor adaptation leads to structural changes in M1-specifically an increase in local grey matter and fractional anisotropy that correlated with the speed of learning (Landi et al. 2011). Further, non-invasive disruption (using transcranial magnetic stimulation) of M1 prior to force-field reach adaptation does not alter the rate of adaptation, but leads to significantly worse performance (increased errors) during a delayed (24 hour) retest of the perturbation (Richardson et al. 2006). This was taken as evidence that whilst the motor cortex is not necessary for the initial adaptation to a novel perturbation, the long-term memory of this perturbation (necessary for exhibiting savings) is dependent on the motor cortex. Supporting this, non-invasive electrical stimulation (transcranial direct current stimulation) over M1 has also been shown to increase retention of a newly learned sensorimotor mapping/internal model (Galea et al. 2011).

In sum, studies in a range of species show that M1 activity is able to form and store motor memories, and may be important in the stabilisation and long term storage of newly formed sensorimotor mappings (internal models) rather than their acquisition (Galea et al. 2011; Della-Maggiore et al. 2015).

1.3.3 Prefrontal cortex

The prefrontal cortex (PFC), found at the very rostral aspect of the mammalian cerebrum, is generally associated with higher cognitive control of behaviours such as maintaining representations of goals and how to achieve them (Miller and Cohen 2001), as well as working memory (reviewed in Funahashi 2017) and longer term memory (reviewed in Euston et al. 2012).

In accordance with a role as an executive controller, the PFC has extensive reciprocal connections, including with the motor cortex and cerebellum (Watson et al. 2009; Watson et al. 2014; Kelly and Strick 2003; Middleton and Strick 2001; Akkal et al. 2007; Bostan et al. 2013). This connectivity allows for involvement of the PFC in aspects of motor control. For example, dissection of the connections between the temporal lobe and PFC in monkeys impaired the learning of novel cue-action associations (Gaffan and Harrison 1988; cited in Wise and Murray 2000). This is paralleled by human neuroimaging data showing increased activity of some prefrontal areas during early stages of similar cue-action 'mapping' tasks (Toni et al. 2001). Similarly, patients with unilateral lesions of the PFC have deficits in oculomotor control (Pierrot-Deseilligny et al. 2003). Specifically, patients had increased occurrences of misdirected reflexive saccades in an anti-saccade task, in which subjects must make saccades in the opposing direction of a target movement. Together, these results suggest a learning role for the PFC in action selection, associating the correct movements with task cues.

Other evidence from human neuroimaging (such as functional magnetic resonance imaging, fMRI) studies supports an influence of the PFC on motor actions through working memory and attentional processes (Wiese et al. 2005), and a specific role in working memory during mental preparation of movement sequences (Pochon et al. 2001). In addition to a role in more general motor control, the influence of the PFC on motor adaptation has also been explored.

1.3.3.1 Prefrontal cortex in adaptation

Neuroimaging studies have shown activation of the PFC during the early stages of sensorimotor adaptation in humans (Shadmehr and Holcomb 1997; Sakai et al. 1998; Seidler and Noll 2008). And studies on healthy ageing have implicated frontal areas in the implementation of 'top-down' cognitive control during adaptation. Lesions to the prefrontal cortices impairs awareness of an applied perturbation, even of large magnitudes (reviewed in Taylor and Ivry 2014). Overall, these findings suggest the PFC may be involved in 'cognitive' aspects of motor adaptation, rather than in the adaptation process *per se*.

Direct evidence for a role of medial PFC (mPFC) in motor adaptation has recently been examined using non-invasive electrical stimulation (using anodal trans-cranial direct current stimulation) applied to the right PFC in humans. The stimulation led to an improvement of performance during re-exposure to a visuomotor (prism) perturbation; i.e. an enhancement in savings with no change in initial adaptation (Seidler et al. 2017). This is in apparent conflict with the neuroimaging data reported above, which showed activations of frontal areas early in learning. This suggests caution when interpreting the significance of imaging results and the need for studies that involve direct recording of neural activity. Recent data has shown that a subset of rodent mPFC neurons show modulation of activity in a 'Go/No Go' object localisation task during

trials in which behavioural adaptations occurred (i.e. a correct response after incorrect response) compared to trials in which no behavioural modifications occurred (de Haan et al. 2018).

As the mPFC is thought to be the loci of maintaining working memory (Euston et al. 2012), as well as task rules and goal concepts (Miller et al. 2002), and high degrees of afferent connections from across the rest of the brain, it is well placed to obtain all necessary information to integrate and compute the necessary adjustments to behaviour in order to adapt and optimise subsequent actions. This is in contrast to other frontal areas such as the anterior cingulate cortex, which has been shown to be involved in error detection and evaluation signalling (Magno 2006) during motor adaptation tasks (Ito et al. 2003), but not in the updating of behaviours (Luauté et al. 2009).

Additionally, although not directly linked to motor adaptation, one theoretical model of prefrontal functioning suggests a general role in developing internal models of the environment (Alexander and Brown 2014). Specifically, the Predicted Response-Outcome model suggests that the PFC is capable of learning action-consequence relationships (the essence of a forward model) and detect discrepancies. Although this model has been developed in relation to attentional or attention-like processes, the proposed ability of the PFC to form predictive associations is important in the context of motor adaptation, as it implies that the capacity to support adaptive learning occurs across multiple areas of the brain.

Overall, evidence that the mPFC may have a broad influence on adaptive processes. As direct evidence is largely derived from data gathered from other motor learning tasks, further investigation is warranted using a task specifically probing motor adaptation.

1.4 Network activity supporting motor adaptation

As indicated above, the cerebellum, M1, and mPFC are all thought to serve roles during motor adaptation. An important question then is how they interact with one another to support adaptive behaviour.

The cerebellum is extensively connected bi-directionally with a myriad of cerebral areas, including the primary motor and prefrontal cortices (Kelly and Strick 2003; Middleton and Strick 2001; Bostan et al. 2013) primarily via afferent inputs from the pontocerebellar tract and efferent pathways via the dentato-thalamo-cortical tract in humans (Buckner et al. 2011). Other efferent pathways originate from the paravermal and vermal compartments and these pathways are known to play significant roles in both motor and non-motor behaviours (Zhang et al. 2016; Pakaprot et al. 2009). Anatomical studies have also shown connection pathways to

the PFC via medial dorsal and ventral lateral thalamic nuclei (Groenewegen 1988; Melik-Musyan and Fanardjyan 1998; Weible et al. 2007).

Given the presence of anatomical connections between the cerebellum, M1, and PFC, along with the distinct roles each area is proposed to serve regarding motor adaptation, it is likely that they form a part of an integrated functional network.

Indeed, microstimulation of cerebellar nuclei leads to a modulation of discharges in M1 neurons (Holdefer et al. 2000; Noda and Yamamoto 1984; Rispal-Padel et al. 1982), showing the impact cerebellar activity has on motor cortical activity. Additionally, transcranial stimulation of the cerebellum in healthy humans results in a suppression of M1 evoked motor potentials, which is not present in subjects with cerebellar dysfunction (Ugawa et al. 1994; Vasant et al. 2015; Fierro et al. 2007; Daskalakis et al. 2004). Further, measures of synchronisation of the local field potential activity in the cerebellar cortex and sensorimotor cortical areas during movement preparations has previously been reported as a potential form of cerebro-cerebellar communication (Courtemanche and Lamarre 2005).

Stimulation of the fastigial cerebellar nucleus has also been shown to evoke neuronal responses in the PFC, and there is a directed coherence of 5-10Hz local field potential activity from the cerebellum to prefrontal areas in rats during active locomotion (Watson et al. 2014). Overall, a body of evidence therefore points to information transmission between the cerebellum, motor and prefrontal cortices during behaviour.

Given the evidence that (i) each of these brain regions may be involved in distinct aspects of motor adaptation, such as state estimation (PFC) or the long term storage of sensorimotor maps (M1); (ii) each of these regions is capable of supporting plastic internal representations; and (iii) the existence of anatomical and physiological pathways between them; the question is raised as to how they might act as an integrated network to support motor adaptation behaviour.

One previous study has explored this issue but in relation to motor sequence learning. Ma *et al.* (2010) fitted structural equation models to neuroimaging data captured at three points (2 weeks apart) during long term motor sequence learning. They found that directed connections from the cerebellum to motor cortex, as well as PFC to both motor cortex and cerebellum decreased as the training progressed, whereas from motor cortex to cerebellum first decreased, and then increased across the training weeks. Overall, the authors suggest their results are consistent with a reduction in cerebellar control (as errors in the motor task decrease) and a reduction in higher cognitive influence (reduction of connections originating from the PFC) during such learning. In contrast, increases in connectivity that occurred between motor cortex and other cortical and non-cortical regions (including the basal ganglia, supplementary and premotor

cortex) was taken to reflect the greater automation of the behaviour as the task became established. Overall, this study demonstrates the dynamic nature of brain-wide structures during longer term motor learning and is consistent with a cerebellar-motor-prefrontal cortical network being crucial during early stages of motor learning.

To date only two studies have attempted to assess such functional connectivity during motor adaptation, using neuroimaging techniques. Functional neuroimaging data from patients with multiple sclerosis- who have deficits in a postural motor adaptation task- showed reduced measures of connectivity between motor cortex and cerebellum (Fling et al. 2015). Additionally, functional neuroimaging on healthy participants has shown changes in a cerebellar, motor, and dorsal premotor cortex resting state network one hour after force-field reach adaptation training compared to prior to experience in the force-field (null field reaching)- with effects highly correlated to behavioural measures of adaptative learning (Vahdat et al. 2011).

Overall, these data suggest longer term changes in brain network activity and connectivity as motor learning and adaptation progresses. It remains to be addressed how such network connectivity may change at shorter timescales (e.g. within a single training session), and how information is encoded by populations of neurons in each of the nodes in the network during motor adaptation.

Considering a single session of adaptation, in which a series of adaptation trials are performed and behavioural errors progressively return to baseline performance levels, it can be hypothesised that cerebellar-motor-prefrontal cortex information transfer is: (i) greatest early on during adaptation (when errors are large and are used to update an internal model); and (ii) minimal when the errors in late adaptation return to baseline levels (when the internal model has been updated).

1.5 The current study

1.5.1 Aims and objectives

The work reported in this thesis seeks to address several questions relating to the neural activity present in the supraspinal motor network during different stages of visuomotor adaptation:

1. Can a neural signature of motor adaptation be observed in the cerebellar cortex, M1 and/or PFC? i.e. are there measurable changes in neural activity in one or more of these nodes that relates to different aspects of adaptation?
2. Is there evidence of enhanced functional connectivity between the cerebellum, M1 and PFC during early adaptation?

To answer these questions, visuomotor adaptation was studied in both human and animal subjects. This allowed investigation of neural activity at multiple scales, ranging from macro scale population activity (human electroencephalography – EEG), through meso scale population activity (animal local field potentials) to micro scale single neuron activity (animal single unit recording).

1.5.2 Organisation of the thesis

This thesis is divided into three results chapters. The first presents human EEG findings during visuomotor adaptation; the second describes the development of a similar behavioural paradigm in the cat. The third reports local field potential and single unit electrophysiological findings during visuomotor adaptation in the animal work. The thesis concludes with a general discussion and summary of the principal findings of the animal and human studies.

Chapter 2 – Human Visuomotor Adaptation

2.1 Introduction to human study

This chapter describes a visuomotor adaptation experiment with healthy adult human participants. Specifically, this experiment used a simple paradigm in which participants use a joystick to control an on-screen cursor, directing it from a start location to a specified on-screen target location. This paradigm has previously been used in both human and non-human (Feingold et al. 2015) motor adaptation studies. This method was chosen over other adaptation paradigms such as those that utilise robotic manipulanda (Diedrichsen et al. 2005; Izawa et al. 2012; Herzfeld, Pastor, et al. 2014; Shadmehr et al. 2010) or 'real-world' reaching to target (Miall et al. 2007) principally due to the ease of implementation of such a paradigm within the EEG recording room.

2.1.1.1 Neurophysiological oscillations and movement

This thesis focusses on the electrophysiological signals recorded during motor adaptation. Consequently, it is appropriate to consider the neuronal processes that generate such signals.

Active neuronal processes involved with the transmission of an action potential (the basic unit of information in the brain) generate small electric fields that superimpose in the extracellular volume, and these can be detected with extracellular recording electrodes. EEG signals are considered to be formed by the synchronisation of large populations of neurons enabling the summation of their electrical charges to a level that can be detected at the surface of the scalp (Cohen and F F Cohen 2017). EEG trades of spatial resolution for sub-millisecond temporal resolution. Reports suggesting synchronous (epileptiform) neocortical surface activity in the order of 19cm^2 is necessary to generate 'well recordable' EEG (Cosandier-Rimélé et al. 2008), suggesting that neurons within this distance must have synchronous activity and be spatially aligned for the electrical moments to sum into a detectable reading at the scalp surface.

This contrasts with more invasive recording electrodes (recording local field potentials), which have better spatial resolution- currently estimated to be in the order of hundreds of microns to a few millimetres (Leski et al. 2013; Lindén et al. 2011). Regardless of the size of the contributing neuronal population, fluctuations in the activity of the neurons as well as the broader architecture of neuronal circuits result in oscillations of these extracellular electrical fields (reviewed in Buzsáki et al. 2012).

There is a widely held belief that various frequency components of recorded electrophysiological signals may embody distinct information about behaviour, including ongoing movement processes. Below is a brief account of oscillation frequencies most relevant to the current thesis and their relationship to voluntary movement.

2.1.1.1.1 Delta

Very low frequency oscillations (1-4Hz; delta) are classically associated with periods of quiescence or sleep, due to their dominant appearance in EEG signals at these times (Rodenbeck et al. 2006; Davis et al. 2011). Recently, these slow waves have been proposed to relate to cognitive processes, such as decision making (Nacher et al. 2013) and attention (Harmony 2013). Specific to movement, delta frequencies in the local field potentials of human M1 were observed to become entrained to inter-movement intervals, which would enable synchronisation of cortical excitability to the ongoing behaviour, which the authors suggest reflects top-down attentional processes to aid in prediction of the task cueing (Saleh et al. 2010). Further, motor cortical neurons in monkey have been shown to exhibit activity within the delta frequency range, synchronous with sub-movements of reaching movements, that was able to encode movement speed and direction (Hall et al. 2014). Thus, there is some evidence that delta frequency oscillations in the motor network may contain useful information about ongoing movement behaviours.

2.1.1.1.2 Beta

Beta frequency oscillations (10-30Hz) have had a primary place in the movement literature. A popular hypothesis for motor cortical beta oscillations is that they signal the 'status quo' of motor processes (Engel and Fries 2010). Specifically, it is proposed that enhanced beta band oscillations reflects the synchronisation of relatively large-scale neural ensembles gathered into a 'default mode' network when they are not actively engaged in motor control (Pfurtscheller et al. 1996). This view follows the observation of decreases in beta oscillations during active phases of movements, when presumably small-scale neural ensembles are required to perform individualised processing tasks. An alternative view is that these beta band oscillations in the sensorimotor areas reflects integration of efferent information from other areas including the periphery, in some way recalibrating the system in preparation for the next series of movements (Baker 2007). Increased beta oscillations are associated with a suppression of movement initiation, as observed in Parkinson's disease patients (Little and Brown 2014). Thus increased beta oscillatory activity has been proposed to promote the current 'motor set' (specific combination of motor plans and commands) and prevents accidental movement execution at the cost of changing these motor plans (Khanna and Carmena 2017).

In the context of adaptation then, if beta oscillations represent the maintenance of select neuronal populations representing a specific motor plan, then during adaptation to a predictable perturbation, beta oscillations are hypothesised to be suppressed, promoting plastic alteration of these neural ensembles.

2.1.1.1.3 Gamma

Motor cortical gamma oscillations (30-80Hz) are thought to be a result of the inhibitory/excitatory loops formed by cortical interneurons and pyramidal cells, although gamma oscillations are possible through inhibitory-inhibitory neuronal connections, and may indeed be produced through a variety of mechanisms in other regions (reviewed in Buzsáki and Wang 2012). Motor cortical gamma oscillations have been associated with active motor control processes, although a role in afferent proprioceptive feedback has been suggested (Nowak et al. 2018). For example, an 80Hz transcranial alternating current stimulation directed over the motor cortex improved performance on a manual cursor tracking task specifically after rapid changes in tracking trajectories (Santarnecchi et al. 2017).

Under this framework, it is hypothesised that high gamma frequencies would be stronger (detected as a greater power in EEG) during early adaptation and early after-effect, reflecting the neural circuits actively modifying motor commands that are no longer suitable (after experiencing prior errors).

2.1.2 Motor adaptation and EEG

A primary goal for this line of experiments was to determine whether adaptation-related changes in neural activity, reflecting that of the motor cortex, can be detected in EEG signals. Previously, Tan and colleagues have shown that post-movement motor cortical beta (13-30Hz) activity is modulated during a joystick reach adaptation task (Tan et al. 2016). Specifically, the oscillatory power was significantly decreased during early stages of adaptation and washout (after-effect) compared to either late baseline, late adaptation or late washout trials. The authors proposed that this modulation of the post-movement beta oscillation reflects the confidence in the (just-used) internal model and signifies the need to either adjust (less beta synchronisation) or maintain (higher beta synchronisation) the internal model. Separately, a study found modulation of beta (16-25Hz) activity over motor cortical regions during a preparatory stage of the reaching movement during the after-effect of a prism adaptation task (Bracco et al. 2018). The lack of effects seen in occipito-parietal regions led the authors to propose that activity in cerebello-thalamo-cortical pathways were a likely candidate of this effect rather than parietal cortical regions. Importantly, both these effects are *in addition to* the well documented movement related desynchronization and post-movement synchronisation of beta band oscillations in the motor cortex (reviewed in Pfurtscheller 2001).

Together, these two studies provide two time-points to assess motor cortical EEG signals during the reaching movement on the present study; immediately prior to the movement, and immediately after the movement. Although it has principally been beta frequencies that have

been considered to date, a wider range of frequencies in the EEG signal was assessed in the current study in relation to visuomotor adaptation task.

2.1.2.1 Cerebellar EEG

A principal focus of this thesis is the contribution of the cerebellum to the wider motor network during motor adaptation. Therefore, it would be preferable to simultaneously record the activity of cerebellar and other brain areas such as the motor cortex. However, there is general agreement that non-invasive recording of electrical activity in the cerebellum (EEG) is not presently reliable (Niedermeyer 2004. cited in Dalal et al. 2013).

Considering the cerebellar anatomy and location, the highly folded cortical surface means that the currents generated by the neurons do not 'line-up' as is the case in less folded frontal cortices of the brain. Thus, the magnitude of the summed currents will be far smaller. Further, the location of the cerebellum in humans, tucked under the occipital lobe and upper neck musculature means that any cerebellar signal must travel through a greater amount of other structures (themselves electrically active) before being able to be detected by surface electrodes. To-date, very few attempts to assess human cerebellar EEG have been published, and these were made using invasive intracortical EEG methods (a.k.a. electrocorticography) (reviewed in Dalal et al. 2013), and present investigations of the cerebellar EEG are limited to combining EEG data with other neuroimaging techniques such as fMRI or positron emission tomography (Canto et al. 2017).

Given these technical issues the present study used a different method to assess the influence of the cerebellum on the activity of frontal cortical structures, utilising a non-invasive technique to modulate cerebellar activity.

2.1.2.2 Non-invasive cerebellar stimulation

There has been a recent resurgence in interest in using non-invasive stimulation of the brain to modulate a broad range of behaviours and clinical symptoms (Utz et al. 2010; Schlaug et al. 2009; Priori 2003), including stimulation of the cerebellum during motor adaptation tasks (Van Dun et al. 2017). There are two main techniques for non-invasively modulating brain activity: Transcranial Magnetic Stimulation (TMS) and transcranial Electrical Stimulation (tES). The latter includes transcranial alternating current and transcranial Direct Current Stimulation (tDCS). All current non-invasive techniques are considered safe with stimulation parameters in common use, with only few reports of mild side effects such as headaches or mild skin irritation (Matsumoto and Ugawa 2017).

2.1.2.2.1.1 Transcranial direct current stimulation

Transcranial direct current stimulation (tDCS) is a technique in which a low current (typically 2mA) is delivered through scalp electrodes to polarise the underlying neural tissue, modulating its activity. tDCS has been reported to have physiological effects on cortical activity both during stimulation and longer term effects (up to 3 hours) post stimulation (Nitsche and Paulus 2000; Ammann et al. 2016). The exact mechanisms of action of tDCS are not understood, but current data suggest that tDCS modulates ongoing plasticity of the affected tissues (Jackson et al. 2016; Stagg and Nitsche 2011).

The effects of motor cortical tDCS on motor learning in humans were reported in a seminal study at the turn of the millennium (Nitsche and Paulus 2000). tDCS had a polarity specific effect on motor skill learning, with anodal current (delivered with the negative terminal electrode over the motor cortex) leading to improvement, whist cathodal stimulation decreased performance.

Cerebellar targeted tDCS has subsequently been reported to modulate behavioural performance of human participants during motor adaptation (Doppelmayr et al. 2016; Taubert et al. 2016; Jayaram et al. 2012). Specifically, in healthy participants, cerebellar targeted anodal tDCS is able to increase measures of adaptation to perturbations in reaching tasks- such as the rate of adaptation or reach trajectory compensation (Galea et al. 2011; Hardwick and Celnik 2014), whilst cathodal stimulation over the cerebellum has been shown to lead to reduced adaptation performance (Herzfeld, Pastor, et al. 2014; Fernandez et al. 2017). However, there is a high degree of variability in the literature regarding effect sizes, with some studies reporting an opposite polarity specific effect, i.e. anodal stimulation impaired adaptation and cathodal stimulation improved adaptation (Panouillères et al. 2015). This inter study variability has been attributed to a multitude of factors, including the specificity of electrode placement, stimulus intensity, underpowered studies, individual susceptibility and age-dependent effects (Thair et al. 2017; Jalali et al. 2017; Ammann et al. 2017).

However, generally speaking, cerebellar anodal tDCS has been shown to be able to facilitate cerebellar processes during visuomotor adaptation (Galea et al. 2011; Herzfeld, Pastor, et al. 2014; Yavari et al. 2015; Doppelmayr et al. 2016). Of interest to the current study is the investigation by Galea et al (2011). In their study, anodal tDCS was targeted over both contralateral motor cortex, and ipsilateral cerebellum, during a cursor-rotation adaptation task. Measurements of the angular errors (angle between start-to-target and start-reach end) in trial epochs across the adaptation procedure (30° rotation mapping between arm position and cursor location) revealed that anodal cerebellar tDCS led to improvements in error reduction (rate of learning) but had no effect on the retention of the rotation transformation (assessed during the washout/after-effect trials). Conversely, anodal tDCS over the motor cortex had no effect on the

initial adaptation to the perturbation but resulted in a reduction in the rate of washout of this memory. The authors concluded that this highlighted the different roles of the cerebellum and motor cortex in visuomotor adaptation: - the cerebellum is involved in the immediate learning of the environmental dynamics on a trial-by-trial basis (via updating of an internal model), whereas the motor cortex is involved in the longer-term retention of the new visuo-motor mappings. This is in line with modelling studies that suggest a multi-rate model of adaptive learning, comprising of a fast-learning/fast-forgetting component and a slow-learning/slow-forgetting process (reviewed in Tanaka et al. 2012).

The anodal cerebellar tDCS during the baseline trials in the study of Galea and colleagues did not affect performance accuracy, only influencing the rate of adaptation to the perturbation. This suggests that cerebellar processes were not essential during the basic reaching task, but only related to the rapid adjustment of the limb movement following errors early in the adaptation. Consequently, it can be hypothesised that the cerebellum and motor cortex communicate specifically during early periods of adaptation, transferring the rapidly learned information about the task dynamics from the cerebellum to the motor cortex for long-term storage and implementation.

In the present study cerebellar targeted tDCS was therefore used (in lieu of cerebellar EEG recording) to assess any changes to the motor cortical and prefrontal cortical signals, which would be indicative of changes to cerebello-cerebro functional connectivity. Any changes in the spectral components of the motor/prefrontal cortical EEG signals because of this stimulation would indicate a cerebellar influence.

2.1.3 Aims

Although the design of the adaptation task and use of cerebellar targeted electrical stimulation were based on relatively standard practices, as this was the first use of such techniques in the lab, a pilot experiment was performed to assess the feasibility of the experiment.

The main experiment aimed to uncover EEG correlates of adaptation across two principal regions of the motor network (sensorimotor and prefrontal cortices), in major frequency band subdivisions of these recorded signals. The influence of the cerebellum on these signals was tested through modulating cerebellar activity by non-invasive electrical stimulation.

2.2 Materials and methods

2.2.1 Ethical statement

Human based experiments were approved by the University of Bristol local ethics committee. All participants gave informed consent to take part and were rewarded with either monetary reimbursement according to local guidelines, or through a course credit system employed by the University of Bristol School of Experimental Psychology.

2.2.2 Participants

Eleven healthy young adult participants (10 female, 1 male, aged between 19 and 21 years) took part for the initial pilot experiment. All pilot participants were undergraduate students of the University of Bristol, right handed (Edinburgh Handedness Inventory mean score: +78.6, SD ±17.9) and had normal or corrected to normal vision. One participant's behavioural data was lost due to corrupt data-file, and so was not included.

Eleven healthy young adults (4 female, 7 male, aged between 21 and 31) took part in the main study. All participants were right handed (Edinburgh Handedness Inventory mean score: +87.5, SD ±14.3) and had normal or corrected to normal vision.

All participants in both pilot and main study took part in two experimental sessions, separated by one week. Each participant performed the task under both 'active' cerebellar tDCS stimulation and a 'sham' cerebellar tDCS stimulation.

2.2.3 Behavioural task equipment and software

The task was run on a computer running Windows XP, within the MATLAB software environment with Psychtoolbox version 3. Task code was modified from that made publicly available under a GNU General Public Licence by D. Goldschmidt at https://github.com/degoldschmidt/motor-experiments. The task ran at approximately 60Hz, thus all behavioural data were captured at this rate.

The visual display was a 20" Iiyama CRT positioned approximately 60cm from the participant's seated position. The control joystick was a Cyborg F.l.y. (Mad Catz, Hong Kong) connected via USB. The joystick was positioned on the right-hand side of the monitor at a distance from the participant to ensure a comfortable reaching behaviour over the full travel of the joystick. The base of the joystick was secured to the table top with duct-tape to prevent movement of the joystick as far as possible. A keyboard was also present to enable the participants to move on from the initial instruction screens.

2.2.4 Behavioural task

The experiment consisted of a simple behavioural task based on similar set-ups used extensively throughout the literature (Miall et al. 2004; Özdenizci et al. 2017; Benson et al. 2011; Bédard and Sanes 2014; Kim et al. 2015; Tan et al. 2014).

In the experiments presented here, each condition (baseline, adaptation, after-effect) consisted of 200 trials. Each trial commenced with the cursor at the centre of the screen, surrounded by sixteen evenly spaced grey markers, positioned at the perimeter of a circle (radius 12cm) forming the task space (**Figure 2.1**). When the participant clicked on the joystick trigger, one of four possible targets was displayed (45°, 135°, 225°, or 315° from vertical). The participant was then able to move the cursor outwards to the target. Trials ended when the cursor crossed the perimeter of the circle formed by the grey markers. The cursor was frozen at the position it crossed the perimeter for a short period of time (500ms) to provide participants with explicit feedback.

Participants were instructed to complete each movement as quickly and accurately as possible, with emphasis on the movements being ballistic – without attempting to stop and check the movement halfway through. As a prompt to maintain a rapid reaching behaviour, the time between target presentation (joystick trigger pull) and trial end was measured, and trials lasting greater than 750ms led to an additional onscreen message requesting the participant to speed up their movements.

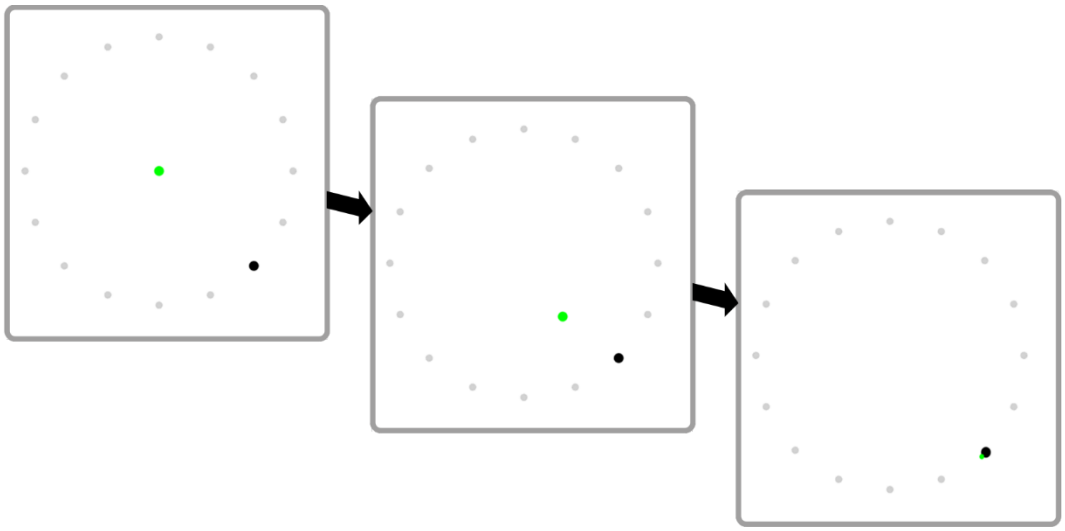

Figure 2.1 Behavioural task space and example trial progression.
Representation of a single trial of reaching. Top left: After clicking the joystick trigger to initiate a trial, one of four black targets and the green cursor appeared. Middle; Participants were required to move the cursor to the appropriate target with a 'ballistic' movement. Bottom right; Upon crossing the perimeter of the task space, the cursor froze at the crossing point to provide visual feedback of the trial.

Targets were presented pseudo randomly in blocks of 20, with each target being presented 5 times. The length of the presentation blocks was chosen as an attempt to minimise the chances

of participants being exposed to long strings of repeated targets or predicting upcoming targets based on prior target appearance. Participants did not receive any breaks between blocks or conditions, other than self-paced inter-trial periods, and between the baseline and adaptation condition for the offline tDCS protocol described below.

The pilot experiment used a 30-degree clockwise rotation during the adaptation condition, whilst the main experiment used a 35-degree clockwise rotation.

The trial duration time (between joystick trigger press and perimeter crossing), endpoint error (angular error between start-to-target and start-perimeter cross), as well as the xy coordinates of the joystick during trials was saved to the PC hard drive and transferred to a data repository server after the experiment.

2.2.5 Cerebellar transcranial direct current stimulation

The tDCS electrodes used in the literature are generally 'conventional' saline soaked sponges (25cm^2 area) (Alam et al. 2016), forming a bi-polar anode/cathode arrangement. Modelling studies have shown that such electrode montages induce electrical fields throughout the cerebellum, and also spread to parts of the occipital cortex (visual cortex) and brainstem (Parazzini et al. 2014). Given the visual nature of the task, it cannot be ruled out that such cerebellar targeted stimulation also influences cortical regions that may be involved in visuomotor adaptation, such as the posterior parietal cortex (Tanaka et al. 2009). A more recent technological refinement, known as High Definition-tDCS (HD-tDCS) uses closely spaced gel-electrodes, not dissimilar to the basic Ag/AgCl EEG electrodes, with a single 'active' electrode in the centre of a number of surrounding 'return' electrodes (Alam et al. 2016; Minhas et al. 2010; Woods et al. 2016).

Modelling studies have shown that, in the cerebral cortex, such electrode montages can produce more spatially specific induced fields with fewer off target effects (Alam et al. 2016). In the cerebellum, modelling of a simple bipolar montage using small electrodes showed relatively precise induced fields in the cerebellum, restricting the greatest field strengths to one cerebellar hemisphere (Fiocchi et al. 2017).

At a practical level, the smaller gel-filled electrodes of HD montages are better suited to concurrent EEG recordings as they can be positioned in between the EEG recording electrodes and the use of viscous gel limits the risk of 'bridging' between the stimulation and recording electrodes- whereas a saline soaked sponge would likely dampen the scalp area and form electrode bridges, rendering the EEG recordings useless.

Therefore, the present study used a 4x1 HD-tDCS (Soterix Medical Inc., USA) electrode montage (1 central, 4 surrounding electrodes evenly spaced approximately 3-4cm away from the anode) with the central 'active' electrode positioned 1cm below inion and 3cm to the ipsilateral (right hand side) cerebellar hemisphere.

During the pilot experiment, 5 participants were given cathodal stimulation (central cathode, surrounding anodes) and 5 were given anodal stimulation (central anode, surrounding cathodes). In the main study, all participants received anodal stimulation.

Based on well-used parameters in the literature (Galea et al. 2011; Thair et al. 2017) a well-used 20 minute, 2mA stimulation was applied, with 30 second ramping of intensity at each end of the stimulation block. During sham stimulation, the starting and ending ramps were given, but the current was reduced to zero for the duration of the block (**Figure 2.2**).

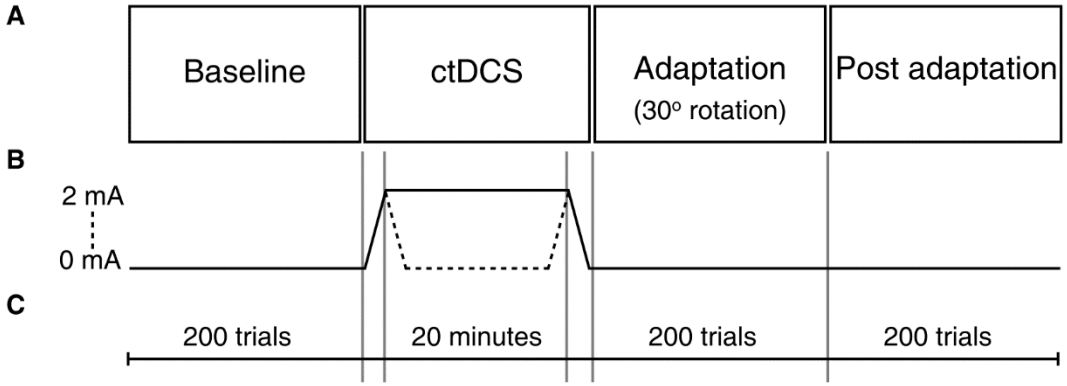

Figure 2.2 Experimental protocol flow.
*Schematic of the experimental timeline. **A**; breakdown of experimental blocks. **B**; timeline of cerebellar tDCS stimulation amplitude, sham session shown in dashed line. **C**; number of trials, or time, in each block.*

2.2.6 Neurophysiological recordings

2.2.6.1 Preparations for recording

EEG signals from participants of the main experiment were captured using 32 active electrodes (ActiCAP, BrainProducts GmbH, Germany) arranged according to the extended international 10/20 system, shown in **Figure 2.3**. Electrodes were fitted into an elasticated cap, appropriately sized for each participant. Once a participant completed all pre-experimental forms (informed consent, Edinburgh-handedness inventory), they were seated in-front of the behavioural computer, within a purpose-built room with electromagnetic shielding. The electrode cap was secured to the participant's head using an elastic chin strap, ensuring that the Fz electrode sat atop the crown of the head, and that the arrangement of other electrodes was not overtly skewed to one side and lying smoothly across the head.

Electrolyte gel (SuperVisc, BrainProducts GmbH, Germany) was applied to each electrode with a blunt needle and syringe as per manufacturer's instructions. The gel was gently massaged into

the scalp area immediately beneath the electrodes by making small circular motions with the blunt needle. This was done until all electrodes achieved a measured impedance value of less than 5kOhm. As electrolyte gel tends to become less viscous over time with body heat amongst other factors, and the EEG recordings being taken over an extended period (~35-45minutes in total), a minimal amount of gel was used at each electrode site to prevent bridging of electrodes during the experiment.

After preparation, the participant was given final reminders about the task, and the experimenter left the Faraday room, closing the door behind them. Recording of EEG signals was begun using the settings described below, and the behavioural task was initiated.

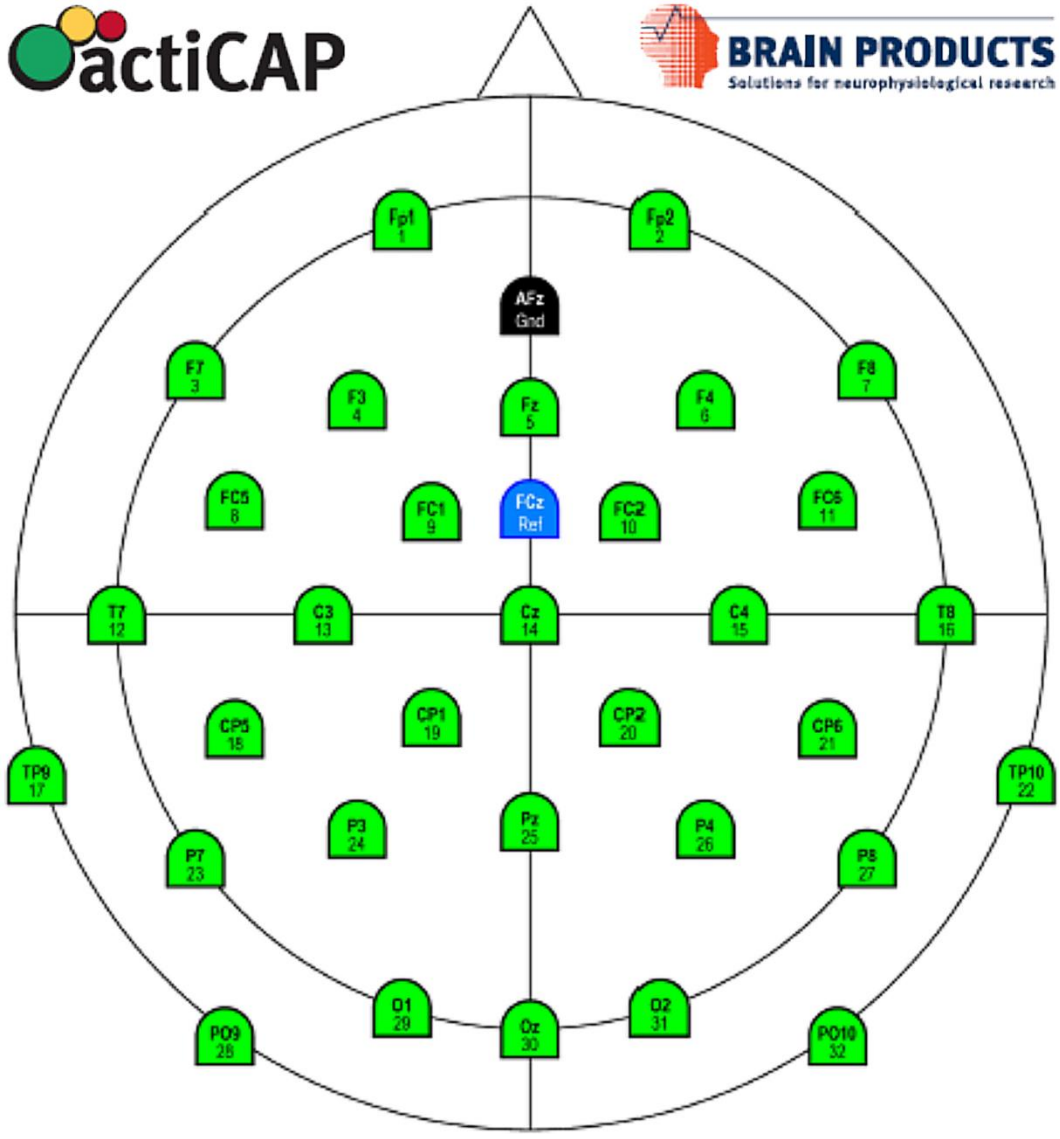

Figure 2.3 EEG electrode positions.
Layout of the 32 EEG electrodes according to the international extended 10-20 standard. Recording electrodes labelled in green, reference and ground locations in blue and black respectively. Taken from Brain Products commercial documentation (Brain Products GmbH).

2.2.6.2 EEG recording settings

Unfiltered EEG signals from the 32 active electrodes were recorded at 2500S/s using a BrainAmp DC amplifier and BrainVision Recorder Software (BrainProducts GmbH, Germany) running on a Windows Vista PC. Data were saved to the PC hard drive during the experiment and subsequently moved to a data repository server for offline analysis. Event marker outputs flags from the behavioural task program, detailing the times of joystick trigger pull and movement end, were relayed via serial port and were embedded into the EEG datafiles.

2.2.7 Data analysis

2.2.7.1 Data pre-processing

2.2.7.1.1 Epochs of interest

Although the principal analysis of the reaching behaviour (endpoint errors – see section 2.2.7.2) used the full number of trials performed, analysis of the electrophysiological data was confined to specific epochs of trials relating to key points in the adaptation behaviour. These consisted of; the final 20 trials of baseline (late baseline), first and final 20 trials of adaptation (early/late adaptation), and the first and final 20 trials of post adaptation (early/late after-effect). Twenty trials were included in each epoch as this guaranteed 5 occurrences of each of the 4 target locations given the pseudorandom programming of target presentation.

2.2.7.1.2 Trial rejection

Trials within epochs of interest were removed prior to analysis of data if: (i) the neural data were contaminated with artefacts in (see section 2.2.7.3.1), (ii) the participant reached toward the wrong target location (judged as an endpoint error greater than 60°), or (iii) the trial duration was longer than the 750ms cut-off period. The number of trials (group mean±SD) remaining in these epochs were as follows; late baseline 17.5±2.7, early adaptation 16.0±1.7, late adaptation 18.2±2.2, early after-effect 17.2±2.7, late after-effect 18.6±1.7. A repeated measures ANOVA showed no statistically significant difference between these values ($F_{(4,40)}$=2.286, p=0.08).

2.2.7.2 Behavioural analysis

Endpoint errors

To extract key parameters of the participant behaviour, a generalised reduced gradient algorithm approach (Lasdon et al. 1974) was used to fit three curves to individual participant endpoint error data, minimising the sum of squared errors by adjusting the constants of the three curves. First, the final 100 trials of the baseline block were used to compute the mean endpoint error. Next, an exponential curve with three parameters (peak, decay constant, and asymptote) was fitted to the adaptation block trials. Finally, a second exponential was fitted to post adaptation block trials, with the asymptote parameter fixed at the original baseline mean.

Reach duration

To gain a measure of the duration of each reaching movement (as a proxy of the reaching velocity), the Euclidian distance from the starting point was computed from the joystick xy coordinates. The reach duration was then computed by subtracting the total trial duration from the final time in which the joystick's position was less than 5 pixels from the zero point.

2.2.7.3 Electrophysiological analysis

Processing of EEG data was done using the EEGLAB toolbox (Delorme and Makeig 2004) in MATLAB 2016a, and further analysis in MATLAB 2016a using custom-made functions.

Raw data from each recording session were filtered between 0.4-100Hz using a fourth order digital Butterworth filter. Then down sampled to 500 samples per second (S/s) for computational efficiency. Data were divided into 2 second windows centred on the initiation of each trial, using the joystick button press event marker embedded in the data (see section 2.2.6.2). This resulted in the generation of 600 individual trial segments for each recording session (200 baseline, 200 adaptation, 200 post-adaptation).

2.2.7.3.1 Artefact rejection

Trials in which online DC correction had been applied to the recordings (to prevent amplifier saturation during recordings) were removed. Subsequently, data were subject to artefact removal procedures using EEGLAB's Infomax Independent Component Analysis (ICA) to identify sources of non-neuronal noise such as eye-blinks- a common approach in processing of EEG data (Chaumon et al. 2015; Urigüen and Garcia-Zapirain 2015). After removing identified sources of extrinsic noise, the components were back-transformed into the time-domain, thus reconstructing the artefact free EEG signal.

2.2.7.3.2 Wavelet analysis

Individual trial data were decomposed into the time-frequency domain by convolving the time series with a Morlet wavelet (wavenumber=6) using an algorithm developed by Torrence and Compo (1998). This resulted in a complex numbered time x frequency matrix output (the wavelet transforms) for each trial. From this, the wavelet power (the product of squaring the absolute value of the complex number) was computed and the oscillatory phase information (the inverse tangent of the complex number) extracted for each time x frequency coordinate of the wavelet transform.

A wavelet based approach was preferred over short-time Fourier transform due to its theoretical properties (such as the non-linear time-bandwidth scaling and lack of assumption of signal

stationarity) better suiting it to the analysis of neurological signals (Samar et al. 1999), although the differences between conventional Fourier and wavelet approaches or other techniques such as the Hilbert transform may be negligible in practice (Zhan et al. 2006; Le Van Quyen et al. 2001). For the purposes of data analysis, the wavelet power was log normalised.

To measure phase relationships between the recorded brain areas on an individual trial basis, an index of phase-locking (sometimes called phase-synchrony) was taken using the single trial methods developed by Lachaux and colleagues- the single trial phase locking value (SPLV) (Lachaux et al. 2000). Briefly, the ongoing (instantaneous) phase difference between two signals (within a predefined frequency range) is computed for a given trial (here subtracting the motor/prefrontal cortical electrode signal from the cerebellar electrode signal). Next, the stability of this phase difference over successive time steps is computed according to the below equation.

$$SPLV_{(f,t)} = \left|\frac{1}{\delta}\int_{t-\delta/2}^{t+\delta/2} \exp\left(j\left(\varphi_x(f,\tau) - \varphi_y(f,\tau)\right)\right) d\tau\right| \qquad \text{Equation 1}$$

By stepping the analysis window (of length φ) across samples, for a given frequency (f) and time (t), this creates a smoothed estimate of the synchronisation of two signals; a value of 1 indicating the two signals are wholly phase-locked, with no variance in the phase difference for the windowed period. In the present analysis, the length of this windowing period was set to equal 6 cycles of the frequency scale under consideration.

2.2.7.3.3 Data analysis

Analysis of the spectral power of EEG signals was only performed on selected electrodes corresponding to recording over the contralateral motor cortex (electrode C3), and the PFC (average of electrodes FP1 and FP2). The two prefrontal electrodes were not averaged prior to the analysis of the phase locking, thus measured of phase locking between the motor cortical electrode and these prefrontal electrodes was performed on both separately.

Prior to data analysis, EEG wavelet transforms were subject to trial normalisation by z-scoring the 2 second wavelet transforms, minimising the contribution of outlier trials and artefacts (Grandchamp and Delorme 2011).

The principal analyses compare the electrophysiological data across the adaptation epochs of interest at four principal frequency bands - delta (1-4Hz), theta (4-9Hz), beta (10-30Hz) and gamma (30-80Hz). Although the boundaries between bands are not strictly defined and variation exists in the literature, the definitions used in this thesis (for all brain structures) are taken from a review of cerebellar oscillatory activity by De Zeeuw *et al.* (2008). Comparisons within these frequency bands have been treated separately.

2.2.7.3.3.1 Times of interest

After computing measures of time-frequency power, and phase locking, the averaged data from within specific times of interest were taken for each frequency band. The first time window of interest was a 100ms window between 120-20ms prior to the detection of movement onset – relating to a movement planning/initiation phase. The second time window was a 100ms window between 20-120ms after the cursor crossed the task perimeter – relating to when the participant is receiving feedback on the accuracy of the reaching movement. Data from within these time windows were averaged in both frequency and time dimensions, resulting in a single value per trial for each of the two time windows.

Formal analyses of the data were performed at the group level, thus the data from trials inside each of the five epochs of interest were averaged to produce one value per participant in each epoch of interest.

2.2.7.3.3.2 EEG during tDCS stimulation

Data during the final two minutes of the online stimulation/sham periods was divided into non-overlapping 2-second 'trials' and pre-processed in the same manner as reaching trials. Analysis of the spectral content was performed by averaging the wavelet transforms in the time dimension (the global wavelet transform) and averaging over trials, generating a single value at each frequency level for each participant during sham, and anodal stimulation.

2.2.7.4 Statistics

No a-priori power calculation was made for the present study. The number of participants was determined by the availability of participants in the allocated usage time of the EEG facilities. Previous studies have used either fewer (5 participants, Tzagarakis et al. 2010) or similar participant numbers (10-15 participants) (Tzagarakis et al. 2015; Tan et al. 2014; Torrecillos et al. 2015; Alayrangues et al. 2019) to observe oscillatory power changes in EEG beta frequencies in similar joystick reaching and adaptation tasks. Although none of these publications provide enough details of the EEG data to carry out a power calculation (principally the variance of the data), it was thought that the number of participants used in the study sufficient for the principle analyses. Nonetheless, the author acknowledges that the present study may be underpowered for some of the tests performed. Comments on the statistical power of key tests are made at the relevant points later in this thesis.

All statistical analyses were performed at $\alpha=0.05$. Parametric tests were used wherever appropriate, and tests are detailed in the text. Where appropriate, if omnibus tests showed statistical significance, all subsequent comparisons were made to the baseline conditions (i.e. full pairwise comparisons not performed).

2.3 Results

2.3.1 Pilot experiment

2.3.1.1 Cerebellar tDCS is well tolerated

During the 'on' and 'off' ramping currents, participants typically described feeling a 'tingling' sensation when prompted. During one participant's first experimental session, the 'relax' function (reducing the current delivered through the electrodes) of the Soterix 4x1 HD-tDCS device was used during the 'on' ramp to improve comfort and ease the participant's anxiety through the first few minutes of the protocol, gradually removing the 'relax' function following agreement by the participant. The session transpired to be this participant's sham session, and so whilst the 'relax' function was suppressing the gradient of the initial current ramp, it's continued use and 'gradual removal' would have had little physiological impact as the delivered current was zero for a significant portion of its use. Nevertheless, the participant was comforted as much as possible to reduce anxiety and reinforce that the system was safe. Toward the end of the protocol, the participant's anxiety had been overcome, and they experienced no discomfort during the 'off' ramp. Moreover, they experienced no discomfort, and did not require the use of the 'relax' function during their second (active) stimulation session.

2.3.1.2 Participants were not aware of adaptation or tDCS schedule

During the post experimental debrief (after the second experimental session), participants were asked to verbally self-report whether they had knowledge of the implemented rotation, or whether they could identify which session had been their sham (vs. active) stimulation session. Whilst all participants acknowledged a worse performance on the task [at the points of changes to the joystick-cursor mapping], none identified a systematic change to the task as the root cause. Similarly, no participant revealed definitive knowledge of which session had been the 'real' stimulation.

2.3.1.3 Adaptation to a visuo-motor perturbation

To assess whether the behavioural paradigm successfully induced motor adaptation in the participants, the endpoint errors of each participant were used to model the behaviour. An example of a single participant's original data and the fitted model data can be found in **Figure 2.5**.

Baseline

After an initial period of improvement, lasting around 50 trials, participants perform the joystick reaching task with group mean endpoint errors over the final 100 trials, of -0.56° with standard deviation of 1.21°. A one sample t-test showed no significant difference to a test value of zero

($t_{(9)}$=-1.463, p=0.177). The variability of the final 100 baseline trials (as measured by the standard deviation) showed a group mean of 8.12°, with a group standard deviation of 1.57°.

Adaptation to 30-degree rotation

Upon addition of the 30-degree clockwise rotation mapping between joystick-cursor position, participants initially observed clockwise errors to their reaches (negative deflection in **Figure 2.4**). Adaptation occurred over subsequent trials until they achieved an asymptote. The modelling of the participant behaviour revealed a group mean peak endpoint error of -23.2°, standard deviation of 12.1°. The group mean half-life of adaptation was 18.0 trials, standard deviation 6.89 trials. The group mean asymptote endpoint error was -4.30°, standard deviation of 1.50°. A one sample t-test showed a significant difference to a test value of zero ($t_{(9)}$=-9.08, p<0.0005).

The values of peak error and adaptation rate were used to inform a sample size calculation. The peak error gave a suggested sample size of 3 at alpha = 0.05 and 1-Beta =0.80, and the adaptation rate a sample size of 2. Consequently, the 11 participants produce enough statistical power to detect the behavioural presence of the visuomotor adaptation in the present task.

After-effect on perturbation removal

Removal of the 30-degree rotation led to anticlockwise endpoint errors (positive deflection in **Figure 2.4**) with a group mean peak endpoint error of 20.2°, standard deviation of 8.12°. A paired sample t-test between the absolute values of peak endpoint errors in the adaptation and after-effect blocks revealed no significant differences ($t_{(9)}$=1.550, p=0.155). The half-life of after-effect was 27.2 trials, standard deviation 13.5 trials.

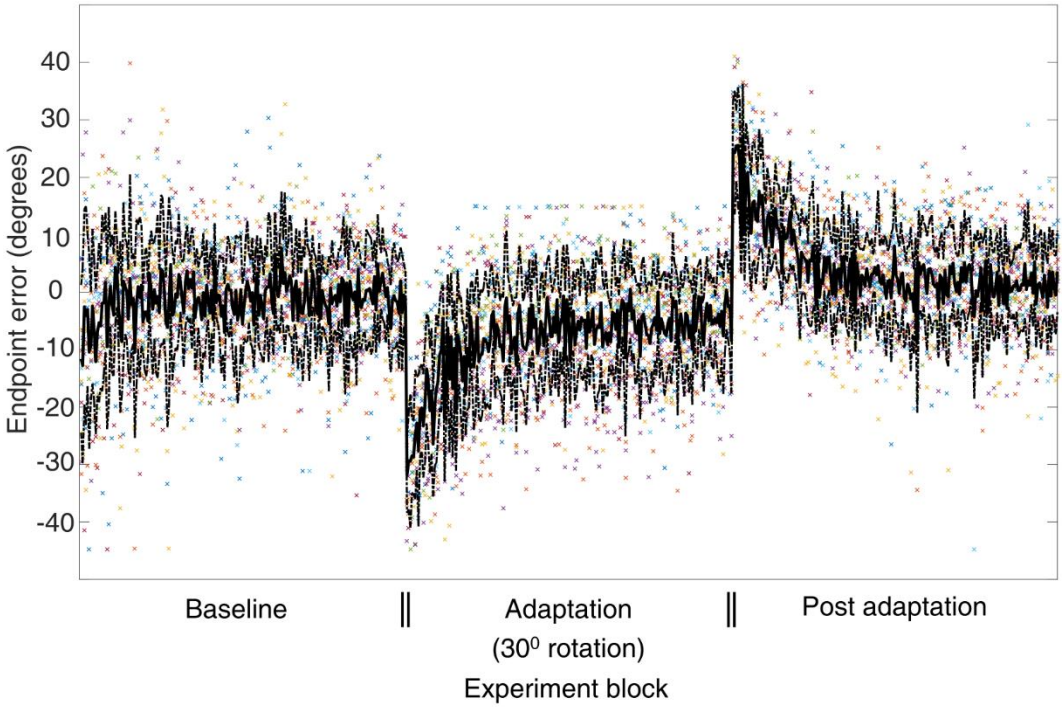

Figure 2.4 Pilot: Behavioural endpoint errors during joystick reaching task.
Data from 10 participants performing the reaching task, adapting to a 30-degree clockwise error. Errors calculated by subtracting the angle of the cursor endpoint (perceived reach position) and target location. Negative values thus represent instances of a perceived clockwise miss direction. Coloured data points represent the angular deviation of the end of individual trials compared to the target, values beyond 45 degrees are removed as 'miss targeting'. Each participant's data are displayed in a unique colour. Thick black line represents the group mean endpoint error, and broken black lines represent the group standard deviation for each trial.

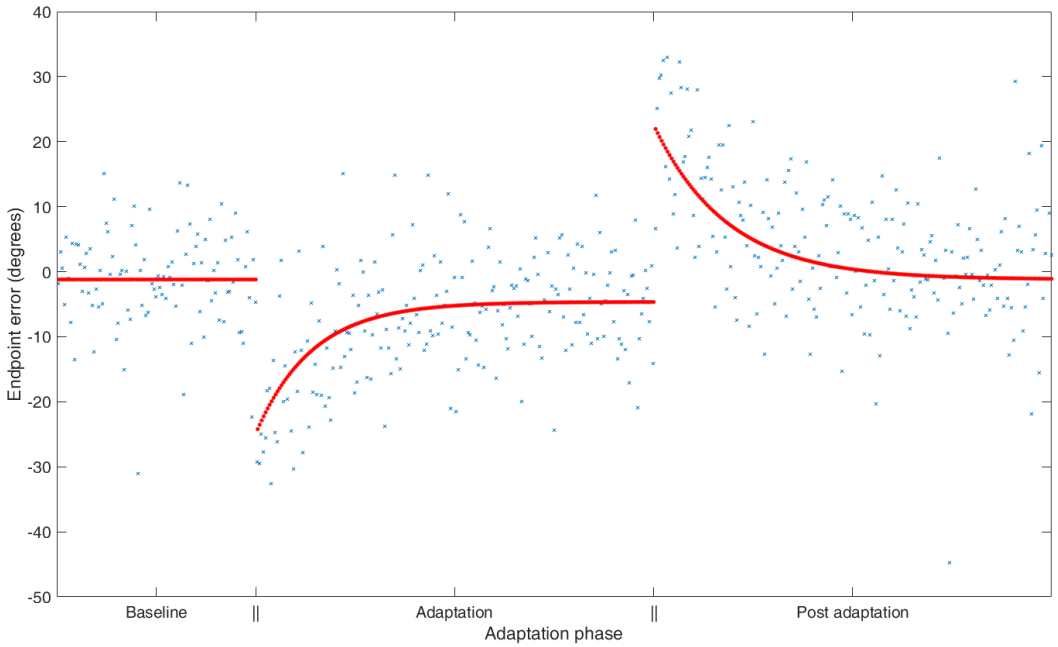

Figure 2.5 Pilot: Example single participant endpoint error model fitting.
Individual trial endpoint errors from one example participant displayed in blue crosses. Generalised reduced gradient model data displayed in red circles.

2.3.1.4 Effect of cerebellar targeted tDCS stimulation

Behavioural model parameters were computed as with the sham session for each participant. Participants were split into those who had received cathodal (**Figure 2.6)** or anodal **Figure 2.7** stimulation, and each stimulation model parameter was compared between stimulation/sham conditions using paired sample t-tests.

Cathodal stimulation

No statistically significant differences were observed in any model parameter between sham and cathodal stimulation (Baseline Error: $t_{(4)}$=-0.64, p=0.559. Adaptation Peak: $t_{(4)}$=-0.69, p=0.529. Adaptation half-life: $t_{(4)}$=-0.67, p=0.540. Adaptation asymptote: $t_{(4)}$=-0.23, p=0.830. After-effect Peak: $t_{(4)}$=0.265, p=0.804. After-effect half-life: $t_{(4)}$=1.351, p=0.248).

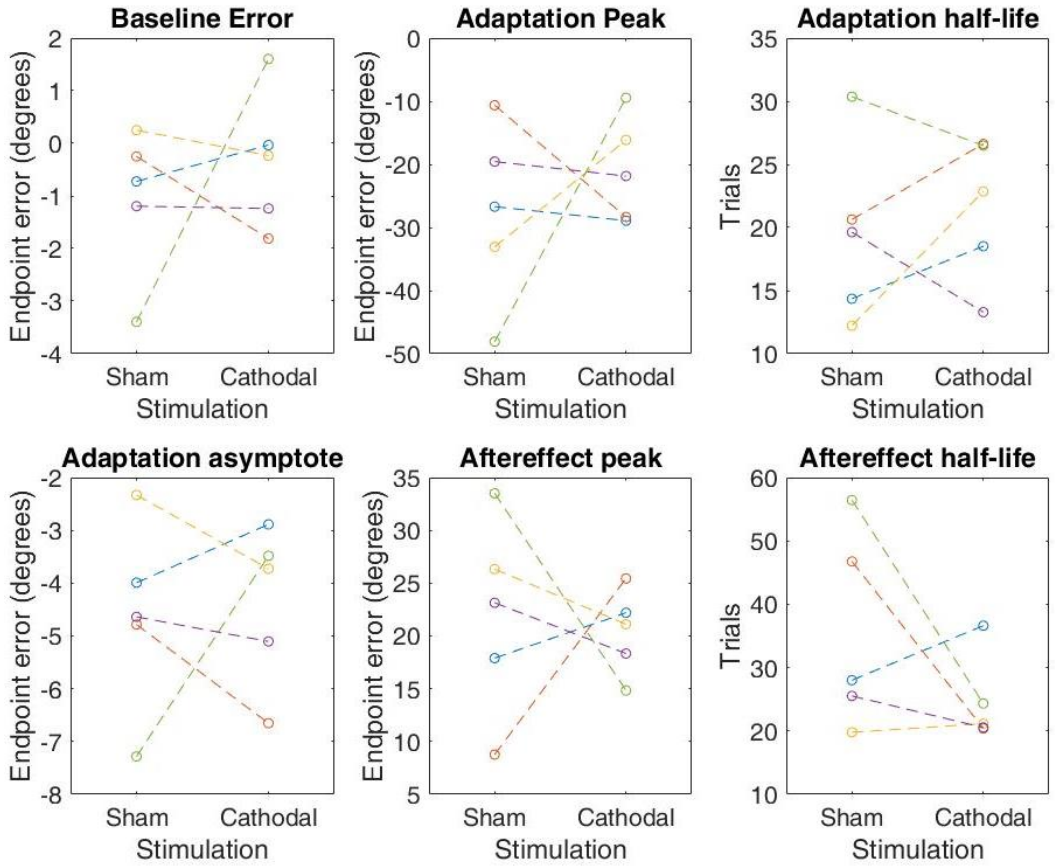

Figure 2.6 Pilot: Effect of 20-minute offline cathodal cerebellar tDCS on behavioural parameters.
Data show behavioural model parameters from individual participants during either a 20-minute cathodal or sham stimulation protocol applied in-between the baseline and adaptation trial blocks. For each parameter, a Wilcoxon signed rank test showed no significant difference in sham or cathodal stimulation.

Anodal stimulation

No statistically significant differences were observed in any model parameter between sham and cathodal stimulation (Baseline Error: $t_{(4)}$=1.09, p=0.339. Adaptation Peak: $t_{(4)}$=-0.46, p=0.668. Adaptation half-life: $t_{(4)}$=0.19, p=0.856. Adaptation asymptote: $t_{(4)}$=1.03, p=0.362. After-effect Peak: $t_{(4)}$=0.21, p=0.843. After-effect half-life: $t_{(4)}$=-1.27, p=0.274).

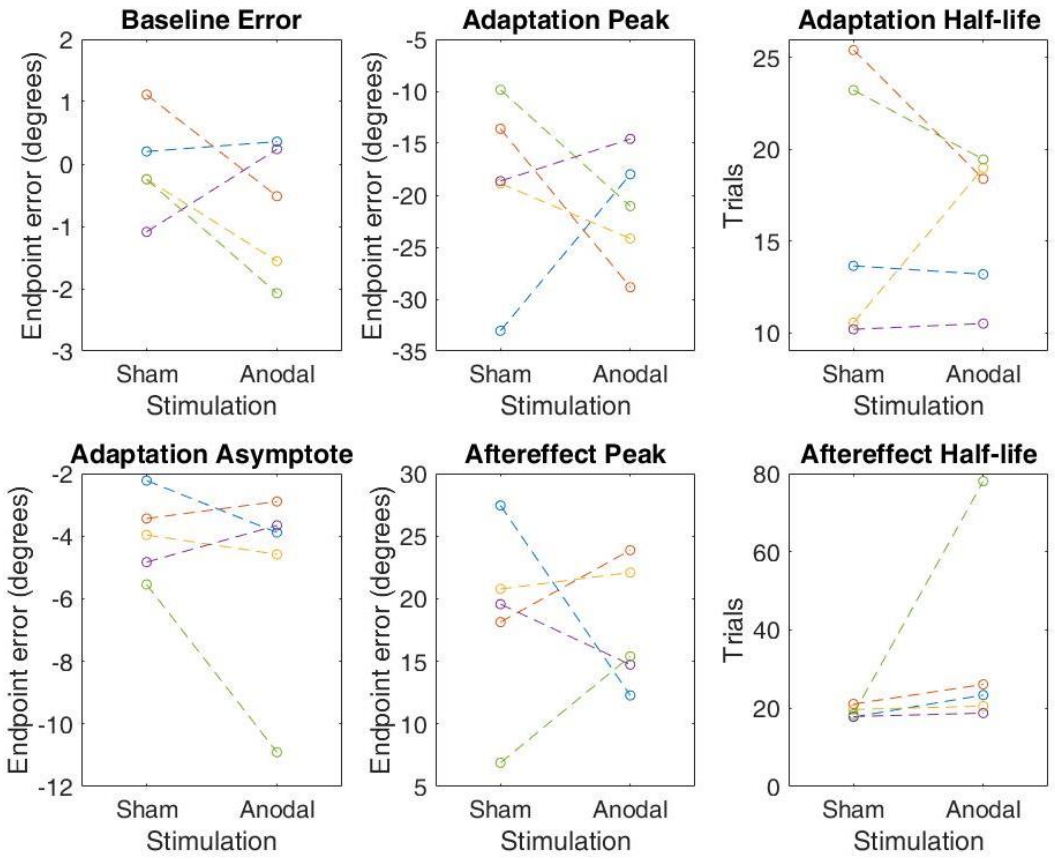

Figure 2.7 Pilot: Effect of 20-minute offline anodal cerebellar tDCS on behavioural parameters.
Data show behavioural model parameters from individual participants during either a 20-minute cathodal or sham stimulation protocol applied in-between the baseline and adaptation trial blocks. For each parameter, a Wilcoxon signed rank test showed a significant increase in after-effect half-life after anodal stimulation, but not in other parameters.

2.3.1.5 Pilot summary

The pilot experiment enabled the testing of the behavioural task with available equipment. In summary, the rotation task was able to induce visuomotor adaptation in the participants, as expected (**Figure 2.4**). The variability of baseline trials, around ±8°, seemed quite high. No definitive explanation can be given here, except that it is possible that the positioning of the joystick, and relative unfamiliarity of using a joystick (compared to a standard mouse) led to a less refined movement control. Although the effects of adaptation were visibly apparent, and the behavioural data showed sufficient statistical power with eleven participants, a greater rotation of 35° was implemented for the main study to further separate perturbed reaches from the intrinsic variability of the action.

The cerebellar targeted stimulation protocol was tolerated well and did not lead to significant adverse effects in the participants. In this small-scale pilot, neither anodal or cathodal stimulation polarities significantly modified the adaptation behaviour. Reasons for such will be discussed further in (2.4.6). Briefly however, there is increasing acknowledgement of the highly variable effects of tDCS (Jalali et al. 2017). Consequently, to increase the experimental power

for the main experiment, only the anodal stimulation polarity was used. Anodal stimulation was chosen due to the more consistent effects reported in the literature compared to cathodal stimulation (Nozari et al. 2014; Wiethoff et al. 2014; Dyke et al. 2016).

2.3.2 Main study

2.3.2.1 Behaviour

No adverse effects of cerebellar trans-cranial direct current stimulation were observed either during or after stimulation, and no participant required the use of the 'relax' function. Again, during debriefing after the second testing session, each participant was asked if they had knowledge of which session had been active or sham stimulation, and whether they were consciously aware of the cursor rotation. No participants reported being convinced of which session had been their sham or active stimulation. Two participants reported being aware of some change in the cursor response but were unable to confirm whether they had attempted to use an explicit strategy to overcome this change. Throughout the analysis, there was no indication that these participants were outliers, and so have not been excluded.

2.3.2.1.1 No difference between targets

Each of the behavioural modelling parameters were computed separately for each of the four target locations and compared with repeated measures ANOVA. No model parameter was significantly difference across target location (Baseline Error: $F_{(3)}$=1.37, p=0.272. Adaptation Peak: $F_{(3)}$=0.88, p=0.463. Adaptation half-life: $F_{(3)}$=1.02, p=0.398. Adaptation asymptote: $F_{(3)}$=1.77, p=0.174. After-effect Peak: $F_{(3)}$=0.51, p=0.676. After-effect half-life: $F_{(3)}$=0.97, p=0.418). Consequently, subsequent analyses pooled all targets together.

2.3.2.1.2 Consistent reach duration across adaptation epochs of interest.

In addition to the modelling of the behavioural errors, the durations of the outward reaches were recorded. The averaged data from within each of five epochs of interest were compared using a repeated measures ANOVA.

As displayed in **Figure 2.8**, participant's average reach duration did not vary greatly over the epochs of interest, the greatest difference from baseline trials (mean= 0.129s, SD=0.036s) was an increase of 0.005s to early after-effect trials (mean= 0.134s, SD=0.012s). The data violated Mauchly's test of sphericity ($\chi^2(9)$=19.585, p=0.023) and so the degrees of freedom were adjusted using Greenhouse-Geisser epsilon (ε=0.535). This test showed no statistically significant effect of adaptation condition ($F_{2.138,21.383}$=0.821, p=0.416).

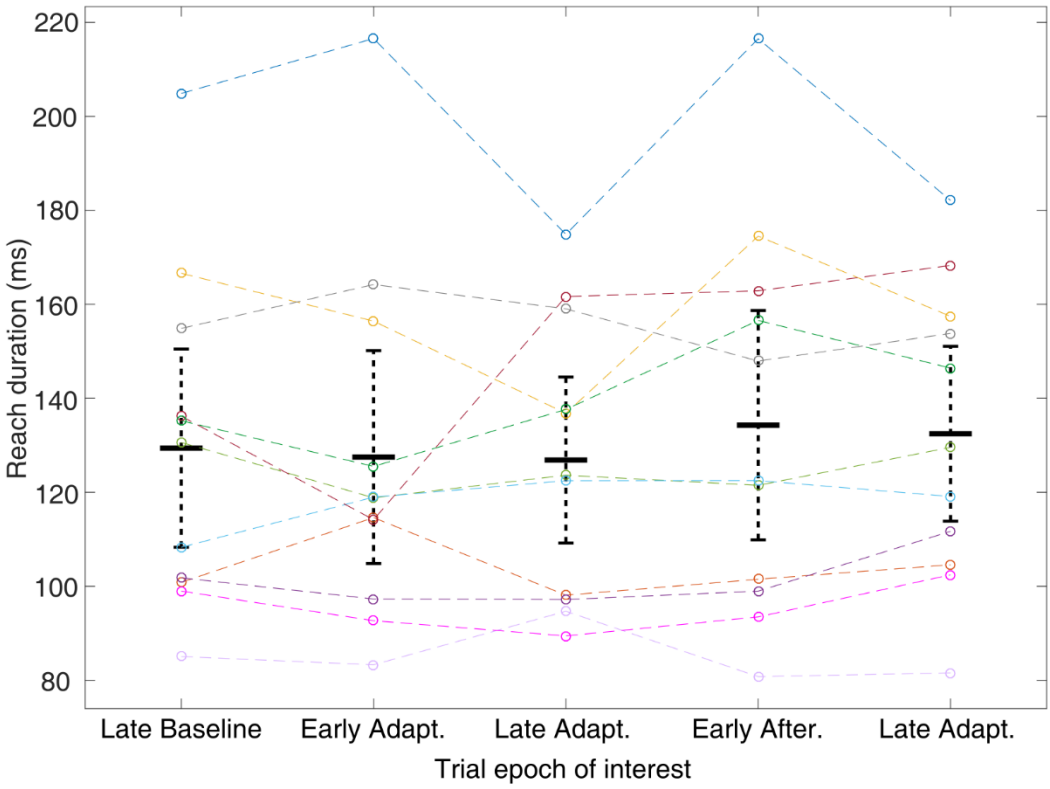

Figure 2.8 Reach duration data for each participant across adaptation epochs.
Trial averaged reaching duration for each participant during each adaptation epoch of interest (20 trials). Individual participant data is linked through dashed lines and unique colour. Black lines and error bars indicate group mean and 95% confidence of the mean.

2.3.2.2 Analysis of EEG signals during adaptation.

The below analyses were performed on data recorded during participants' sham tDCS session to establish whether the EEG signals recorded over the prefrontal and contralateral motor cortex were modulated by the visuomotor adaptation.

2.3.2.2.1 Motor network activity pre-movement.

2.3.2.2.1.1 Motor cortical EEG corelates of motor adaptation

Figure 2.9A-D shows average data of the reaction time window split into frequency bands. Delta and theta frequency bands have a unique pattern of data, while both beta and gamma bands appear to share a common pattern. Briefly, the greatest deviation from baseline (mean = 0.061, SEM = 0.053) in delta frequencies appears to be an increased band power in the late adaptation period (mean change= 0.079, SEM= 0.052). Compared to baseline trials, theta frequencies appear to have decreased band power in both early adaptation and after-effect periods (mean change= -0.099 & -0.072, SEM 0.072 & 0.100 respectively), whilst both late adaptation/after-effect periods have increased band power (mean change= 0.064 & -0.031, SEM 0.064 & 0.078 respectively). Again, comparing to baseline trials in both beta and gamma frequency bands (mean= -0.005 & 0.007, SEM= 0.022 & 0.047 respectively), the greatest deviation is in the early

adaptation trials which have a decreased power (mean change= -0.149 & 0.117, SEM= 0.049 & 0.043 respectively).

A repeated measures ANOVA was performed on each frequency band. Beta frequencies showed a statistically significant effect of adaptation ($F_{4,40}$=3.46, p=0.016). The observed power of this test was 0.814, and partial eta squared measure of effect size was 0.257. Comparing each condition to the baseline epoch revealed a significant difference between baseline, and early adaptation ($F_{1,10}$=9.29, p= 0.012). The other three bands showed no significant differences across the adaptation epochs; delta ($F_{4,40}$=1.20, p=0.328), theta ($F_{4,40}$= 1.73, p=0.162), and gamma ($F_{4,40}$ = 2.21, p=0.085), although gamma frequencies do show the same trend as in beta frequencies. Of these three frequency bands, the observed power in the main effect tests ranged between 0.34 (delta) and 0.60 (gamma), showing an insufficiency of statistical power in these tests. The effect size (partial eta squared) in delta, theta, and gamma bands were 0.107, 0.482, and 0.181 respectively.

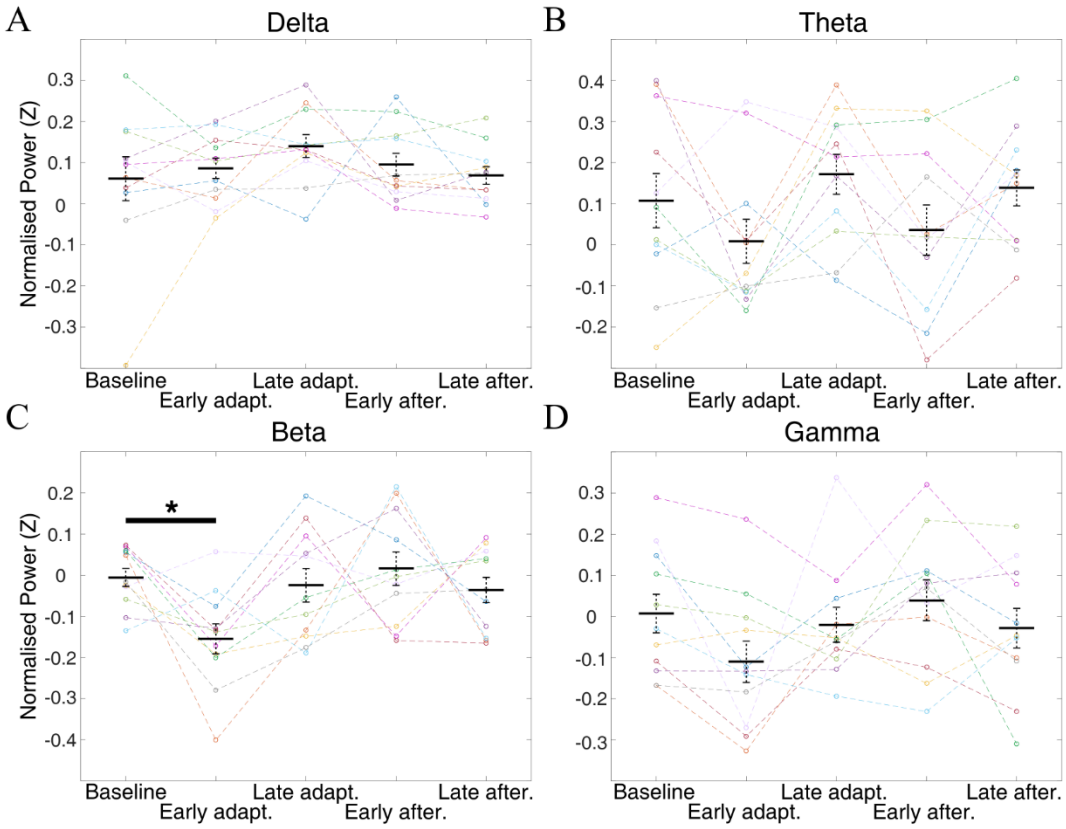

Figure 2.9 Pre-movement motor cortical electrode (C3) band power across adaptation epochs.
Trial averaged EEG band-power recorded at C3 electrode during the pre-movement window for four main frequency bands. ***A****. Average delta (1-4Hz) band power.* ***B****. Average theta (4-9Hz) band power.* ***C****. Average beta (10-30Hz) band power.* ***D****. Average gamma (30-80Hz) band power. Individual participant data displayed as coloured points and dashed lines, each represented by a unique colour. Black bars indicate group mean, error bars are 95% confidence of the mean. Asterisk and bar indicate significant difference (p<0.05).*

2.3.2.2.1.2 Prefrontal cortical EEG correlates of motor adaptation

Figure 2.10 shows the trial average band power for each participant in each frequency band. Again, a consistent decrease is apparent between the baseline and early adaptation trials in

band power for all frequencies (delta mean change= -0.128, SEM= 0.017, theta mean change= -0.120, SEM 0.088, beta mean change= -0.121, SEM=0.053, gamma mean change=-0.128, SEM=0.017). However, a repeated measures ANOVA test showed no statistically significant effect of adaptation condition for any frequency band (delta: $F_{4,40}$= 1.149, p=0.348, theta: $F_{4,40}$=1.396, p=0.253, beta: $F_{4,40}$=1.838, p=0.141, gamma: $F_{4,40}$=2.208, p=0.085). Observed power in these tests ranged between 0.33 and 0.60, suggesting a lack of statistical power to detect the changes in power seen.

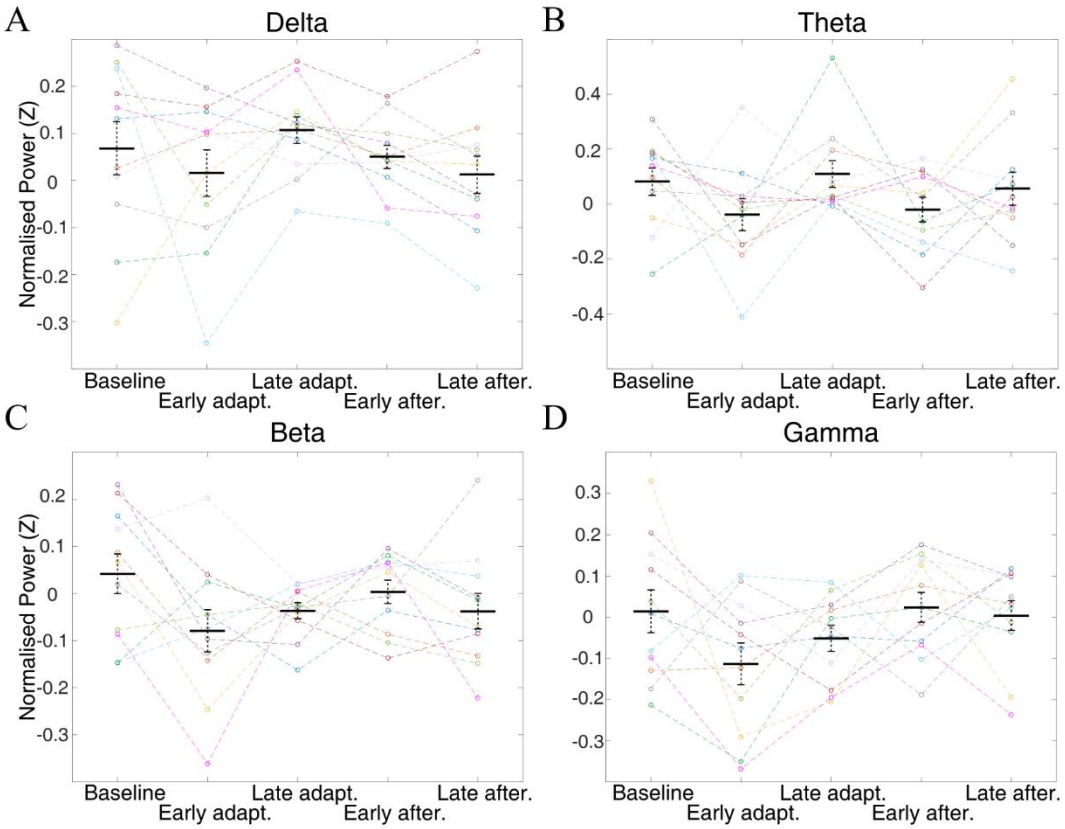

Figure 2.10 Pre-movement band power on FP1/2 electrodes across adaptation epochs.
Trial averaged EEG band-power recorded at FP1/2 electrodes during the pre-movement window for four main frequency bands. ***A****. Average delta (1-4Hz) band power.* ***B****. Average theta (4-9Hz) band power.* ***C****. Average beta (10-30Hz) band power.* ***D****. Average gamma (30-80Hz) band power. Individual participant data displayed as coloured points and dashed lines, each represented by a unique colour. Black bars indicate group mean, error bars are 95% confidence of the mean.*

2.3.2.2.2 Motor network activity after reaching

2.3.2.2.2.1 Motor cortical EEG corelates of motor adaptation

Analysis of the motor cortical electrode data extracted during the post movement window (**Figure 2.11**) showed no statistically significant differences in any frequency band across the adaptation epochs (delta: $F_{4,40}$=0.165, p=0.955, theta: $F_{4,40}$=0.699, p=0.597, beta: $F_{4,40}$=0.402, p=0.806, gamma: $F_{4,40}$=0.209, p=0.932). Measures of observed power showed very low statistical power in these tests (range: 0.08-0.21).

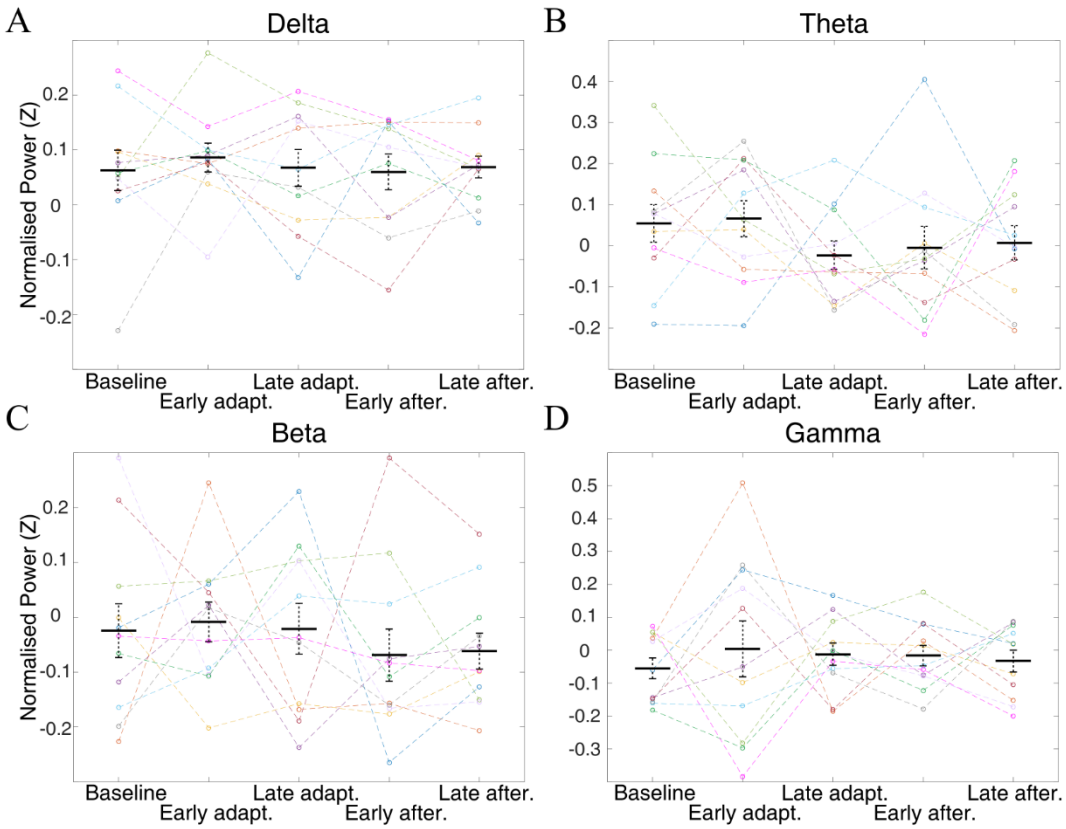

Figure 2.11 Post-movement motor cortical (C3) band power across adaptation epochs.
Trial averaged EEG band-power recorded at C3 electrode during the post-movement window for four main frequency bands. ***A****. Average delta (1-4Hz) band power.* ***B****. Average theta (4-9Hz) band power.* ***C****. Average beta (10-30Hz) band power.* ***D****. Average gamma (30-80Hz) band power. Individual participant data displayed as coloured points and dashed lines, each represented by a unique colour. Black bars indicate group mean, error bars are 95% confidence of the mean.*

2.3.2.2.2.2 Prefrontal EEG corelates of motor adaptation

As with the pre-movement window, analysis of the post-movement EEG spectral power over the PFC electrodes with a repeated measured ANOVA showed no statistically significant effect of adaptation epoch (delta: $F_{4,40}$=0.560, p=0.693, theta: $F_{4,40}$=1.054, p=0.392, beta: $F_{4,40}$=0.513, p=0.726, gamma: $F_{4,40}$=0.704, p=0.594), and the observed power of all tests was less than 0.50.

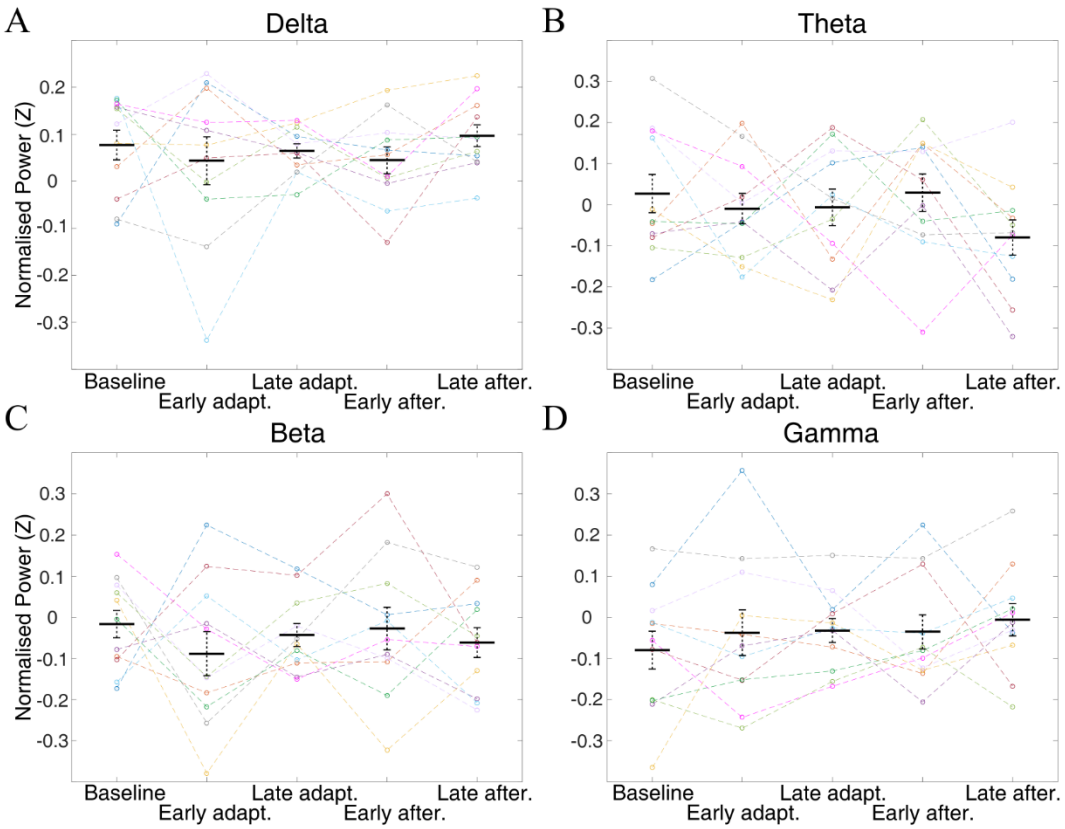

Figure 2.12 Post-movement band power on FP1/2 electrodes across adaptation epochs.
Trial averaged EEG band-power recorded at FP1/2 electrodes during the post-movement window for four main frequency bands. ***A****. Average delta (1-4Hz) band power.* ***B****. Average theta (4-9Hz) band power.* ***C****. Average beta (10-30Hz) band power.* ***D****. Average gamma (30-80Hz) band power. Individual participant data displayed as coloured points and dashed lines, each represented by a unique colour. Black bars indicate group mean, error bars are 95% confidence of the mean.*

2.3.2.2.3 Motor network functional connectivity during adaptation.

2.3.2.2.3.1 Motor cortical to prefrontal phase locking pre-movement

To assess any potential changes in functional connectivity between M1 and Pfc, a measure of phase locking between the motor cortical (C3) electrode and the two frontal electrodes (FP1/FP2) was taken for every trial. As with previous analysis, data were averaged within the conditions, resulting in a single summary value for each participant's adaptation condition.

Representative data from the contralateral motor cortex- contralateral PFC electrode pairing (C3-FP1) is shown in **Figure 2.13**. In delta and gamma frequencies (**Figure 2.13A,D**), there is a general decrease from baseline (delta: mean=0.581, SEM=0.026, gamma: mean=0.532, SEM=0.017) over the adaptation conditions, with the lowest mean value during late after-effect (delta: mean=0.516, SEM=0.012, gamma: mean=0.505, SEM=0.008). Theta frequencies also show a general decrease in phase locking values over the adaptation conditions, although the lowest value comes during early after-effect (mean=0.506, SEM= 0.010). Average phase locking at beta frequencies on the other hand decreases between baseline and early adaptation trials (baseline: mean=0.540, SEM 0.015, early adaptation: mean=0.497, SEM=0.010), and proceeds

to increase this value over the subsequent conditions, up to late after-effect (mean=0.512, SEM=0.011).

Frequency band-averaged data were analysed with repeated measures ANOVA, with data from both electrode pairings and each adaptation conditions input as repeated measures. After adjusting degrees of freedom for violations of Mauchly's test of sphericity for delta, theta and beta frequencies, none of the frequency bands exhibited statistically significant interaction between the electrode pair and adaptation epoch (delta; $F_{1.819,18.195}$=1.205, p=0.319. Theta; $F_{1.687,16.874}$=0.918, p=0.403. Beta; $F_{1.541,15.410}$=0.946, p=0.387. Gamma; $F_{4,40}$=1.280, p=0.294). Further, no frequency band had a statistically significant main effect of adaptation epoch (delta; $F_{4,40}$=1.876, p=0.134. Theta; $F_{4,40}$=1.384, p=0.257. Beta; $F_{1.635,16.353}$=0.995, p=0.375. Gamma; $F_{4,40}$=1.074, p=0.382). Measures of observed power for the main effect of condition tests ranged between 0.285, and 0.518.

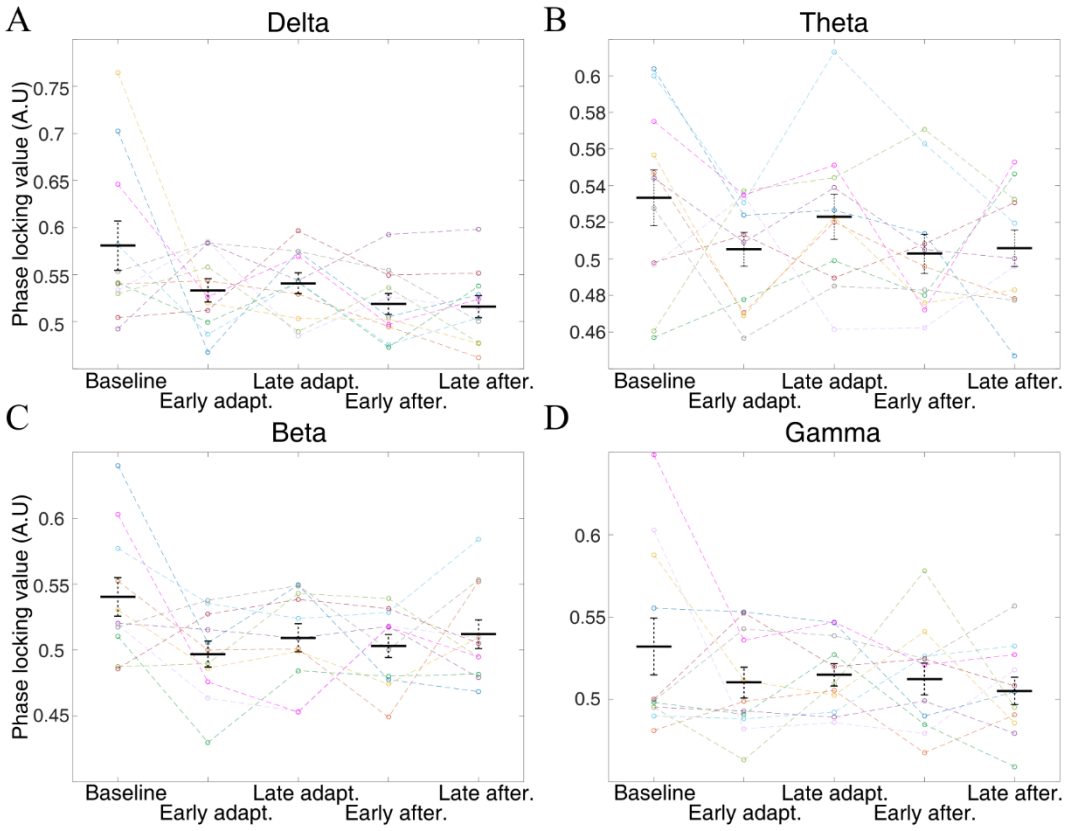

Figure 2.13 Pre-movement phase locking between motor cortical (C3) and FP1 electrodes across adaptation epochs. *Trial averaged EEG phase locking between C3 and FP1 electrodes during the pre-movement window for four main frequency bands.* ***A****. Average delta (1-4Hz) phase locking.* ***B****. Average theta (4-9Hz) phase locking.* ***C****. Average beta (10-30Hz) phase locking.* ***D****. Average gamma (30-80Hz) phase locking. Individual participant data displayed as coloured points and dashed lines, each represented by a unique colour. Black bars indicate group mean, error bars are 95% confidence of the mean.*

2.3.2.2.3.2 Motor cortical to prefrontal phase locking post movement

To assess any changes to the functional connectivity between the motor cortex and prefrontal areas during the different stages of adaptation, a measure of phase locking between the electrodes of interest was extracted as described in section 2.2.7.3.2.

Frequency band-averaged data were analysed with repeated measures ANOVA, with data from both electrode pairings and each adaptation conditions input as repeated measures. After adjusting degrees of freedom for violations of Mauchly's test of sphericity for delta, theta and beta frequencies, none of the frequency bands exhibited statistically significant interaction between the electrode pair and adaptation epoch (delta; $F_{2.122,21.224}$=1.570, p=0.231. Theta; $F_{4,40}$=0.343, p=0.847. Beta; $F_{1.420,14.196}$=1.548, p=0.243. Gamma; $F_{1.593,15.932}$=1.210, p=0.314). Further, no frequency band had a statistically significant main effect of adaptation epoch (delta; $F_{4,40}$=1.855, p=0.137. Theta; $F_{4\ 40}$=1.542, p=0.208. Beta; $F_{1.226,12.261}$=914, p=0.379. Gamma; $F_{2.015,20.152}$=0.211, p=0.813). Measures of observed power for the main effects of condition were less than 0.80 for all frequencies.

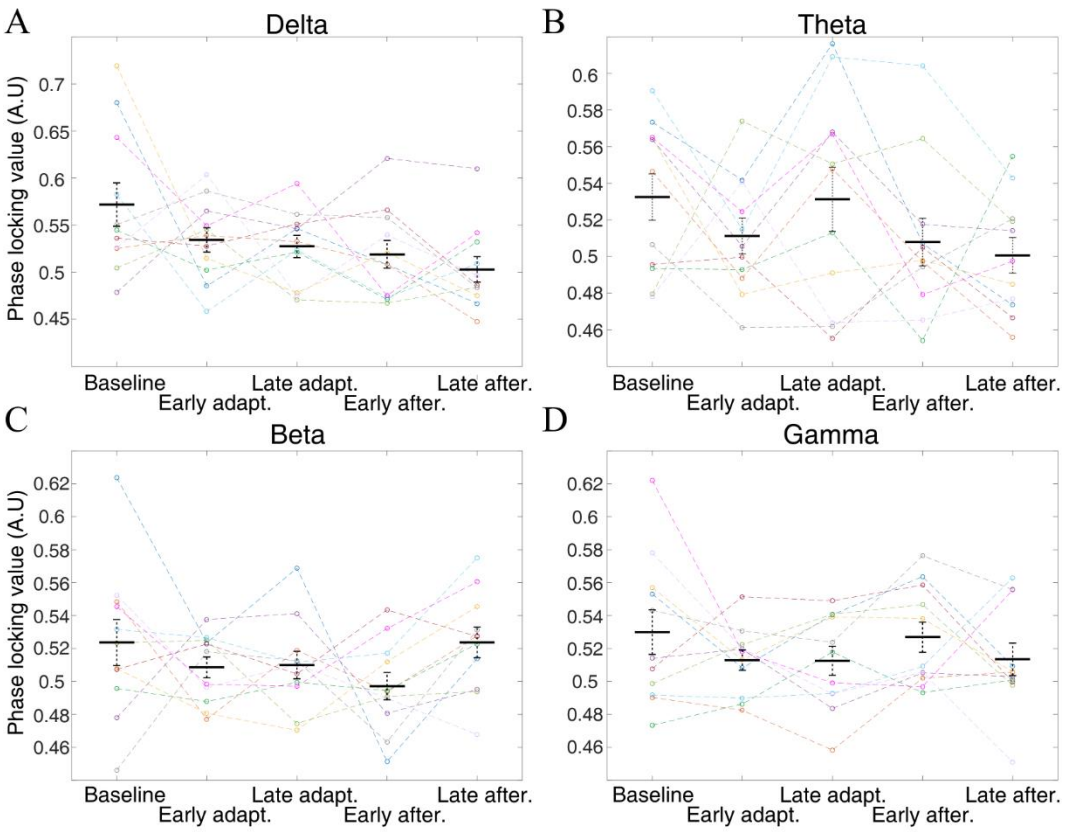

Figure 2.14 Post-movement phase locking between motor cortical (C3) and FP1 electrodes across adaptation epochs.
Trial averaged EEG phase locking between C3 and FP1 electrodes during the post-movement window for four main frequency bands. ***A****. Average delta (1-4Hz) phase locking.* ***B****. Average theta (4-9Hz) phase locking.* ***C****. Average beta (10-30Hz) phase locking.* ***D****. Average gamma (30-80Hz) phase locking. Individual participant data displayed as coloured points and dashed lines, each represented by a unique colour. Black bars indicate group mean, error bars are 95% confidence of the mean.*

2.3.2.3 Anodal cerebellar tDCS did not affect adaptation behaviour

Behavioural modelling parameters for each participant under sham, and anodal cerebellar tDCS are shown in **Figure 2.15**. Paired sample t-tests for each parameter revealed no statistically significant effect of cerebellar tDCS on the behavioural measures (Baseline Error: $t_{(10)}$=1.091, p=0.301. Adaptation Peak: $t_{(10)}$=0.88, p=0.402. Adaptation half-life: $t_{(10)}$=-0.76, p=0.466.

Adaptation asymptote: $t_{(10)}$=0.31, p=0.760. After-effect Peak: $t_{(10)}$=-0.12, p=0.911. After-effect half-life: $t_{(10)}$=1.12, p=0.290).

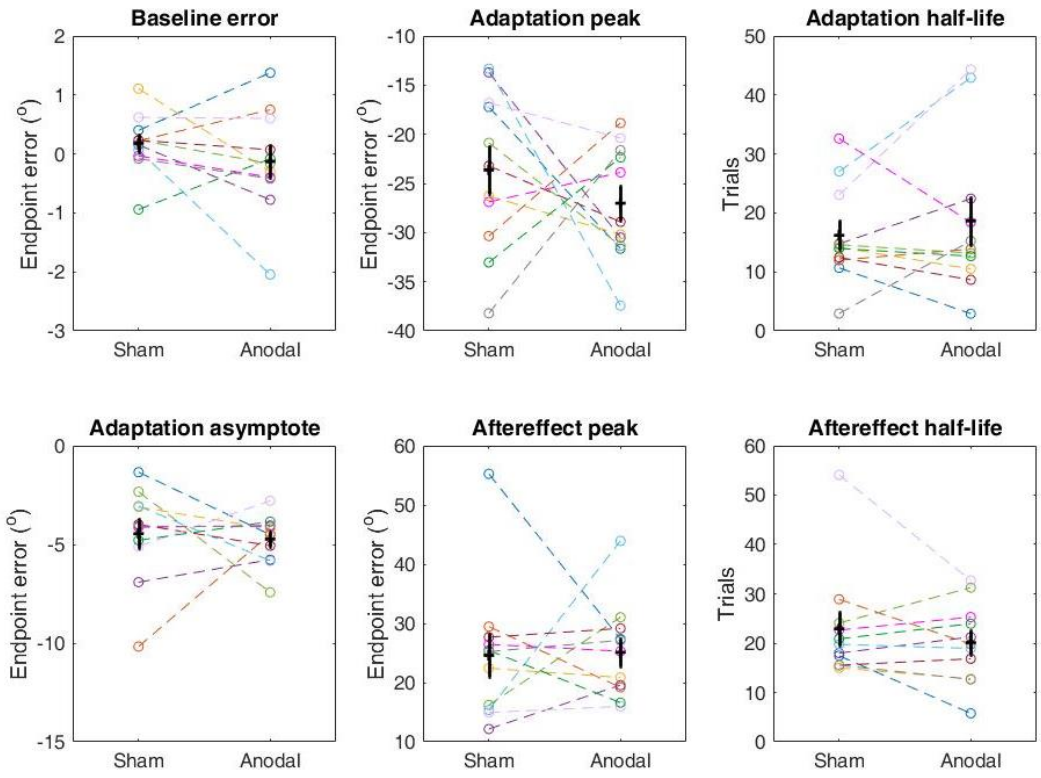

Figure 2.15 Behavioural model parameters after offline sham, and anodal cerebellar tDCS.
Endpoint error modelling parameters from sham and active tDCS sessions. Individual participant data shown in unique colours. Black bars and error bars indicate group mean and standard error of mean.

2.3.2.4 No detectable effect of cerebellar tDCS on motor cortical EEG

To assess whether the non-invasive cerebellar stimulation had any direct effect on motor cortical activity, EEG signals recorded during final two minutes of the twenty-minute stimulation protocol were decomposed into the frequency domain for spectral analysis.

As shown in **Figure 2.16**, at the group level, averaged delta, theta and beta frequencies had marginally increased spectral power during active anodal stimulation compared to sham (delta change= 0.069dB, SD= 0.225dB, theta change= 0.2944dB, SD= 0.195dB, beta change=0.007dB, SD=0.127dB) whilst averaged gamma frequencies had marginally decreased power (change=0.011dB, SD=0.171dB). Paired sample t-tests for each frequency band showed no statistically significant effect of stimulation in any frequency, (delta $t_{(10)}$=-1.015, p=0.334, theta $t_{(10)}$=-0.501, p=0.627, beta $t_{(10)}$=-0.185, p=0.857, gamma $t_{(10)}$=0.209, p=0.838).

Overall, the HD cerebellar tDCS has had no statistically significant effect on motor adaptation behaviour, nor detectable effects on EEG signals over the sensorimotor cortex.

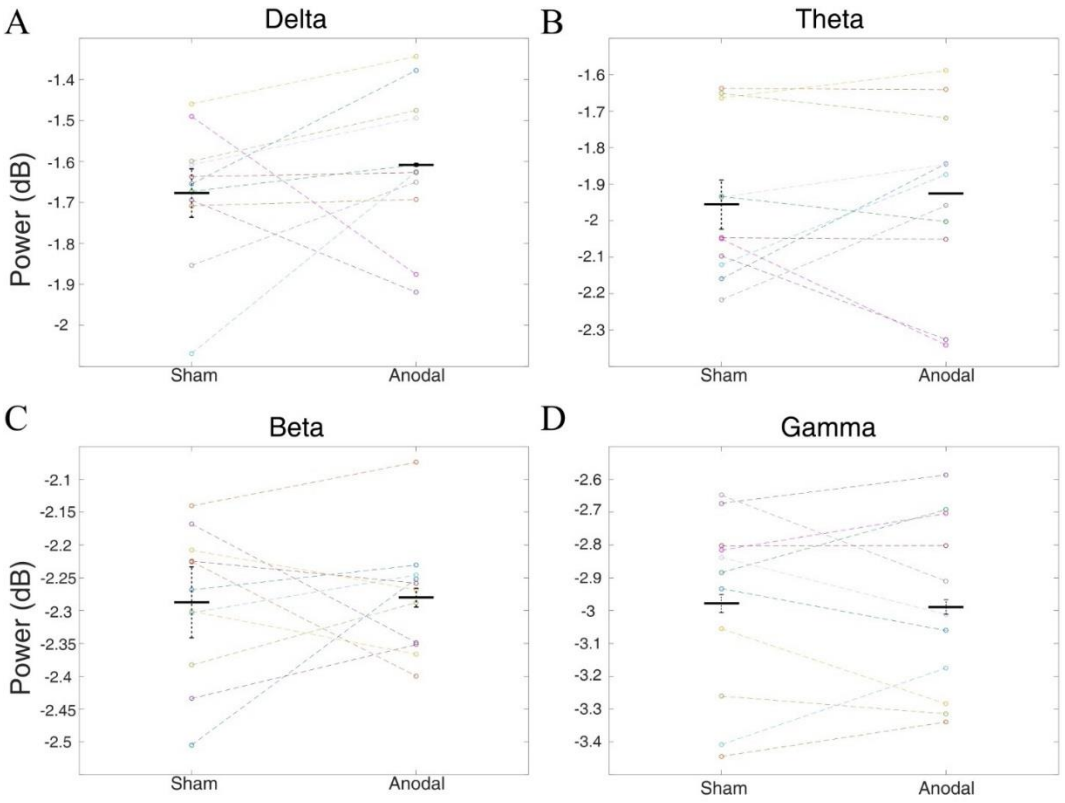

Figure 2.16. Motor cortical electrode (C3) band power during final 2 minutes of a 20-minute sham/anodal cerebellar tDCS session.

Individual participant data displayed in unique colour. Participant group mean and standard error of mean (n=11) displayed as black horizontal line and dashed error bars. Individual participant data displayed as coloured points and dashed lines, each represented by a unique colour. ***A****. Average delta (1-4Hz) band power.* ***B****. Average theta (4-9Hz) band power.* ***C****. Average beta (10-30Hz) band power.* ***D****. Average gamma (30-80Hz) band power. Black bars indicate group mean, error bars are 95% confidence of the mean.*

2.4 Discussion

2.4.1 Motor adaptation in human participants

The present study used a well-characterised behavioural task to elicit visuomotor adaptation by manipulating visual feedback. As expected, all participants adapted to the clockwise perturbation. Further, an equal and opposite after-effect was observed upon removal of the perturbation. When measured at the group level, both phases of adaptation followed an approximately exponential decay function. Consistent with the extensive literature on motor adaptation behaviour (Shadmehr et al. 2010; Haith and Krakauer 2013), this pattern of behaviour is good evidence that the task induced motor adaptation.

The individual variance in endpoint errors was relatively large (section 2.3.1.3). Although this variance did not seem to prevent adaptation from occurring, it is possible that it influenced the parameters of the fitted exponential functions fitted to participant data. The source of this trial-to-trial variability is likely a combination of intrinsic and extrinsic sources. Extrinsic factors could include the measurement error of the joystick itself – involving a presumed delay between the actual position of the hand/joystick, and the task program's logging of the joystick location on each screen refresh (running at approximately 60Hz). An intrinsic factor might be an arm error of the specific push/pull movement geometry used in this task. The joystick was positioned to the right-hand side of the screen to allow a relaxed positioning of the hand on the joystick, similar to where a normal right-handed computer mouse would be. Although the neutral position of the joystick would have been familiar, the specific movements to the four quadrants may not have been familiar motions to the participants, and the muscle activations to move the sprung joystick would likely be novel. Further, dominant muscle groups may have biased the arm movements into specific trajectories, which may not have 'aligned' well to the target locations. As such, precision of the movements would have diminished.

2.4.2 Modelling motor adaptation behavioural parameters

To simplify the individual trial data from each participant to a few comparable parameters, the time-courses of reach endpoint errors were modelled using a general reduced gradient algorithm.

The General Reduced Gradient algorithm is a method to find the local minimum of some reference value by iteratively varying the input variables. Consequently, the solution of the algorithm is dependent on the starting values of the input variables and may not represent the so-called global minimum; the absolute optimum value possible. This dependence on the starting point formed the driving reason to seed the algorithm with expected values of each input variable, so that the model data approximated a well-fitting line running through the

middle of the participant data distributions. For example, the peaks of the adaptation and after-effect decay functions were expected to be equal to the value of the perturbation (35 degrees). Overall, visual comparisons between the participant data and their respective modelled data exhibited a good likeness- the model data generally being centred within the participant data.

Interestingly, the adaptation asymptote was consistently biased away from the baseline mean error value, in the direction on the perturbation. This offset is a common feature reported in previous literature (Van der Kooij et al. 2016), and has been used as an indication of a formed equilibrium between adaptive learning and a reversion to the baseline state, perhaps via a forgetting process, or reversion to the (presumably stronger) baseline internal model state (Kitago et al. 2013; Vaswani et al. 2015).

This phenomenon is not surprising considering that the mapping of the joystick-cursor movements during the baseline trials was the same as a standard computer mouse (forward=up). As all participants were known to readily use desktop computers at work, the baseline movements would have been very familiar to them. In the future it would be interesting to test whether an asymptote is indeed influenced by a prior internal model using an adaptation task in which both baseline, and perturbed movements are not well known to the participants.

2.4.3 Sensorimotor cortical oscillations during adaptation

2.4.3.1 Pre-movement beta desynchronization during early adaptation

In this study, there was a significant decrease in beta frequency power specifically during the pre-movement period of the early adaptation trials (**Figure 2.9**). This statistically significant decrease in oscillatory power was frequency specific, although gamma frequencies exhibited the same trend. Further, this effect was only evident at the motor cortical (C3) electrode, and not the prefrontal (FP1/2) electrodes, suggesting a localised effect in the sensorimotor cortex. Additionally, the effect was temporally specific, occurring only during the pre-movement period, and not during the post-movement period.

This result is consistent with modulation of beta power prior to visuomotor (Bracco et al. 2018) and force-field adaptation (Torrecillos et al. 2015) tasks. In the force-field study of Torrecillos and colleagues, the pre-movement attenuation of beta oscillations was specifically related to reaching errors that drive sensorimotor adaptation, suggesting a role in the updating of motor commands. The present results are thus consistent with the idea that disruption of beta oscillations prior to movement execution may promote plastic changes in the neural ensembles containing motor plans.

As detailed in the results section above, the adaptation related changes in pre-movement beta power had enough power even with the low sample size tested. It was not possible to perform

a power calculation for other frequency bands as to the best of the author's knowledge at the time of writing, there are no equivalent published data of such comparisons.

It is interesting that a similar effect on beta oscillations was not found during the early stages of the after-effect. Given the equal and opposite nature of the behaviour, it might be expected that there is an equivalent drive to promote plasticity in the motor cortical circuitry to enable changes to the motor commands being generated – reversing the changes made during the initial adaptation. The absence of a significant neural response to the behavioural after-effect is evidence that the two processes might be supported by differing mechanisms. Studies on ageing effects have shown differential effects of healthy ageing on adaptation and after-effects (Buch 2003), supporting the idea that there are separate mechanisms at play.

2.4.3.2 Post-movement oscillatory power in the motor cortex.

There was no significant effect of adaptation on the spectral power of the motor cortical EEG signal in any of the frequencies of interest (**Figure 2.10**).

The present results appear to conflict with those of Tan and colleagues (2016), who observed a post-movement decrease in beta power over the sensorimotor cortex during early stages of adaptation. Importantly, Tan and colleagues took measures of the EEG spectral power at a time-point much later than that of the present study- around 750ms after the termination of the movement, compared to 20-120ms used in the present study. If the decreased beta synchronisation (proposed by Tan and colleagues as an index of the motor system's confidence in an internal model) selectively occurs after a delay of around 750ms after movements, then this suggests a natural 'speed-limit' on the adaptive updating of internal models.

Participants of the present study were not required to stop and hold the cursor over the target location, unlike the participants of Tan and colleagues who held the outward position until the target returned to the centre position. This makes a direct comparison between studies difficult, as an analysis window of around 750ms after the end of the outbound reach would fall over a period in which the participants of the current session were returning, or were already back at the starting location, either resting, or preparing for the next trial.

2.4.4 Prefrontal cortical oscillations during adaptation

There were no significant differences in EEG spectral power measures at either pre-or post-movement time windows across the epochs of interest for electrodes overlaying the prefrontal cortices (FP1 and FP2). This was unexpected given previous neuroimaging data showing changes in blood flow in the prefrontal cortex during early stages of a force-field adaptation task (Shadmehr and Holcomb 1997), and temporary disruption of PFC (using TMS) has led to deficits

in motor learning tasks, notably with a lack of conscious awareness of the perturbation, even with large magnitude errors (reviewed in Taylor and Ivry 2014).

It has been proposed that sensorimotor adaptation learning may be supported by both implicit and explicit processes, with the implicit component associated with cerebellar dependent error-based learning, whilst the explicit component is associated with cognitive strategy, reliant on frontal areas (McDougle et al. 2015; Taylor et al. 2014; Taylor and Ivry 2014; Liew et al. 2018). If this is the case then, given that in the present study the instruction was to make rapid, ballistic movements to the targets as soon as they were presented, it is possible that an explicit component was minimal and therefore frontal areas would not be greatly involved in the task.

2.4.5 Functional connectivity between motor cortex and prefrontal cortex is unchanged during motor adaptation

There was no detectable change in phase synchrony between contralateral motor cortex and either ipsi- or contralateral prefrontal cortical regions either per- or post-movement (**Figure 2.14**, **Figure 2.13**). This suggests that the functional connectivity between sensorimotor and prefrontal cortical regions remained similar during motor adaptation.

As detailed above, the PFC is hypothesised to contribute explicit strategy processes to overcome behavioural errors. As there appears to be no effect of adaptation on the EEG signals recorded over the PFC in the present data, it may not be surprising that measures of functional connectivity between the prefrontal and sensorimotor areas are also not sensitive to the adaptation task.

Alternatively, it may be that the nodes of the motor network involved in adaptation are 'constitutively connected' during voluntary movements, and adaptation related processes are accomplished with these already established lines of communication. This will be considered further in the general discussion (section 5.7).

2.4.6 Cerebellar tDCS did not influence motor adaptation behaviour

In the experiments presented here, a standard offline protocol of 2mA for 20 minutes anodal stimulation did not reliably alter the participant group's adaptation behaviour, compared to a sham stimulation. Anodal cerebellar tDCS was hypothesized to improve adaptation through an effect on the half-life of adaptation, in accordance with previously published studies (Galea et al. 2011; Block and Celnik 2013).

Although the data did not support the hypothesised behavioural effect, it was not wholly unexpected, given the acknowledgement of substantial variability in efficacy of the technique in the literature (Jalali et al. 2017). Studies on tDCS have begun to investigate factors influencing

both the efficacy and directionality of effects present uses of tDCS have on behaviour, some of which are highlighted below.

Assessment of the effect size of tDCS on motor adaptation has suggested that the majority of published studies are greatly underpowered, and a sample size of at least 75 has been recommended (Jalali et al. 2017; Minarik et al. 2016). Considering these recent guides, the present study is clearly underpowered. Even so, the absence of a discernible trend in adaptation half-life between sham and anodal stimulation (**Figure 2.15**) is perhaps some indication that, in the current set-up at least, the stimulation had no influence on the adaptation process.

A principal distinction between the present study and many previously published studies on cerebellar tDCS is the use of HD-tDCS. The majority have used the traditional large saline soaked sponge electrodes, with the so-called active electrode over the cerebellar target and the other over either a frontal brain region, buccinator muscle, or deltoid muscle (Ferrucci and Priori 2014; Van Dun et al. 2016; Oldrati and Schutter 2018; Van Dun and Manto 2018). The use of the smaller electrodes in the present study was intended to restrict the induced fields to the ipsilateral cerebellar hemisphere, in line with a modelling study (Fiocchi et al. 2017). However, it is plausible that the specific electrode montage used here (different to that modelled by Fiocchi and colleagues) delivered insufficient current to the cerebellum to effect neurophysiological activity.

As well as consideration of the induced currents, variability in the effect of tDCS has also been attributed to many factors, including; gender (Russell et al. 2014), skull morphology (Brunoni et al. 2012), and even genetic background (Nieratschker et al. 2015; Wiegand et al. 2016). Although these effects are yet to be systematically studied in relation to the influence on motor adaptation and motor learning, it is reasonable to assume that there is a similar range of confounds to non-invasive DC stimulation.

2.4.7 Cerebellar tDCS did not influence motor cortical or prefrontal activity

As well as the lack of detectable effect on motor adaptation behaviour, the concurrent EEG recordings were used to assess the impact of DC cerebellar stimulation on motor cortical and prefrontal signal spectra. At the group level, there was no statistically significant change in spectral power between the active and sham sessions over several frequency bands of interest.

The hypothesis that anodal cerebellar DC stimulation leads to changes in cortical EEG signals is in line with previous studies showing that the inhibitory drive between the cerebellar cortex and motor cortex (cerebellar-brain inhibition) is modulated by cerebellar tDCS (Ferrucci et al. 2016; Galea et al. 2009). It follows that if cerebellar activity can be directly manipulated by anodal

tDCS, then this might be observed in other regions of the motor network as changes in EEG signal.

The lack of observable effect on the EEG recording over both sensorimotor and prefrontal regions during stimulation parallels the null behavioural effect discussed previously. It is therefore difficult to determine whether this is because of insufficient cerebellar stimulation, or a genuine lack of effect on the frontal areas as a result of cerebellar anodal stimulation.

2.4.8 Summary

The present findings suggest that beta frequencies generated in the human sensorimotor cortex - contralateral to the reaching limb - are desynchronized in early adaptation compared to unperturbed reaches (**Figure 2.9**). This adaptation related beta desynchronization occurred immediately prior to the reaching movement and was not statistically significant post movement. This may be interpreted as a role for beta oscillations in the sensorimotor cortex in the preparatory control of movements, perhaps enabling plastic changes to the motor commands used for the upcoming movement.

By contrast, no adaptation-related modulation of EEG signals was detected over pre-frontal areas, suggesting this effect was localised to the sensorimotor cortex. In addition, no systematic change in phase locking between the contralateral sensorimotor and prefrontal regions was observed, suggesting that functional connectivity between these brain regions remained similar throughout adaptation.

The anodal cerebellar tDCS parameters used in the present study did not modify the adaptation behaviour and did not affect EEG signals over the contralateral sensorimotor cortex during the stimulation.

These results have informed subsequent experiments translating the visuomotor adaptation task into an animal model to gain complementary data, which are reported in the remainder of this thesis.

Chapter 3 – Animal Visuomotor Adaptation. Part I. Behaviour

3.1 Introduction

This chapter describes translation of the human visuomotor adaptation task used in chapter 2 into an animal model. This allowed direct recording of the electrophysiological activity in the brain regions of interest. These results will be described in chapter 4.

3.1.1 Animal model of visuomotor adaptation

Previous literature has combined a variety of adaptation paradigms with electrophysiological recordings in animals. Although it is generally thought that there are common mechanisms underlying both visuomotor and force-field adaptation (Seidler et al. 2013), it is possible that different forms of adaptation, such as upper limb vs eye saccade adaptation, elicit different neural mechanisms depending on the localised circuitry involved (Panouillères et al. 2015). This seems likely considering the growing evidence suggesting that the cerebellar circuitry is not a uniform structure as originally suggested in the original anatomical descriptions and theoretical ideas of cerebellar function. Instead, there is variation of physiological properties across different microcircuits of the cerebellar cortex that likely results in differences in information processing (reviewed in Cerminara et al. 2015).

In the present study a cat reach-retrieve task was chosen to implement a visuo-motor adaptation paradigm, as this type of reaching task has been used previously in the lab to study aspects of cerebellar contributions to voluntary forelimb movements and internal models (Apps et al. 1997; Edge 2005; Miles et al. 2006; Cerminara et al. 2009; Cerminara et al. 2005).

Adaptation was induced by fitting prism glasses to displace the cat's visual field, and thus closely resembles many features of classic adaptation in humans. Such an approach also allows comparison with the visuomotor adaptation results described in the previous chapter. Whilst adaptation of eye movements (Baker et al. 1987; Evinger and Fuchs 1978) and the effects of unexpected perturbations to locomotion (Marple-Horvat et al. 1998; Andersson and Armstrong 1987) have been previously studied in cat, the present study is the first to use a prism paradigm in an animal model to study visuomotor adaptation.

3.1.2 Aims of the study

The analysis presented in this chapter determines whether prism glasses can induce visuomotor adaptation in the cat. This is followed in chapter 4 by the analysis of electrophysiological data from the cerebellum, M1 and PFC to compare with the results obtained in the human EEG study (section 2.3.2.2.1.1). Direct neural recording simultaneously from all three brain regions also allowed cerebello-cerebral connectivity to be studied during motor learning.

3.2 Materials and methods

The majority of methods used for the animal experiments were based extensively on those previously used in the lab (Montgomery 1994; Apps et al. 1997; Miles et al. 2006; Edge 2005; Cerminara et al. 2005; Cerminara et al. 2009), primarily extending these to incorporate the prism adaptation paradigm as well as multi-site electrophysiological recordings (detailed in chapter 4).

3.2.1 Ethical statements and animal use

All animal experiments conformed to the UK Animals (Scientific Procedures) Act (1986) and were approved by the University of Bristol Animals and Ethical Review Body. Three adult male cats (denoted as A, B and C) weighing between 4-6kg were used to collect the data presented in this thesis. No negative reinforcement, food or water restriction was used. Thus, all task rewards were on top of the regular diet and *ad libitum* water.

3.2.2 Recording apparatus and training

3.2.2.1 Recording apparatus

A schematic diagram of the recording apparatus is shown in **Figure 3.1**. The recording apparatus consisted of:

a) Recording alcove- a covered steel base mounted atop a 4-foot-high frame, Faraday cage sides, with clear Perspex inner walls, and inner Perspex baffles positioned using magnetic anchors. A copper plate was also secured to the base beneath the approximate location that the reaching forelimb of the cats would rest. Two USB web cameras were affixed to the upper corner of the Faraday cage to achieve a view of the left aspect of the cats.

   The two USB web cameras were operated by a dedicated Windows computer (PC) running the open source software Bonsai (Lopes et al. 2015), with a start trigger delivered from the NSP via an Arduino UNO (configured as a digital-analogue converter) used to start the video capture in synchrony with the neural data acquisition.

b) Cables linking the head implant connectors to associated acquisition hardware were organised into a single bundle (the 'umbilicus') to prevent distraction. The umbilicus was directed upwards from the head, with slack to allow unrestricted movement, using a string on a retracting coil.

c) Cables carrying the neural signals were connected to dedicated neural acquisition hardware (Cerberus system: Blackrock Microsystems LLC, USA). This consisted of a pre-amplifier positioned atop the Faraday cage, digitising the signal and passing this onto the main processing unit (Neural Signal Processor, NSP) via an optic fibre. The Neural

Signal Processor was operated by a Windows PC running the associated commercial software. Acquisition settings are detailed in (section 4.2.2).

d) Cables carrying EMG signals connected to the NSP, via a custom-made analogue filter bank, and visualised on an oscilloscope.

e) Cables carrying event marker signals (see below) were passed to both the NSP and visualised on an oscilloscope.

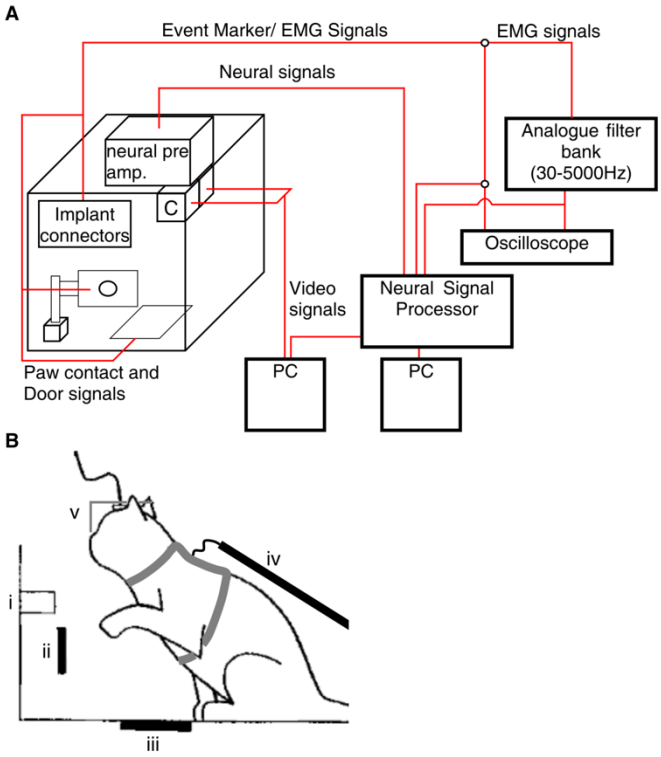

Figure 3.1 Schematic of recording apparatus with major electronic signal pathways.
A *Event marker signals include; Paw contact, door open, and tube entry signals. Implant connectors include those for neural probes, EMG wires, paw contact and peripheral nerve stimulation wires. PC1 represents the dedicated video capture computer (PC), PC2 represents the dedicated neural, EMG, and event marker data capture PC.* ***B*** *Schematic showing relative location of cat within behaviour environment with the reward tube (i) at 'arm's length' covered by a sliding door (ii). The cat sat within the environment with the reaching paw resting on the copper contact plate (iii) and was loosely restrained by a per harness and attachment (iv). The prism glasses (v) were clipped onto the implant headpiece, 'floating' in front of the cat's eyes so as not to come into contact with the animal directly. Adapted from Apps et al. (1997).*

3.2.2.1.1 Reward tube

The target for the reaching task was a clear Perspex tube (internal diameter 30mm) positioned to allow a comfortable forward reaching action – approximately 20cm in front and 28cm above the resting left paw position. The tube was secured to the base of the recording alcove by a magnetic base, which allowed the tube structure to be removed when bringing the animal in and out of the alcove. The opening of the tube on the animal's side was surrounded by a clear Perspex façade extending 4cm above/below, and 8cm to each side of the centre of the tube. The opening on the animal's side was also covered by an opaque Perspex door. This could be

manually slid downwards by the human operator from the rear of the tube apparatus to reveal the tube to the cat and allow it to reach into the tube.

3.2.2.1.2 Event markers

To provide reliable timings of important events through the reaching behaviour, a few signalling lines were used. These lines offered a TTL level (0-5V) binary signal depending on the status of the sensor, which was sent to the NSP for recording synchronously with the neural and EMG data. Transitions between the high and low states served as timestamps of the key events; opening of the reward tube door, paw lift-off, and entry of the paw into the reward tube.

3.2.2.1.2.1 Door open

Opening the door to the reward tube (the cue for the animal to begin reaching) triggered a lever style micro-switch. This controlled a TTL output line which was high when the door was closed, and low when the door was open.

3.2.2.1.2.2 Contact plate

A copper plate was situated on the base of the recording alcove, where the cat's left paw would rest when not reaching. The plate was energised with a 30kHz, 400mV sine wave. When the paw was in contact with the plate, a circuit was closed, and a control box detected the presence of the carrier wave in the cat's implant lead. This control box controlled a TTL output line which was high when the paw was in contact with the plate, and low when the circuit was broken.

3.2.2.1.2.3 Reward tube entry

The mouth of the reward tube was fitted with a horizontal infra-red beam emitter/detector arrangement. When the beam was uninterrupted, a logic board maintained a high TTL output signal, when the cat's paw reached into the tube, the infra-red beam would be broken, and the logic board would set the output TTL signal low.

3.2.2.2 Training

A strong rapport was established between each cat and the researchers through daily handling prior to any training. Approximately 2 months prior to implantation surgery, the cats were introduced to the reaching task in gradual stages. Firstly, the cats were introduced to morsels of fish placed within a handheld clear Perspex tube (identical to the reward tube used on the recording apparatus, but without the door and façade). The cats were initially allowed to explore the Perspex tube and retrieve the fish morsels in any manner. The Perspex tube was gradually held such that the tube was approximately at the cat's shoulder height and at 'arm's length'. Typically, the cats quickly adopted a forelimb reach strategy, but both forelimbs were used. To train only a left paw reach retrieve, a rule was enforced whereby the Perspex tube was retracted if the cats attempted to reach with the right forelimb.

Once the cats were proficient in retrieving the reward from the handheld tube, they were introduced to the recording alcove (see section 3.2.2.1 for details, and **Figure 3.1B**). After a short acclimatisation period to the Faraday cage, the cats were introduced to the reward tube and training was continued in the recording rig. Here, the training introduced a waiting period between reaches using an opaque, manually operated shutter covering the face of the reward tube. Thus, the trained behaviour consisted of a waiting period, a reaction time, and a reaching period. If the cat successfully reached into the tube and retrieved the reward but dropped the morsel outside of the tube when attempting to eat it, the fish was picked up by the operator and fed to the cat by hand.

To build and maintain a relationship between the recording room and the behavioural task and not 'playtime', the cats were only brought into the recording room to perform the task and were not allowed to explore the recording room further.

Cats were loosely connected to the inside of the recording alcove by means of a pet harness. The harness provided no restraint to the forelimbs or head, and only served to prevent the cats from suddenly leaving the Faraday cage whilst the recording cables were plugged in. If at any time the animal displayed signs of boredom, disinterest in the task or desire to exit the rig, they were immediately disconnected from all recording equipment and taken back to the home pen.

To prepare the cats for the expected duration of recording sessions, the training sessions lasted approximately 45 minutes, during which the cats typically performed up to 100 reaches. Sessions were ended when either the allotted time had elapsed, or the cat had reached satiety and no longer performed the task.

3.2.3 Design and build of custom components

3.2.3.1 Prism glasses

The prism glasses were constructed from a clear 59x 59mm acrylic frame, with 1mm diameter holes machined into the corners. The holes enabled aluminium wires to be passed and cinched in place with grub screws. The aluminium wires were flexible enough to adjust by hand and allowed clipping the glasses onto a post fitted to a bayonetted post included into the front of the implanted headpiece (see section 3.2.4.5). The frame had an adjustable front-piece to which the 40 dioptre Fresnel prism screen (Press-On™, 3M, DE) was secured with grub screws. The Fresnel prism screen was cut to provide maximal coverage of the animal's gaze without contacting the face- a triangular cut-out to accommodate the nose was also made. Images of the glasses can be seen in **Figure 3.2**. The total weight of the glasses was approximately 19.4 grams.

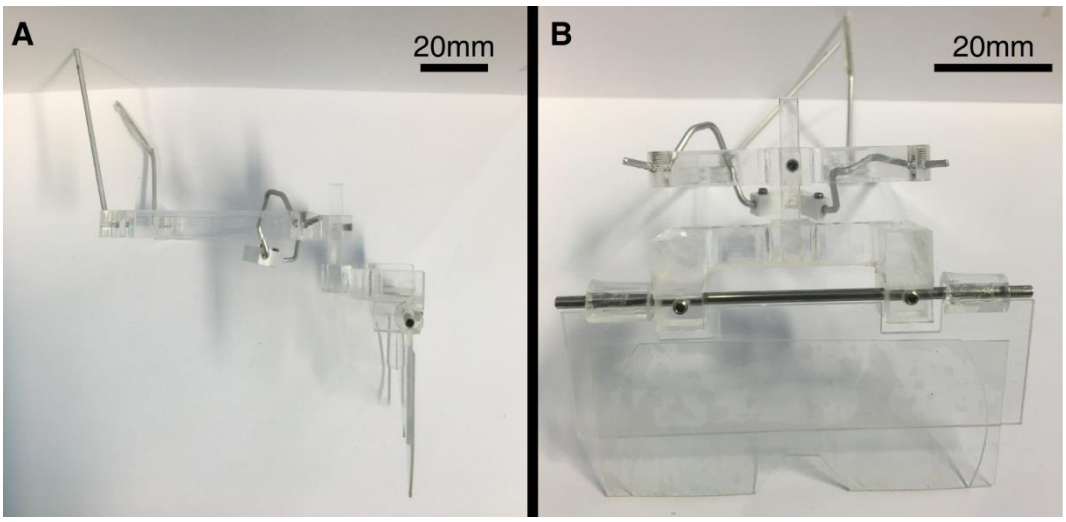

Figure 3.2 Images of prism glasses.
***A**; profile view and **B**; Front view of prism glasses.*

3.2.3.2 Implantable components

All implant connectors were designed to result in as minimal and unobtrusive implant structure as possible. Electrical continuity of the peripheral implants was confirmed prior to implantation. Peripheral implants were gas sterilised with an Ethylene Oxide system prior to implantation.

3.2.3.2.1 EMG leads

Three forelimb muscles were chosen to record electromyographical signals from; cleidobrachialis (major flexor muscle), triceps medial head, and triceps lateral head (extensor muscles). EMG leads were implanted in these muscles in the left forelimb.

Each muscle's activity was recorded using a bipolar electrode arrangement; therefore, three pairs of Teflon insulated braided stainless-steel wires (Cooner wire Co., Chatsworth, USA) measuring 60cm in length were soldered to a male micro-D connector with the excess plastic clipped off. A 1¼ inch 23-gauge hypodermic needle was cut from its plastic base and crimped onto the free end of the wires, and wire pairs were coloured with enamel paint (Humbrol™, Hornby Hobbies Ltd, UK) to differentiate them.

A single Teflon coated stainless-steel wire measuring 30cm was prepared in the same manner as the EMG wires, to serve as a ground electrode for the peripheral implant electronics. Solder joints were carefully covered and sealed with an epoxy resin (Araldite®, Huntsman International LLC, USA) to provide electrical isolation.

The excess length of these wires was intended to enable easy implant routing through the limbs and subsequent intramuscular implant. Individual wires would be trimmed to an appropriate length during the surgery.

3.2.3.2.2 Stimulation leads

Bipolar nerve cuff electrodes were used in each limb to deliver electrical stimulation to superficial radial nerve to evoke cerebellar field responses. Therefore, two pairs of peripheral wires were made up in the same manner as the EMG leads, with the exception that they were attached to a separate male micro-D connector.

3.2.3.2.3 Contact event marker lead

To record whether the cat had its left paw resting on the base of the Faraday cage, an electrical cable was implanted into the left wrist, which would carry a 400mV peak-to-peak 30KHz sine wave signal until the paw lifted from the copper base plate in the recording alcove- thus indicating paw lift-off at the initiation of the reach.

A single Teflon coated stainless-steel wire (Cooner wire Co., USA) measuring 60cm was soldered to a female gold socket (Fine Science Tools®, DE), and a 1¼ inch 23-gauge hypodermic needle crimped onto the free end as per the EMG leads. In Cat A this was an independent connector in the headpiece structure, whilst in cats B and C, this socket was incorporated into a bank of four sockets, grouping the contact lead, cerebellar electrode reference and ground wires.

3.2.3.2.4 T-bolts

To provide anchorage for the dental acrylic headpiece structure created during surgery, several pan head bolts (in a range of lengths between 3-7mm) were machined down into a 'T' shape with a Dremel. This allowed the bolt head to be inserted through a drilled slot in the skull and twisted 90° to lock into place.

3.2.4 Implantation surgery

Prior to any exposure to the prism glasses during the reach behaviour, the cats underwent two implantation surgeries separated by one week's recovery. During the first surgery, EMG electrodes, and event marker detection components were implanted, these are detailed below. Details of the implantation of the peripheral stimulation leads and neural recording electrodes will be detailed in the next chapter (section 4.2.1).

3.2.4.1 Disclosure of surgical team roles

Conforming to best practices regarding the three R's of animal research in the UK, surgeries were performed by an experienced team. A veterinary anaesthetist managed induction, maintenance, and recovery from anaesthesia as required. Most surgical procedures were performed by the Principle Investigator (PI) and post-doctoral fellow, assisted by the PhD candidate and a senior technician. Physiological mapping of the motor and cerebellar cortex, as well as the positioning of neural electrodes were performed by the PhD candidate, supervised by the PI and post-doctoral fellow as required. Implantation of the peripheral electrodes was

performed by the PI, post-doctoral fellow, and PhD candidate, assisted by the veterinary anaesthetist and senior technician.

3.2.4.2 General surgical methods

Due to the complex nature of the surgeries, and the modifications made to the type of cerebellar implant used for cats B and C, the following is a general outline of the surgeries. Further, only the implants necessary for the analysis of the cats' behaviour are given here, details of the implantation procedures of the extracellular electrodes will be given in the next chapter (section 4.2.1).

Surgical procedures were performed according to local aseptic surgical best practices. All surgical tools and equipment were sterilised by either autoclave, or ethylene oxide gas as appropriate.

3.2.4.3 Anaesthesia and stereotaxic set up

Cats were sedated with intramuscular dexmetomidine (15µg/kg), and the fur covering regions of interest was clipped away. These regions included; top of skull, frontal forelimbs (over the muscles identified for peripheral implantation, see section 3.2.4.4) and inside right hindlimb.

An intra-venous line was inserted into the right hindlimb, and trachea intubated. Under the direction of the veterinary anaesthetist, anaesthesia was induced with intra-venous Propofol (Propoflo™ Plus, 10mg/ml, Abbott Animal Health, USA) and maintained on gaseous Isoflurane for the duration of the surgical procedures, except during periods of electrophysiological investigations in which anaesthesia was transferred to ketamine (10µg/kg/hr) for motor cortical mapping (section 4.2.1.1.2), and Propofol for cerebellar cortical mapping (section 4.2.1.2.2). Isoflurane was delivered with oxygen enriched air produced by an oxygen concentrator (Clinipath Equipment Ltd., UK).

Cats were positioned into a stereotaxic frame (David Kopf Instruments®, USA) using atraumatic ear bars, prepared with a local analgesic (lidocaine) on the tips, and by bars supporting the upper jaw, and lower aspects of the orbits. The eyes were protected with Lacrilube. A homeothermic blanket (Harvard Apparatus, USA) was placed beneath a layer of VetBed® to maintain body temperature throughout surgery.

Throughout surgery peripheral capillary O_2 saturation, end tidal CO_2, electrocardiogram and body temperature was monitored by the veterinary anaesthetist and exact dosages of anaesthetic agents adjusted at their discretion. Opioid pain relief (Buprenorphine) and antibiotics (cefuroxime, Zinacef, GlaxoSmithKline, UK) were also given intra-venously at the veterinary anaesthetist's discretion.

3.2.4.4 Peripheral implantation

The peripheral implants (EMG, stimulation leads and contact event marker lead) were implanted during the first surgery, after having already implanted neural electrodes into the frontal cortical targets.

Prior to implanting the peripheral electrodes, the connectors were affixed to the skull caudal to the frontal craniotomy. The two micro-D connectors were positioned and held in place by the two stereotaxic manipulators, and the gold socket connectors manually held with custom made adapters while dental acrylic was used to secure them in place and form a headpiece structure (see section 3.2.4.5).

A small skin pocket was made into the caudal end of the head incision, to accommodate excess cabling post-surgery. Small incisions were made to the shaved skin areas on both forelimbs. The superficial fascia was reflected to expose the muscles and nerves to be implanted. A trocar was wetted with saline and pushed subcutaneously from the skin pocket down each limb to the limb incisions. The appropriate implant wires were passed down each limb through the trocar.

In the case of the EMG wires, a small double knot was formed at an appropriate length in each wire to provide enough slack to the final length so as not to impede natural movement, and to prevent the wires being pulled too far through the muscle during insertion. The Teflon insulation distal to this knot was scraped away with a scalpel and the electrode pairs inserted into their designated muscle with the attached hypodermic needles. Wire pairs were arranged in parallel with the muscle fibres with an approximate separation of 3mm. A second double knot was tied at the point where the wire emerged from the muscle, securing the wires in place. Excess wire was cut away.

Peripheral nerve cuff pairs were positioned around the superficial radial nerves in each forelimb wrist area. The insertion of wire pairs followed the same procedure as muscle implants. The pairs were inserted into the perineural tissue on opposing sides of the nerve. Finally, the single Teflon wire designed to carry the Contact signal was stitched into the connective tissue under the left wrist. Approximate routing of the cables through the forelimb can be seen in **Figure 4.4C**.

Successful implantation of the peripheral wires was tested by stimulation of each cable pair separately using an isolated stimulation box (Digitimer Ltd.®, UK), and observing the evoked muscle twitch.

Finally, the free end of the peripheral grounding wire was sutured into the connective tissue on the back around the mid thoracic level. Once the peripheral electrodes had been implanted, all limb incisions were stitched with suture material (Ethicon, Johnson & Johnson Medical, BE). The

cable slack was placed into the skin pocket. The skin pocket was then stitched firmly closed to the boundary of the headpiece, and recovery then proceeded as below.

3.2.4.5 Headpiece structure

Once all implant components had been secured in position, dental cement was used to build up a single implant structure. A guide to the organisation of electrode connectors on the headpiece, as used during surgeries, can be found in the Appendix. Dummy connectors were attached to all interface connections during this process to protect the electrical contacts, and to prevent fouling of the connectors. The boundaries of the structure were contained between prefabricated Nylon shells. The shells had an overhanging ledge on the top surface and had previously been coated in a silver sulfadiazine antimicrobial dressing (Coatings2Go™ LLC, USA) to reduce probability of post-surgical infection. At the very rostral aspect of the structure, a bayonet style bolt was cemented, enabling the quick attachment of a 10cm aluminium post to which the prism glasses would attach.

The top surface of the dental cement was moulded to be as 'streamlined' as possible, limiting the extent to which connectors protruded from the structure, whilst not fouling them. Cement surfaces were smoothed using a wetted cotton tip.

Once the headpiece structure had been finalised and cured, all manipulators were removed from the various connectors, and the skin incision was stitched back around the headpiece with suture material. Recovery then proceeded as described below.

3.2.4.6 Recovery

Under the direction of the veterinary anaesthetist, anaesthesia was stopped, the animal removed from the stereotaxic frame, monitoring instruments were removed, and the cat extubated. The cat was transferred to a large pet cage lined with VetBed® in the home pen (though separate from the other cats). The cat was then left to recover under observation until fully recovered (10-24 hours). Post-operative pain relief (Buprenorphine 20mgkg-1, Buprecare®) was administered as advised by the veterinary anaesthetist.

The cat was returned to grouped housing with the other cats once all involved parties (including Named Veterinary Surgeon and Named Animal Welfare Officer) were happy with the state of recovery. A minimum period of one week was observed between the first and the second surgery, and between the second surgery and resumption of the behavioural task/recording sessions.

3.2.5 Recording procedures

After the minimum one-week recovery period, and once the cats were deemed fully recovered from the surgeries. the implanted cats were brought through to the recording room and harnessed into the recording alcove as described in section 3.2.2.2.

3.2.5.1 Video recordings

To allow offline review of the reaching behaviour, two webcams (Kayeton Technology Co. Ltd, China) were positioned in a stereoscopic manner within the recording alcove, allowing an unobscured view of the cat's reaching paw from the typical resting position on the copper contact plate, to the full extent of a reach into the entrance of the reward tube.

3.2.5.2 Adaptation behaviour

Once all recording apparatus was initiated, the operator (previously attending to the cat) opened the reward tube door, and the cat began reaching for fish morsels as trained. The intra-session timeline of reach trials followed that of a standard adaptation paradigm: - The first 20 reaches served as a daily baseline. Next, the prism glasses were fitted to the bayonet fitting in the headpiece. Reaching continued under the prism condition, noting whether each reach missed the tube (miss), the reach was corrected to enter the tube (corrected hit), or successfully entered the tube as in the baseline period (hit).

Adaptation was considered to have occurred once the cat had successfully performed 20 hits in succession. Once this had been achieved, the prism glasses were removed, and reaching continued, again noting the classification of reaches until 20 consecutive hits were recorded. The specific number of reaches in each condition was a balance between collecting as many reaches as possible for data analyses for each condition and completing all conditions before the cat was sated and lost interest in the task.

3.2.5.2.1 Switching prism directions

During the recordings, it became apparent that the animals may have been exhibiting longer-term savings rather than short term adaptation (detailed in section 3.3.2.1). To re-invoke short-term adaptation, the prism glasses were 'flipped' from the original leftward displacement to a rightward displacement.

3.2.6 Pharmacological experiments (cats B and C)

After the completion of the behavioural experiments outlined above, cats B and C were subject to a final experiment designed to confirm that the region of cerebellum that was targeted indeed had a role in the behaviour.

3.2.6.1 Lidocaine blockade

After initially performing the reaching task as normal (no-prism baseline), a 22-gauge bevelled needle was affixed to the micro-drive tower in-place of a recording electrode and advanced to a depth approximately equal to that used during previous recordings (~2mm from cortical surface). A 6µl dose of lidocaine was infused 1µl/min by means of an infusion pump (Harvard Apparatus, USA) connected to the needle via surgical tubing. The animal was then allowed to proceed reaching with no prisms for ten trials before the prisms were fitted.

3.2.7 Perfusion fixation

At the termination of the experiments, the cats were deeply anaesthetised with intra-peritoneal injection of sodium pentobarbitone (40mg/kg, Euthatal, Merial Animal Health Ltd., UK), and trans-cardially perfused with one litre of heparine saline (0.9% heparin), followed by 2 litres of 4% paraformaldehyde. After the perfusion, the brain was carefully removed from the skull, and stored in 4% paraformaldehyde at 4°C. The brain was transferred to a 30% sucrose solution after a week and allowed to sink.

3.2.8 Statistics

Parametric tests were performed whenever possible, and the type of test used is highlighted in the text.

Regarding the behavioural metrics (reaction time and reach duration), the data generally appeared to conform to an ex-Gaussian or gamma distribution rather than a true normal distribution, not uncommon for reaction time data (Whelan 2008; Heathcote et al. 1991; Palmer et al. 2011; Mcgill and Gibbon 1965). Moreover, the unbalanced nature of the data groupings (adaptation and after-effect misses being rarer than hits due to the adaptive behaviour) led to a violation of the assumption of homogeneity of variance (levene's test). Consequently, a generalised linear model, which has less stringent assumptions of homogeneity of variance than general linear models, detailing a gamma distribution with a log-link function for reaction time data, was chosen as the principal test for the behavioural data.

3.3 Results

3.3.1 Forelimb reaching behaviour in cats

As described in previous work from the lab (Cerminara et al. 2005), the cats were trained to reach to retrieve a food reward from a shoulder height Perspex tube. Each daily recording session lasted approximately 20-30 minutes (plus additional time at the start and end for electrode set up and removal) with around 80 reach trials being made by the cats within each session (group average 79.5, SD 12.7).

3.3.1.1 Cats remained engaged throughout recording sessions

A potential issue with any repetitive, reward-based behavioural task is that over the course of a recording session animals may become fatigued or disengaged with the task as they become sated. We assessed this possibility in two cats (cats B and C) by extending the duration of individual recording sessions (without any prism glasses) on 5 consecutive days to determine when the animals might cease performing the task and show signs of wanting to return to their home pen (e.g. being restless and no longer attending to the task).

Both cats performed 150 reaches within the regular 30-minute session length with little or no indication of showing a decline in task performance or interest. This number of reaches substantially exceeded that typically performed in the prism adaptation recording sessions (mean total of 90 and 78 per session for cats A and B respectively). It was therefore concluded that fatigue and/or changes in motivation were unlikely to be major factors in the experimental trials.

3.3.1.2 Forelimb reaching is visually driven

Due to the static arrangement of the target (the reward tube was always directly ahead of the animals), and the over-trained nature of the reaching behaviour, it was possible that the cats might learn to forego using vision to target the tube and favour a more automatic 'habit' reaching behaviour. To confirm that the cats were not simply executing an over-trained motor program, we assessed cats B and C's ability to reach to the tube when moved to different locations.

On two consecutive recording sessions, these two cats performed 20-25 reaches with the reward tube in the standard location, directly in front and in line of sight of the cats (without prisms). The reward tube was then moved either to the left or right extremities of the recording cage (maintaining approximately the same distance from the cats). The cats then performed 20-25 additional reaches with the reward tube in each of these locations. The operator noted reach accuracy - i.e. if trials were on-target (hits) or not (miss).

Regardless of the reward tube location, neither cat missed the reward tube on any trial (example still shown in **Figure 3.3**). Moreover, the cats clearly attended to the location of the reward tube, tracking its position with their eyes.

Figure 3.3 Visual targeting of reward tube.
Still from video recording of cat B's first reach to left-hand target location. The reward tube (white arrow) was moved to the cat's left hand extreme. Note the cat's clear attention on the tube location, and accuracy of the paw as it enters the reward tube. Timer in bottom right of image details current time of recording session.

3.3.1.3 Reaching limb EMG signals are consistent across reaches

EMG signals were recorded in three proximal forelimb muscles of the reaching limb of the cats; a flexor muscle (cleidobrachialis) and two extensors (triceps brachii long head and lateral head). An example reach is illustrated in **Figure 3.4**, showing EMG recordings, and three event marker channels – reward tube door state, paw contact state, and tube entry state. Whilst each individual animal exhibits a unique pattern of EMG activity (**Figure 3.5**, **Figure 3.6** and **Figure 3.7**), activity was very consistent across trials, and all three display similar gross sequence of activation which has been described in prior literature (Schepens and Drew 2003).

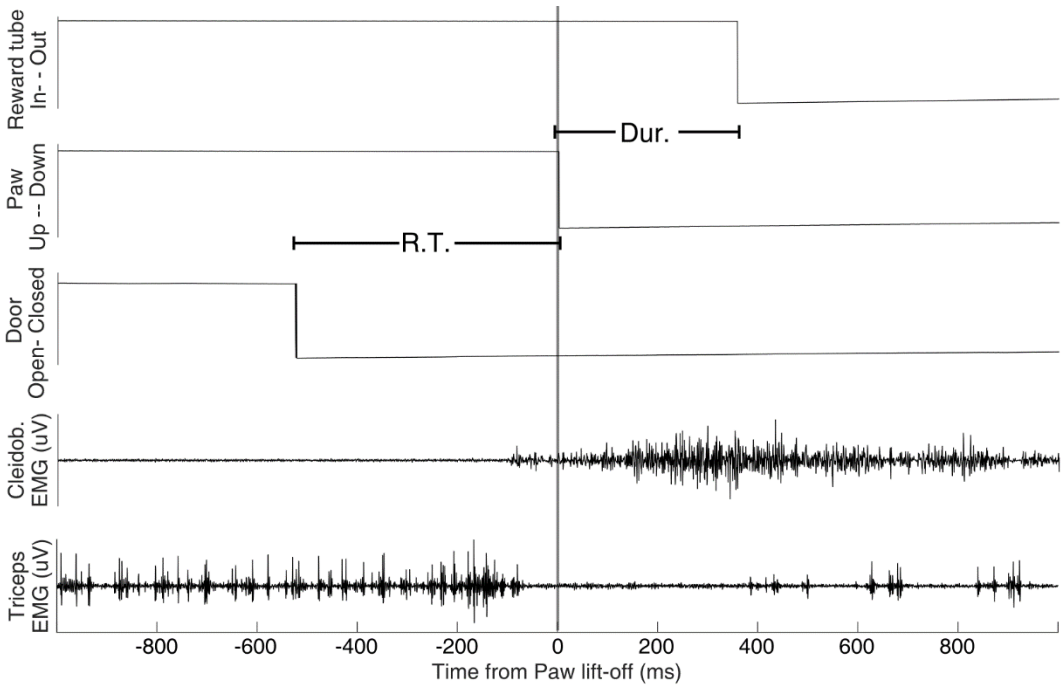

Figure 3.4 Example time series of event markers and EMG signals.
Forelimb extensor (Triceps) and flexor (Cleidobrachialis) EMG activity shows stereotyped antagonistic activity during the reach. R.T: - reaction time between door opening and paw lift-off. Dur: - reach duration between paw lift-off and reward tube entry.

There was an EMG burst in one or both triceps brachii muscles starting approximately 200ms prior to paw lift-off, as the cats made small postural adjustments prior to the reach. This pre-lift bursting of extensor muscle was apparent in the lateral head triceps of cat A, the long head triceps of cat B, and both triceps of cat C. The long head channel of cat A did not record any clear EMG activity (likely due to a failure of the implant), and the lateral head activity of cat B appeared more consistent with recording of a flexor muscle, possibly due to inaccurate implantation. The flexor muscle (cleidobriachialis) was generally quiescent prior to the paw-lift signal, and then 'ramped-up' to sustained EMG activity during the reach, initiating shortly before the paw lift-off signal (~150-200ms).

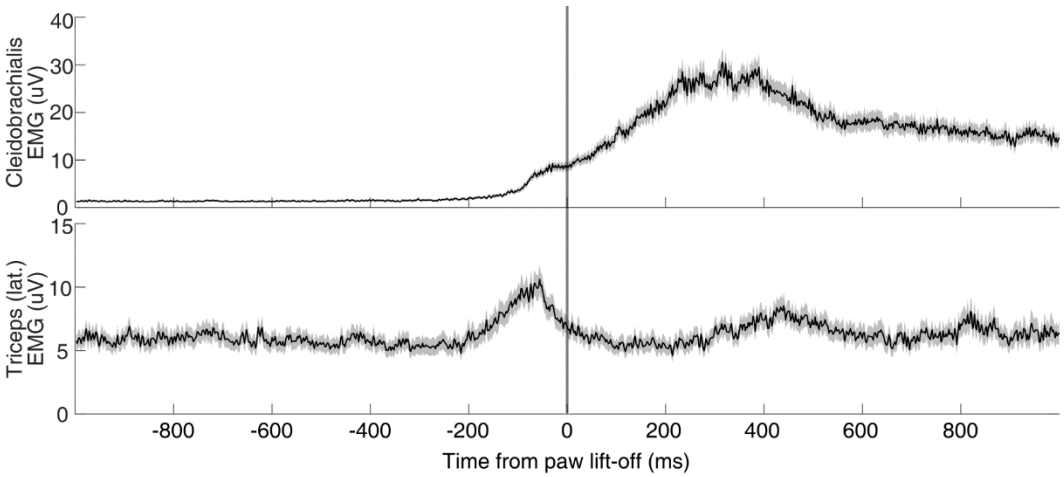

Figure 3.5 Rectified EMG signals in muscles of reaching limb in cat A.
EMG activity of two major forelimb muscles (Cleidobrachialis, and lateral head of triceps) during a reaching movement. Triceps long head EMG not shown due to faulty implant. Black lines indicate average EMG activity over all trials, aligned to paw lift-off. Shaded areas represent 95% confidence intervals of the mean.

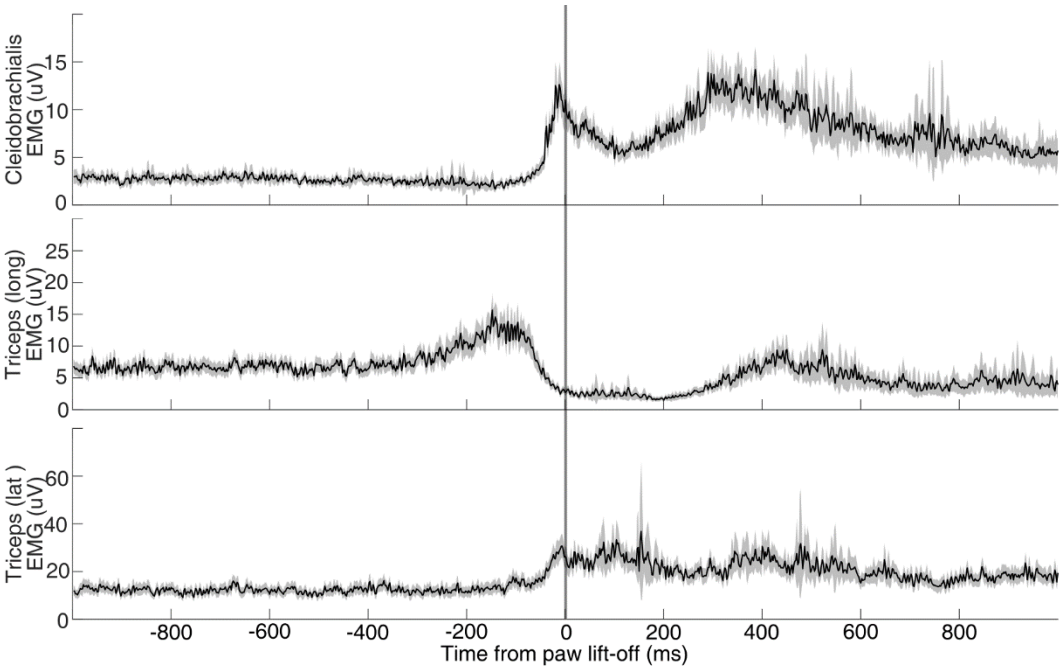

Figure 3.6 Rectified EMG signals in three muscles of the reaching limb in cat B.
EMG activity of three major forelimb muscles (Cleidobrachialis, long head and lateral head of triceps) during a reaching movement. Note activity of lateral triceps channel appears antagonistic to long head triceps channel, indicating a missed implantation. Black lines indicate average EMG activity over all trials, aligned to paw lift-off. Shaded areas represent 95% confidence intervals of the mean.

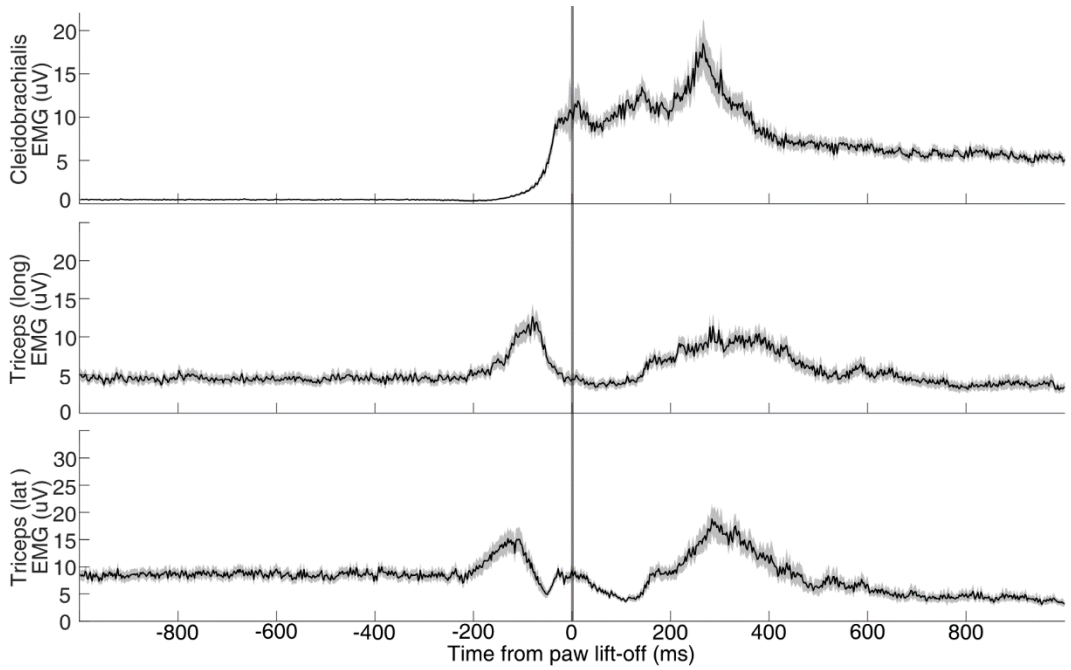

Figure 3.7 Rectified EMG signals in three muscles of the reaching limb in cat C.
EMG activity of three major forelimb muscles (Cleidobrachialis, long head and lateral head of triceps) during a reaching movement. Black lines indicate average EMG activity over all trials, aligned to paw lift-off. Shaded areas represent 95% confidence intervals of the mean.

3.3.2 Prisms elicit visuomotor adaptation in cats

All three cats tolerated the prism glasses well, carrying out the reaching task with their left forelimb (ipsilateral to the cerebellar recording site). There were no gross behavioural reactions from any of the cats to having the prism glasses put on. Further, once the glasses were put on and the reward tube opened for subsequent reaching, the cats directed their focus back to the reward tube and task. This was taken as good evidence that the presence of the prisms was not a distractor or otherwise altering the behaviour of the animals beyond the intended function of the prisms.

Evidence of prism adaptation was found over the first 5 consecutive recording sessions of exposure to the prism glasses in all three animals. In each of these recording sessions, when the prism glasses were first put on, the cats' reaching was perturbed, with the reaching paw initially missing the reward tube mouth to the left. The cats would progressively adapt their reaching movement until the paw reached directly into the tube as in baseline trials. Across all the recording sessions, adaptation to the prisms took around 10 trials of misses before 'hits' were made (Cat A mode =9, Cat B mode=8, Cat C mode=11).

Furthermore, when the prisms were removed, the animals missed the tube in the opposing direction to the prism displacement, consistent with an after-effect phenomenon - a hallmark

of visuomotor adaptation (Taylor and Ivry 2014). Once again, upon repeated trials the animals were able to regain task accuracy, reaching into the tube as in baseline trials.

Reaches were categorised into two main groups within either pre-prism (Baseline), prism on (adaptation) or prism off (after-effect) trials:

1. 'Miss' trials consisted of reaches in which the animal reached forward and hit the façade of the reward tube, having to make a secondary corrective movement to place the paw into the tube.
2. 'Hit' trials, by contrast, consisted of reaches in which the animal reached forward and placed their paw directly into the tube in a smooth motion, as in the baseline trials.

A third, intermediary category ('corrected hits') of reaches was defined as reaches that did not fall into the other two defined categories. Specifically, as the trials continued, the size of the lateral reach error decreased such that the paw would brush past the reward tube perimeter and appear to deflect into the reward tube, with no need for a secondary corrective movement. As discussed later (section 3.4.5), these trials were excluded from the analyses in this thesis because they likely reflect trials when online corrections are made, rather than error driven adaptation. Consequently, the reaching trials constituting the analyses in this thesis fell into five major conditions: baseline, adaptation miss (early adaptation), adaptation hit (late adaptation), after-effect miss (early after-effect) and after-effect hit (late after-effect). Examples of the four main reach conditions (baseline, early adaptation, early after-effect, and late after-effect) are shown in **Figure 3.8** below to provide an indication of the degree of errors made.

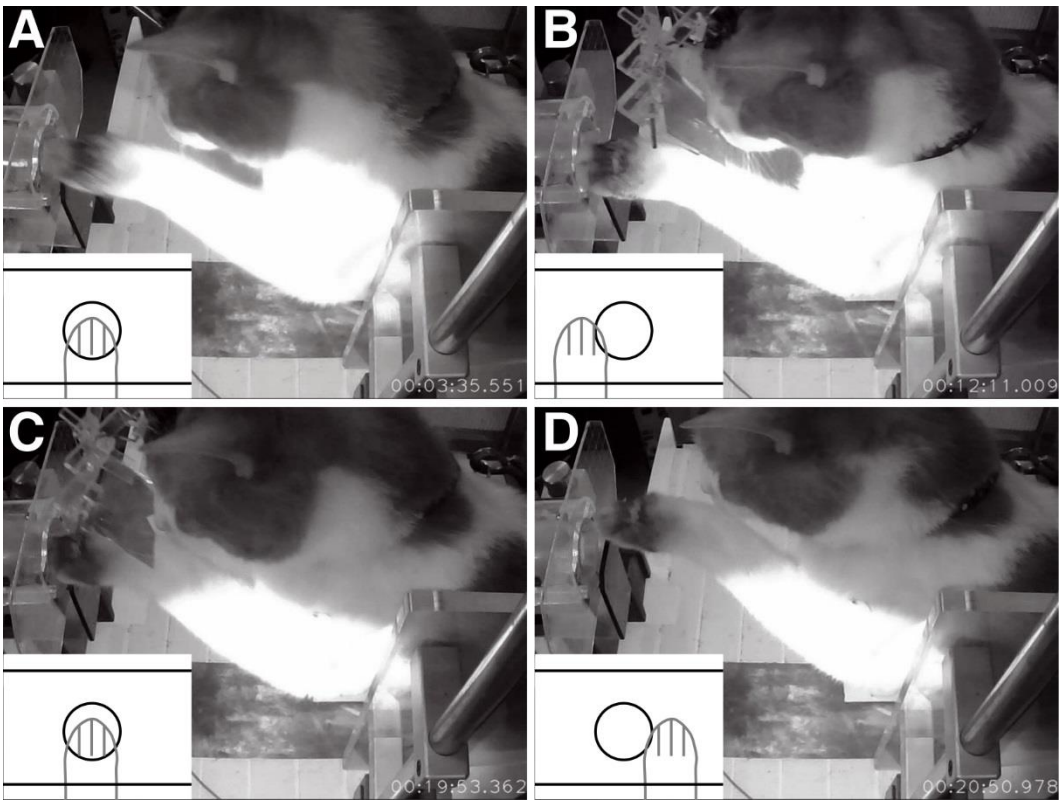

Figure 3.8.Major Reach category examples.
*Example video stills from cat B recording session showing; **A**- baseline, when reaches are accurately placed into the tube; B- early adaptation when reaches are perturbed to the left of the tube entrance; **C**-late adaptation, when reaches are now on-target; and **D**- early after-effect, when reaches are displaced to the right of the tube. Late after-effect examples not show as they appear the same as baseline reaching. Images show reaching endpoints as the paw hits the plane of the reward tube façade. Insets show schematic representation of paw location from in front of the tube.*

3.3.2.1 Savings over weeks

In addition to short term motor adaptation occurring within each recording session (intra-session adaptation), improvements in task performance – such as a more rapid rate of adaptation to the same perturbation – are also possible over longer-term periods (typically over numerous experimental sessions over many days). This inter-session improvement is referred to as savings in the motor learning literature (Krakauer 2009). Whilst cat A continued to display classical intra-session adaptation over several weeks, cats B and C ceased to exhibit intra-session adaptation after only one week of exposure to the prism glasses. Instead, after the initial recording week, both cats during prism trials would successfully reach into the reward tube after only one or two miss reaches. The performance of both animals was similar when the prism glasses were on and off, with no evidence of an after-effect.

Two approaches to re-invoke intra-session adaptation in these cats were attempted. A washout period of one week (5 consecutive recording days) was performed during which the cats were not exposed to the prism glasses. Instead, the time was used for control experiments such as assessing the engagement in the task (see sections 3.3.1.1 and 3.3.2.3). However, when the

prisms were re-introduced, intra-session adaptation was not restored. Subsequently, the prisms were reversed, which was successful at evoking intra-session adaptation, as already detailed.

Similarly, once cats B and C had been exposed to the rightward prisms for 5 consecutive recording sessions, intra-session adaptation was no longer apparent. The prisms were once again reversed, but neither cat appeared to undergo intra-session adaptation, again requiring only one or two miss reaches before consistently performing accurate reaches. This suggests a long-term memory for the previously experienced visuomotor perturbation, and although not within the scope of this study, data captured in these periods may provide insights into the mechanisms of switching established internal models.

3.3.2.2 Savings over days

To assess whether the three cats exhibited significant savings-like behaviour in the 5 recording sessions prior to the longer term savings behaviour became apparent, the total number of erroneous reaches (combining both misses and corrected hits) occurring on each of the 5 recording days was plotted as a measure of the duration of intra-session adaptation (i.e., the total number of trials in a session before 'hits' occurred). If a process of savings was occurring, a reduction in the number of inaccurate reaches as a function of recording day would be expected.

There is some evidence for this as shown in **Figure 3.9**, in which all three cats show a negative trend between the number of inaccurate reaches and recording session number over the first 5 consecutive recording days (group gradient = -2.8 inaccurate reaches per day, R^2=0.249). However, this trend is less evident when the prisms are removed (the after-effect), with a group gradient of only -0.311 reaches per day (**Figure 3.10**).

A mixed-model ANOVA (Prism on/off x Prism direction x recording day), revealed no statistically significant 3-way interaction ($F_{(4,5.118)}$=2.23, p=0.199), or 2-way interactions (Day x Prism direction; $F_{(4,5.118)}$=1.85, p=0.255. Day x prism on/off; $F_{(4,5.118)}$=2.276, p=0.193. Prism direction x prism on/off; $F_{(1,11.326)}$=0.824, p=0.383). There was a significant main effect of prism on/off ($F_{(1,11.326)}$=42.725, p<0.000), and prism direction ($F_{(1,11.326)}$=0.022), but no significant effect of day ($F_{(4,5.118)}$=3.264, p=0.111). Overall, it appears that there are only modest savings occurring over the 5 consecutive recording sessions.

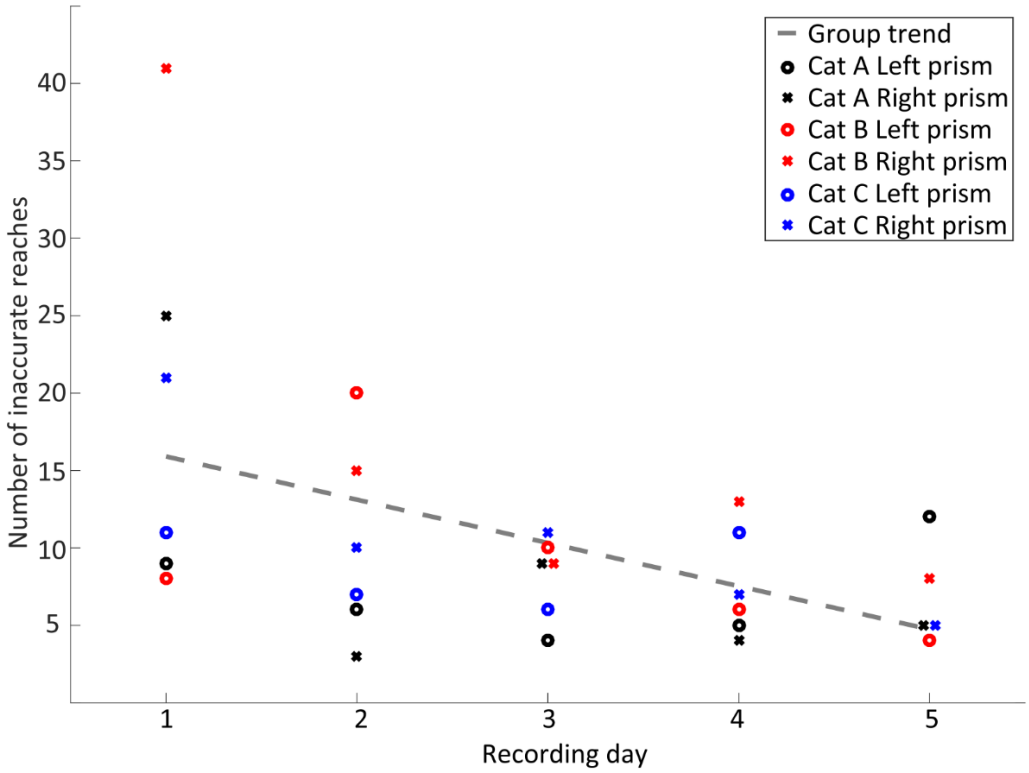

Figure 3.9 Number of reach errors per day with prisms on.
Scatter plot showing the number of inaccurate (miss and corrected) adaptation reaches for each day. Each animal represented by a specific colour, left prism reaching indicated by circles, right prism reaching denoted by crosses. The linear trend of the group is shown as a grey dashed line.

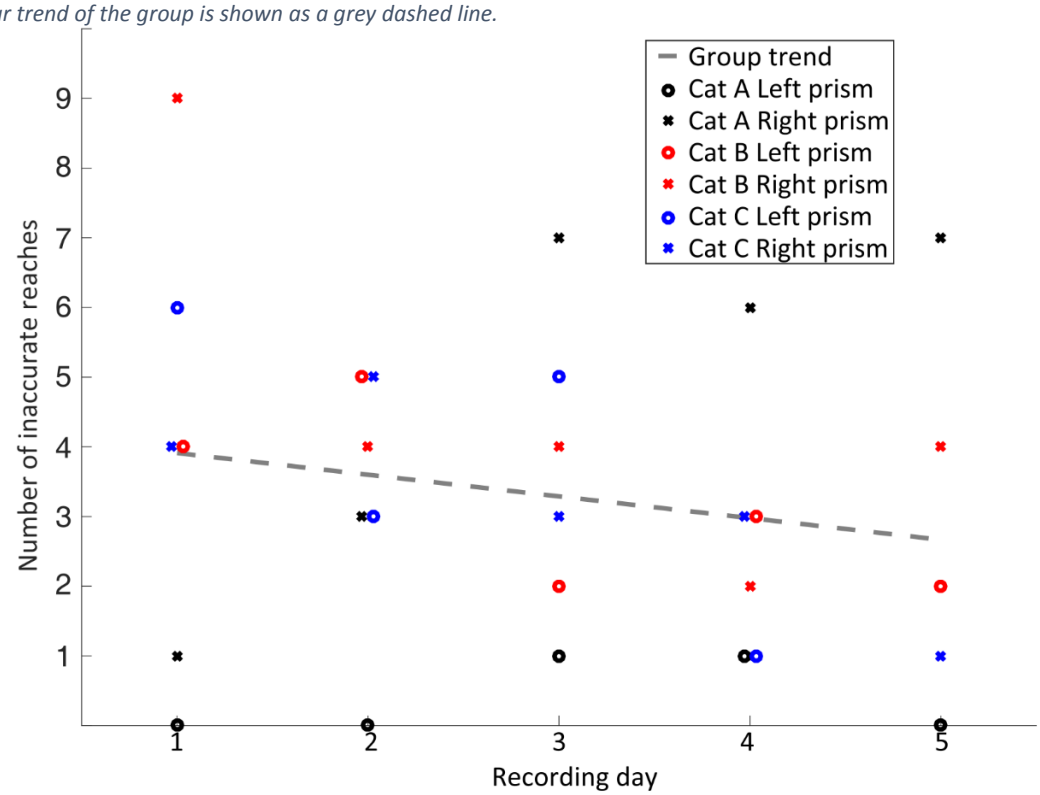

Figure 3.10 Number of reach errors per day after prims removal.
Scatter plot showing the number of inaccurate (miss and corrected) after-effect reaches for each day. Each animal represented by a specific colour, left prism reaching indicated by circles, right prism reaching denoted by crosses. The linear trend of the group is shown as a grey dashed line.

3.3.2.3 Cerebellum paravermal lobule V influences forelimb motor adaptation in the cat

To provide direct evidence that the cerebellar cortical regions targeted in each cat were involved in forelimb visuomotor adaptation, reversible pharmacological inactivation was performed in cats B and C by injecting lidocaine (a voltage-gated sodium channel blocker) into the vicinity of the cerebellar recording sites. This was possible because of the open chamber design of the cerebellar implant in cats B and C and was carried out at the end of the recording lifetime of each animal. Technical limitations prevented both cannula and recording electrode from being used concurrently, therefore no neural data were collected with the drug infusion.

Behavioural effects of lidocaine injection (6µl, 20% lidocaine in saline) were not observed in cat B but were evident in cat C. In contrast to normal reaching, ataxic symptoms manifested as markedly slower reaching in baseline trials, but the animal was still able to successfully enter the tube. Moreover, in contrast to prior recording sessions in which intra-session adaptation was no longer observed (because of long term savings, see above), after the lidocaine infusion the cat missed the target several times when the prism glasses were first applied. Prism adaptation occurred at a similar rate as observed in the first week of prism exposure, requiring 11 trials before successful hits were established. Through the prism-on period, the reaches became less ataxic-like until the animal no longer displayed any motor symptoms. Interestingly, when the prisms were removed, there was no evidence of an after-effect.

3.3.3 Refining the reach dataset

To form a useable dataset, describing the typical reaching behaviour of each animal, individual reaching trials were excluded from further analysis if:

(i) They displayed excessively short or long reaction times (less than 150ms or greater than 1500ms);

(ii) They displayed ‘abnormal’ reach durations (greater than 2.5 standard deviations from the mean a commonly used [if arbitrary] threshold for limiting limb reaching data (Miller 1991)).

(iii) The neural recordings were corrupted by electrical artefact.

The proportion of trials excluded based on criteria (i) and (ii) was quite consistent across animals (group mean=15.05%, SD=2.70%), whilst the number of trials containing some form of electrical artefact in the neural data (criteria iii) varied much more between the animals (mean=37.19%, SD=27.45%). **Table 3.1** shows the breakdown of these numbers for each cat. Cat B had a much greater overall loss of data than the other two cats mainly because of instability in the neural recording.

	Cat A	Cat B	Cat C
Total reaches performed	757	856	677
Proportion excluded for behavioural criteria	16.25%	16.94%	11.96%
Proportion of remainder excluded for neural data criterion	14.04%	67.51%	30.03%
Total remaining 'clean' reaches	545	231	417
Percentage of total reaches excluded	28.01%	73.01%	38.40%

Table 3.1 Proportion of excluded trials through data pre-processing.
Table showing total number of performed reaches by each cat for all days with intra-session adaptation, the proportion of reaches excluded at each successive stage of pre-processing, and the total remaining trials for analysis.

3.3.3.1 Trials are not evenly distributed between adaptation condition

Table 3.2 shows the total number of pre-processed trials performed by each cat, divided into the main stages of adaptation: baseline (pre-prism), prism adaptation (hit and miss), and post-prism after-effect (hit and miss). As expected, the number of 'miss' trials are much less than 'hits'. Moreover, the number of early after-effect trials available after pre-processing is extremely small. To minimise the impact of such small number of trials, the early after-effect condition was excluded from subsequent statistical analyses.

Adaptation condition	Cat A	Cat B	Cat C
Baseline	179	64	127
Early adaptation (miss)	54	27	26
Late adaptation (hit)	123	52	129
Early after-effect (miss)	6	4	9
Late after-effect (hit)	183	84	126

Table 3.2 Number of analysed reaches in each adaptation condition.
For each cat, the total number of trials analysed in this report is shown for each stage of adaptation.

3.3.3.2 Reaching metrics of each cat differ

Descriptive values of the reach metrics of each animal can be found in **Table 3.3**. Cat A had a median reaction time 73.8% slower than cat B, and cat C had a median reaction time 17.1% slower than cat B. Further, cat A also had the broadest range of reaction times, 25.9% greater than those of cat B, and cat C had a range 19.9% greater than cat B. In terms of reach duration; cat A again had the slowest median, 66.8% greater than cat C, and cat B had a median reach duration 43.6% slower than cat C.

	Metric	Mean (ms)	Median (ms)	Mode (ms)	Range (ms)
Cat A	Reaction time	616.8	547.7	529.0	1339.0
	Reach duration	385.6	376.5	368.0	536.3
Cat B	Reaction time	355.3	315.2	271.2	1063.3
	Reach duration	331.2	324.2	337.0	355.4
Cat C	Reaction time	434.5	369.0	169.3	1275.1
	Reach duration	231.7	225.7	218.6	182.8

Table 3.3 Descriptive statistics of cat reach metrics.
For both reaction time and reach duration, a selection of common descriptive values is displayed.

Reaction time data appeared as gamma distributions (positive valued, positively skewed-**Figure 3.11**). Gamma (and closely associated ex-Gaussian) distributions are often associated with individual reaction time data and has previously been used to describe movement parameters in humans, including reach-to-grasp actions (Mcgill and Gibbon 1965; Palmer et al. 2011).

A generalised linear model revealed statistically significant differences between the cats' reaction times (Wald $\chi^2(2)=295.220$, $p<0.0005$), and reaching duration (Wald $\chi^2(2)=1739.771$, $p<0.0005$).

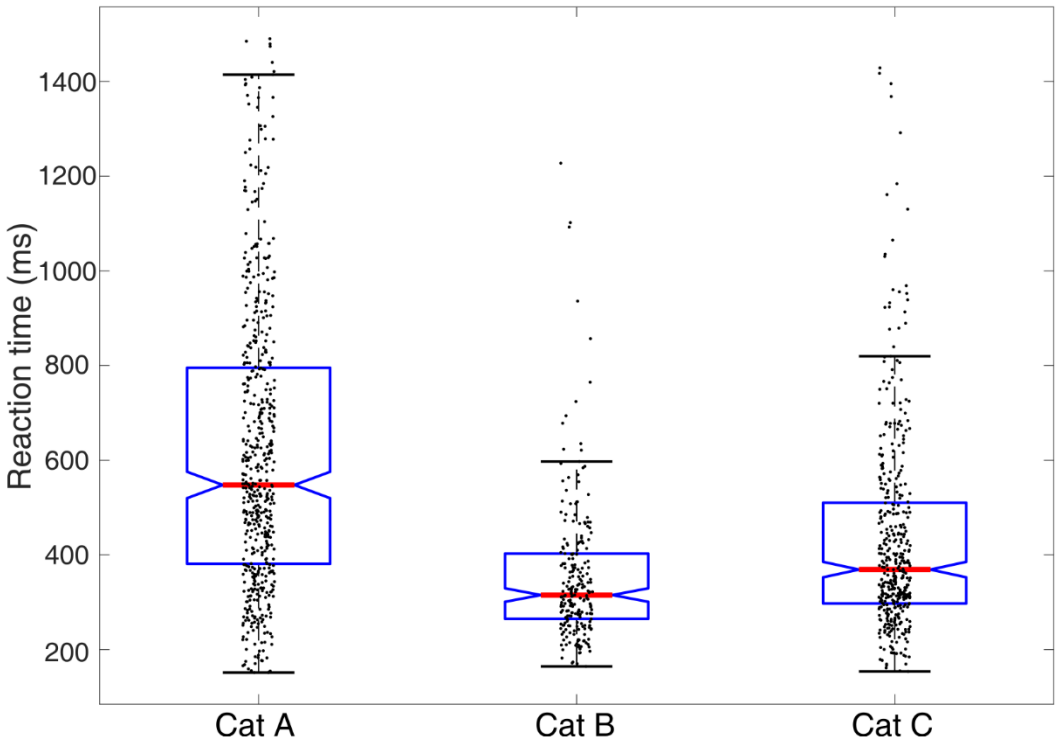

Figure 3.11 Reaction times of each cat.
Box/scatter plot showing reaction times of pre-processed trials from each animal. Black dots show individual reach datum. Central red bar of boxes indicates group medians, top and bottom limits of boxes demark interquartile ranges. Notches in boxes indicates 95% confidence intervals of the median values.

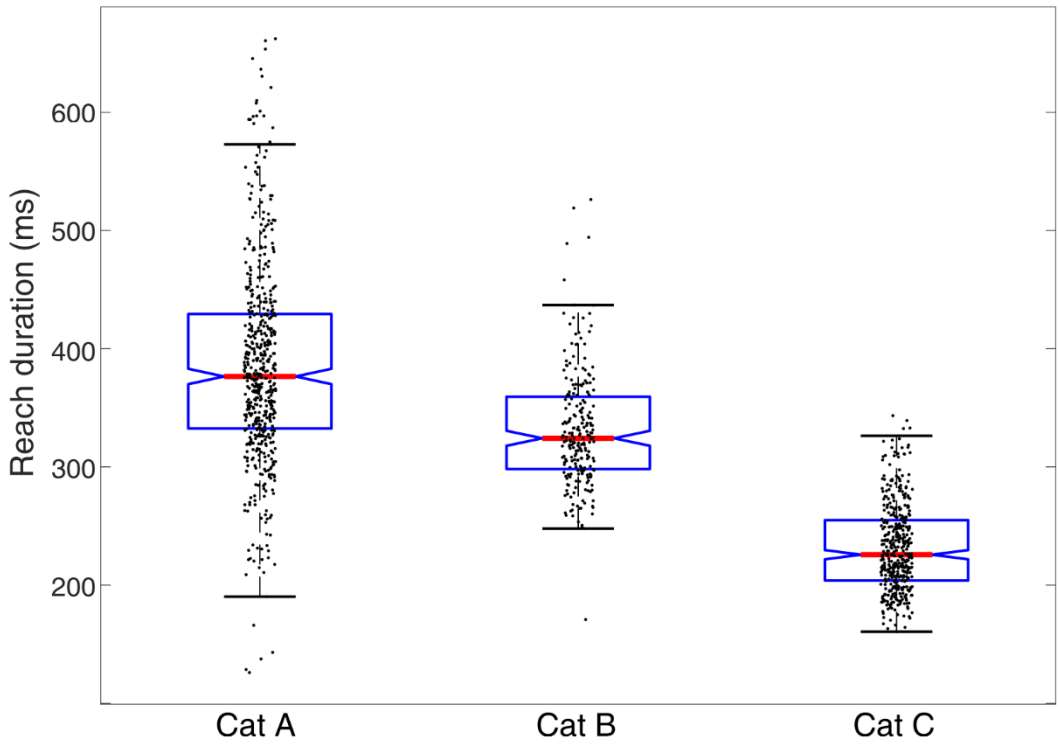

Figure 3.12 Duration of outward reaching of each cat.
Box/scatter plot showing reach durations of pre-processed trials from each animal. Black dots show individual reach datum. Central red bar of boxes indicates group medians, top and bottom limits of boxes demark interquartile ranges. Notches in boxes indicates 95% confidence intervals of the median values.

3.3.4 Reaching metrics are not consistent between study conditions

For comparison of the neural activity between the different adaptation conditions, the reaching behaviour should ideally be consistent between them. To assess this, both reaction time and reach duration metrics were analysed by a generalised linear model (cats x adaptation condition).

Reaction time

The model found a statistically significant interaction between animals and adaptation condition (Wald $\chi^2(6)=13.294$, $p=0.39$). Subsequent models for each animal separately showed no statistically significant main effect of adaptation condition in cat A (Wald $\chi^2(3)=5.243$, $p=0.155$), cat B (Wald $\chi^2(3)=4.834$, $p=0.184$), but a significant effect of adaptation condition in cat C (Wald $\chi^2(3)=28.053$, $p<0.000$). Post-hoc Bonferroni corrections revealed significant comparisons between baseline-late adapt. ($p=0.061$) and baseline- late after. ($p<0.0005$) trials.

Reach duration

The model found a statistically significant interaction between animals and adaptation condition (Wald $\chi^2(6)=49.145$, $p<0.0005$). Subsequent models for each animal separately showed statistically significant main effect of adaptation condition in cat A (Wald $\chi^2(3)=58.952$, $p<0.0005$. All Bonferroni corrected comparisons to baseline $p<0.0005$) and B (Wald $\chi^2(3)=13.104$, $p=0.004$. Bonferroni corrected comparisons; baseline-early adapt. $p=0.051$,

baseline-late adapt. p=0.006, baseline-late after. p=0.013), but not cat C (Wald $\chi^2(3)=0.595$, p=0.897).

3.4 Discussion

3.4.1 Task paradigm

The basic reaching behaviour of the cat's in this study was consistent with previously published studies (Apps et al. 1997; Cerminara et al. 2005; Edge 2005). The cats were able to successfully reach into the tube when it was moved to one side of the recording alcove, and the cats notably attended to the target. Although this is consistent with the notion that it was a visually guided voluntary reaching movement, it does not exclude the possibility that the central position used in most of this study was a more habitual, less sensory driven behaviour. However, the fact that the introduction of the prism glasses was able to induce behavioural errors in the direction of the visual displacement lends further credence that the movements were indeed visually guided.

On initial exposure to the prism glasses, all three cats exhibited behaviours consistent with visuomotor adaptation; initially missing the target in the direction of the prism displacement and regaining accurate reaches after a few trials (mean trials ±SD= 10.5±7.9). Further evidence of a visuomotor adaptation process was found on removal of the prisms when all cats exhibited behaviour consistent with an after-effect. Overall, it seems reasonable to conclude that the prism glasses induced visuomotor adaptation in all three cats used in this study.

3.4.2 Cerebellar involvement in visually guided reaching

Infusion of lidocaine into the region of the cerebellar cortex region of interest led to an ataxic-like reaching behaviour of cat C, with slower reaches post infusion. This is consistent with prior literature suggesting that paravermal lobule V of the cerebellar cortex is involved in the control of voluntary forelimb movements (reviewed in Ishikawa et al. 2016), and confirmed accurate targeting of the chamber implant in cat C. Without the concurrent electrophysiological recordings, it was not possible to deduce whether the lack of behavioural effect of a similar infusion of lidocaine in cat B was due to a failure of drug infusion, or a genuine null effect of lidocaine on the reaching behaviour. Considering the overwhelming consensus that the anterior lobe including lobule V is involved in sensorimotor control of voluntary limb movements, it seems most likely that the infusion was unsuccessful.

In cat C, in addition to the ataxic-like reaching behaviour, the lidocaine infusion resulted in a return to intra-session adaptation, contrasting with previous recording sessions in which the cat was able to switch readily between prism-on and off conditions (discussed in section 3.4.4). This is similar to the effects of lidocaine infusion into the postero-lateral cerebellar cortex of monkeys (Norris et al. 2011). The monkeys had been trained on a prism-reaching task and successfully switched between no-prism and prism-on conditions without reaching errors. Infusion of

lidocaine immediately prior to putting prisms on re-invoked the classic prism-induced behavioural errors. However, these monkeys did not adapt to the prisms under the influence of the lidocaine (instead continuing to miss the reaching targets). In contrast, in cat C adaptation did occur to the prisms. This suggests the target area in the present study (lobule V, C2/ C3 zone) may not be involved in the process of adaptation *per se*, instead this may be a site of longer-term storage of the prism adaptation internal model.

However, the absence of an after-effect in cat C is noteworthy. An after-effect is considered the tell-tale sign that motor adaptation has occurred. It is possible that classical adaptation had not occurred during drug infusion in the prism-on trials. Instead, the cat may have implemented alternative mechanisms to overcome the perturbation, perhaps through aiming strategies or online correction of the movements. Given that the reaching behaviour at this stage was markedly slow, the latter explanation seems likely.

A similar experiment in monkeys also lesioned various areas of the cerebellar cortex and found that only lesions that covered the dorsal paraflocculus and uvula led to abolition of visuomotor adaptation, whilst lesions of areas including the paramedian lobule V did not (Baizer et al. 1999). Considering this, we cannot rule out that lobule V is not a site of adaptive processing during visuomotor adaptation, rather it is the posterior lobe that receives most of the visual-cortical originating mossy fibre inputs that underpin adaptive changes in these tasks (Baizer et al. 1999). Yet, human neuroimaging experiments suggest lobule V is activated during early stages of visuomotor adaptation tasks (Luauté et al. 2009; Donchin et al. 2012; Diedrichsen et al. 2005), and the complex spikes in the intermediate hemispheric lobules IV-VI of monkeys can encode reach error signals (Kitazawa et al. 1998).

Overall, the evidence from one cat suggests that local inactivation of the cerebellum is sufficient to disrupt the switch from a newly learned internal model to another. However, it remains unclear whether lobule V in cats is solely responsible for the process of forelimb visuomotor adaptation.

3.4.3 Savings

It has been proposed that savings are either a result of retrieving memories of prior successful actions (Huang et al. 2011), or instead an increased sensitivity to previously experienced errors (Herzfeld, Vaswani, et al. 2014). An experiment set up to distinguish between these two hypotheses found that the error-based model, was both sufficient and necessary for savings in a visuomotor task in humans, whilst the prior action model was neither sufficient or necessary for savings to occur (Leow et al. 2016). This suggests that the neural mechanisms occurring over

the different days of prism exposure are likely to remain essentially the same, but perhaps a greater gain in error-sensitivity in the latter days of exposure to the same perturbation.

Although not found to be statistically significant, all three cats appeared to show some evidence for an increased rate of adaptation over the 5 consecutive days of prism exposure that were studied in detail (increased rate inferred from fewer trials needed before establishing hits). The greater trend in the prism-on condition (**Figure 3.9**) compared to the prism-off condition (**Figure 3.10**) appears to be largely driven by the first day of right hand prism exposure, whilst subsequent days appear much closer to the number of erroneous reaches produced by left hand prism. Given that the right-hand prism direction was presented after the left-hand prism direction, this may indicate an interference effect of the previous perturbation schedule on the first exposure to the right-hand prisms. Such anterograde interference has been observed in force-field adaptation tasks in humans (Sing and Smith 2010). The authors propose that anterograde interference is explained by the contribution of a slow learning component of a multi-rate model (putatively proposed to be supported by posterior parietal cortex activity (Della-Maggiore 2004)), while the fast learning component (residing within the cerebellar circuitry (Smith et al. 2006)) is not responsible for the interference effect.

Taken together, although there appears an interference of the left-hand prisms on the rate of adaptation to the right-hand prisms, current theories suggest that cerebellar dependent, error-based learning mechanisms are not affected. Therefore, the data collected during the first day of right-hand prism adaptation has been retained for electrophysiological analysis reported in the next chapter.

3.4.4 Multiple internal models

The rapid cessation of intra-session adaptation in cats B and C after the first 5 recording days is notable. The ability to readily change the reaching behaviour in response to the altered condition (prisms on/off) without the process of iterative adaptation is likely a contextual switching behaviour in which the brain can readily call up pre-established internal models when the context of the task is changed (i.e. when the prisms are put onto the cat). The concept of individuals being capable of learning, maintaining and switching between multiple internal models is addressed by the MOdular Selection And Identification for Control (MOSAIC) model (Haruno et al. 2001), which has experimental evidence supporting it in humans (Martin et al. 1996b; Wada et al. 2003), and monkeys performing a prism based reach adaptation task (Norris et al. 2011).

In the present study, this apparent support of multiple internal models (one for prism off/prism on) was evidently robust to long periods of disuse, as shown by the failure of multiple weeks of reaching behaviour with no prism exposure to wash out the switching behaviour.

As the principal focus of this thesis is on neural processes supporting visuomotor adaptation, the data collected during these stages was not addressed. Nevertheless, it may be a useful paradigm to investigate the neural processes surrounding the switching of available internal models.

3.4.5 Exclusion of 'corrected hit' trials

'Corrected hits', being at the transition between misses and hits makes these reaches potentially interesting because they reflect a time when adaptation mechanisms are transitional. For instance, as the behavioural errors begin to cross into the boundaries of the individual's baseline variance, there is the possibility of a credit assignment problem in which the error may be a result of the perturbation (and so initiate the adaptive error-correction processes that are of interest to this study), or it may be assigned to the natural variance of that movement - potentially instigating alternative motor skill learning mechanisms rather than adaptive ones. Such decision making processes have been recently attributed largely with areas of the prefrontal cortices (Stolyarova 2018).

3.4.6 Considerations for the electrophysiological analyses

3.4.6.1 Behavioural variability

A major reason for analysing the behaviour exhibited during the task was to understand whether the reaching behaviour in each of the different conditions of adaptation was equivalent.

It is evident that there is significant variability in the basic measures of reaching behaviour collected during this study, both between individual animals (section 3.3.3.2), and across the stages of adaptation (section 3.3.4). Consequently, the behavioural differences may be a confounding issue when interpreting any effects in the neural data. As an attempt to combat this potential confound, the individual animals have been kept as separate case studies, and the reach metrics have been included as covariates in the analysis of electrophysiological data, reported in Chapter 4.

3.4.7 Analysis time windows

Following on from the analysis of the human EEG data (section 2.3.2), the key time-points of interest for the present thesis are during the movement preparation (during which the human EEG beta oscillations were significantly reduced in early adaptation), and immediately after the

movement (hypothesised as a critical time window for error processing and updating of internal models).

In the cats, reviewing the EMG signals shows that there is clear movement related activity prior to the paw lift-off signal (**Figure 3.5**, **Figure 3.6**, and **Figure 3.7**). To avoid analysis of data after the start of the up-swing of the forelimb (presumed to occur on increased activity of the cleidobrachialis flexor muscle), these averaged EMG signals were used to determine the 'pre-movement' period of data analysis, rather than the paw lift-off event marker. Consequently, the pre-movement analysis window was set from 400-200ms prior to the paw lift-off event marker, and a post-movement analysis window was set from 20-220ms after the termination of the outward reach (dictated by the tube entry/miss event marker).

3.4.8 Summary

The present results show that a visuomotor adaptation paradigm can be successfully applied to a cat forelimb reaching task. Two behavioural metrics, the reaction time and duration of the outbound reach, were assessed across the principal stages of adaptation and it was found that they varied significantly between the 3 animals. Accordingly, these metrics will be incorporated into the statistical analyses of the electrophysiological data as covariates to control for any effect they may have on the neural data described in the final results chapter.

Chapter 4 – Animal Visuomotor Adaptation. Part II. Electrophysiology

4.1 Introduction

Development of a forelimb reaching visuomotor adaptation task in the cat enabled direct interrogation of the neural activity within three nodes of the motor network (cerebellar cortex, M1, and medial PFC) during adaptation. This chapter will detail the electrophysiological data recorded and analysed from this task that complements the human work in Chapter 2.

4.1.1 Invasive neuroelectric recordings

Whilst the EEG data recorded from the human participants provides a readout of the synchronous activity of large neuronal populations, the spatial resolution of corresponding neuronal circuits is much finer. Moreover, as described previously (section 2.1.2.1), it was not possible to monitor cerebellar activity in the human study using EEG. In contrast, the use of an animal model allows for the implantation of recording electrodes into specific brain sites including the cerebellum. Behavioural information is likely to be encoded within the action potential activity (e.g. firing rate) of small clusters of individual neurons (Gallego et al. 2017; Li et al. 2001). Consequently, assessing the neuronal activity underpinning motor adaptation at multiple scales from the single cell to neuronal populations provides us with a much richer database from which to assess how the brain functions (during motor adaptation in this case). This includes direct measures of adaptation-related changes in neural activity and functional connectivity in and between all three of the principal regions under investigation in this thesis (cerebellum, M1 and PFC).

4.1.1.1 The local field potential

The Local Field Potential (LFP) is the low frequency component of an extracellular voltage recording, typically less than 100 Hz. Like EEG, LFP signals are commonly subdivided into frequency bands.

There is significant commonality in hypotheses of the functional role of these different oscillations between EEG and LFP in the cerebral cortices, and those relevant to the present study have already been discussed (section 2.1.1.1). Whilst the proposed roles of cortical oscillations have largely been reported to have similar interpretations between the EEG and LFP scales, the lack of a convincingly attainable cerebellar EEG has prevented a useful avenue of investigations into the causes and consequences of cerebellar generated rhythms. Nevertheless, there have been some attempts to establish this, and most of the current understanding has been encompassed in reviews by De Zeeuw *et al*. (2008) and Courtemanche *et al.* (2013).

Briefly, the granule cell layer networks, containing reciprocal connections between excitatory mossy fibre inputs, excitatory granule cells, and inhibitory interneurons, such as Golgi cells has been shown to generate rhythmic activity in the 13-18Hz (beta) range. This rhythmic activity is

most pronounced during periods of immobility in monkeys (Pellerin and Lamarre, 1997; cf. Courtemanche, Robinson and Aponte, 2013). By comparison, in the rat, granule cell related oscillatory activity has been reported at lower frequencies, within the range of standard definitions of theta (4-9Hz) frequencies (Hartmann and Bower, 1998; cf. De Zeeuw, Hoebeek and Schonewille, 2008).

These oscillations in the cerebellum have been proposed to aid in the organisation of cerebellar circuits in preparation for movement-related processing; with data from monkeys showing an enhanced magnitude of the oscillations in the paramedian cerebellar cortex during a delay period before an active forelimb movement (active expectancy), which was greater than during a passive waiting condition (Courtemanche et al. 2002). In the same series of experiments, Courtemanche and colleagues found these oscillations to be associated with the organisation of cerebello-cerebro networks, showing an enhanced phase synchrony between the cerebellar cortex and primary sensory cortex during the active expectancy condition (Courtemanche and Lamarre 2005).

Oscillations in the cerebellar cortex within gamma frequencies (30-80Hz) are proposed to originate from Purkinje cell activity and interneurons situated in the molecular layer (Middleton et al. 2008). Although the functional role of these higher frequency oscillations has not been addressed in the literature, preliminary evidence from a self-paced finger-tapping task in humans (recording cerebellar cortical surface activity by electrocorticography) suggests that cerebellar gamma rhythms are dynamic during the behaviour with an increase in power at the time of finger tap (Dalal et al. 2008). If cerebellar gamma rhythms are driven by Purkinje cell activity, this rhythmic activity may reflect a task dependent burst of oscillatory cerebellar cortical activity during active movements. Given that all cerebellar cortical processing must impact on Purkinje cell activity due to the circuit architecture, gamma rhythms may be the most reliable measure of changes in cerebellar cortical activity.

4.1.2 Cerebellar cortical zones

As the invasive recording electrodes enable a much finer spatial resolution than other techniques, it is appropriate to briefly note the finer anatomical details of the cerebellar cortex. The cerebellar cortex has been shown to be subdivided into anatomical zones, which send projections to distinct subregions of the inferior olive, and receive afferent inputs from distinct subregions of the cerebellar nuclei (Apps et al. 2018; Trott and Armstrong 1987).

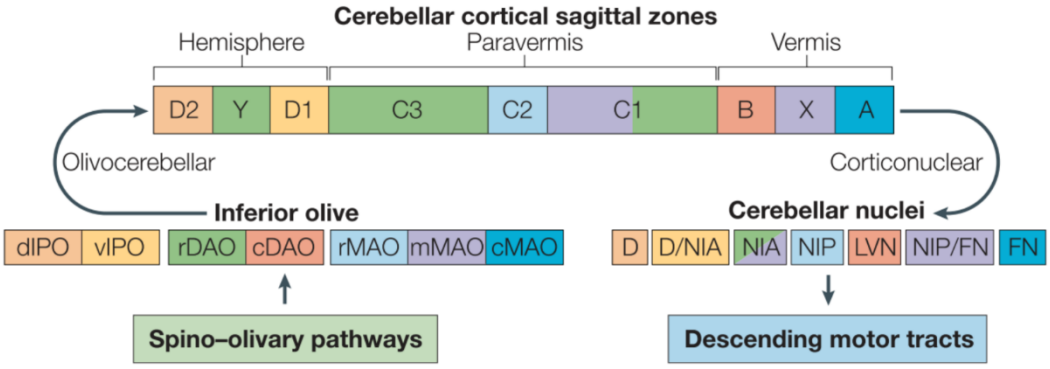

Figure 4.1 Cerebellar cortical zones and their afferent and efferent connection pathways.
Schematic representation of cerebellar cortical modules and their connections in cat. Modules are defined by their distinct olivocerebellar inputs from the inferior olive, and corticonuclear outputs to the cerebellar nuclei. Connected areas are shown in matching colours. Inferior olive abbreviations: - cDAO, caudal part of dorsal accessory olive; rDAO, rostral part of dorsal accessory olive; dlPO, dorsal lamella of the principle olive; vlPO, ventral lamella of the principle olive; cMAO, caudal medial accessory olive; mMAO, middle part of medial accessory olive; rMAO, rostral medial accessory olive. Cerebellar nuclei abbreviations: - D, dentate nucleus; FN, fastigial nucleus; LVN, lateral vestibular nucleus; NIA, nucleus interpositus anterior; NIP, nucleus interpositus posterior. Taken from (Apps and Garwicz 2005), *reproduced with permission of Springer Nature.*

Relevant to this study are the C1, C2 and C3 cortical zones within the cerebellar paravermis, that receive their olivary input from the rostral medial and ventral dorsal accessory olives respectively, and project to the posterior and anterior interpositus nucleus respectively. Further, C1 and C3 zones receive only ipsilateral forelimb projections through the ventral dorsal accessory olive, whilst C2 zone receives bilateral input through the rostral medial accessory olive (Oscarsson 1980; Apps et al. 1997; Oscarsson 1979). By stimulating the ipsi- and/or contralateral superficial radial nerve in the anaesthetised animal characteristic responses can be identified in each zone. Medially within paravermis, the C1 zone can be identified by a short latency (11-14ms) response evoked by ipsilateral limb stimulation only, whilst further laterally the C2 zone is identified by a longer latency (18-21ms) response evoked by ipsi-and contralateral stimulation (Apps et al. 1997). Lateral to the C2 zone can be found the C3 zone which has a similar pattern of response to limb stimulation as the medially located C1 zone (Trott and Apps 1991).

Based on previous work identifying the involvement of these paravermal zones in the control of visuomotor forelimb movements in the cat, these zones were the target of the present study.

4.1.3 Cerebello-cerebral functional connectivity

A key aim of this thesis was to investigate evidence of communication between the cerebellum and motor cortex over the course of a motor adaptation task. Previous work has linked the ascending drive from the cerebellum to cortical structures to supporting motor and sensory cortical gamma frequency connectivity (Popa et al. 2013). Specifically, pharmacological inactivation of the cerebellar interpositus nucleus with muscimol disrupted gamma band (25-49Hz) coherence between sensory and motor cortices during mouse whisking behaviours, indicating a cerebellar drive. Additionally, low frequency oscillations (5-12Hz) in the cerebellar

cortex and medial PFC of the guinea pig have previously been shown to become synchronised after presentation of a conditioned stimulus during early stages of a trace eyeblink conditioning paradigm, which positively correlated with adaptive performance (Chen et al. 2016). These data suggest a cooperative function between the medial PFC and cerebellar cortex early in the adaptation process.

4.1.4 Aims

Based on the observed decrease in beta band oscillation power during early adaptation of the pre-movement EEG recorded over the contralateral sensorimotor cortex in the human study, a key aim of the animal study was to assess whether a similar modulation of beta oscillations could be observed in the LFP signals recorded from the cat contralateral forelimb motor cortex and other nodes in the network (PFC and paravermal cerebellar cortex).

Additionally, the ability to record directly from the cerebellar cortex offered the opportunity to assess the functional connectivity between the cerebellar and frontal cortices over the course of the visuomotor adaptation task.

4.2 Methods

4.2.1 General surgical methods

As detailed in section 3.2.4, experimental cats underwent two surgeries to implant the electrophysiological recording and stimulation devices. For both surgeries, the same general anaesthesia and preparation procedures were followed, details of which can be found in section 3.2.4.3. Arrangement of the stimulator and recording electrodes and associated connectors followed the same plan for each of the animals, with any changes being minor and made on an ad-hoc basis during the surgery. A copy of the arrangement plan as used in the surgeries can be found in the appendix.

4.2.1.1 First surgery

4.2.1.1.1 Frontal craniotomy

Prior to any incision, the skin area was washed with a 5% hibitane solution. A midline incision to skin and scalp musculature was made from just caudal to the brow to the top of the neck. Skin and musculature were reflected laterally with skin retractors attached to the stereotaxic frame. Saline soaked surgical swabs were packed onto the exposed musculature to keep it hydrated throughout surgery. The exposed skull was scraped and washed with 70% ethanol to clean and remove remaining connective tissue.

A dental burr attached to a dental drill was used to shave down the occipital ridge, in preparation for the cerebellar implant during the second surgery. The burr was also used to create a small opening into the frontal sinuses to the left of midline, forming an “L” shape approximately 5x5mm. Next, a frontal craniotomy was made over the right hemisphere; starting at the approximate location of M1 (AP+23, ML+8) and expanded with rongeurs to span an area between the sagittal suture to 10mm lateral, and 8mm rostral from Bregma, to the coronal suture. The mucous membranes of the frontal sinus were removed with forceps and swabs and the sinus openings filled with gelfoam (Sterispon, Allan and Hanbury Ltd., UK).

The right M1 and PFC were revealed by making a small burr hole in the thin bone overlying it and clipping away the rest with small rongeurs. The dura mater was cut away using a fine hypodermic needle and iris scissors, revealing the whole area surrounding the cruciate sulcus. A sketch was made of the exposure detailing the cortical surface and vasculature for later use to map motor cortical responses (section 4.2.1.1.2). An image of the exposure can be seen in **Figure 4.2**. The exposure was then covered in saline soaked swabs to protect the exposed brain whilst preparations were made for the motor cortex mapping and probe implant procedure.

An anchoring T-bolt was secured into the “L” shaped slot over the left sinus with a small washer and nut. The nut was gently tightened to fix the bolt firmly, but not so to cause necrosis of the

bone. Two further burr holes were made near to the main exposure, and skull screws were partially screwed in to be later used as reference and grounding locations for the neural probes.

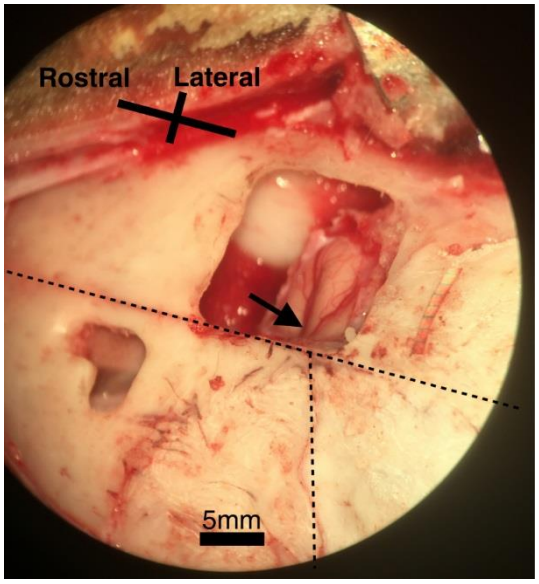

Figure 4.2 View of frontal exposure through surgical microscope.
Image taken through surgical microscope showing the exposed right motor and prefrontal cortex, and frontal sinus. Dashed lines indicate midline (left to right) and left coronal suture (top to bottom) intersecting at Bregma. Black arrow points to cruciate sulcus. 5mm scalebar shown at bottom of image.

4.2.1.1.2 Motor cortex physiological mapping

A micro-manipulator was fitted to the stereotaxic frame and a sprung ball electrode fitted. This electrode was connected to a constant current stimulator box (Digitimer Ltd.®, UK). The reference electrode consisted of a 1 inch 25-gauge hypodermic needle inserted into the exposed temporal muscles.

The swabs covering the brain were removed, excess moisture wicked away and the ball electrode was carefully positioned onto the surface of the brain around the cruciate sulcus. Bodily motor responses to motor cortex pulses (11 pulse 330Hz trains (Kobaiter-Maarrawi et al. 2011)) were observed and noted on the surgical sketch before moving the electrode to a new position and repeating the process.

A region corresponding to selective stimulation of the left forelimb was identified and selected as the target for the motor cortical probe implant. Once this was achieved, the electrophysiological equipment was removed from the theatre.

4.2.1.1.3 Motor cortex/prefrontal cortex probe implant

Two stereotaxic manipulators (David Kopf Instruments®, USA) were positioned on the stereotaxic frame, and the silicon probes were mounted to them using custom-made adaptors. The PFC probe was a 5mm, single shanked 16 channel linear array (site spacing 150µm), whilst the motor cortex was a 2mm, 16 shanked 'comb', with a single channel per shank, spaced 100µm

apart (NeuroNexus, USA). The probes were aligned over the identified regions of interest (PFC targeted by literature coordinates (Markowitsch and Pritzel 1977)), see **Figure 4.4A**. The probes were then carefully driven into the brain as per manufacturers' directions. The PFC probe was driven to a depth of between 4-6mm whilst motor cortex probe was driven to a depth of between 1-2mm.

The probe's reference and ground wires were then wound around the previously installed skull screws (one screw serving as the reference, and the other as the ground for both probes). In cats B and C, the cerebellar probe reference and ground jumper wires were also wound around the skull screws at this time. The screws were then tightened to clinch the wires in place. To protect the brain surface from damage, artificial dura compound (Dura-Gel, Cambridge NeuroTech Ltd., UK) was poured over the exposed brain tissue and a silicon sealant (Kwik-Cast™, World Precision Instruments, USA) poured on top of that.

The probes were then initially secured in place by building up a bridge to the t-bolt and skull screws using dental acrylic. Care was taken to build up enough cement without obscuring the area required for the peripheral implants. Once the cement had cured, the manipulators were gently removed from the probes, and moved caudal in preparation for the peripheral implants.

After the peripheral electrodes had subsequently been implanted (section 3.2.4.4), The excess peripheral cable was placed into the caudal aspect of the skin pocket made by the initial incision of the scalp. The skin pocket was then stitched firmly closed to the boundary of the headpiece using suture material (Ethicon, Johnson & Johnson Medical, BE). Recovery then proceeded as in section 3.2.4.6.

4.2.1.2 Second surgery

After the preparatory stages and anaesthesia had been completed as previously described, the scalp sutures from the first surgery were cut away, the sagittal incision re-opened, and the skin and muscles reflected away as before. Great care was taken to avoid severing the peripheral implant wires. Once again, the integrity of peripheral implants was confirmed with an isolated stimulator (Digitimer Ltd.®, UK), in case any repair to the peripheral implants were required.

4.2.1.2.1 Cerebellar craniotomy

After cleaning the skull surface with 70% ethanol, an orthopaedic burr attached to a dental drill was used to create an initial exposure at approximately 12mm rostral to the occipital crest, and 7mm left from midline. After confirming correct location by identifying the bony tentorium, the exposure was extended to between midline and 8mm lateral, and 8mm rostro-caudal to uncover an area over the approximate target area of the paravermis immediately lateral to the paravermal vein. The bony tentorium that occludes the target area was clipped away with

rongeurs. The dura mater was carefully removed, and a sketch made of the exposure and surface vasculature, to be used later as a map to mark neural probe target positions. An image of the exposure can be seen in **Figure 4.3**.

Saline soaked swabs were placed over the exposed brain to protect the surface. Next, up to 4 holes were made around the exposure and either t-bolts or skull screws secured at these points. These would later serve as anchoring points for the final implant headpiece.

4.2.1.2.2 Cerebellar cortical zone mapping

A fine manipulator was attached to the stereotaxic frame, and a small sprung ball electrode fitted to the manipulator. The electrode was connected to an analogue bandpass filter set to 30-5,000Hz, and then visualised on an oscilloscope. An earthing electrode was wrapped in saline soaked swab and placed in the cat's mouth, and a reference wire soldered to a fine hypodermic needle inserted into the reflected scalp connective tissue. Two fine hypodermic needles were inserted into the left forepaw to act as stimulating electrodes and these were connected to an isolated stimulator box (Digitimer Ltd.®, UK).

The protective swabs were removed from the cerebellar surface, and excess moisture wicked away. The ball electrode was placed on the cerebellar surface and single pulse stimuli were delivered to the left forepaw, gradually increasing the stimulus intensity to evoke a reflex twitch of the forepaw.

The cerebellar evoked field responses to the stimuli were observed on the oscilloscope, and the type of olivo-cerebellar zonal response noted on the sketched map at the position of the ball electrode. The electrode was then moved around the exposure to map the evoked responses across the exposure. Responses were classified according to previously defined response latencies and the presence of contralateral responses. Importantly, C2 zone were defined as having longer (19-27ms) response latencies to both ipsi- and contralateral stimulation, whereas C1 and C3 zones were defined as having shorter (12-16ms) response latencies only to ipsilateral stimulation (Trott and Armstrong 1987; Ekerot and Larson 1979). C1 and C3 responses were differentiated by the anatomical location, with C3 lying further lateral than the C2 zone.

Once the boundaries between C1, C2 and C3 zones had been identified. The exposure was re-covered with a saline soaked swab whilst the electrophysiological equipment was removed.

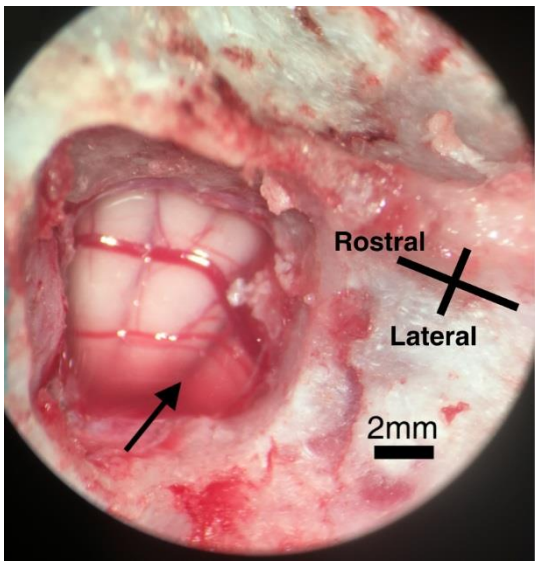

Figure 4.3 View of caudal exposure through surgical microscope.
After removal of the bony tentorium, the lobule V target region is clearly visible. Black arrow indicates the primary fissure, and the thick red paravermal vein can be seen running rostro-caudally. Scale bar is an approximation.

4.2.1.2.3 Cerebellar cortex probe alignment and implant

The cats were next implanted with either neural probes (cat A) or a recording chamber (cats B and C).

In response to the failure of the chronically implanted silicon electrode arrays to yield extracellular spiking activity in cat A, the decision was made to alter the cerebellar implant design to incorporate acutely implanted electrode arrays. This enabled electrodes to be advanced into the cerebellar cortex each day, 'hunting' for spiking activity with much fresher electrodes. This was intended to overcome the impact of a glial scar forming around the electrode shank, insulating the electrode from neural activity- a known issue in long-term neural recordings (reviewed in Polikov et al. 2005).

Cat A probe implant

Two 16 channel silicon probes (Cambridge NeuroTech Ltd., UK) were manoeuvred using stereotaxic manipulators to target a region within the C1 zone, and the other to a C2 zone according to the physiological mapping. Advancement of the probes into the brain proceeded as per the manufacturer's instructions. Once this was achieved, they were initially secured to nearby t-bolts with small amounts of dental cement. Both neural probes were connected via ribbon cables to an Omnetics interface board, allowing a single Omnetics Neuro Nano connector (Omnetics Connector Corp., USA) to be used. The interface board was cemented to the skull with dental cement and reference/ground wires secured to nearby skull screws, which were then tightened to clinch the wires tightly.

Cats B and C chamber implant

A custom made polyeteretherketone cylindrical chamber was selected from the range of sizes available to be able to span the depth between the cerebellar surface and the desired height of the chamber above the skull (accounting for the additional height of the final implant headpiece).

The chamber was attached to a stereotaxic manipulator, and then manoeuvred such that the bore of the chamber overlay a region of the cerebellar exposure spanning the C2/C3 boundary (see **Figure 4.4**). Care was taken to ensure that the chamber was not positioned in such a way that the electrode drive towers would not foul the connectors already implanted in the first surgery. The chamber was then fixed in place with dental cement, anchoring the chamber to the surrounding t-bolts. Once the initial anchoring cement had cured, the manipulator was carefully removed, and the position of the chamber bore confirmed to be over the lobule V target region.

Once the manipulator had been removed, the brain surface within the chamber was covered with some artificial dura and approximately 6mm of silicon sealant (Kwik-Cast™, World Precision Instruments, USA). Once the sealant had cured, a Nylon cap was tightened onto the chamber with a worm screw.

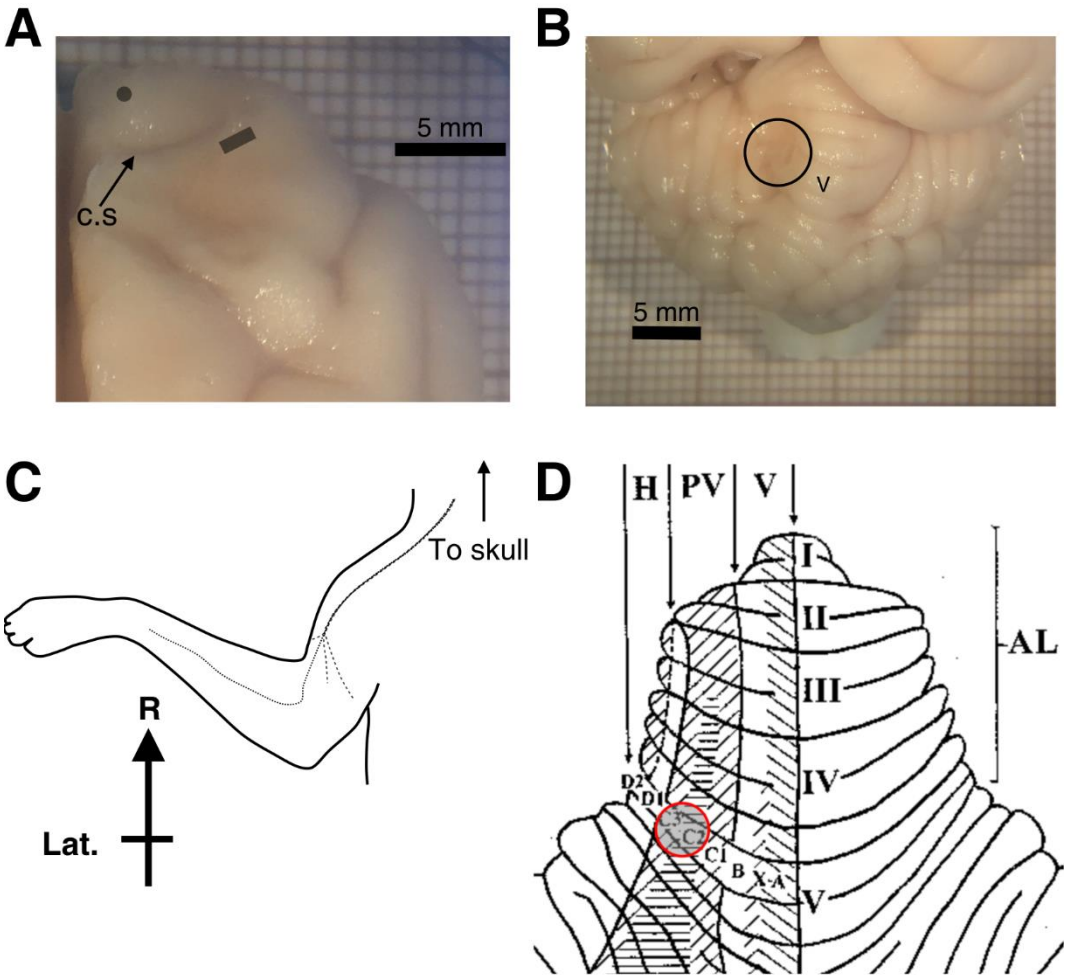

Figure 4.4 Locations of recording and stimulator electrodes.
A *Whole brain image of cat C left forebrain (post mortem) showing implant location of Pfc (grey circle) and M1 (grey rectangle). Location of the cruciate sulcus (c.s.) noted.* ***B*** *Whole brain image of cat C cerebellum showing extent of cerebellar chamber implant area (black circle). Location of lobule V indicated.* ***C*** *Schematic of dorsal view of left forelimb, as presented during surgery, showing routes of peripheral implant wires (dashed lines). The longest line indicates radial nerve stimulator and paw contact signal detector, shorter lines indicate EMG electrodes to cleidobrachialis, and the long and lateral head of the triceps.* ***D*** *Schematic of anterior cat cerebellum showing the extents of the cerebellar cortical zones. Target location for cerebellar recordings denoted by red circle. Adapted from Apps 1999, with permission of Elselvier Science.*

4.2.2 Electrophysiological recordings

During the daily recording surgeries, the recording equipment, booted up prior to the animal being brought to the recording room, was plugged into the head implant as required and the cable umbilicus arranged to avoid interference with either the view of the video cameras, or movement of the cat's head.

In cats B and C, the cerebellar probe needed to be driven down into the brain. This was done using the computer controlled microdrive towers on the recording stage (NaN Instruments Ltd., IL). The recording probe was driven slowly, with an audio output of a single channel played through speakers and visualised on an oscilloscope. The operator(s) listened to the tell-tale sounds of neuronal activity, such as a sudden increase in background activity noise indicating successful penetration of dura. If a single unit or robust multi-unit activity could be identified

and appeared stable, then the approximate depth of the probe was noted using the scale on the drive towers, recording of the datafiles was commenced and the session proceeded. Alternatively, if no unit activity was apparent within a reasonable time, the probe was halted at a depth similar to previous days, and the session proceeded.

Signals captured using the Neural Signal Processor, were captured at either 2kS/s (cat A) or 10kS/s (cats B and C). Continuous neural data was amplified and filtered by the Front-End Amplifier (1st-order high-pass, 0.3Hz and 3rd-order low-pass, 7500Hz), digitised and passed to the Neural Signal Processor. They were then filtered (4^{th} order digital Butterworth low pass 500Hz filter), and an adaptive line noise cancellation implemented to reduce power-line interference. EMG signals were filtered by a custom-made analogue filter bank (30-5kHz Bandpass) before being passed to the Neural Signal Processor. Event Marker channels underwent no filtering process. Raw data was also captured at 30kS/s. The Neural Signal Processor saved continuous data files to a native format (.nsX) onto the PC's hard drive.

4.2.2.1 Field potentials and receptive fields

Once the reaching data had been captured, the neural filter settings were switched to allow observation of evoked field potentials (30-2500Hz bandpass 4^{th} order digital Butterworth), and new recording files were initiated.

Isolated stimulator boxes (Digitimer Ltd.®, UK) were used to deliver a low intensity (non-noxious) periodic paired-pulse stimulation to either the ipsi- or contralateral limb via the peripheral superficial radial nerve cuffs. The stimulation intensity was started at zero, and gradually increased until a small, but robust limb twitch was observed. As the strength of the evoked twitch was variable, changing with the cat's posture, the stimulus intensity was adjusted accordingly to maintain the small but robust twitch.

Whilst the peripheral stimulation was occurring, the cerebellar recordings were visualised on an oscilloscope to look for signs of an evoked response. If signs of a response were observed, the latency of response was used to establish a cerebellar cortical zone (see section 4.2.3.3), and these were noted.

4.2.2.2 Data storage

At the completion of each recording session, electrophysiological and video recordings were terminated, the umbilicus cables were disconnected, and the cat returned to the home pen. Data files from both PCs were uploaded to a secure network server for later offline analysis.

4.2.3 Data analysis

Modern literature is awash with different methods of extraction, pre-processing and analysis of extracellular signals with little standardisation, especially regarding LFP signals. The analysis in the present thesis takes the conscious philosophy of 'less is more', with the minimal amount of pre-processing performed as possible to retain closeness to the original recordings.

All analyses of the extracellular recordings (both LFP and spike train data) were performed offline using custom MATLAB 2016a functions.

4.2.3.1 LFP recordings

4.2.3.1.1 Neural data pre-processing and trial extraction

The raw .ns6 files were imported from the data repository servers, and data back-converted to voltage readings. To remove the influence of movement related artefacts and other non-neuronal sources of noise, four pre-selected channels from each neural electrode array were averaged together and re-referenced to the averaged signal from four other (distal) sites on the same electrode, resulting in bi-polar electrode recordings from within the local area (approximate distance of 1.2mm between these 'virtual channels'), see **Figure 4.5**.

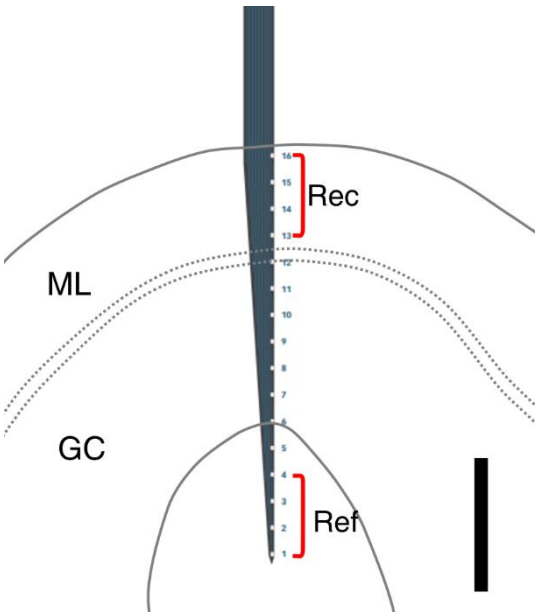

Figure 4.5 Schematic of implanted location of cerebellar electrode.
Indication of ideal recording locations obtained from cerebellar cortical recordings. ML; molecular cell layer. GC; granule cell layer. The recording sites indicated located in the molecular cell layer, whilst reference sites are in the white matter below the cortical lobule. Exact location of electrode sites relative to cortical layers cannot be guaranteed due to variable implant angles and unknown cortical fold arrangement. The four electrodes selected as reference sites for the four recording pseudo-tetrode sites indicated by red braces. Black bar denotes 500um scale.

The re-referenced neural signals were then lowpass filtered (100Hz corner frequency) with a 4th order Butterworth digital filter run forwards and backwards to prevent phase distortion. This also served as an anti-aliasing filter before data was down-sampled to 500S/s for computational efficiency and data management. An additional high pass filter (4Hz corner frequency) with a 4th

order Butterworth digital filter run forward and back over the data. Finally, a 4th order Butterworth notch filter (47-53Hz corner frequencies) was applied forwards and backwards to remove any mains line noise.

Two second epochs of data were extracted, centred on the paw lift-off event marker timestamps (i.e. one second either side), from reach trials. Trials were then inspected for the occurrence of obvious electrical artefact during the epochs and these trials were removed from the dataset.

Given that recordings were made on multiple days, and the cerebellar electrodes used for cats B and C were to be plugged in and implanted each day, it was possible that there would be variation in the recorded signals over the different days due to a myriad of factors (for example the fractional changes in impedances of the cerebellar electrode sites). To account for any day-to-day variation of local field potential oscillations, the time series data was z-score normalised to same-day-trials.

After this pre-processing of the data, trials were subjected to time-frequency decomposition to extract frequency and phase information.

4.2.3.1.2 Wavelet analysis

The individual trial data was subjected to the same wavelet decomposition algorithms as used in the human study (section 2.2.7.3.2). After computing the time-frequency wavelet power and phase synchrony from the neural signals, the data within specific windows of interest (200-to-400ms prior to paw lift-off and 20-to-220ms post reward-tube entry/miss) was extracted. For each trial, the median values of both time and frequency dimensions were computed from within the specific windows of interest. This provides an estimate of the state of the ongoing frequency activity at these times of the reaching behaviour. This data was the stored and subsequently used for statistical analysis in this thesis.

4.2.3.2 Single unit recordings

During the daily recording sessions, any apparent spiking activity was noted as to which channel it appeared on, what the general features may be (single/multi-unit activity, presence of a complex spike). This information was used as a guide for the offline channel selection protocols described below.

It should be noted that the height of the electrode drive towers made them susceptible to unstable recordings with movement of the animal's head. This was a greater issue in cat B who tended to make short-sharp head movements, following actions of the reward tube operator (such as when replacing fish reward into the back of the tube).

Each daily recording was imported into Spike2v7 (Cambridge Electronic Design, UK) for manual visualisation and identification of candidate channels for spike extraction. Once candidate channels were identified, they were grouped into 'virtual tetrodes' comprising of 4 proximal channels. This was a requirement of the spike sorting software used (described below).

4.2.3.2.1 Spike extraction

Raw recordings were imported into MATLAB 2016a and back-converted to voltage readings. If multiple recording files had been made on a given day, these were appended onto one another. The previously identified virtual tetrodes were isolated in the recordings and subsequent extraction was performed on these individually.

Data was bandpass filtered (500-10000Hz corners) using a 4th order digital Butterworth filter run forwards and backwards over the data. This filter is in line with previous work on cat cerebellar spike recordings (Edge 2005; Cerminara et al. 2009).

Spikes were next identified using a non-linear (squared) energy algorithm (Mukhopadhyay and Ray 1998) (available courtesy of M. Gaidica as a MATLAB toolbox from https://github.com/LeventhalLab/EphysToolbox). Simply, this outputs timestamps of detected spikes above a user chosen threshold after squaring and applying a cost function based on neighbouring samples to the input signal. In lay terms, this non-linear approach amplifies narrow, spikey features, whilst broader features are amplified less, thus improving the signal to noise ratio in neuroelectric recordings and allowing more precise thresholding. The timestamps of identified spikes were saved for subsequent spike sorting procedures.

4.2.3.2.2 Spike sorting

MClust, a MATLAB based application (A.D. Redish, University of Minesota, USA) was used to cluster and sort the detected spikes. This was chosen over other programmes due to the lab's familiarity with its use, as well as its implementation of the popular KlustaKwik sorting algorithm. A consequence of this was that only 4 channels could be handled at a time, requiring the creation of the virtual tetrodes. Due to the large physical separation of channels (consecutive sites 50µm apart) compared to standard wire tetrodes, there was less chance of detecting the same neuron across multiple virtual tetrodes. Moreover, of visual inspection of the data, it appears that the silicon probes offered very good discrimination between sites, with even strong single unit recordings being isolated to only one channel (see **Figure 4.18** for example). A second consequence of using MClust was that it considers only 32 data samples centred around the peak of the spike timestamp. Using a sample rate of 30KS/s meant that the sorting window was 1.07ms wide. Whilst this is enough to encompass a standard spike event, it is not long enough to encompass the expected duration of Purkinje cell complex spikes. Thus, the current spike

sorting techniques would not be sufficient to isolate and extract complex spike activity. As a result, the data presented in this thesis focusses on the simple spiking activity of putative Purkinje cells, and does not attempt to consider adaptation related changes in complex spiking activity.

Spike times and the 32 data point waveforms from the spike extraction routine were imported into MClust, and four features of the detected spikes were used for the clustering algorithm: waveform peak, waveform trough, spike energy, and the 1st principle component.

After implementing the automated clustering algorithm in MClust, returned clusters were then manually inspected and assessed according to the following criteria. To be considered as a single unit, a cluster's Isolation distance had to be equal to or above 15, the L-ratio less than or equal to 0.35, and the number of inter-spike intervals less 2ms had to be less than 1% of the total number of spikes. Details of these measures of cluster quality have been described previously (Schmitzer-Torbert et al. 2005; Schmitzer-Torbert 2004).

4.2.3.2.2.1 Identification of putative Purkinje cells

As the principle output neuron of the cerebellar cortex, a focus has been put on analysis of the spiking activity of these cells. The presence of a complex spike in a unit recording is the gold standard for identifying the presence of a Purkinje cell (Miles et al. 2006), however it is not always possible to comprehensively identify complex spikes especially in the context of awake animal recordings (Edge 2005). A common approach in lieu of identifiable complex spikes is to classify putative Purkinje cell simple spikes based on features of their waveform and inter-spike interval histograms (Marple-Horvat et al. 1998; Cerminara et al. 2005; Miles et al. 2006; Cerminara et al. 2009).

For the purposes of this thesis, single units have been identified as putative Purkinje cells if the spike width of the average waveform was approximately between 0.4-0.8ms (Armstrong and Rawson 1979) and a median inter-spike interval above 35Hz, displaying a 'narrow' positively skewed inter-spike interval histogram (Marple-Horvat et al. 1998). This is in contrast to other cortical neurons including Golgi cells, which have typically longer duration spikes, and a lower tonic firing rate between 7 and 21 spikes/second (Edgley and Lidierth 1987; Edge 2005), and mossy fibres, which have a wide dynamic range of discharge rate, resulting in a wide, flat inter-spike interval histogram (Garwicz and Andersson 1992).

4.2.3.2.3 Single unit analysis

To establish whether any of the putative Purkinje cells in the present recordings had altered firing rates in relation to the reaching movements, peri-event time histograms (PETHs) were computed around the paw lift-off event marker, as well as the reward tube entry/miss

timestamp. Spikes were sorted into 20ms bins for ±1000ms around each event marker. Responses were deemed significant if two consecutive bins fell outside 2SD of a baseline period defined between -1000 and -500ms prior to the paw lift-off event marker- representing a period when the animal would not have been actively reaching (Cerminara et al. 2009). Further, to assess tonic changes in discharge rate, the mean rate for the 200ms period prior to the movement initiation (-400 to -200ms pre paw lift-off, see section 3.4.7) was compared to the 200ms immediately following paw lift-off by means of a student's t-test (Edge 2005).

4.2.3.3 Statistical analysis

As with the behavioural data, the unbalanced nature of motor adaptation (target misses being less frequent than target hits), the generalised linear model was the preferred parametric model. All electrophysiological data appeared approximately normal (after log normalising wavelet power data) and so a generalized linear model was set with a normal distribution and an identity link function.

Moreover, following the analysis of the reaching behaviour revealing significant variation in reaching parameters (reaction time and reach duration) across the adaptation behaviour (section 3.3.4), as well as previous literature indicating that LFP oscillations may encode such kinematic parameters (Flint et al. 2012; Mehring et al. 2003), these were included in the statistical model as covariates.

Evaluating whether the single-trial phase locking values at a given frequency are statistically significant is achieved by comparing them to a surrogate data set in which the phase relationships of the original data is randomised. To this end, a surrogate trial was created with randomised phase differences, and the phase-locking values for all frequencies computed and stored. This process was repeated 10,000 times, generating a null distribution of phase-locking values for each frequency of the wavelet transforms, against which the experimental data could be compared.

4.3 Results 1 – localisation of cerebellar recordings

During the implantation of the cerebellar recording probes in cat A, evoked fields were initially recorded on the cerebellar cortical surface evoked by stimulation of the superficial radial nerve in the ipsilateral and contralateral forelimbs (**Figure 4.6**). This allowed mapping of the location of the paravermal cortical zones to guide the implantation of the chronic recording probes (section 4.2.1.2.2). One probe was implanted into a cortical region where C1 zone responses were recorded on the surface, while the second probe was implanted approximately 1.4mm further laterally where C2 zone responses were recorded on the surface. For purposes of identification, the two probes are termed accordingly.

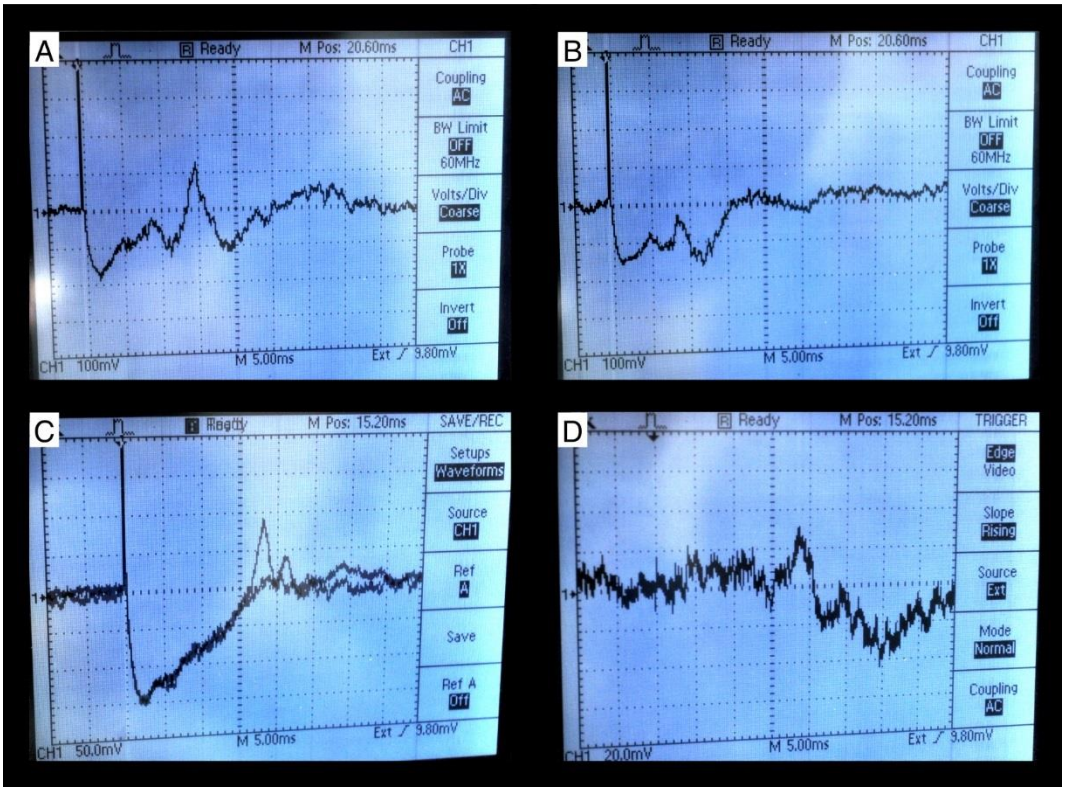

Figure 4.6 Images of example evoked fields recorded during surgery.
*Images of oscilloscope screen taken during cat A's surgery. **A** and **B**; C1 zonal responses to ipsilateral forelimb stimulation, latency of responses was ~11ms and ~7ms respectively. **C** and **D**; C2 zonal responses to ipsilateral stimulation (null response to contralateral stimulation not imaged). **C** shows a double trace of two stimulation events, one response latency ~17ms, second response latency ~20ms. Stimulation intensity turned down for image D, removing large negative deflection after stimulus artefact. All oscilloscope scales; 5ms/ 100mV per large division.*

4.3.1 Differential LFP signals across cerebellar cortical zones

A comparison of the LFP power

spectrum between the C1 and C2 localised probes was made to identify any differences between these recording sites. Trial averaged power spectra were compared over the 2 second reaching epochs made during the 179 baseline reaching trials (**Figure 4.7**). The C1 zone probe had stronger theta and high gamma band oscillations (4-9Hz and 50+ Hz respectively), whilst the

C2 zone probe had stronger beta and low gamma band oscillations (10-30Hz and 30-50Hz respectively).

These observed differences were statistically significant for all frequency bands, tested with a two-way mixed model ANOVA (interaction between electrode and frequency; $F_{(3,782.632)}$ = 361.466, p<0.0005. Paired sample t-tests subsequently run on each frequency band; theta $t_{(178)}$=4.809, p<0.0005, beta $t_{(178)}$=-14.378, p<0.0005, low gamma $t_{(178)}$=-6.1, p<0.0005, high gamma $t_{(178)}$=31.639, p<0.0005).

Given these differences it seems reasonable to conclude that the C1 and C2 probes were recording at least partially distinct LFP signals. The data have therefore been analysed separately in the following results.

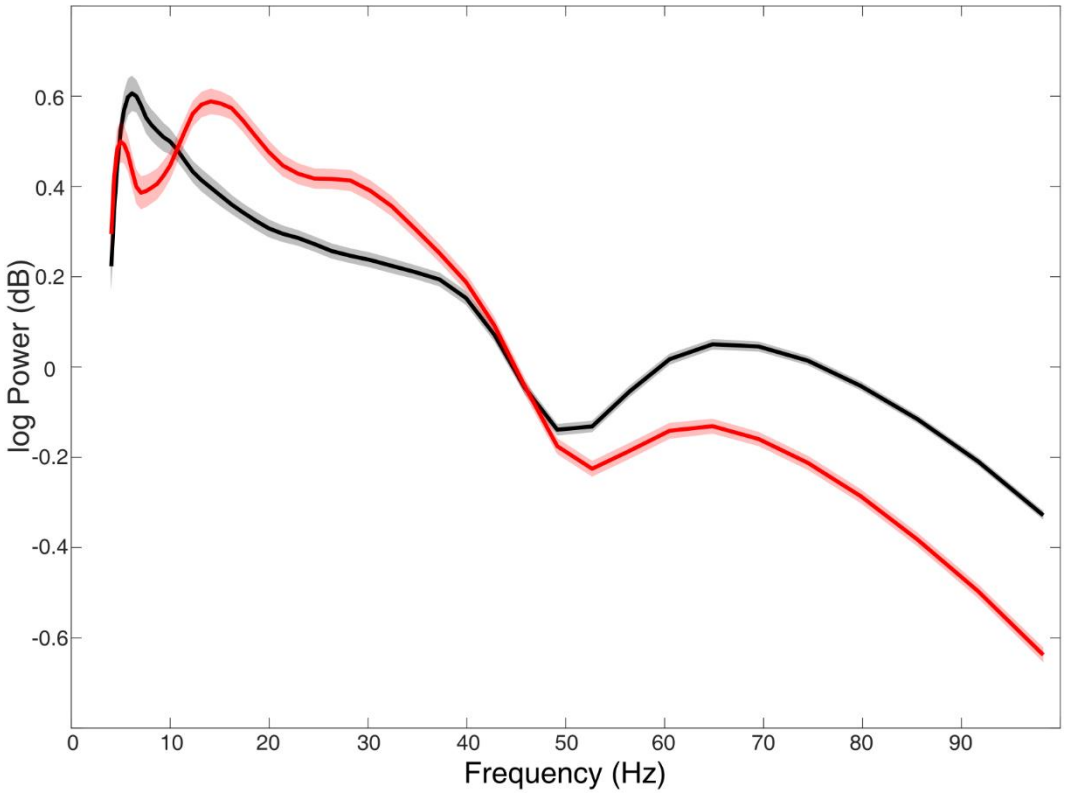

Figure 4.7 Comparison of C1 and C2 localised power spectra in cat A.
Mean power spectra during baseline trial 2 second epochs. Black line denotes trial averaged spectrum for C1 localised electrode, red line denotes trial averaged power spectrum for C2 localised electrode. Shaded areas indicate 95% confidence of the mean for each electrode.

In cats B and C during implant surgery, evoked field potentials were mapped on the cortical surface identifying the C2 and C3 zones. However, in these animals a different design of chamber was used which allowed electrodes to be introduced temporarily into the brain during recording sessions (rather than permanently at the initial implant as in cat A, see 4.2.1.2.3). As a result, we attempted to record evoked fields during individual behavioural recording sessions to determine the cerebellar zones being recorded from on each day.

Evoked field responses were isolated in Cat C but not Cat B. The responses were mainly consistent with recording from the C2 zone, with only one day resulting in C3 zone (**Figure 4.8**). Given the lack of identifiable evoked responses in cat B, and the evidence that both C2 and C3 zones were recorded from in cat C, the electrophysiological results from cats B and C should be considered as deriving from a mixture of the C2 and C3 zones of lobule V.

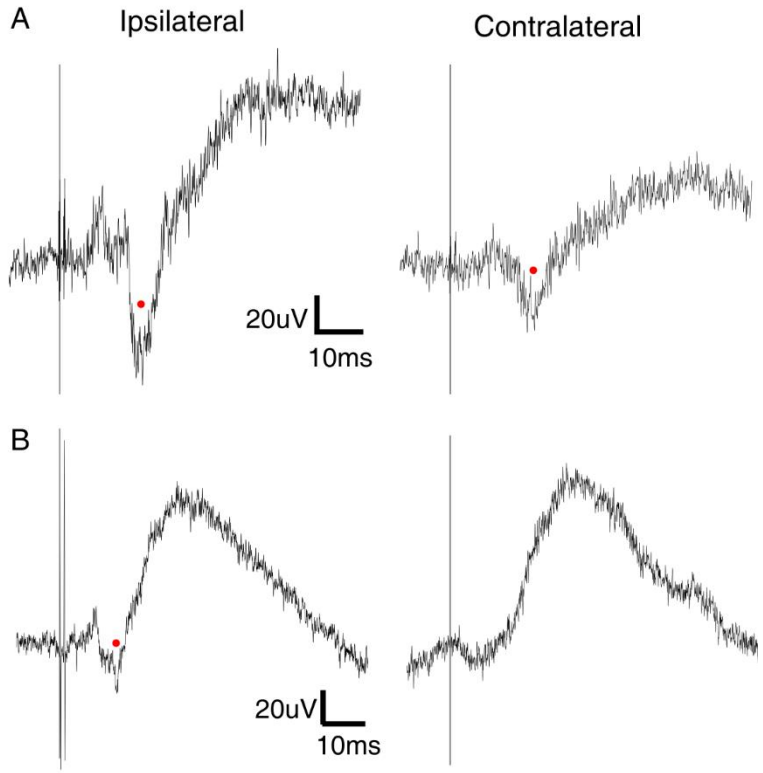

Figure 4.8 Example evoked field responses in cat C.
Averaged responses (n=20) aligned to the stimulation. ***A****. Bilaterally evoked response occurring at 15ms post stimulus, indicates C2 zone.* ***B****. Evoked response at 10ms post stimulus, only during ipsilateral stimulation putatively indicates C3 zone. Red dots indicate maximal evoked response, grey vertical bars denote time of peripheral nerve stimulation.*

4.4 Results 2– Local field potentials

4.4.1 Local field potential spectral power changes during reaching

Figure 4.9 shows an example spectrogram revealing the dynamic nature of the frequency components of the LFP signal recorded from the motor cortex in cat A during the reaching task. For ease of visualisation of the whole frequency spectrum (overcoming the 1/frequency scaling property of LFPs (Buzsáki et al. 2012)), the data have been adjusted by dividing by its wavelet scale ('adjusted power' **Figure 4.9B**). Note that this adjustment is for visualisation only. All quantitative analysis is performed on the original power data computed from the wavelet transform.

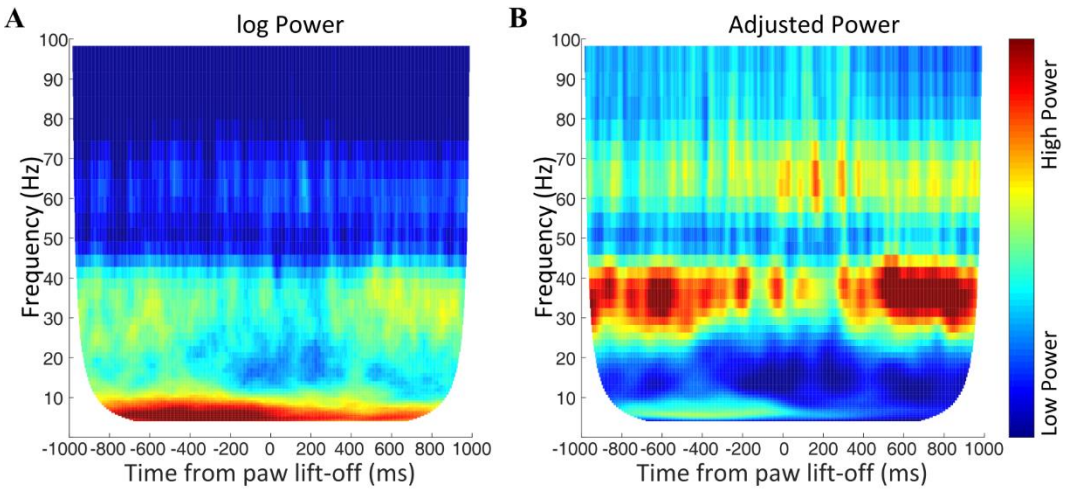

Figure 4.9 Baseline trial averaged time x frequency spectrograms for cat A motor cortex.
Trials aligned to paw lift-off event marker. White space indicates data potentially unreliable due to edge effects (cone of influence). Colour bar indicates spectral power, note that the units are not equivalent between the two plots. ***A*** *log normalised power showing non-stationary spectral components of the LFP during reaching* ***B*** *Adjusted power better shows the dynamic nature of spectral features at all frequencies. Note the broad patterning is the same as observed in the log normalised power, but now we are better able to observe a band of power between 60-80Hz.*

During the period 500-1000ms prior to paw lift-off, there is an increase in the 4-10Hz frequency band (theta), another more prominent increase between 25-40Hz (low gamma). After paw lift-off, there is also an increase in a 60-80Hz band (high gamma).

There is also a decrease in beta frequency power (defined here as 10-25Hz to distinguish from the theta and low gamma bands), that occurs approximately 300-400ms prior to paw lift-off, and continues until approximately 400ms after paw lift-off. This movement related decrease in beta power is well reported in the literature (Chung et al. 2017; Feingold et al. 2015; Hosaka et al. 2016; Khanna and Carmena 2017; Engel and Fries 2010). Similarly, the increase in high gamma frequency power (60-80Hz) during movement (0-400ms after paw lift) is another feature that is consistent with previous literature on movement related oscillations in the motor cortex (Nowak et al. 2018; Ball et al. 2008). Taken together this suggests that the pre-processing of the data in the current experiments has been effective at extracting neural related LFP signal from noise.

4.4.2 Beta oscillations during adaptation

4.4.2.1 Motor cortex

One of the chief aims of the animal-based experiments was to determine whether similar frequency band LFP signals were present to those found in the human EEG experiments, using a similar task. A key finding of the human study was that, prior to the reaching movements, beta oscillations in the EEG signal recorded over the contralateral sensorimotor cortex that occurred were decreased during early adaptation (section 2.3.2.2.1.1). **Figure 4.10** shows the corresponding pre-movement Beta (10-25Hz) LFP data recorded from the forelimb region of the contralateral motor cortex in each animal.

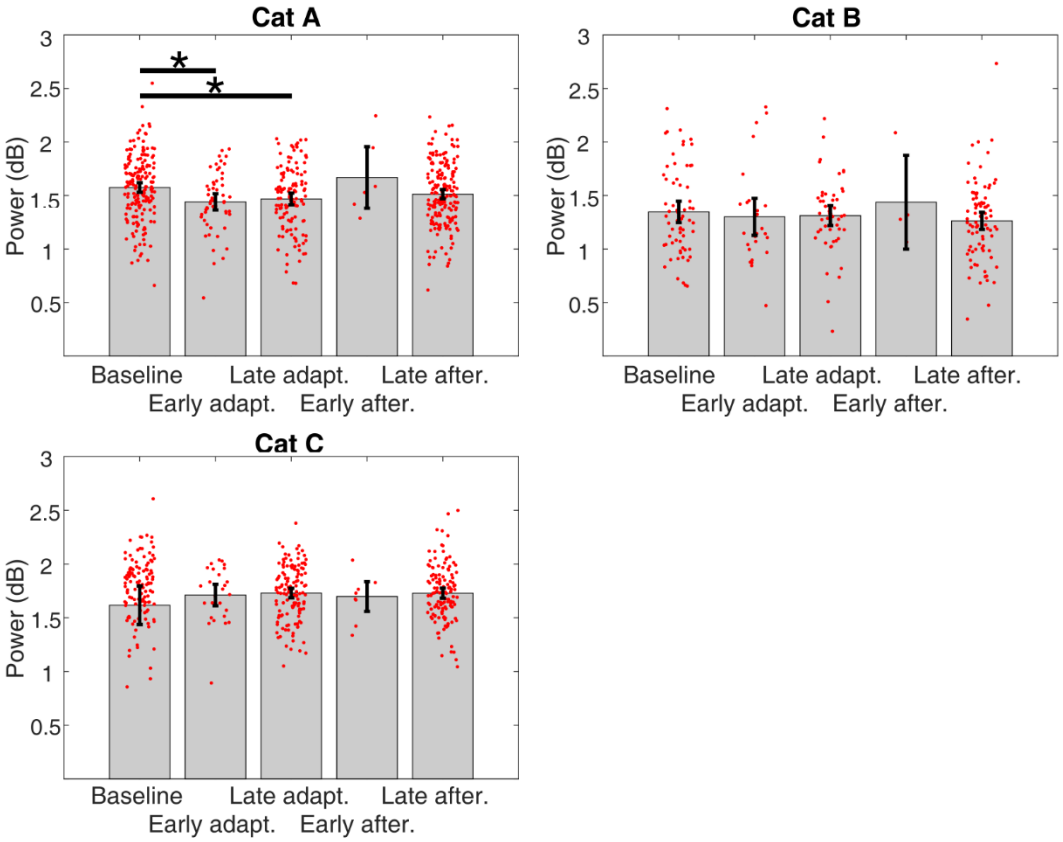

Figure 4.10 Pre-movement beta power modulation in forelimb motor cortex.
Bar charts showing trial averaged beta power (10-25Hz) during different stages of adaptation. Error bars indicate 95% confidence of the mean. Asterisks and bars indicate Bonferroni corrected comparisons (p<0.05). Red points indicate individual trial data.

According to a generalized linear model, cat A was the only animal with statistically significant differences across the adaptation phases (Cat A; Wald $\chi^2(3)=10.79$, p=0.013. Cat B; Wald $\chi^2(3)=1.738$, p=0.629. Cat C; Wald $\chi^2(3)=1.625$, p=0.654). Specifically, compared to baseline, both early and late adaptation phases had statistically significant decreases in beta power (Bonferroni corrected p-value: Baseline-early adapt. =0.01, Baseline-late adapt. =0.06, Baseline-late after. =0.395). Whilst not statistically significant, the data from cat B does show a similar trend to that of cat A, with a small decrease in power relative to baseline in both adaptation phases. Regarding the early after-effect trials, both cats A and B show a non-significant increase in power compared to baseline trials. Conversely, cat C shows little change in beta power across stages of adaptation.

In contrast to the human EEG data, the modulation of beta power in cat A did not appear specific to the pre-movement period. Indeed, the statistically significant decrease is evident in a post-movement time window; Wald $\chi^2(3)=27.919$, p<0.0005 (**Figure 4.11**). Further, Bonferroni corrected comparisons revealed that in the post-movement window, there was also a significant decreased power in the late after-effect trials (Baseline-early adapt. p<0.0005, Baseline-late

adapt. p<0.0005, Baseline-late after. p=0.013). Again, neither cats A or B showed a statistically significant effect of adaptation (Cat B; Wald $\chi^2(3)=7.922$, p=0.048, all Bonferroni corrected p-values for comparisons to baseline >0.05. Cat C; Wald $\chi^2(3)=3.101$, p=0.376).

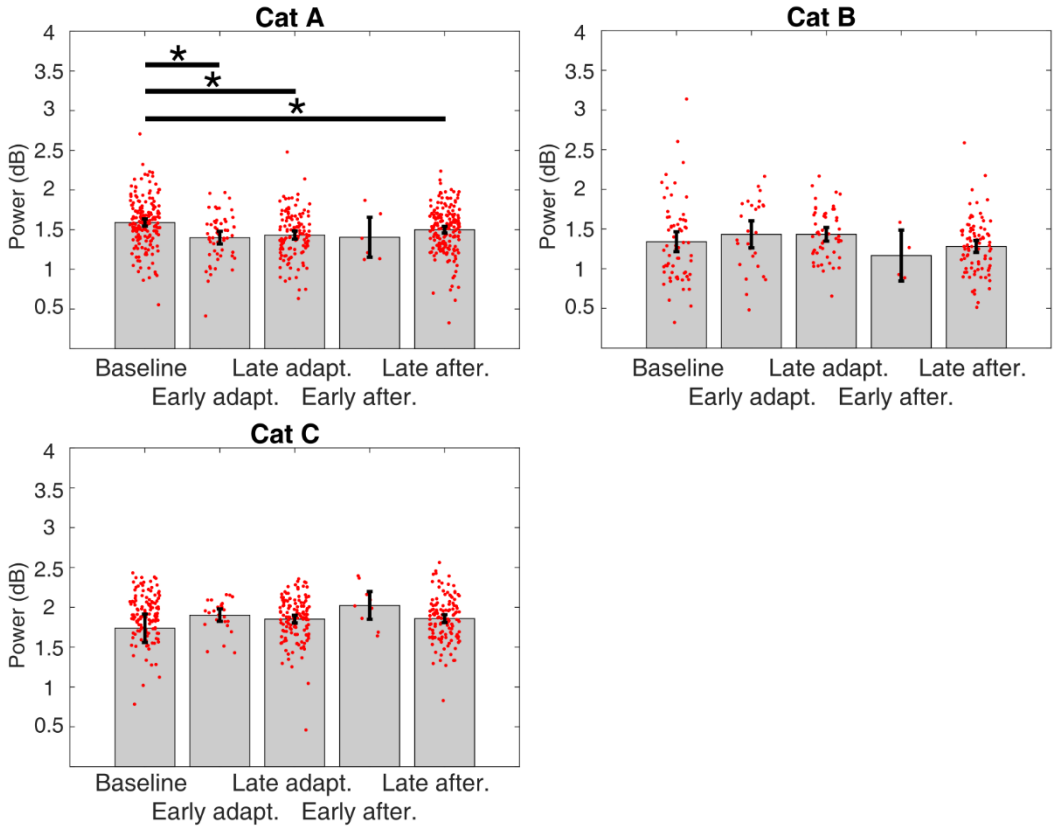

Figure 4.11 Post-movement beta power modulation in forelimb motor cortex.
Bar charts showing trial averaged beta power (10-25Hz) during different stages of adaptation. Error bars indicate 95% confidence of the mean. Asterisks and bars indicate Bonferroni corrected comparisons (p<0.05). Red points indicate individual trial data.

4.4.2.2 Cerebellar cortex

As discussed in section 4.1.1.1, beta oscillations have been proposed to be driven by granule cell layer networks in the cerebellar cortex (De Zeeuw et al. 2008), and have been associated with cerebro-cerebellar communication during movement tasks.

Figure 4.12 shows trial averaged beta power in the cerebellar cortex during the movement preparation window. A generalized linear model showed no statistically significant differences between adaptation conditions for cats A or B (Cat $A_{(C2\ zone)}$; Wald $\chi^2(3)=6.705$, p=0.082. Cat $A_{(C1\ zone)}$; Wald $\chi^2(3)=1.895$, p=0.594. Cat B; Wald $\chi^2(3)=2.986$, p=0.394), but a significant increase in Cat C (Wald $\chi^2(3)=9.314$, p=0.025) specifically during early and late adaptation trials (Bonferroni post-hoc comparisons; Baseline-early adapt. p=0.047, Baseline-late adapt. p= 0.031, Baseline-late after. p=0.380). Although not significant, both C1 and C2 electrodes in cat A do appear to share the same trend as cat C of an increase in beta power early in adaptation.

Figure 4.13 shows trial averaged power in the cerebellar cortex during the post-movement (20-220ms after reward tube entry). A generalized linear model showed no statistically significant differences between adaptation conditions in cat A (Cat A $_{(C2\ zone)}$; Wald $\chi^2(3)=3.363$, p=0.339. Cat A $_{(C1\ zone)}$; Wald $\chi^2(3)=2.682$, p=0.443.), or cat B after Bonferroni corrections (Wald $\chi^2(3)=10.845$, p=0.013, all Bonferroni corrected p-values for comparisons to baseline >0.05). In contrast, a generalised linear model did yield a statistically significant difference in data from cat C between baseline and both early and late after-effect trials (Wald $\chi^2(3)=12.871$, p=0.005. Bonferroni corrected p-value: baseline-early adapt. =0.083, baseline-late adapt. =0.014, baseline-late after. =0.001).

Overall, the analyses suggest that cerebellar cortical beta power may increase during the adaptation trials, especially at the movement preparation stage.

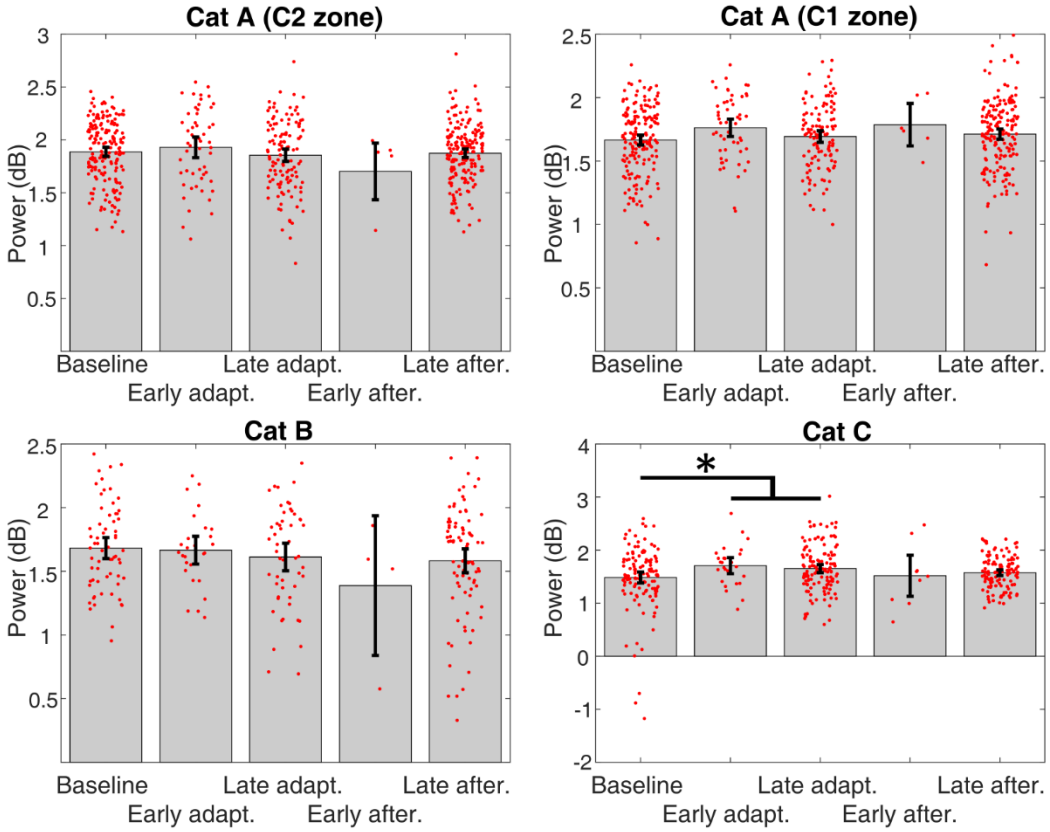

Figure 4.12 Movement preparation beta (10-25Hz) frequency modulation in cerebellar cortex.
Bar charts showing trial averaged beta power (10-25Hz) during different stages of adaptation. Error bars indicate 95% confidence of the mean. Red points indicate individual trial data.

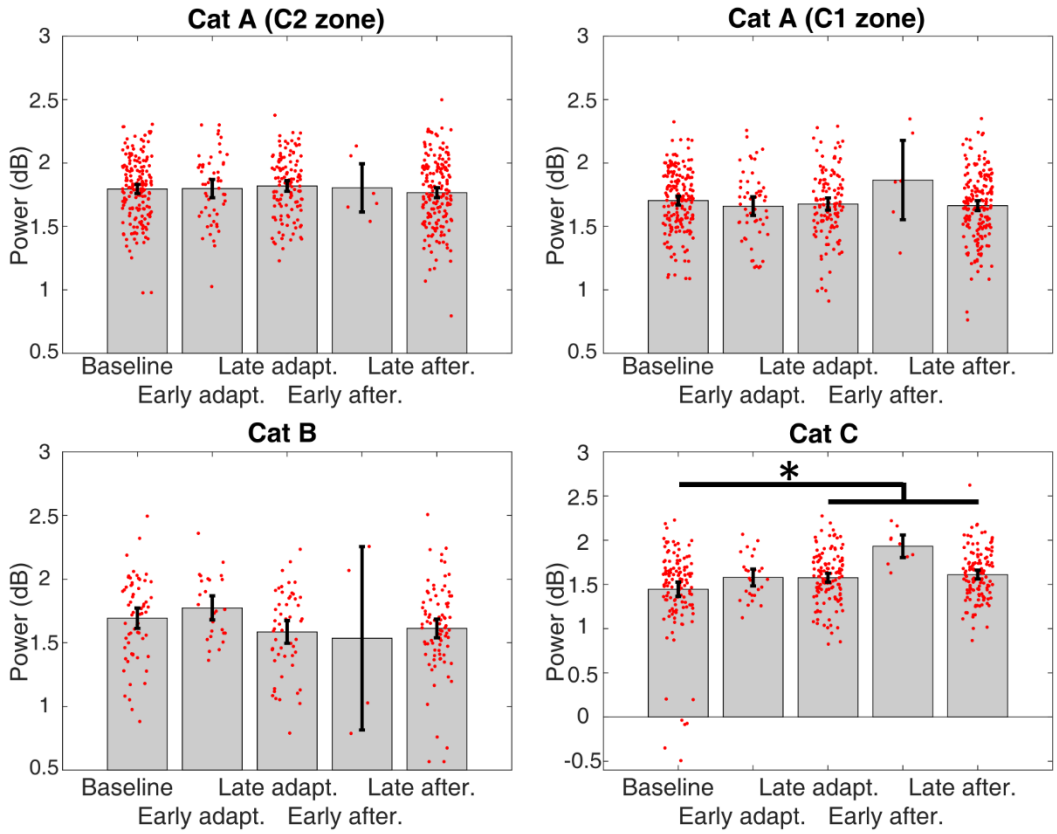

Figure 4.13 Post-movement beta (10-25Hz) frequency modulation in cerebellar cortex.
Bar charts showing trial averaged beta power (10-25Hz) during different stages of adaptation. Error bars indicate 95% confidence of the mean. Asterisks and bars indicate Bonferroni corrected comparisons (p<0.05). Red points indicate individual trial data.

4.4.2.3 Cerebro-cerebellar phase coherence

Another key aim of this thesis was to assess whether there was any evidence in the LFP signal to suggest a transfer of newly learned sensorimotor mappings between the cerebellum and M1 during adaptation, as proposed by Galea et al 2011. To this end, functional connectivity was inferred through phase locking between the cerebellum and M1. It was hypothesised that a change in connectivity will occur between the two structures during early adaptation (and possibly during early after-effect) compared to other time periods, since this is a time when an internal model is most likely to require updating.

Figure 4.14 shows the beta band phase locking data between cerebellar cortex and motor cortex during a post-reach period. All three animals show a slight decrease in phase-locking value during the early adaptation trials relative to the baseline trials. Generalized linear models revealed no significant differences in cerebellar-M1 phase locking in cat B, C or the C1 zone probe in cat A (cat $A_{(\text{cerebellar cortex C1 zone})}$: Wald $\chi^2(3)=7.79$, $p=0.051$. Cat B: Wald $\chi^2(3)=2.665$, $p=0.446$. Cat C: Wald $\chi^2(3)=0.781$, $p=0.854$), and no significant differences after Bonferroni correction in the C2 zone of cat A (Cat $A_{(\text{cerebellar cortex C2 zone})}$: Wald $\chi^2(3)=7.868$, $p=0.049$. Bonferroni corrected comparisons: baseline-early adapt. $p=0.428$, baseline-late adapt. $p=0.803$, baseline-late adapt. $p=0.678$).

Likewise, there does not appear to be any significant change in beta frequency phase locking between the cerebellar cortex and PFC during the post-movement period (**Figure 4.15**: Cat A $_{(\text{cerebellar cortex C2})}$: Wald $\chi^2(3)=3.46$, $p=0.326$. Cat A $_{(\text{cerebellar cortex C1 zone})}$: Wald $\chi^2(3)=2.423$, $p=0.489$. Cat B: Wald $\chi^2(3)=1.087$, $p=0.78$. Cat C: Wald $\chi^2(3)=2.152$, $p=0.542$).

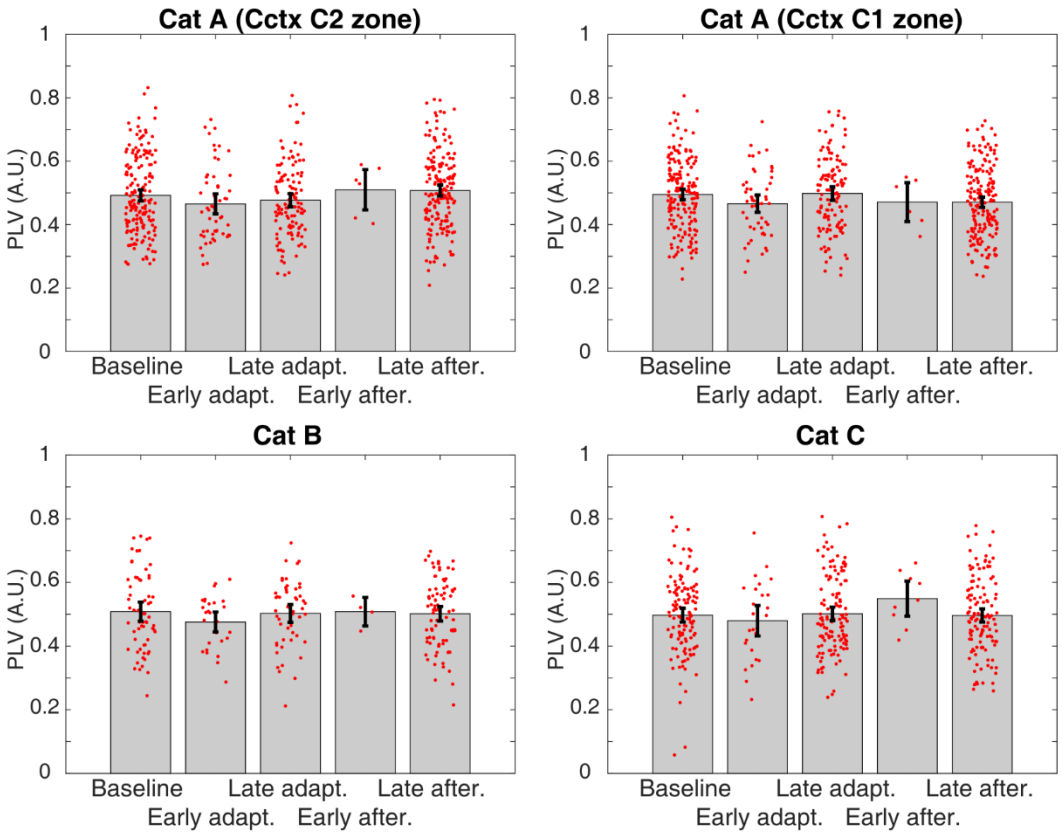

Figure 4.14 Post-movement local field potential beta (10-25Hz) phase locking between cerebellar cortex and forelimb motor cortex during adaptation.
Bar charts showing trial averaged beta power (10-25Hz) during different stages of adaptation. Error bars indicate 95% confidence of the mean. Red points indicate individual trial data.

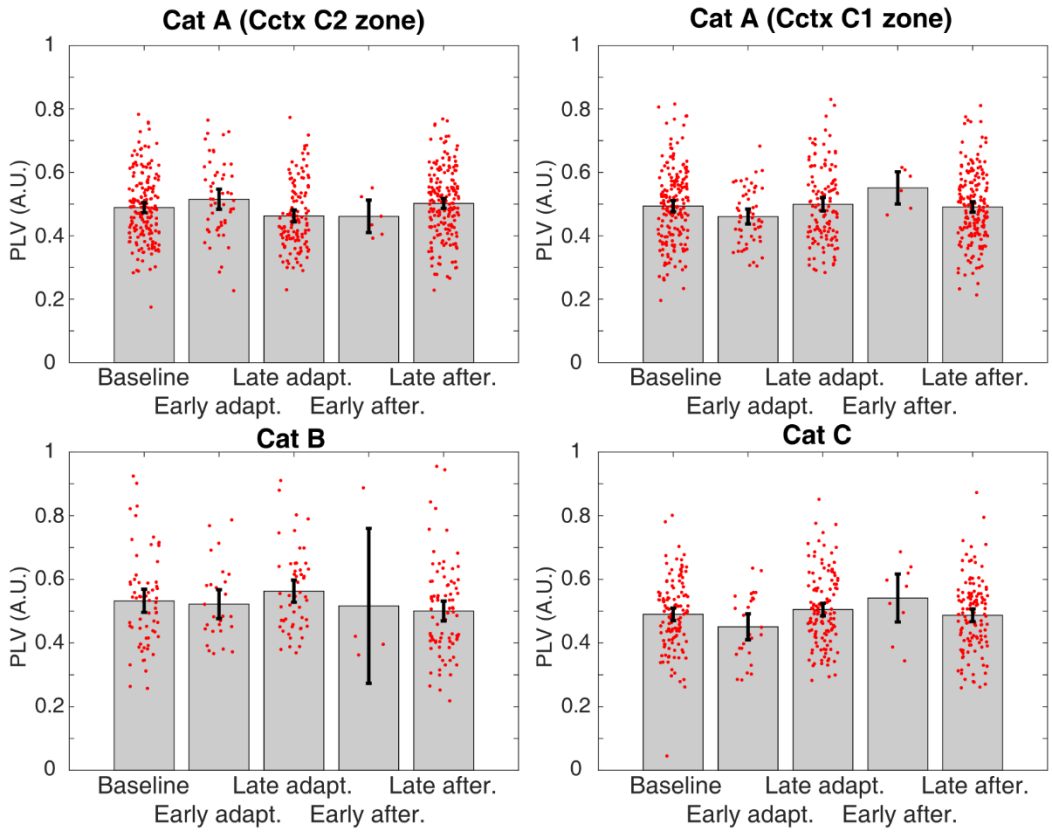

Figure 4.15 Post-movement local field potential beta (10-25Hz) phase locking between cerebellar cortex and prefrontal cortex during adaptation.
Bar charts showing trial averaged beta power (10-25Hz) during different stages of adaptation. Error bars indicate 95% confidence of the mean. Red points indicate individual trial data.

4.4.3 Theta and Gamma oscillation cerebro-cerebellar phase synchrony

In the current experiments, when the phase locking data are compared to a surrogate dataset in which the relative phase of the two recordings (cerebellar and motor cortical) has been randomised, values of phase locking for gamma frequencies are, on average, not above surrogate [chance] values (**Figure 4.16**). Thus, it appears cerebellar-cortical gamma oscillations are not significantly phase synchronised during the current reach-retrieve task.

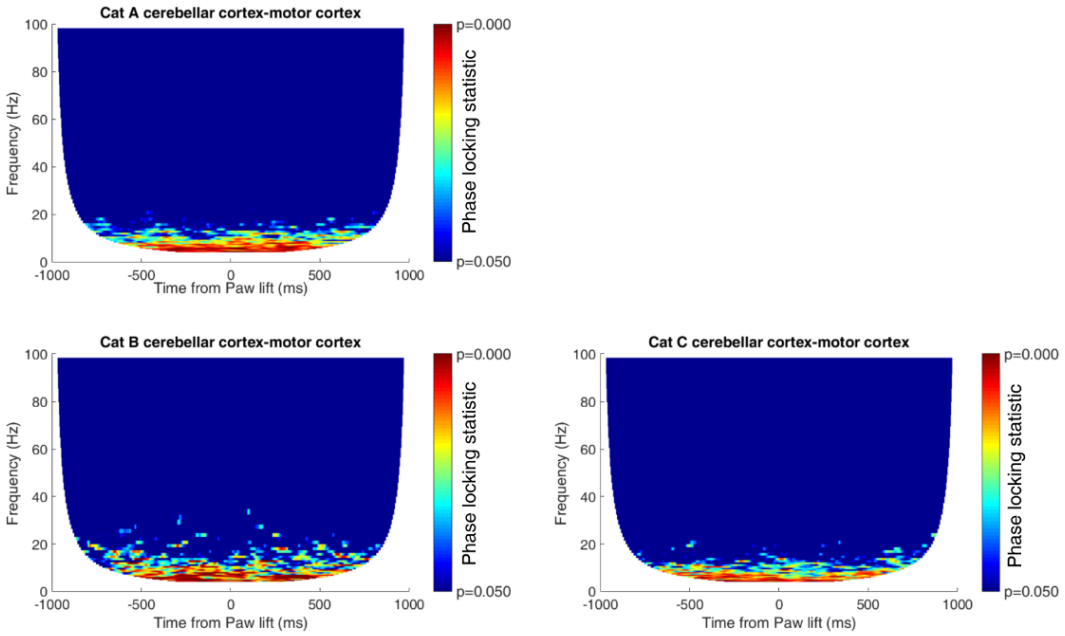

Figure 4.16 Example time-frequency plots of phase locking statistic between the cerebellar cortex and motor cortex. *Trial averaged heatmaps showing comparison of the strength of phase locking to trial shuffled surrogate data. White space indicates data potentially unreliable due to edge effects (cone of influence). Colour bar indicates p-value comparing random data. Note that in all three cats, gamma frequencies (>30Hz) do not show levels of phase locking above chance levels, whilst lower frequencies show above chance levels.*

To test whether the cat visuomotor adaptation task could elicit similar effects on cerebellar cortex-to-medial PFC coherence, the phase-locking value between cerebellar cortex LFP signals and the medial PFC LFP signal was taken from a 100ms time window centred on the midpoint (in time) of the forward reaching movement (i.e. half the time between paw lift-off event marker and reward tube entry/miss). A generalised linear model showed no effect of adaptation condition for any of the individual animals (Cat A $_{\text{(cerebellar cortex C2 zone)}}$: Wald $\chi^2(3)=1.284$, p=0.733. Cat A $_{\text{(cerebellar cortex C1 zone)}}$: Wald $\chi^2(3)=0.657$, p=0.883. Cat B: Wald $\chi^2(3)=1.493$, p=0.684. Cat C: Wald $\chi^2(3)=1.211$, p=0.75). Moreover, as with other frequencies shown previously, it appears there is a wide distribution of trial-to-trial values spanning almost the full range of phase locking values. Consequently, no statistically significant change in phase locking of theta oscillations between the cerebellar cortex and medial PFC was found during the current visuomotor adaptation task.

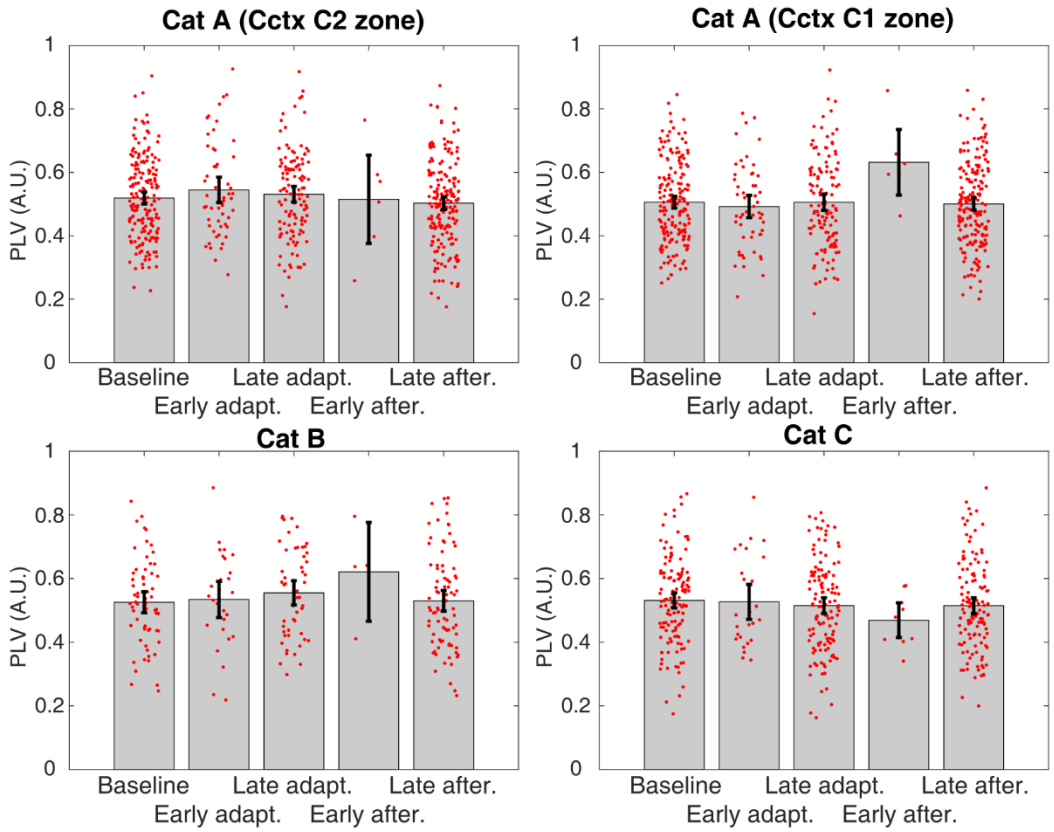

Figure 4.17 Theta (4-9Hz) phase locking between cerebellar cortex and medial prefrontal cortex.
Bar charts showing trial averaged theta (4-9Hz) power during different stages of adaptation. Error bars indicate 95% confidence of the mean. Red points indicate individual trial data.

4.4.4 Other analyses

As well as the above analyses, gamma band oscillations in the cerebellar and motor cortical LFPs were assessed in the same manner. Results of these comparisons can be seen in the appendix. Overall, there appeared to be no adaptation related modulation of gamma band oscillations in either the cerebellar, or motor cortical data.

4.4.5 Summary

Local field recordings made in forelimb regions of the motor cortex in a cat visuomotor adaptation task show evidence of decreased beta frequency oscillatory power during early stages of adaptation in two of the three animals. By contrast, no consistent effects on cerebellar LFP power was observed at either beta or gamma frequencies. Moreover, there was no evidence of adaptation related modulation of the cerebello-cerebral phase locking in the LFP signals.

4.5 Results 3– Cerebellar spiking activity

As noted above in section 4.2.1.2.3, we were unable to record any extracellular spiking activity in the frontal cortex targets, or the cerebellar cortex of cat A. Although not formally quantified, there was no indication from initial recordings that there was any temporal degradation of any signals. However, as described in the methods section 3.2.4.6 there was a mandated recovery

period of one week from the second surgery in which recordings were not made (resulting in a 2-week delay between the motor cortical implant surgery and the initial recordings). Additionally, although it was possible to make field recordings for the purposes of cortical mapping of the cerebellum with basic apparatus in the available operating theatre, it was not practically possible to accommodate all the computing equipment necessary to record activity from electrodes as they were advanced into the brain. Consequently, it is not possible to know whether the probes were ever able to detect such activity.

4.5.1 Recording of spiking activity in cats B and C

In cats B and C, we were able to successfully record extracellular spiking activity in the cerebellar cortex, an example recording trace can be seen in **Figure 4.18**. Over 10 days of adaptation recordings yielded 36 single units in cat B and 86 single units in cat C.

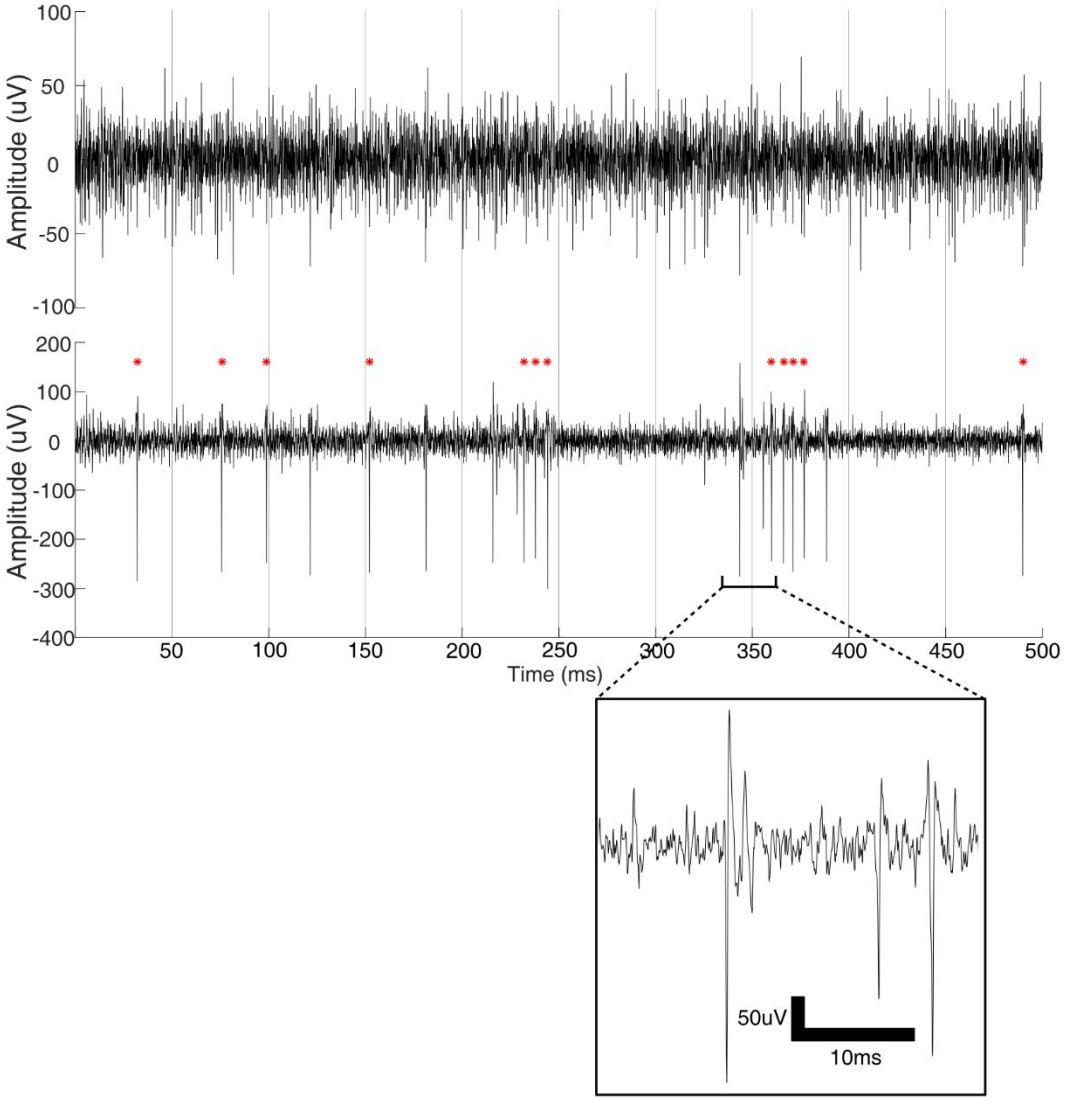

Figure 4.18 Example extracellular recordings from cerebellar cortex.
Two voltage recordings from adjacent probe channels, upper trace showing multi-unit activity, lower trace showing a dominant single unit. Red asterisks denote positions of putative Purkinje cell simple spikes from one isolated cluster.

Lower trace also exhibits two examples of Purkinje cell complex spikes, each followed by a simple spike burst and pause. Inset shows expanded view of a complex spike and two subsequent simple spikes.

4.5.1.1.1 Classification of single units

Out of the 88 single units from cat C, 10 were identified as putative Purkinje cells with one of these also present with a complex spike (**Figure 4.18**). One of the 36 single units was identified as putative Purkinje cells in cat B. Example waveforms and inter-spike intervals of the putative Purkinje cells can be seen in **Figure 4.19**.

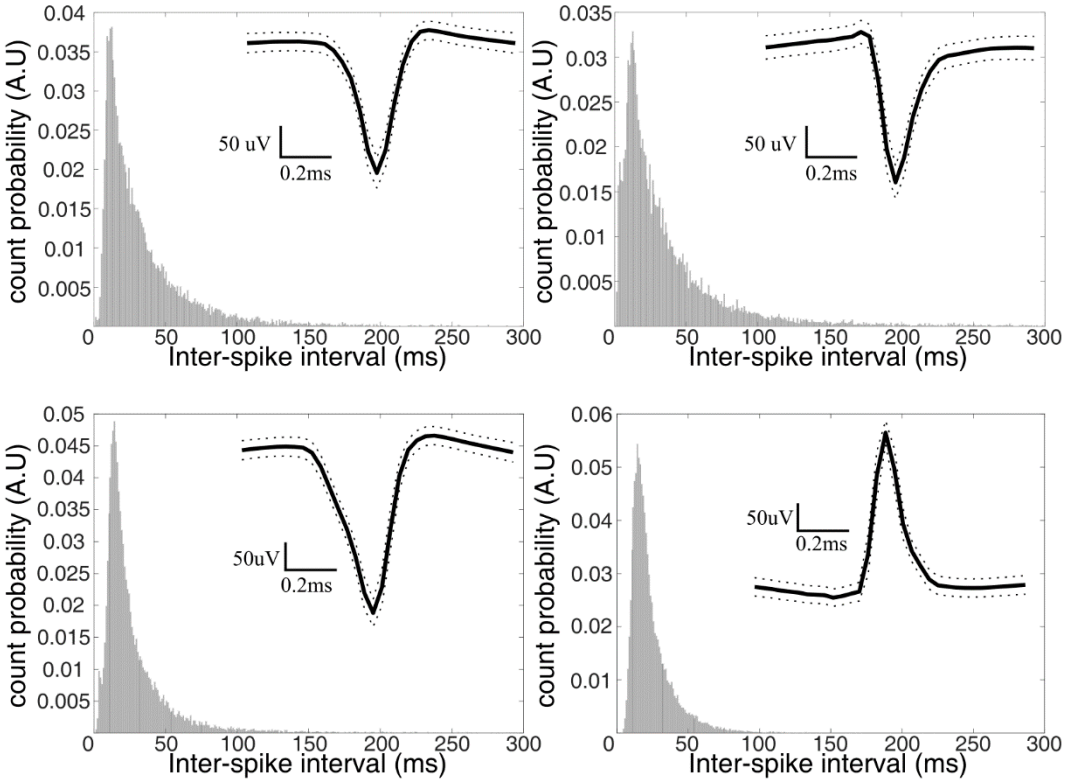

Figure 4.19 Example inter-spike interval histograms and average waveforms from 4 putative Purkinje cell single units.
Histograms formed using 1ms bins and normalised to give y-axes of probability densities. Insets of each histogram show average waveform of the unit computed on the tetrode channel with the largest waveform. Dotted lines indicate bounds of the waveform standard error.

4.5.2 Movement related responses in single unit activity

The activity of Purkinje cells from across the cerebellar cortex have been documented to be modulated by external sensory cues (Cerminara et al. 2009; Cerminara et al. 2005; Marple-Horvat et al. 1998), features of limb (Hewitt et al. 2015), and eye-movements (Kojima et al. 2010; Herzfeld et al. 2018; Thier et al. 2002).

Example PETHs of putative Purkinje cells are shown in **Figure 4.20**. Out of the 11 putative Purkinje cells, 2 showed no detectable change in firing rate (**Figure 4.20F)**, 3 showed a significant increase in firing rate either immediately after paw lift-off (**Figure 4.20D**), or after the tube entry event marker, and 6 showed decreased spike activity (**Figure 4.20A,B,C,E**). None of the putative Purkinje cells exhibited what would be considered as a time-locked phasic response to either

the paw lift-off or tube entry event markers, instead showing relatively prolonged changes lasting upwards of 100ms. Consequently, it appears that the putative Purkinje cells reported in this study exhibit tonic changes in firing rate during the reaching behaviour.

A statistical comparison of unit activity pre-movement and during movement showed differences in all but 3 of the putative Purkinje cells (**Table 4.1**). This is in general agreement with the above, showing tonic firing rate changes during the movement period except for one unit that showed no significant tonic changes, but did show increased discharge in the PETHs.

The remaining units not-classified as putative Purkinje cells were not comprehensively assessed according to their PETHs, because of their low firing rate and the small number of trials available to calculate average activity. Nonetheless, there were a small number of units that displayed movement-related modulation (**Figure 4.21**).

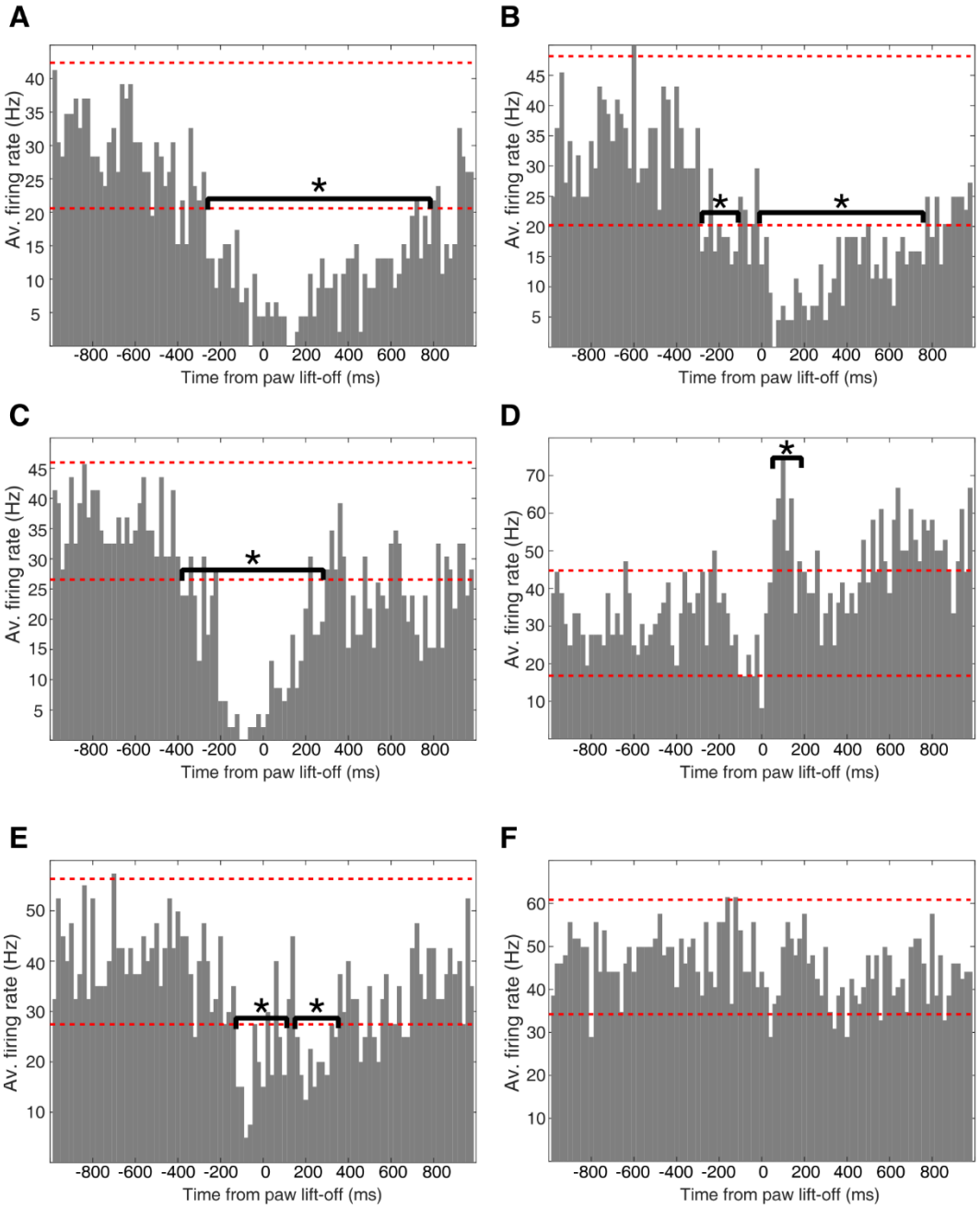

Figure 4.20 Peri-event time histograms of putative Purkinje cells.
Six example trial averaged peri-event time histograms (20ms bins) aligned to the paw lift-off event marker. Red dashed lines indicate 2 standard deviations from the baseline period between -1000 and -500ms. Asterisks and brackets denote regions of discharge rate beyond the dashed lines for 2 consecutive bins (40ms).

Unit ID	Activity description	Condition tested	t-test p-value
280317_2_3	Broad movement decrease	Baseline	<0.0005
280317_2_5	Steady ramp up post-movement	Baseline	0.0048
280317_2_7	Broad movement decrease	Late adaptation	<0.0005
290317_1_8	Silent around paw lift-off	Baseline	<0.0005
290317_2_2347	Short decrease during movement	Late adaptation	0.0035
300317_1_12	No observed change	Baseline	0.2315
100517_1_5	Not enough trials	-	-
100517_1_6	Rapid drop in rate at paw lift, possible increase after tube entry	Late after-effect	0.0014
110517_1_6	Short increase after paw lift, over by tube entry	Baseline	0.1321
110517_1_7	Decrease during movement period	Late Adaptation	<0.005
090517	Increase at -200ms from paw lift-off and larger increase after tube entry (long lasting)	Baseline	0.0039

Table 4.1 Student's t-test comparisons between trial averaged discharge rates in pre-movement and movement periods.

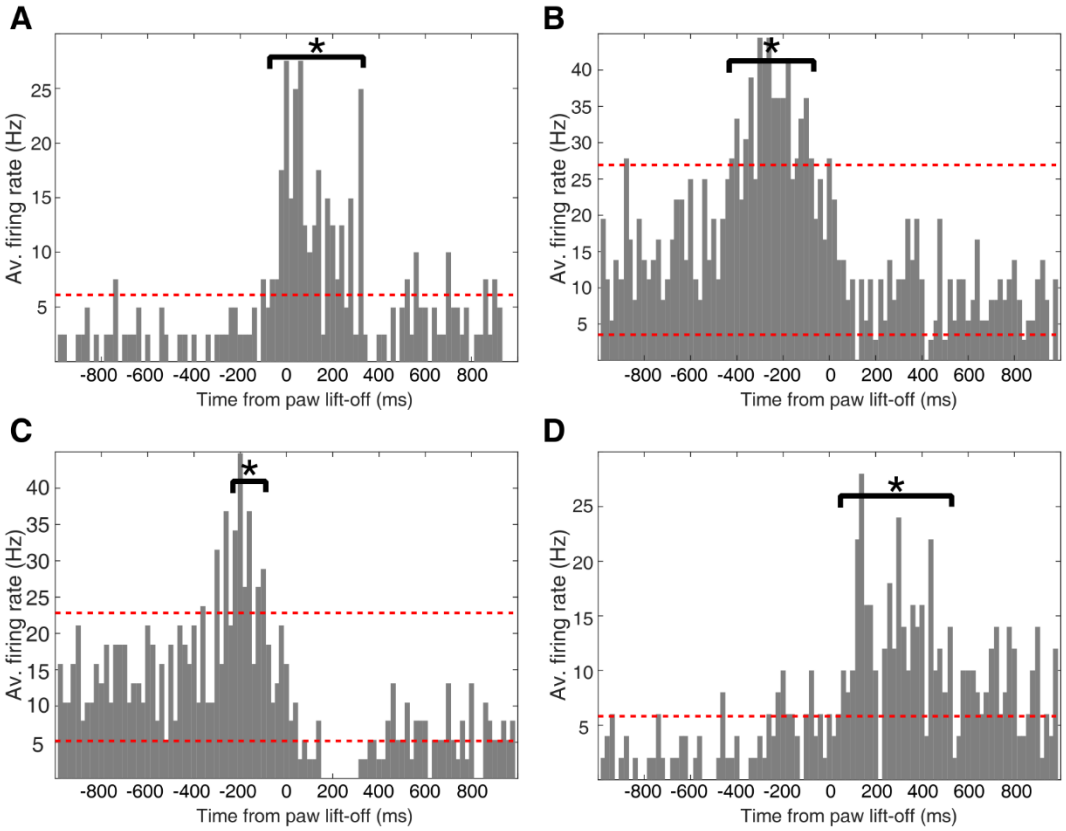

Figure 4.21 Peri-event time histograms of unclassified units.
Four example trial averaged peri-event time histograms (20ms bins) aligned to the paw lift-off event marker. Red dashed lines indicate 2 standard deviations from the baseline period between -1000 and -500ms. Asterisks and brackets denote regions of discharge rate beyond the dashed lines for 2 consecutive bins (40ms).

4.5.3 Modulation of single unit spiking through motor adaptation.

Of primary interest to this thesis is whether there is evidence to suggest that the neuronal activity within the cerebellum change because of the adaptation process. As Purkinje cells provide the sole output signals of the cerebellar cortex, they should form the keystone of the cortical processing and thus an informative measure of any changes to the activity. Given the technical challenges of the recordings it was possible to isolate and examine only a small number of single units in this dataset, and most were not recorded during the entire adaptation behaviour.

Two putative Purkinje cell units were recorded in enough trials to give at least a qualitative indication of adaptation related changes to their discharge profiles. These examples can be seen in **Figure 4.22**. Although the variance in the PETH plots changes between the adaptation conditions, due to the variable number of trials in each, there is no striking change in the discharge profiles of either example. The timing and pattern of the decrease in discharge of the second unit (**Figure 4.22B**) remains similar in early adaption and late adaptation - suggesting that *this neuron* does not encode features of the motor adaptation such as movement errors occurring in the early adaptation phase. Nor is there any striking difference between late adaptation and late after-effect - suggesting that *this neuron* does not encode features of an

updated internal model, given that the limb movement is similar (in both cases the animal accurately reaches the target) but the internal model is likely to have been revised to account for the prism displacement.

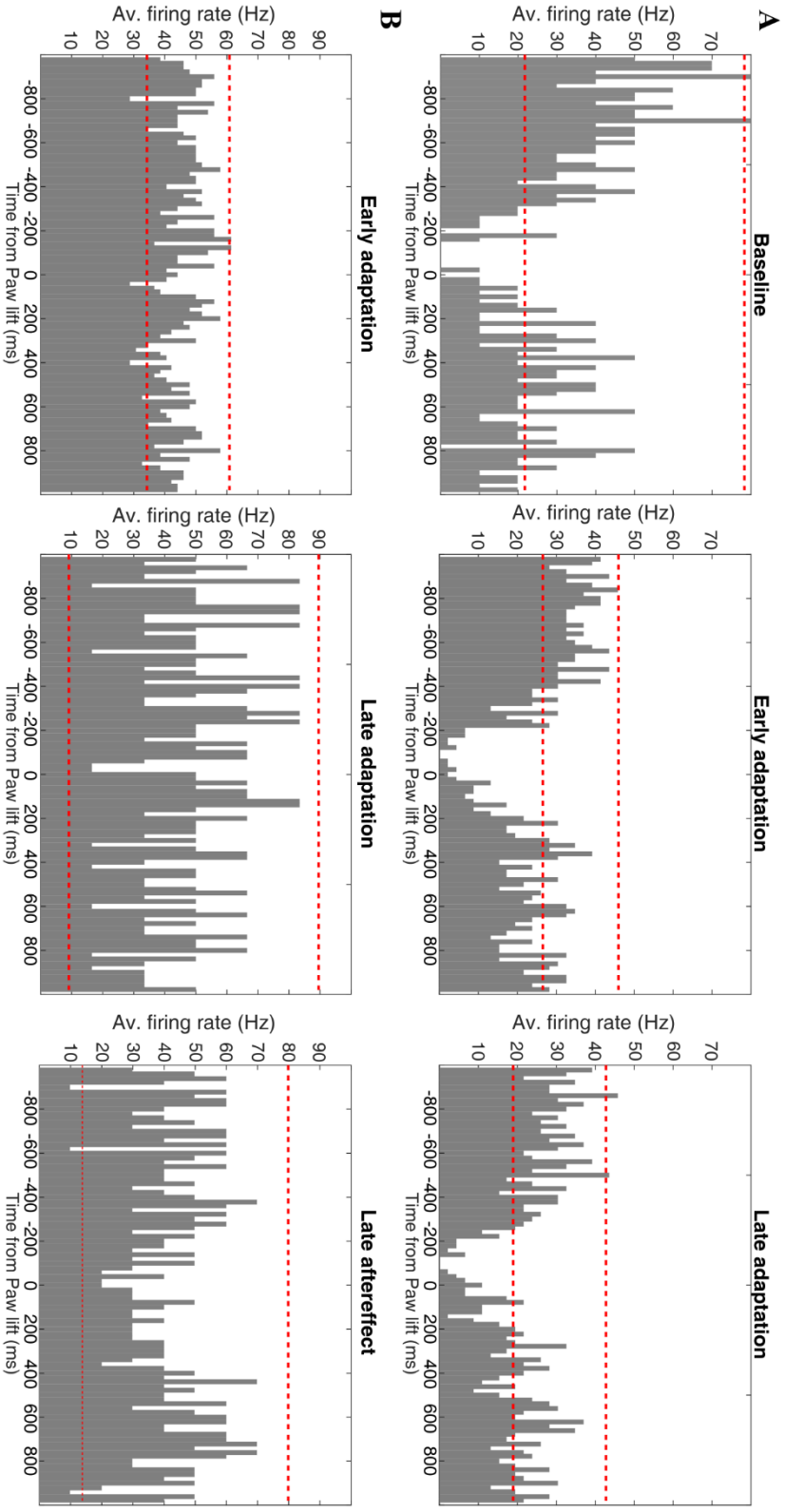

Figure 4.22 Comparison of movement related spike discharge profile across adaptation conditions.
*Two examples of putative Purkinje cell units (**A** responsive to movement and **B** unresponsive to movement) showing similar spike discharge profiles across multiple stages of adaptation. Red dashed lines indicate ±2SD from the -1000 to -500ms mean discharge rate.*

4.5.4 Movement related responses of neuronal populations

The single unit data obtained from both cats were pooled to form an indication of population activity in the cerebellar cortex. PETHs (20ms bins as before) of the cumulative spike count of pooled units were created, aligned to paw lift-off (**Figure 4.23**). As a result, differences in population discharge rate between non-adapting and adaptation states are evident. Specifically, in baseline, late adaptation and late after-effect trials, there is a prominent increase in spike discharge occurring from 200ms to paw lift-off. This is not present during either early adaptation or early after-effect trials. To control for differences in number of trials between phases, notably the lower trials numbers for early adaptation and after-effect periods, the analysis procedure was repeated with 10,000 randomly resampled trials from each of the separate conditions. A prominent increase in discharge rate remains evident in the non-adaptation states but is not present in the early adaptation and after-effect phases (**Figure 4.24**).

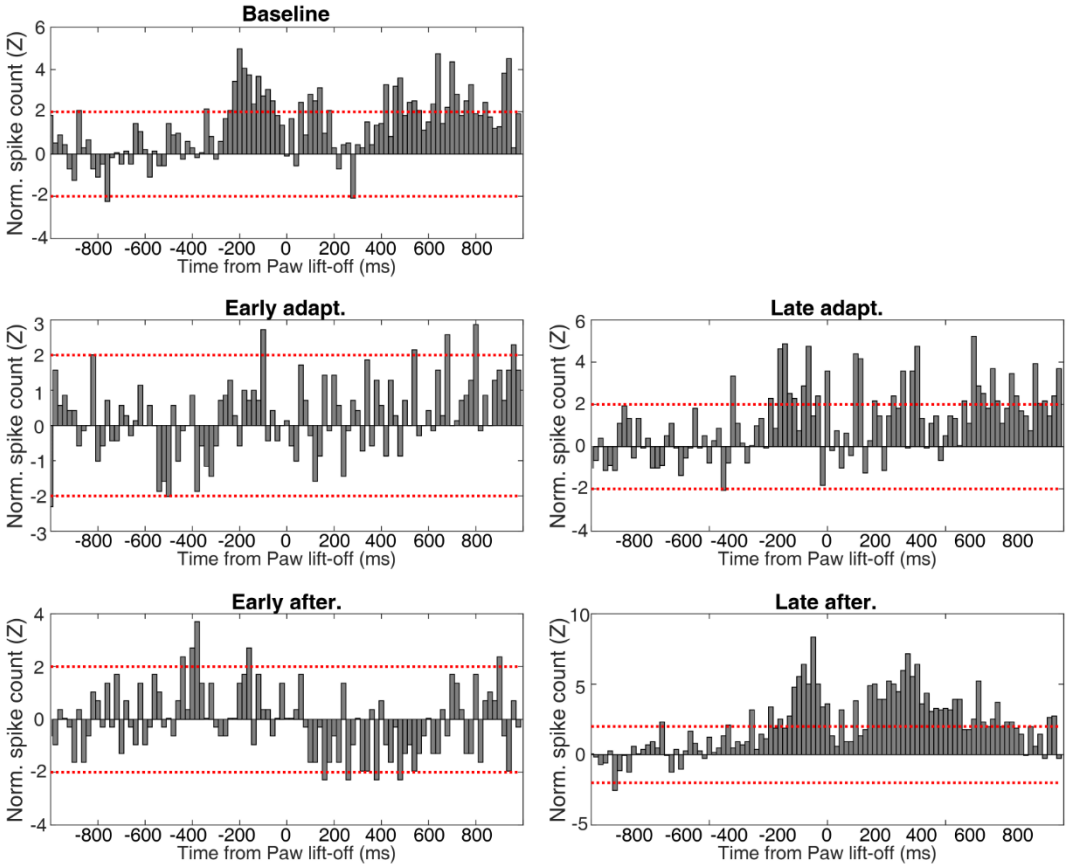

Figure 4.23 Population spike histograms over adaptation.
Cumulative spike counts from pooled single units arranged in 20ms bins aligned to paw lift-off and normalised to -1000 to -500ms period. Red dashed lines denote 2 SD boundary from baseline period.

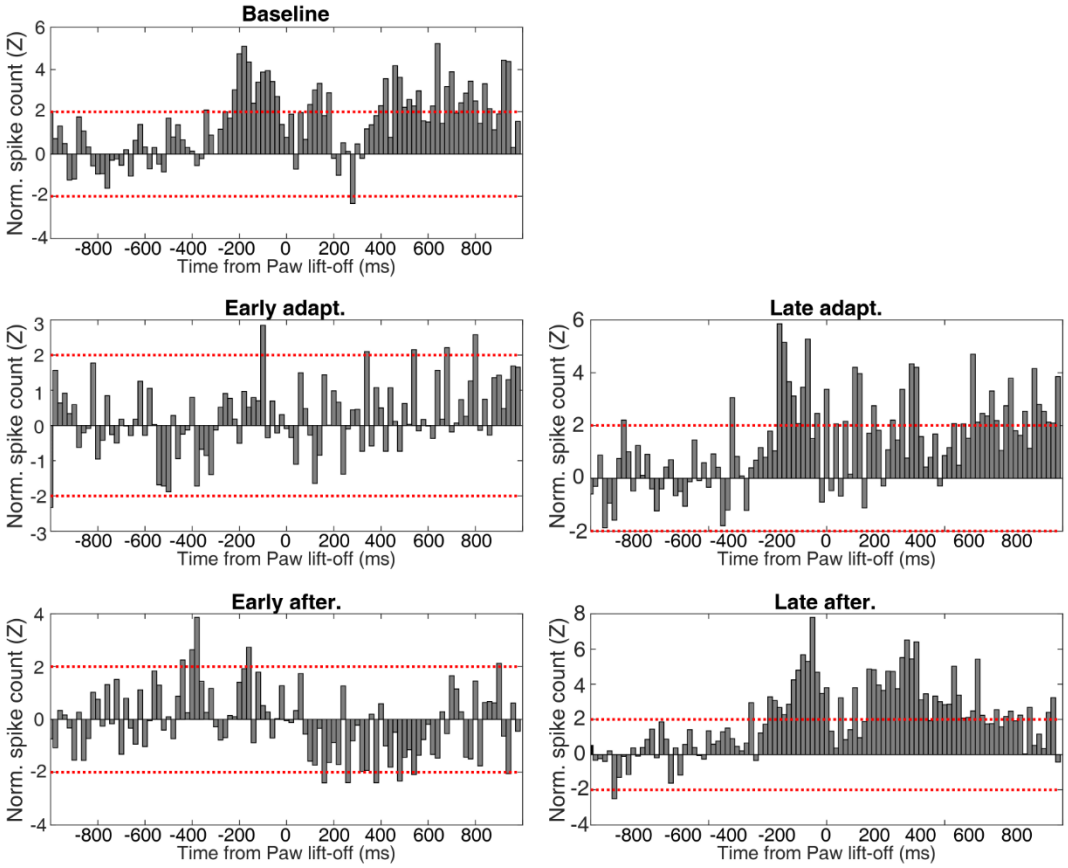

Figure 4.24 Bootstrapped population spike histograms over adaptation.
Bootstrap resampled cumulative spike counts from pooled cat C single units (20ms bins aligned to paw lift-off), normalised to -1000 to -500ms period. Red dashed lines denote 2 SD boundary from baseline period. 10000 resampled trials taken from each adaptation period.

The change in population activity prior to paw lift-off occurs during the initial increases in cleidobrachialis EMG activity (see section 3.3.1.3) suggesting this may be a critical time during the task when adaptation-related processing may be occurring.

To test whether the LFP signals also showed early adaptation/after-effect specific changes during this increased multi-unit activity, power spectra were computed by averaging the wavelet transforms in the period between 200 and 100ms prior to the paw lift-off signal (**Figure 4.25**). Overall, no clear difference between the early adaptation/after-effect trials and the other three conditions was found.

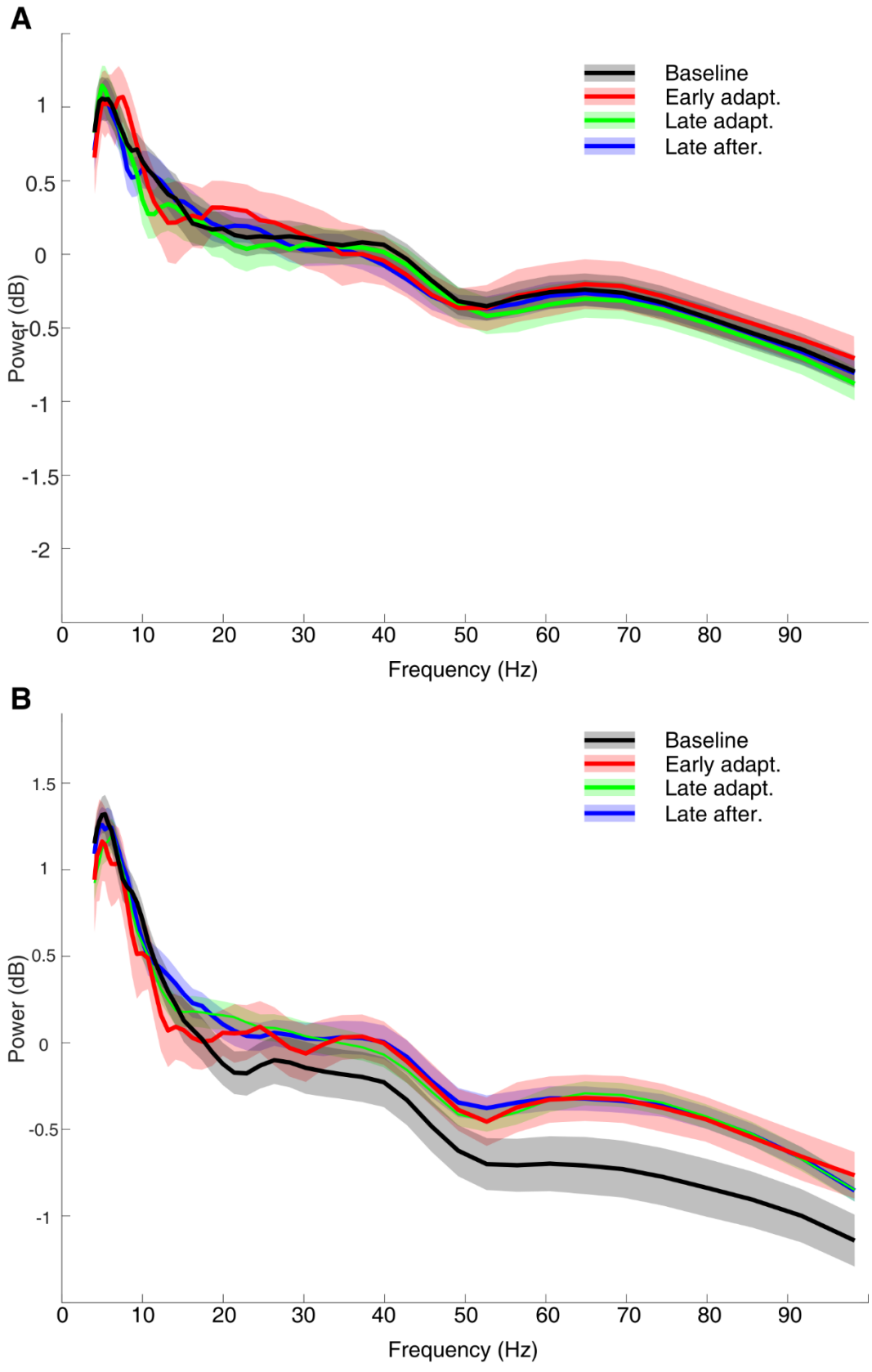

Figure 4.25 Local field potential power spectra during multi-unit bursting.
Local field potential spectral power was averaged over a 100ms window during increased multi-unit activity (200-100ms prior to paw lift-off). ***A****; trial averaged spectra for cat B.* ***B****; trial averaged spectra for cat C. Shaded areas give 95% confidence intervals for respective condition.*

4.5.5 Summary

Cerebellar cortical recordings made during days in which visuomotor adaptation was observed yielded a small number (11) of putative Purkinje cell units. None of these units altered their pattern of firing in a way that was tightly coupled to the major event markers of the reaching behaviour. Instead most displayed longer lasting changes in spike rate that occurred throughout the task. While at a single unit level of analysis there was little evidence to suggest adaptation related changes, when the data were considered as a population, adaptation-related changes were found. Specifically, changes in modulation were evident during the initiation of the reaching movement. This change in single unit population activity was not found in the LFP signal.

4.6 Discussion

4.6.1 Cerebellar zonal activity

In the present analysis, there was a significant difference in the LFP signals between the electrodes positioned in the paravermal C1 and C2 zones of cat A. Although direct evidence is still elusive, the distinct olivocerebellar and cortico-nuclear projections to the cerebellar cortical zones suggests distinct functions of each. Moreover, different electrophysiological properties of the C1/3 and C2 zones have been shown during behaviour. Specifically, the modulation ('gating') of climbing fibre transmission (as determined through the magnitude of evoked field responses) is maximal in the C1/3 zone during the swing phase of the step cycle of cat, whilst it was most consistently (but more variable) maximal during the stance phase (Lidierth and Apps 1990; Apps et al. 1990). However, contrasting activity was not seen during a reaching task, similar to the one used in the present study (Apps et al. 1997). Finally, while not directly relevant to the present data, even greater distinctions may be made between the hemispheric D2 zone, which has activity linked with predictions of the trajectories of external stimuli, and paravermal C2 zone, linked to the control of voluntary limb movements (reviewed in Cerminara and Apps 2011).

Variability in cerebellar zonal LFP has so far not been systematically investigated but given the known differences in afferent/efferent connectivity, the distinct LFP signals recorded from the C1 and C2 electrodes in cat A (**Figure 4.7**) suggest that these two lobule V zonal regions of the cerebellar cortex might perform different functional processes (supported by different oscillatory activity in the zones) during a forelimb reaching behaviour.

4.6.2 Local field potentials

The present analysis of the LFP spectral content highlights inter-individual differences between the three cats, with no clear and consistent effects. Nevertheless, the present data give some evidence of adaptation related changes in neural population activity.

4.6.2.1 Beta oscillations in motor cortex are modulated by adaptation

Cat A exhibited a significant decrease in beta power during adaption to prism glasses, with another showing the same trend in data (**Figure 4.10**). This adaptation related decrease is somewhat similar to data from primate studies, revealing that beta oscillations in the LFP of supplementary motor cortex are suppressed specifically when motor plans are required to be actively updated (Hosaka et al. 2016). Here, monkeys were trained to perform a bimanual sequential motor sequence task in response to a cue. After repetition of one motor sequence for several trial blocks, the required motor sequence was changed, requiring the monkeys to change the generated motor plans. The authors argued that the observed suppression of beta

oscillations during the pre-movement phase reflects a 'volatility' in the neural assemblies of the supplementary motor cortex as new local networks are engaged in response to the new motor demands. In the context of the present motor adaptation task, the observed decrease in beta oscillations during the pre-movement stage may reflect the same 'volatility' of neural assemblies in response to the new motor plan demands.

Contrary to this however, our data shows that the decreased beta oscillation is not restricted to early stages of adaptation but persists into the late adaptation stages (**Figure 4.11**) when the neural ensembles active for the task might be presumed to have stabilised. One explanation for this might be that the unperturbed reaching motion is highly over-learned (whilst the monkeys tested by Hosaka and colleagues had several new and variable motor sequences presented) and so there remains an instability in the motor cortical network, with the neurones represented in the unperturbed neural ensemble still 'competing' against alternative ensembles.

4.6.2.2 Cerebellar cortical local field potentials

None of the LFP oscillatory activity in the cerebellar cortex appeared to show a strong adaption related modulation, with inconsistent data between the three individual animals (data in the appendix). This is certainly unexpected, given the wealth of literature indicating a role for the cerebellum in error detection, error-processing, and motor adaptation (Seidler et al. 2013; Bernard and Seidler 2013), and we expected local field potentials to largely reflect ongoing neuronal processes (Buzsáki et al. 2012; De Zeeuw et al. 2008).

It is plausible that the neuronal populations contributing to the LFP signals were not principally involved in the adaptive changes made to the reaching movement. However, the magnitude of the adaptive changes (a lateral displacement of up to a few centimetres) in relation to the overall movement may have been too small to detect such changes, and there was no restriction on which muscle groups were utilised to adapt the reaching motion. This contrasts with other adaptation paradigms in which the task requires adaptation of specific muscles (i.e. adaptation of saccade, or vestibulo-occular reflex gain which better isolates adaptation of specific ocular muscles depending on the direction of the adaptive movement). It may be that the adaptation process was achieved through modifying neuronal activity that only contributed a small fraction of the total LFP recorded here.

In cat, both olivary and mossy fibre inputs to individual Purkinje cells show quite refined peripheral receptive fields, with Purkinje cells within 200µm by 100+µm sagittal microzones exhibiting highly overlapping receptive fields (Oscarsson 1979). In cats, moving laterally across different microzones by as little as 1mm however leads to receptive fields spanning the entire forelimb (Ekerot and Jörntell 2001). Whilst the extent of the 'catchment zone' of LFP sources is

still debated (Kajikawa and Schroeder 2011; Herreras 2016), and is likely a non-uniform rule depending on neuronal type and activity (Leski et al. 2013; Lindén et al. 2011). Current estimates, based on modelling cerebral cortex, lie between 200-1000µm (Leski et al. 2013; Lindén et al. 2011). Consequently, the LFP signals recorded in the present thesis are likely to span multiple cortical microzones and may even include activity from more than one cortical zone, which may have differential functional activity during the behaviour as discussed previously.

Considering then that the signals constituting the recorded LFP signals likely constitute sensory information pertaining to much of the reaching forelimb, and the adaptive changes required to regain task success may be relatively minor, it is plausible that neural activity reflecting adaptive changes was masked by the activity of a larger number of neurons that did not encode the adaptation behaviour.

4.6.2.3 Cerebello-cerebral functional connectivity

The functional connectivity between the cerebellum and motor and prefrontal cortices was assessed through the phase relationships of their local field potential oscillations. Overall there was no adaptation related changes in phase synchrony between network nodes at any frequency. This null result seems to contrast with a previous study, showing an increased phase synchrony of theta frequency LFPs during adaptive responses to a trace eyeblink conditioning experiment (Chen et al. 2016). However, Chen and colleagues compared theta band phase synchrony between animals, grouped into adaptive learners and non-adaptive learners. Looking closely at the reported data, whilst there is an increase in theta phase synchrony between animals that adapt and those that do not, there does not appear to be a change in the phase synchrony across the time-course of adaptation behaviour for the adaptive learners. Consequently, the theta phase synchrony may better reflect the intrinsic ability of the motor network to adapt. Considering that all the animals used in the present study were able to sufficiently adapt to the prism glasses, it may be that the cerebro-cerebellar networks were indeed performing in a continually synchronised state throughout the behaviour (highlighted by the significant theta synchrony compared to surrogate data during baseline conditions (**Figure 4.16**)).

Further, there was large inter-trial variability with single trial phase synchrony ranging from low synchrony to high synchrony. This raises the possibility that the cerebello-cerebral network in question does not utilise strict phase relationships to transmit information across the network, allowing phase synchrony to vary substantially on a trial by trial basis.

4.6.3 Spiking activity

Single unit spiking activity was recorded from two out of the three cats in this study, and mainly from cat C. It is regrettable that the chronically implanted silicon probes positioned in the frontal cortices in the three animals, or the cerebellar cortex in cat A did not yield any spiking activity, as it would have been very interesting to assess potential coupling/covariation of spiking activity across these regions. Nevertheless, the spiking activity presented in this thesis gives an indication of adaptation related modulation of neuronal activity in the cerebellar cortex.

4.6.3.1 Putative Purkinje cell responses to movement

Of the 11 putative Purkinje cells- identified through their firing properties (**Figure 4.19**), and one presence of a complex spike (**Figure 4.18**), none appeared to exhibit a temporally specific phasic response to either the paw lift-off, or reward tube entry/miss events. Instead, those that did show changes in their discharge rates showed changes lasting upwards of 100ms and extending the full movement duration, beyond the initial outward reach (**Figure 4.20**).

Purkinje cells have been shown to elicit short, phasic responses to sensori-motor events, as shown in air-puff stimulation of whisker pads of awake mice, and mechanical whisker stimulation of anaesthetised mice, with responses typically lasting around 33ms (Bosman et al. 2010). However, similar experiments by this lab, recording lateral cerebellar responses to a variety of events during visually guided reaching in cats, found little or no phasic responses to the paw lift-off event marker, whilst a number of Purkinje neurons elicited phasic responses (typically an approximately 50ms increase in discharge rate, initiating up to 50ms after the event of interest) in response to certain visual sensory events (Miles et al. 2006; Cerminara et al. 2009). Longer lasting changes in simple spike discharges during forelimb movements has also been reported previously (Mano and Yamamoto 1980; Mano et al. 1986), and so it is these 'types' of Purkinje neuron that are likely to have been recorded from in this study.

4.6.3.2 Putative Purkinje cell responses to adaptation

Out of the limited number of neurons available in this study, there was no general impression from the PETHs that the activity of single neurons was modified throughout the visuomotor adaptation task. This is in contrast to previous literature that has shown changes in the simple spike discharge rate during a force-field adaptation task in primates in a majority of recorded Purkinje neurons (Hewitt et al. 2015), and that the simple spike discharge can encode feedback errors in a wrist tracking task (Popa et al. 2012). Considering the very small number of putative Purkinje cells available to this study, we cannot dismiss the possibility that, by chance, the cells isolated in this study happened not to have such activities, and given further investigations a

population of Purkinje cells that did have such representations of error would be found in this region of lobule V.

4.6.3.3 Population spiking responses to adaptation

In contrast to the stability of the putative Purkinje cell discharge rates throughout the visuomotor adaptation behaviour, the present data gives some indication that the cerebellar cortical population as a whole may exhibit adaptation related changes. Pooled single unit responses exhibited an ensemble increase in discharge rate during a period of movement initiation (-200ms to paw lift-off) for baseline, late after-effect, but not during periods of early adaptation or after-effect (**Figure 4.23** and **Figure 4.24**). Although we do not see changes in the activity of individual Purkinje neurons in this dataset, the change in the ensemble activity in response to a need to adjust the task movements leaves open the suggestion that the cerebellar cortical activity was in some way involved in the adaptation modification of the reaching movement.

It is interesting that the adaptation related change in neural ensemble activity occurs early in the movement, prior to the paw lift-off event. This suggests that there may be predictive correction mechanisms occurring at the population level, as opposed to error feedback responses which would be expected after the tube entry/miss event. The cerebellum has been implicated in rapid, online control of skilled movements, stemming from the suitability of the cerebellum to act as a forward model (Sokolov et al. 2017). Consequently, in the early adaptation stages of motor adaptation, the changes seen in the cerebellar code occurring very early during the movement could represent signals reflecting a sensory prediction error from this forward model, based on the previous (erroneous) trial, potentially allowing rapid online correction of the movements and reducing the behavioural error made. By contrast, during situations in which prior trials have been sufficiently accurate, no sensory prediction error will be generated from the output of the forward model, and the planned movements can proceed unaffected.

In this data, we are unable to tease apart the probable outcome of this ensemble activity on the downstream nuclei. Even if we could assume that it was non-Purkinje cell activity (based on the firing properties), there remains a homogenous mix of neuronal types that elicit both excitatory and inhibitory influences on the Purkinje cells, and thus the ultimate output of the cerebellar cortex.

Despite the indications of an adaptation related change in cerebellar cortical activity found in the spiking data, this did not translate into an adaptation specific change in the LFP spectrum (**Figure 4.25**). This disparity suggests that the contribution of spiking activity to the local field potentials in the cerebellar cortex may be minor.

4.7 Summary

Overall, the electrophysiological results have shown:

1. Different physiological activity is present within the C1 and C2 cerebellar cortical zones during a reaching task.
2. Adaptation related decrease in motor cortical beta oscillations during movement preparation/initiation, consistent with the human EEG data presented in Chapter 2.
3. No modulation of cerebellar LFP during motor adaptation.
4. No modulation of cerebello-cerebral LFP phase synchrony during motor adaptation.
5. Adaptation related suppression of multi-unit activity in the cerebellar cortex during movement initiation.

Chapter 5 – General Discussion

The studies reported in this thesis aimed to investigate how neuronal activity across three major nodes in a motor network (cerebellum, M1, and PFC) might vary in response to a visuomotor perturbation during reaching, including how the information flow across the network may vary at different stages of the behaviour. To achieve this, a translational approach was taken, with studies involving both human and animals, to provide complementary lines of investigation at multiple scales of resolution of neuronal activity. This final chapter briefly considers the principal findings of these studies.

5.1 General experimental considerations

5.1.1 Use of multi-site silicon probes

The decision to use multi-site silicon probes was largely practical. As the recording of neural signals during surgical implantation of the probes was not practically possible, the presence of many recording sites spread along the probe shank was thought to offer a greater chance of obtaining single unit type recordings from the principle neurons in the implanted regions. Furthermore, the recording apparatus was designed for easy compatibility with the type of connector sockets on commercially available silicon probes, circumventing the need for adaptors that could lead to electrical noise, and add extra cabling and bulk to the animal implant, which was designed to be as streamlined and light as possible.

Contrary to this, in light of the failure of the silicon probes to record spiking activity in the frontal cortices, on repeating the present experiments, these chronically implanted electrodes may have benefitted from custom made platinum/iridium electrodes which have been used previously in the motor cortex of cats (Amos 1989).

5.1.2 Further experiments

The inter animal variability in the neural data suggests that these experiments would need to be repeated a number of times to increase the reliability of the data. This was not possible given ethical and licencing considerations of the project. Given the good evidence of motor adaptation behaviour in all three cats, repetition of the same behavioural task would certainly be possible. Nonetheless, it should be noted that the presented data comprises a small fraction of the total data recorded from each animal (ten recording sessions of a total of ~50 recording sessions) and the spiking data from cats B and C is presently being used toward a larger ongoing study of cerebellar cortical activity during voluntary forelimb movements.

It would be interesting to correlate changes in neural states with the kinematic action of the reaching limb during adaptation. These forms of analyses are possible when using forcefield adaptation tasks, from which high-resolution kinematic data can be extracted from the position and forces applied to the robotic manipulanda during a task. This is potentially one reason why

forcefield adaptation tasks have become the preferred choice for human and non-human primate-based experiments. Using a manipulandum, whilst un-tested, seems an unlikely prospect for a cat whose natural repertoire does not encompass grasping and manipulating objects. In order to gain similar data in the cats, the stereo video captured during the experiment could be used to re-construct 3D trajectories of the reaching limb. This was intended at the onset of the project; however, it was not completed due to insufficiencies in the available tracking methods. Recently a group has developed a powerful open-source platform (DeepLabCut) using artificial neural networks to perform kinematic tracking (Mathis et al. 2018). This tool should enable a rapid and user-friendly way of generating detailed limb trajectories from the existing video data.

Finally, the animal data presented in this thesis comprises a small portion of that gathered from the three cats. As noted previously, after exposure to the prisms, cats B and C developed the ability to seamlessly switch between prism on and prism off conditions with little to no reach errors. Comparing the neural activity between these sessions and those in which classical motor adaptation was elicited may reveal the neural contributions toward contextual switching mechanisms in the frontal cortices and across the motor network described in this thesis.

5.1.3 Consideration of sample size

Foremost in the limitations of both studies is the lack of statistical power in some of the assessments driven by the small sample populations (11 humans and 3 cats).

In the case of the human study, the observed power of the main effect of beta band oscillations across adaptation epochs was 81.4% and an effect size (partial Eta squared) of 0.257 – considered a large effect according to the 'rules of thumb' in the behavioural research community (Miles and Shevlin 2001; Bakeman 2005). However, regarding the null effect of the cerebellar targeted tDCS, in particular the change in adaptation half-life – expected from the observation in the literature (Galea et al. 2011; Herzfeld, Pastor, et al. 2014) – the effect size of the paired t-test is considered small (Cohen's d=0.23) with an observed power of 10.5%. Using this effect size suggests that a sample size of 153 would be necessary to achieve an observed power of 80%. A sample of this size was impractical given the use restrictions of the EEG lab space available for this study, and is indeed a very large number compared to published literature, although in line with recent estimates suggesting sample sizes of 75 are still slightly underpowered (Minarik et al. 2016).

Regarding the spiking activity recorded in the cats, the technical limitations of the recordings were such that maintaining a single unit recording for the duration of a session proved highly challenging. The principal factors leading to the loss of a seemingly stable unit appeared to be

the fitting and removal of the prism glasses- which led to excessive movement in the electrode drive towers, destabilising the recordings at these times. Two obvious alternatives exist; either use prism glasses that do not require complete removal (possibly hinging away from the gaze) and using chronically implanted probes instead of the large tower driven probes, which should be less susceptible to mechanical instability.

As this was the first known implementation of a prism adaptation task in cats, we did not know how well the cats would tolerate wearing glasses. Moreover, the design of the glasses was such as to be as minimalistic as possible, reducing both complexity and weight. Consequently, the employment of some sort of 'hands free' removal of the prisms, although considered, was not pursued. The reasons for choosing to use acutely introduced probes has been detailed in the body of the thesis (section 4.2.1.2.3), and so will not be considered further here.

5.2 Adaptation vs. after-effect

In the animal study, the lack of available data in the early after-effect (prisms off, miss reaches) was disappointing as this was a principal condition of interest after the early adaptation trials, given that the individual is now 're-adapting' to use the original sensorimotor mapping (internal model). Moreover, the human EEG data pointed toward a difference in the neuronal activity during early adaptation and early after-effect, thus comparison of the LFP data in these two conditions was desirable.

The lack of data in this condition is perhaps an indication of the strength of the original internal model 'prior' (no-prism model), with the animal being able to revert to it more rapidly than the new, with-prism model. In this light, the existence of after-effects is perhaps curious given the presumably well-defined internal model of standard reaching and cats A and B showed ability to rapidly alternate between multiple internal models (section 3.4.4). If the standard internal model is crystallised in some form of long-term memory network, and individuals can switch to the correct model as-needs-be, why do after-effects exist when the correct internal model is available? To date, this has not been addressed in the literature, however the following may serve as a potential explanation.

If the two internal models (standard and perturbed) are available, but they have not yet been associated to separable conditions, then the brain is unable to determine that a switch is possible, and so the progressive error-based after-effect occurs. Later, once a strong and separable context has been linked to each of the internal models, the brain is able to make the association and switch models. Thus, it might be that the development of the rapid switching behaviours is subject to a slower, associative learning process that occurs once the two internal

models have been learnt. Specific experiments to dissociate the development of internal models from the associative learning of context will be required to test this idea.

5.3 Cerebellar transcranial direct current stimulation

The lack of a statistically significant effect of cerebellar targeted tDCS on the adaptation rate in humans was disappointing, though perhaps not wholly surprising given the mixture of results in the wider literature. Exemplifying the unpredictability of tDCS, a recent study attempted to replicate the findings of Galea and colleagues (2011) and was unable to do so (Jalali et al. 2017). Moreover, varying the experimental design – such as gradually increasing, or implementing small stepping of the visuomotor rotation – did not lead to significant effects between anodal and sham conditions. Relevant to this work specifically, Jalali et al. (2017) were unable to observe a significant behavioural effect of offline anodal tDCS- as was found in the present study. Overall, it appears there is a publication bias toward positive effects of non-invasive electrical stimulation. Pooling large datasets from across the research community would be able to more accurately estimate the effect size of such non-invasive stimulation methods.

5.4 Motor cortical beta oscillations

The present study found a significant decrease in beta frequency EEG oscillations over the contralateral motor cortex during early stages of a visuomotor reach adaptation task. Preliminary evidence in two out of the three animals supports this finding, with decreased beta frequency LFP oscillations in a forelimb region of the contralateral cat motor cortex. In both the animal and human studies, this suppression of beta oscillations was observed in a pre-movement time, prior to the execution of the reaching movements. This suggests that similar neural mechanisms operate across species within this frequency range that can be detected by LFP and EEG recording. Consistent with other literature, this may reflect activity in the motor cortex relating to the generation and selection of motor plans (Torrecillos et al. 2015), perhaps from a 'library' of inverse models. Consequently, during early stages of learning, there may be a drive to decrease cortical synchronisation (at beta frequencies) which may enable recruitment of alternative ensembles of motor neurons (selection of a different inverse model) as a means to modify the muscle synergies provoked by the motor commands.

5.5 Cerebellar activity

The cerebellar cortical data recorded from the animal study provided mixed results during adaptation. At the population level (LFP), there was no convincing modulation of spectral activity during adaptation, yet at a smaller population level (pooled single-unit spike activity), a change in pre-movement activity was evident (specific to early adaptation and after-effect). Current evidence suggests that the LFP reflects the activity of *synchronously* firing neurons (Buzsáki et

al. 2012; Denker et al. 2011). If this is the case, then the present findings suggest that the multi-unit activity observed in the present data originates from a sub group of neurons contributing to the LFP whose activity is masked by a larger population of synchronised neurons.

The behavioural effect of pharmacological blockade of cerebellar cortical activity suggested a disruption in the switching from the baseline to the prism internal models. This is consistent with the idea of the cerebellum acting as a site of an internal model but does not distinguish between forward and inverse models.

If the cerebellum acts as a forward model, the data might be interpreted as the failure (due to the blockade) of generating a prediction error, thus preventing the motor system from updating the motor commands, leading to an error in reach. If instead the cerebellum acts as an inverse model, the data might be interpreted as a disruption of the conversion from an intention signal into the appropriately synchronised/timed motor commands, thus leading to a behavioural error.

Although there was evidence of preserved intra-session motor adaptation after the pharmacological blockade, the absence of an after-effect suggests that an alternative form of error-based learning may have been at play, perhaps a greater influence of cognitive strategy supported by the PFC. It is therefore disappointing that neuronal recordings were not feasible at this time, as a contrast between activity recorded during typical adaptation sessions and the cerebellar blocked session may have revealed differential activity in the PFC related to top-down control of the motor behaviour.

5.6 Adaptation vs after-effect

In both human and animal studies presented here, there was a disparity between data collected during the early adaptation trials, and early after-effect trials. This supports the suggestion that the neural mechanisms associated with these two phenomena are distinct.

Behavioural measures of motor adaptation and the after-effect have previously been shown to be dissociable. For example, patients with disorders of the basal ganglia (Parkinson's and Huntington's) exhibit the same rate of initial adaptation to a visuomotor perturbation as healthy controls, but had significantly reduced after-effects (Fernández-Ruiz et al. 2003), suggesting a change in involvement of the basal ganglia between initial adaptation and after-effects.

Of course, as the removal of the visuomotor perturbation reverts the task back to a previously experienced (and in the animals an over-trained) environment dynamic the after-effect could be mediated by a retrieval of/switching to a previously established sensorimotor mapping. However, if the pre-existing no-prism internal model was readily available, we would expect a

rapid switching back to it, as is the case in humans (White and Diedrichsen 2013), and in cats B and C in the later weeks of the experiment (section 3.3.2.1). Instead, there is a persistence of a relatively slow, trial-to-trial reduction of error in both the humans and cats. This suggests that the presence of an appropriate internal model is not on its own sufficient to enable rapid switching, but a slower process – perhaps an associative learning of contextual features (Huang et al. 2011)– is required to develop such switching capability. Thus, prior to such associative learning, the motor system still requires an error-based mechanism to overcome the removal of the perturbation.

5.7 Functional connectivity stable within sessions.

Investigating the dynamics of the functional connectivity between the nodes of the motor network is likely to further our understanding of the neural processes that support the motor adaptation behaviours. Whilst there are still knowledge gaps in respect of what the local circuitry is doing within each of the major structures discussed throughout this thesis, it is clear from current literature that these disparate regions of the brain all act to support motor adaptation. This indicates that there ought to be high levels of information flow between each node, to enable accurate computations to be made. A current unknown is how and when information may be passed between these centres to enable the rapid and accurate computations performed.

The measures of phase synchrony between the PFC, and sensorimotor cortex in human EEG, and between the cerebellum and motor cortex LFP in cats, remained unchanged across the different epochs of the adaptation tasks. This challenges the hypothesis that functional connectivity between these motor network nodes would be enhanced during early stages of adaptation and after-effect, in which the proposed mechanisms of updating internal models would be expected to be most active. This raises a couple of possibilities.

Firstly, the indirect pathways from the cerebellum to both motor and prefrontal cortices (via the cerebellar and thalamic nuclei) may disrupt phase relationships between these regions through processing at the intermediary loci. ‘Long-range’ phase synchrony between distal brain areas has previously been observed (Lachaux et al. 1999; Sellers et al. 2016; Liebe et al. 2012) including from the cerebellar cortex to sensorimotor cortex (Courtemanche and Lamarre 2005), and phase synchrony can be sustained across networks with long delay lines (Barardi et al. 2014); however a direct assessment of the effects of intermediate processing steps (pons and thalamus) would be required to test this issue directly. Processing of the bi-directional information by intermediary nuclei might introduce non-linear relationships between nodes in the network. Consequently, standard measures of coherence – which address linear relationships between signals – may be insufficient to fully elucidate the underlying communication. A number of non-

linear analysis approaches exist (Pereda et al. 2005; Guevara Erra et al. 2017; Kantz and Schreiber 2003), and further investigations might be able to reveal distributed brain network effects by removing the assumptions of linearity.

The alternative possibility is that network connectivity does not vary throughout visuomotor adaptation, suggesting that the neural computations associated with adaptation can exploit the same communication lines that are used during a 'standard' reach movement. Further studies will be required to explore this more fully.

References

Akkal, D., Dum, R.P., and Strick, P.L., 2007. Supplementary motor area and presupplementary motor area: targets of basal ganglia and cerebellar output. *The Journal of Neuroscience*, 27(40):10659–73.

Alam, M., Truong, D.Q., Khadka, N., and Bikson, M., 2016. Spatial and polarity precision of concentric high-definition transcranial direct current stimulation (HD-tDCS). *Physics in Medicine and Biology*, 61(12):4506–4521.

Alayrangues, J., Torrecillos, F., Jahani, A., and Malfait, N., 2019. Error-related modulations of the sensorimotor post-movement and foreperiod beta-band activities arise from distinct neural substrates and do not reflect efferent signal processing. *NeuroImage*, 184(May 2018):10–24.

Alexander, W.H. and Brown, J.W., 2014. A general role for medial prefrontal cortex in event prediction. *Frontiers in Computational Neuroscience*, 8:69.

Ammann, C., Lindquist, M.A., and Celnik, P.A., 2017. Response variability of different anodal transcranial direct current stimulation intensities across multiple sessions. *Brain Stimulation*, 10(4):757–763.

Ammann, C., Spampinato, D., and Márquez-Ruiz, J., 2016. Modulating motor learning through transcranial directcurrent stimulation: an integrative view. *Frontiers in Psychology*, 7:1981.

Amos, A.J., 1989. *The role of the cat motor cortex in skilled locomotion*. University of Bristol.

Andersson, G. and Armstrong, D.M., 1987. Complex spikes in Purkinje cells in the lateral vermis (b zone) of the cat cerebellum during locomotion. *The Journal of Physiology*, 385(1):107–134.

Apps, R., Atkins, M.J., and Garwicz, M., 1997. Gating of cutaneous input to cerebellar climbing fibres during a reaching task in the cat. *The Journal of Physiology*, 502(1):203–214.

Apps, R. and Garwicz, M., 2005. Anatomical and physiological foundations of cerebellar information processing. *Nature reviews. Neuroscience*, 6(4):297–311.

Apps, R., Hawkes, R., Aoki, S., Bengtsson, F., Brown, A.M., Chen, G., Ebner, T.J., Isope, P., Jörntell, H., Lackey, E.P., Lawrenson, C., Lumb, B., Schonewille, M., Sillitoe, R. V., Spaeth, L., Sugihara, I., Valera, A., Voogd, J., Wylie, D.R., and Ruigrok, T.J.H., 2018. Cerebellar Modules and Their Role as Operational Cerebellar Processing Units. *The Cerebellum*, :1–29.

Apps, R., Lidierth, M., and Armstrong, D.M., 1990. Locomotion-related variations in excitability of spino-olivocerebellar paths to cat cerebellar cortical c2 zone. *The Journal of Physiology*, 424:487–512.

Armstrong, D.M. and Edgley, S.A., 1984. Discharges of nucleus interpositus neurones during locomotion in the cat. *The Journal of Physiology*, 351(1):411–432.

Armstrong, D.M. and Rawson, J.A., 1979. Activity patterns of cerebellar cortical neurones and climbing fibre afferents in the awake cat. *The Journal of Physiology*, 289(1):425–448.

Avanzino, L., Bove, M., Pelosin, E., Ogliastro, C., Lagravinese, G., and Martino, D., 2015. The cerebellum predicts the temporal consequences of observed motor acts. *PLoS ONE*, 10(2).

Baizer, J.S., Kralj-Hans, I., and Glickstein, M., 1999. Cerebellar lesions and prism adaptation in macaque monkeys. *The Journal of Neurophysiology*, 81(4):1960–1965.

Bakeman, R., 2005. Recommended effect size statistics for repeated measures designs. *Behavior*

Research Methods, 37(3):379–384.

Baker, J., Wickland, C., and Peterson, B., 1987. Dependence of cat vestibulo-ocular reflex direction adaptation on animal orientation during adaptation and rotation in darkness. *Brain Research*, 408(1–2):339–343.

Baker, S.N., 2007. Oscillatory interactions between sensorimotor cortex and the periphery. *Current Opinion in Neurobiology*, 17(6):649–655.

Ball, T., Demandt, E., Mutschler, I., Neitzel, E., Mehring, C., Vogt, K., Aertsen, A., and Schulze-Bonhage, A., 2008. Movement related activity in the high gamma range of the human EEG. *NeuroImage*, 41(2):302–310.

Barardi, A., Sancristóbal, B., and Garcia-Ojalvo, J., 2014. Phase-Coherence Transitions and Communication in the Gamma Range between Delay-Coupled Neuronal Populations. *PLoS Computational Biology*, 10(7):e1003723.

Bédard, P. and Sanes, J.N., 2014. Brain representations for acquiring and recalling visual-motor adaptations. *NeuroImage*, 101:225–235.

Benson, B.L., Anguera, J.A., and Seidler, R.D., 2011. A spatial explicit strategy reduces error but interferes with sensorimotor adaptation. *The Journal of Neurophysiology*, 105(6):2843–51.

Bernard, J.A. and Seidler, R.D., 2013. Cerebellar contributions to visuomotor adaptation and motor sequence learning: an ALE meta-analysis. *Frontiers in Human Neuroscience*, 7:27.

Bizzi, E. and Cheung, V.C.K., 2013. The neural origin of muscle synergies. *Frontiers in Computational Neuroscience*, 7:51.

Block, H.J. and Celnik, P. a, 2013. Stimulating the cerebellum affects visuomotor adaptation but not intermanual transfer of learning. *Cerebellum*, 12(6):781–793.

Bosco, A., Breveglieri, R., Hadjidimitrakis, K., Galletti, C., and Fattori, P., 2016. Reference frames for reaching when decoupling eye and target position in depth and direction. *Scientific Reports*, 6(1):21646.

Bosman, L.W.J., Koekkoek, S.K.E., Shapiro, J., Rijken, B.F.M., Zandstra, F., van der Ende, B., Owens, C.B., Potters, J.W., de Gruijl, J.R., Ruigrok, T.J.H., and De Zeeuw, C.I., 2010. Encoding of whisker input by cerebellar Purkinje cells. *The Journal of Physiology*, 588(19):3757–3783.

Bostan, A.C., Dum, R.P., and Strick, P.L., 2013. Cerebellar networks with the cerebral cortex and basal ganglia. *Trends in Cognitive Sciences*, 17(5):241–54.

Bostan, A.C. and Strick, P.L., 2018. The basal ganglia and the cerebellum: nodes in an integrated network. *Nature Reviews Neuroscience*, 19(6):338–350.

Bracco, M., Veniero, D., Oliveri, M., and Thut, G., 2018. Prismatic Adaptation Modulates Oscillatory EEG Correlates of Motor Preparation but Not Visual Attention in Healthy Participants. *The Journal of Neuroscience*, 38(5):1189–1201.

Brunoni, A.R., Nitsche, M.A., Bolognini, N., Bikson, M., Wagner, T., Merabet, L., Edwards, D.J., Valero-Cabre, A., Rotenberg, A., Pascual-Leone, A., Ferrucci, R., Priori, A., Boggio, P.S., and Fregni, F., 2012. Clinical research with transcranial direct current stimulation (tDCS): Challenges and future directions. *Brain Stimulation*, 5(3):175–195.

Buch, E.R., 2003. Visuomotor Adaptation in Normal Aging. *Learning & Memory*, 10(1):55–63.

Buckner, R.L., 2013. The cerebellum and cognitive function: 25 years of insight from anatomy and neuroimaging. *Neuron*, 80(3):807–815.

Buckner, R.L., Krienen, F.M., Castellanos, A., Diaz, J.C., and Yeo, B.T.T., 2011. The organization of

the human cerebellum estimated by intrinsic functional connectivity. *The Journal of Neurophysiology*, 106(5):2322–2345.

Buzsáki, G., Anastassiou, C. a., and Koch, C., 2012. The origin of extracellular fields and currents — EEG, ECoG, LFP and spikes. *Nature Reviews Neuroscience*, 13:407–420.

Buzsáki, G. and Wang, X.-J., 2012. Mechanisms of Gamma Oscillations. *Annual Review of Neuroscience*, 35(1):203–225.

Cantarero, G., Spampinato, D., Reis, J., Ajagbe, L., Thompson, T., Kulkarni, K., and Celnik, P. a, 2015. Cerebellar direct current stimulation enhances on-line motor skill acquisition through an effect on accuracy. *The Journal of Neuroscience*, 35(7):3285–90.

Canto, C.B., Onuki, Y., Bruinsma, B., van der Werf, Y.D., and De Zeeuw, C.I., 2017. The Sleeping Cerebellum. *Trends in Neurosciences*, 40(5):309–323.

Cerminara, N.L. and Apps, R., 2011. Behavioural significance of cerebellar modules. *Cerebellum*, 10(3):484–94.

Cerminara, N.L., Apps, R., and Marple-Horvat, D.E., 2009. An internal model of a moving visual target in the lateral cerebellum. *The Journal of Physiology*, 587:429–442.

Cerminara, N.L., Edge, A.L., Marple-Horvat, D.E., and Apps, R., 2005. The lateral cerebellum and visuomotor control. *Progress in Brain Research*, 148:213–226.

Cerminara, N.L., Lang, E.J., Sillitoe, R. V, and Apps, R., 2015. Redefining the cerebellar cortex as an assembly of non-uniform Purkinje cell microcircuits. *Nature Reviews Neuroscience*, 16(2):79–93.

Chaumon, M., Bishop, D.V.M., and Busch, N.A., 2015. A practical guide to the selection of independent components of the electroencephalogram for artifact correction. *The Journal of Neuroscience Methods*, 250:47–63.

Chen, H., Wang, Y.-J., Yang, L., Sui, J.-F., Hu, Z., and Hu, B., 2016. Theta synchronization between medial prefrontal cortex and cerebellum is associated with adaptive performance of associative learning behavior. *Scientific Reports*, 6(1):20960.

Chung, J.W., Ofori, E., Misra, G., Hess, C.W., and Vaillancourt, D.E., 2017. Beta-band activity and connectivity in sensorimotor and parietal cortex are important for accurate motor performance. *NeuroImage*, 144:164–173.

Cohen, M.X. and F F Cohen, D.I., 2017. Where Does EEG Come From and What Does It Mean? *Trends in Neurosciences*, 40(4):208–218.

Cosandier-Rimélé, D., Merlet, I., Badier, J.M., Chauvel, P., and Wendling, F., 2008. The neuronal sources of EEG: Modeling of simultaneous scalp and intracerebral recordings in epilepsy. *NeuroImage*, 42(1):135–146.

Courtemanche, R. and Lamarre, Y., 2005. Local field potential oscillations in primate cerebellar cortex: synchronization with cerebral cortex during active and passive expectancy. *The Journal of Neurophysiology*, 93(4):2039–2052.

Courtemanche, R., Pellerin, J.-P., and Lamarre, Y., 2002. Local Field Potential Oscillations in Primate Cerebellar Cortex : Modulation During Active and Passive Expectancy. *The Journal of Neurophysiology*, 88(2):771–782.

Courtemanche, R., Robinson, J.C., and Aponte, D.I., 2013. Linking oscillations in cerebellar circuits. *Frontiers in Neural Circuits*, 7:125.

Dalal, S., Osipova, D., Bertrand, O., Jerbi, K., Dalal, S., Osipova, D., Bertrand, O., and Jerbi, K., 2013. Oscillatory activity of the human cerebellum: The intracranial electrocerebellogram

revisited. *Neuroscience and Biobehavioral Reviews*, 37(4):585–93.

Dalal, S.S., Guggisberg, A.G., Edwards, E., Sekihara, K., Findlay, A.M., Canolty, R.T., Berger, M.S., Knight, R.T., Barbaro, N.M., Kirsch, H.E., and Nagarajan, S.S., 2008. Five-dimensional neuroimaging: Localization of the time-frequency dynamics of cortical activity. *NeuroImage*, 40(4):1686–1700.

Daskalakis, Z.J., Paradiso, G.O., Christensen, B.K., Fitzgerald, P.B., Gunraj, C., and Chen, R., 2004. Exploring the connectivity between the cerebellum and motor cortex in humans. *The Journal of Physiology*, 557(2):689–700.

Davis, C.J., Clinton, J.M., Jewett, K.A., Zielinski, M.R., and Krueger, J.M., 2011. Delta Wave Power: An Independent Sleep Phenotype or Epiphenomenon? *The Journal of Clinical Sleep Medicine*, 7(5):S16-18.

Della-Maggiore, V., 2004. Stimulation of the Posterior Parietal Cortex Interferes with Arm Trajectory Adjustments during the Learning of New Dynamics. *The Journal of Neuroscience*, 24(44):9971–9976.

Della-Maggiore, V., Landi, S.M., and Villalta, J.I., 2015. Sensorimotor Adaptation: Multiple Forms of Plasticity in Motor Circuits. *The Neuroscientist*, 21(2):109–125.

Delorme, A. and Makeig, S., 2004. EEGLAB: an open sorce toolbox for analysis of single-trail EEG dynamics including independent component anlaysis. *The Journal of Neuroscience Methods*, 134:9–21.

Denker, M., Roux, S., Lindén, H., Diesmann, M., Riehle, A., and Grün, S., 2011. The local field potential reflects surplus spike synchrony. *Cerebral Cortex*, 21(12):2681–2695.

Deuschl, G., Toro, C., Zeffiro, T., Massaquoi, S., and Hallett, M., 1996. Adaptation motor learning of arm movements in patients with cerebellar disease. *The Journal of Neurology, Neurosurgery & Psychiatry*, 60(5):515–519.

Diedrichsen, J., Hashambhoy, Y., Rane, T., and Shadmehr, R., 2005. Neural correlates of reach errors. *The Journal of Neuroscience*, 25(43):9919–31.

Donchin, O., Rabe, K., Diedrichsen, J., Lally, N., Schoch, B., Gizewski, E.R., and Timmann, D., 2012. Cerebellar regions involved in adaptation to force field and visuomotor perturbation. *The Journal of Neurophysiology*, 107(1):134–47.

Doppelmayr, M., Pixa, N.H., and Steinberg, F., 2016. Cerebellar, but not Motor or Parietal, High-Density Anodal Transcranial Direct Current Stimulation Facilitates Motor Adaptation. *The Journal of the International Neuropsychological Society*, 22(9):928–936.

Van Dun, K., Bodranghien, F., Manto, M., and Mariën, P., 2017. Targeting the Cerebellum by Noninvasive Neurostimulation: a Review. *The Cerebellum*, 16(3):695–741.

Van Dun, K., Bodranghien, F., Mariën, P., and Manto, M.U., 2016. tDCS of the Cerebellum: Where Do We Stand in 2016? Technical Issues and Critical Review of the Literature. *Frontiers in Human Neuroscience*, 10:199.

Van Dun, K. and Manto, M., 2018. Non-invasive Cerebellar Stimulation: Moving Towards Clinical Applications for Cerebellar and Extra-Cerebellar Disorders. *The Cerebellum*, 17(3):259–263.

Dyke, K., Kim, S., Jackson, G.M., and Jackson, S.R., 2016. Intra-Subject Consistency and Reliability of Response Following 2 mA Transcranial Direct Current Stimulation. *Brain Stimulation*, 9(6):819–825.

Ebbesen, C.L. and Brecht, M., 2017. Motor cortex - To act or not to act? *Nature Reviews Neuroscience*, 18(11):694–705.

Eccles, J.C., Llinás, R., and Sasaki, K., 1966. The excitatory synaptic action of climbing fibres on the Purkinje cells of the cerebellum. *The Journal of Physiology*, 182(2):268–296.

Edge, A., 2005. *The role of the lateral cerebellum in visually guided movement*. University of Bristol.

Edgley, S.A. and Lidierth, M., 1987. Discharges of cerebellar golgi cells during locomotion. *The Journal of Physiology*, 392:315–332.

Ekerot, C.-F. and Larson, B., 1979. The dorsal spino-olivocerebellar system in the cat. I. Functional organization and termination in the anterior lobe. *Experimental Brain Research*, 36(2):201–17.

Ekerot, C.F. and Jörntell, H., 2001. Parallel fibre receptive fields of Purkinje cells and interneurons are climbing fibre-specific. *The European Journal of Neuroscience*, 13(7):1303–10.

Ekerot, C.F., Jörntell, H., and Garwicz, M., 1995. Functional relation between corticonuclear input and movements evoked on microstimulation in cerebellar nucleus interpositus anterior in the cat. *Experimental Brain Research*, 106(3):365–376.

Engel, A.K. and Fries, P., 2010. Beta-band oscillations-signalling the status quo? *Current Opinion in Neurobiology*, 20(2):156–165.

Euston, D.R., Gruber, A.J., and McNaughton, B.L., 2012. The role of medial prefrontal cortex in memory and decision making. *Neuron*, 76(6):1057–70.

Evinger, C. and Fuchs, A.F., 1978. Saccadic, smooth pursuit, and optokinetic eye movements of the trained cat. *The Journal of Physiology*, 285(1):209–229.

Feingold, J., Gibson, D.J., DePasquale, B., and Graybiel, A.M., 2015. Bursts of beta oscillation differentiate postperformance activity in the striatum and motor cortex of monkeys performing movement tasks. *Proceedings of the National Academy of Sciences of the United States of America*, 112(44):13687–13692.

Fernández-Ruiz, J., Díaz, D., Hall-Haro, C., Vergara, P., Mischner, J., Nunez, L., Drucker-Colin, R., Ochoa, A., and Alonso, M.E., 2003. Normal prism adaptation but reduced after-effect in basal ganglia disorders using a throwing task. *European Journal of Neuroscience*, 18(3):689–694.

Fernández-Ruiz, J. and Díaz, R., 1999. Prism Adaptation and Aftereffect: Specifying the Properties of a Procedural Memory System. *Learning & Memory*, 6(1):47–53.

Fernandez, L., Albein-Urios, N., Kirkovski, M., McGinley, J.L., Murphy, A.T., Hyde, C., Stokes, M.A., Rinehart, N.J., and Enticott, P.G., 2017. Cathodal Transcranial Direct Current Stimulation (tDCS) to the Right Cerebellar Hemisphere Affects Motor Adaptation During Gait. *The Cerebellum*, 16(1):168–177.

Ferrier, D., 1874. Experiments on the Brain of Monkeys. *Proceedings of the Royal Society of London*, 23:409–430.

Ferrucci, R., Bocci, T., Cortese, F., Ruggiero, F., and Priori, A., 2016. Cerebellar transcranial direct current stimulation in neurological disease. *Cerebellum & Ataxias*, 3(1):16.

Ferrucci, R. and Priori, A., 2014. Transcranial cerebellar direct current stimulation (tcDCS): Motor control, cognition, learning and emotions. *NeuroImage*, 85:918–923.

Fierro, B., Giglia, G., Palermo, A., Pecoraro, C., Scalia, S., and Brighina, F., 2007. Modulatory effects of 1 Hz rTMS over the cerebellum on motor cortex excitability. *Experimental Brain Research*, 176(3):440–447.

Fiocchi, S., Chiaramello, E., Gazzola, V., Suttrup, J., Ravazzani, P., and Parazzini, M., 2017.

Assessment of the capability to target cerebellar sub-regions with high-definition transcranial direct current stimulation high-definition transcranial direct current stimulation (HD-tDCS) over the cerebellum. In: *2017 IEEE 3rd International Forum on Research and Technologies for Society and Industry (RTSI)*. Modena, pp.1–6.

Fling, B.W., Gera Dutta, G., and Horak, F.B., 2015. Functional connectivity underlying postural motor adaptation in people with multiple sclerosis. *NeuroImage: Clinical*, 8:281–289.

Flint, R.D., Lindberg, E.W., Jordan, L.R., Miller, L.E., and Slutzky, M.W., 2012. Accurate decoding of reaching movements from field potentials in the absence of spikes. *The Journal of Neural Engineering*, 9(4):046006.

Funahashi, S., 2017. Working memory in the prefrontal cortex. *Brain Sciences*, 7(5).

Galea, J.M., Jayaram, G., Ajagbe, L., and Celnik, P. a, 2009. Modulation of cerebellar excitability by polarity-specific noninvasive direct current stimulation. *The Journal of Neuroscience*, 29(28):9115–22.

Galea, J.M., Vazquez, A., Pasricha, N., Orban De Xivry, J.J., and Celnik, P. a, 2011. Dissociating the roles of the cerebellum and motor cortex during adaptive learning: The motor cortex retains what the cerebellum learns. *Cerebral Cortex*, 21(8):1761–1770.

Gallego, J.A., Perich, M.G., Miller, L.E., and Solla, S.A., 2017. Neural Manifolds for the Control of Movement. *Neuron*, 94(5):978–984.

Gandolfo, F., Li, C.S., Benda, B.J., Schioppa, C.P., and Bizzi, E., 2000. Cortical correlates of learning in monkeys adapting to a new dynamical environment. *Proceedings of the National Academy of Sciences of the United States of America*, 97(5):2259–63.

Garwicz, M. and Andersson, G., 1992. Spread of synaptic activity along parallel fibres in cat cerebellar anterior lobe. *Experimental Brain Research*, 88(3):615–622.

Grandchamp, R. and Delorme, A., 2011. Single-trial normalization for event-related spectral decomposition reduces sensitivity to noisy trials. *Frontiers in Psychology*, 2:236.

Graziano, M.S.A., Taylor, C.S.R., and Moore, T., 2002. Complex movements evoked by microstimulation of precentral cortex. *Neuron*, 34(5):841–851.

Groenewegen, H.J., 1988. Organization of the afferent connections of the mediodorsal thalamic nucleus in the rat, related to the mediodorsal-prefrontal topography. *Neuroscience*, 24(2):379–431.

Gross, C.G., 2007. The discovery of motor cortex and its background. *The Journal of the History of the Neurosciences*, 16(3):320–331.

Guevara Erra, R., Perez Velazquez, J.L., and Rosenblum, M., 2017. Neural Synchronization from the Perspective of Non-linear Dynamics. *Frontiers in Computational Neuroscience*, 11:98.

de Haan, R., Lim, J., van der Burg, S.A., Pieneman, A.W., Nigade, V., Mansvelder, H.D., and de Kock, C.P.J., 2018. Neural Representation of Motor Output, Context and Behavioral Adaptation in Rat Medial Prefrontal Cortex During Learned Behavior. *Frontiers in Neural Circuits*, 12:75.

Haith, A.M. and Krakauer, J.W., 2013. Model-Based and Model-Free Mechanisms of Human Motor Learning. In: M. J. Richardson, M. A. Riley, & K. Shockley, eds. *Progress in Motor Control, Advances in Experimental Medicine and Biology*. Advances in Experimental Medicine and Biology. Springer New York, pp.1–21.

Hall, T.M., DeCarvalho, F., and Jackson, A., 2014. A Common Structure Underlies Low-Frequency Cortical Dynamics in Movement, Sleep, and Sedation. *Neuron*, 83(5):1185–1199.

Hardwick, R.M. and Celnik, P.A., 2014. Cerebellar direct current stimulation enhances motor learning inolder adults. *Neurobiology of Aging*, 35(10):2217–2221.

Harmony, T., 2013. The functional significance of delta oscillations in cognitive processing. *Frontiers in Integrative Neuroscience*, 7:83.

Harris, C.S., 2012. Adaptation to Displaced Vision: Visual, Motor, or Proprioceptive Change? *Science*, 140(3568):812–813.

Hartmann, M.J. and Bower, J.M., 1998. Oscillatory activity in the cerebellar hemispheres of unrestrained rats. *The Journal of Neurophysiology*, 80(3):1598–1604.

Haruno, M. and Wolpert, D.M., 1999. Multiple Paired Forward-Inverse Models for Human Motor Learning and Control. *Advances in Neural Information Processing Systems*, 11:31–37.

Haruno, M., Wolpert, D.M., and Kawato, M., 2001. MOSAIC Model for Sensorimotor Learning and Control. *Neural Computation*, 13(10):2201–2220.

Heathcote, A., Popiel, S., and Mewhort, D.J.K., 1991. Analysis of response time distributions: An example using the Stroop task. *Psychological Bulletin*, 109(2):340–347.

Herculano-Houzel, 2010. Coordinated scaling of cortical and cerebellar numbers of neurons. *Frontiers in Neuroanatomy*, 4:12.

Herreras, O., 2016. Local Field Potentials: Myths and Misunderstandings. *Frontiers in Neural Circuits*, 10:101.

Herzfeld, D.J., Kojima, Y., Soetedjo, R., and Shadmehr, R., 2018. Encoding of error and learning to correct that error by the Purkinje cells of the cerebellum. *Nature Neuroscience*, :1.

Herzfeld, D.J., Pastor, D., Haith, A.M., Rossetti, Y., Shadmehr, R., and O'Shea, J., 2014. Contributions of the cerebellum and the motor cortex to acquisition and retention of motor memories. *NeuroImage*, 98:147–58.

Herzfeld, D.J., Vaswani, P.A., Marko, M.K., and Shadmehr, R., 2014. A memory of errors in sensorimotor learning. *Science*, 345(6202):1349–1353.

Hewitt, A.L., Popa, L.S., and Ebner, T.J., 2015. Changes in Purkinje Cell Simple Spike Encoding of Reach Kinematics during Adaption to a Mechanical Perturbation. *The Journal of Neuroscience*, 35(3):1106–1124.

Hobson, J.A. and McCarley, R.W., 1972. Spontaneous discharge rates of cat cerebellar purkinje cells in sleep and waking. *Electroencephalography and Clinical Neurophysiology*, 33(5):457–469.

Holdefer, R.N., Miller, L.E., Chen, L.L., and Houk, J.C., 2000. Functional connectivity between cerebellum and primary motor cortex in the awake monkey. *The Journal of Neurophysiology*, 84(1):585–590.

Holmes, G., 1917. The symptoms of acute cerebellar injuries due to gunshot injuries. *Brain*, 40(4):461–535.

Holmes, G., 1939. The cerebellum of man. *Brain*, 62(1):1–30.

Honda, T., Nagao, S., Hashimoto, Y., Ishikawa, K., Yokota, T., Mizusawa, H., and Ito, M., 2018. Tandem internal models execute motor learning in the cerebellum. *Proceedings of the National Academy of Sciences*, 115(28):7428–7433.

Hosaka, R., Nakajima, T., Aihara, K., Yamaguchi, Y., and Mushiake, H., 2016. The Suppression of Beta Oscillations in the Primate Supplementary Motor Complex Reflects a Volatile State During the Updating of Action Sequences. *Cerebral Cortex*, 26(8):3442–3452.

Huang, V.S., Haith, A., Mazzoni, P., and Krakauer, J.W., 2011. Rethinking motor learning and savings in adaptation paradigms: model-free memory for successful actions combines with internal models. *Neuron*, 70(4):787–801.

Hunter, T., Sacco, P., Nitsche, M.A., and Turner, D.L., 2009. Modulation of internal model formation during force field-induced motor learning by anodal transcranial direct current stimulation of primary motor cortex. *The Journal of Physiology*, 587(12):2949–2961.

Ishikawa, T., Tomatsu, S., Izawa, J., and Kakei, S., 2016. The cerebro-cerebellum: Could it be loci of forward models? *Neuroscience Research*, 104:72–79.

Ito, M., 2000. Mechanisms of motor learning in the cerebellum11Published on the World Wide Web on 24 November 2000. *Brain Research*, 886(1–2):237–245.

Ito, M., 2002. Historical review of the significance of the cerebellum and the role of purkinje cells in motor learning. *Annals of the New York Academy of Sciences*, 978:273–288.

Ito, S., Stuphorn, V., Brown, J.W., and Schall, J.D., 2003. Performance monitoring by the anterior cingulate cortex during saccade countermanding. *Science*.

Ivry, R.B., Spencer, R.M., Zelaznik, H.N., and Diedrichsen, J., 2002. The cerebellum and event timing. *Annals of the New York Academy of Sciences*, 978:302–17.

Izawa, J., Criscimagna-Hemminger, S.E., and Shadmehr, R., 2012. Cerebellar Contributions to Reach Adaptation and Learning Sensory Consequences of Action. *The Journal of Neuroscience*, 32(12):4230–4239.

Jackson, M.P., Rahman, A., Lafon, B., Kronberg, G., Ling, D., Parra, L.C., and Bikson, M., 2016. Animal models of transcranial direct current stimulation: Methods and mechanisms. *Clinical Neurophysiology*, 127(11):3425–3454.

Jalali, R., Miall, R.C., and Galea, J.M., 2017. No consistent effect of cerebellar transcranial direct current stimulation on visuomotor adaptation. *The Journal of Neurophysiology*, 118(2):655–665.

Jayaram, G., Tang, B., Pallegadda, R., Vasudevan, E.V.L., Celnik, P. a, and Bastian, A., 2012. Modulating locomotor adaptation with cerebellar stimulation. *The Journal of Neurophysiology*, 107(11):2950–7.

Kajikawa, Y. and Schroeder, C.E., 2011. How local is the local field potential? *Neuron*, 72(5):847–858.

Kantz, H. and Schreiber, T., 2003. *Nonlinear Time Series Analysis*. Cambridge: Cambridge University Press.

Kawato, M., 1993. Inverse dynamics model in the cerebellum. *Proceedings of 1993 International Conference on Neural Networks (IJCNN-93-Nagoya, Japan)*, 2:1329–1335.

Kelly, R.M. and Strick, P.L., 2003. Cerebellar loops with motor cortex and prefrontal cortex of a nonhuman primate. *The Journal of Neuroscience*, 23(23):8432–8444.

Khanna, P. and Carmena, J.M., 2017. Beta band oscillations in motor cortex reflect neural population signals that delay movement onset. *eLife*, 6.

Kim, S., Ogawa, K., Lv, J., Schweighofer, N., and Imamizu, H., 2015. Neural Substrates Related to Motor Memory with Multiple Timescales in Sensorimotor Adaptation. *PLoS Biology*, 13(12).

Kitago, T., Ryan, S.L., Mazzoni, P., Krakauer, J.W., and Haith, A.M., 2013. Unlearning versus savings in visuomotor adaptation: comparing effects of washout, passage of time, and removal of errors on motor memory. *Frontiers in Human Neuroscience*, 7:1–7.

Kitazawa, S., Kimura, T., and Yin, P.-B., 1998. Cerebellar complex spikes encode both destinations and errors in arm movements. *Nature*, 392(6675):494–497.

Knudsen, E.I., 1994. Supervised learning in the brain. *The Journal of Neuroscience*, 14(7):3985–97.

Kobaiter-Maarrawi, S., Maarrawi, J., Abou Zeid, H., Samaha, E., Okais, N., Garcia-Larrea, L., and Magnin, M., 2011. Stereotactic functional mapping of the cat motor cortex. *Behavioural Brain Research*, 225(2):646–650.

Kojima, Y., Soetedjo, R., and Fuchs, A.F., 2010. Changes in simple spike activity of some Purkinje cells in the oculomotor vermis during saccade adaptation are appropriate to participate in motor learning. *The Journal of Neuroscience*, 30(10):3715–27.

Van der Kooij, K., Overvliet, K.E., and J, S.J.B., 2016. Temporally Stable Adaptation is Robust, Incomplete and Specific. *European Journal of Neuroscience*, 44(9):2708–2715.

Koziol, L.F., Budding, D., Andreasen, N., D'Arrigo, S., Bulgheroni, S., Imamizu, H., Ito, M., Manto, M., Marvel, C., Parker, K., Pezzulo, G., Ramnani, N., Riva, D., Schmahmann, J.D., Vandervert, L., and Yamazaki, T., 2014. Consensus paper: the cerebellum's role in movement and cognition. *Cerebellum*, 13(1):151–77.

Krakauer, J.W., 2009. Motor learning and consolidation: The case of visuomotor rotation. *Advances in Experimental Medicine and Biology*, 629:405–421.

Kuczynski, V., Telonio, A., Thibaudier, Y., Hurteau, M.-F., Dambreville, C., Desrochers, E., Doelman, A., Ross, D., and Frigon, A., 2017. Lack of adaptation during prolonged split-belt locomotion in the intact and spinal cat. *The Journal of Physiology*, 595(17):5987–6006.

Lachaux, J.-P., Rodriguez, E., Le van Quyen, M., Lutz, A., Martinerie, J., and Varela, F.J., 2000. Studying single-trials of phase synchronous activity in the brain. *International Journal of Bifurcation and Chaos*, 10(10):2429–39.

Lachaux, J.P., Rodriguez, E., Martinerie, J., and Varela, F.J., 1999. Measuring phase synchrony in brain signals. *Human Brain Mapping*, 8(4):194–208.

Landi, S.M., Baguear, F., and Della-Maggiore, V., 2011. One week of motor adaptation induces structural changes in primary motor cortex that predict long-term memory one year later. *The Journal of Neuroscience*, 31(33):11808–13.

Lang, E.J., Apps, R., Bengtsson, F., Cerminara, N.L., De Zeeuw, C.I., Ebner, T.J., Heck, D.H., Jaeger, D., Jörntell, H., Kawato, M., Otis, T.S., Ozyildirim, O., Popa, L.S., Reeves, A.M.B., Schweighofer, N., Sugihara, I., and Xiao, J., 2017. The Roles of the Olivocerebellar Pathway in Motor Learning and Motor Control. A Consensus Paper. *Cerebellum*, 16(1):230–252.

Lasdon, L.S., Fox, R.L., and Ratner, M.W., 1974. Nonlinear optimization using the generalized reduced gradient method. *Revue Francaise d'Automatique, Informatique et Recherche Opérationnelle*, 3(3):73–104.

Leow, L.-A., de Rugy, A., Marinovic, W., Riek, S., and Carroll, T.J., 2016. Savings for visuomotor adaptation require prior history of error, not prior repetition of successful actions. *The Journal of Neurophysiology*, 116(4):1603–1614.

Leski, S., Lindén, H., Tetzlaff, T., Pettersen, K.H., and Einevoll, G.T., 2013. Frequency Dependence of Signal Power and Spatial Reach of the Local Field Potential. *PLoS Computational Biology*, 9(7):e1003137.

Li, C.-S.R.S., Padoa-Schioppa, C., and Bizzi, E., 2001. Neuronal correlates of motor performance and motor learning in the primary motor cortex of monkeys adapting to an external force field. *Neuron*, 30(2):593–607.

Lidierth, M. and Apps, R., 1990. Gating in the spino-olivocerebellar pathways to the c1 zone of the cerebellar cortex during locomotion in the cat. *The Journal of Physiology*, 430:453–69.

Liebe, S., Hoerzer, G.M., Logothetis, N.K., and Rainer, G., 2012. Theta coupling between V4 and prefrontal cortex predicts visual short-term memory performance. *Nature Neuroscience*, 15(3):456–462.

Liew, S.-L., Thompson, T., Ramirez, J., Butcher, P., Taylor, J.A., and Celnik, P.A., 2018. Variable neural contributions to explicit and implicit learning during visuomotor adaptation. *Frontiers in Neuroscience*, 12:610.

Lindén, H., Tetzlaff, T., Potjans, T.C., Pettersen, K.H., Grün, S., Diesmann, M., and Einevoll, G.T., 2011. Modeling the spatial reach of the LFP. *Neuron*, 72(5):859–872.

Little, S. and Brown, P., 2014. The functional role of beta oscillations in Parkinson's disease. *Parkinsonism & Related Disorders*, 20:S44–S48.

Livingston, A. and Phillips, C.G., 1957. Maps and Thresholds for the Sensorymotor Cortex of the Cat. *Quarterly Journal of Experimental Physiology and Cognate Medical Sciences*, 42(2):190–205.

Llinás, R.R., 2011. Cerebellar motor learning versus cerebellar motor timing: the climbing fibre story. *The Journal of Physiology*, 589(14):3423–3432.

Lopes, G., Bonacchi, N., Frazao, J., Neto, J.P., Atallah, B. V, Soares, S., Moreira, L., Matias, S., Itskov, P.M., Correia, P.A., Medina, R.E., Calcaterra, L., Dreosti, E., Paton, J.J., and Kampff, A.R., 2015. Bonsai: an event-based framework for processing and controlling data streams. *Frontiers in Neuroinformatics*, 9:7.

Luauté, J., Schwartz, S., Rossetti, Y., Spiridon, M., Rode, G., Boisson, D., and Vuilleumier, P., 2009. Dynamic changes in brain activity during prism adaptation. *The Journal of Neuroscience*, 29(1):169–78.

Ma, L., Wang, B., Narayana, S., Hazeltine, E., Chen, X., Robin, D.A., Fox, P.T., and Xiong, J., 2010. Changes in regional activity are accompanied with changes in inter-regional connectivity during 4 weeks motor learning. *Brain Research*, 1318:64–76.

Magno, E., 2006. The Anterior Cingulate and Error Avoidance. *Journal of Neuroscience*.

Mano, N.-I., Kanazawa, I., and Yamamoto, K.-I., 1986. Complex-Spike Activity of Cerebellar Purkinje Cells Related to Wrist Tracking Movement in Monkey. *The Journal of Neurophysiology*, 56(1):137–157.

Mano, N. and Yamamoto, K.-I., 1980. Simple-spike activity of cerebellar Purkinje cells related to visually guided wrist tracking movement in the monkey. *The Journal of Neurophysiology*, 43(3):713–28.

Markowitsch, H.J. and Pritzel, M., 1977. A stereotaxic atlas of the prefrontal cortex of the cat. *Acta Neurobiologiae Experimentalis*, 37(2):63–81.

Marple-Horvat, D.E., Criado, J.M., and Armstrong, D.M., 1998. Neuronal activity in the lateral cerebellum of the cat related to visual stimuli at rest, visually guided step modification, and saccadic eye movements. *The Journal of Physiology*, 506(2):489–514.

Martin, T.A., Keating, J.G., Goodkin, H.P., Bastian, A.J., and Thach, W.T., 1996a. Throwing while looking through prisms. I. Focal olivocerebellar lesions impair adaptation. *Brain*, 119(4):1183–98.

Martin, T.A., Keating, J.G., Goodkin, H.P., Bastian, A.J., and Thach, W.T., 1996b. Throwing while looking through prisms: II. Specificity and storage of multiple gaze-throw calibrations.

Brain, 119(4):1199–1211.

Mathis, A., Mamidanna, P., Cury, K.M., Abe, T., Murthy, V.N., Mathis, M.W., and Bethge, M., 2018. DeepLabCut: markerless pose estimation of user-defined body parts with deep learning. *Nature Neuroscience*, 21(9):1281–1289.

Matsumoto, H. and Ugawa, Y., 2017. Adverse events of tDCS and tACS: A review. *Clinical Neurophysiology Practice*, 2:19–25.

McDougle, S.D., Bond, K.M., and Taylor, J.A., 2015. Explicit and Implicit Processes Constitute the Fast and Slow Processes of Sensorimotor Learning. *The Journal of Neuroscience*, 35(26):9568–79.

Mcgill, W. and Gibbon, J., 1965. The general-gamma distribution and reaction times. *The Journal of Mathematical Psychology*, 2(1):1–18.

Mehring, C., Rickert, J., Vaadia, E., de Oliveira, S.C., Aertsen, A., and Rotter, S., 2003. Inference of hand movements from local field potentials in monkey motor cortex. *Nature Neuroscience*, 6(12):1253–1254.

Melik-Musyan, A.B. and Fanardjyan, V. V, 1998. Projections of the central cerebellar nuclei to the intralaminar thalamic nuclei in cats. *Neurophysiology*, 30(1):39–47.

Miall, R.C., Christensen, L.O.D., Cain, O., and Stanley, J., 2007. Disruption of state estimation in the human lateral cerebellum. *PLoS biology*, 5(11):e316.

Miall, R.C., Jenkinson, N., and Kulkarni, K., 2004. Adaptation to rotated visual feedback: A re-examination of motor interference. *Experimental Brain Research*, 154(2):201–210.

Middleton, F. a and Strick, P.L., 2001. Cerebellar projections to the prefrontal corex of the primate. *The Journal of Neuroscience*, 21(2):700–712.

Middleton, S.J., Racca, C., Cunningham, M.O., Traub, R.D., Monyer, H., Knöpfel, T., Schofield, I.S., Jenkins, A., Whittington, M.A., Knöpfel, T., Schofield, I.S., Jenkins, A., and Whittington, M.A., 2008. High-Frequency Network Oscillations in Cerebellar Cortex. *Neuron*, 58(5):763–774.

Milardi, D., Arrigo, A., Anastasi, G., Cacciola, A., Marino, S., Mormina, E., Calamuneri, A., Bruschetta, D., Cutroneo, G., Trimarchi, F., and Quartarone, A., 2016. Extensive Direct Subcortical Cerebellum-Basal Ganglia Connections in Human Brain as Revealed by Constrained Spherical Deconvolution Tractography. *Frontiers in Neuroanatomy*, 10:29.

Miles, J. and Shevlin, M., 2001. *Applying Regression and Correlation*. SAGE Publications.

Miles, O.B., Cerminara, N.L., and Marple-Horvat, D.E., 2006. Purkinje cells in the lateral cerebellum of the cat encode visual events and target motion during visually guided reaching. *The Journal of Physiology*, 571(3):619–637.

Miller, E.K. and Cohen, J.D., 2001. An Integrative Theory of Prefrontal Cortex Function. *Annual Review of Neuroscience*, 24(1):167–202.

Miller, E.K., Freedman, D.J., and Wallis, J.D., 2002. The prefrontal cortex: categories, concepts and cognition. *Philosophical Transactions of the Royal Society B: Biological Sciences*, 357(1424):1123–1136.

Miller, J., 1991. Reaction Time Analysis with Outlier Exclusion: Bias Varies with Sample Size. *The Quarterly Journal of Experimental Psychology*, 43(4):907–912.

Minarik, T., Berger, B., Althaus, L., Bader, V., Biebl, B., Brotzeller, F., Fusban, T., Hegemann, J., Jesteadt, L., Kalweit, L., Leitner, M., Linke, F., Nabielska, N., Reiter, T., Schmitt, D., Spraetz, A., and Sauseng, P., 2016. The Importance of Sample Size for Reproducibility of tDCS

Effects. *Frontiers in Human Neuroscience*, 10:453.

Minhas, P., Bansal, V., Patel, J., Ho, J.S., Diaz, J., Datta, A., and Bikson, M., 2010. Electrodes for high-definition transcutaneous DC stimulation for applications in drug delivery and electrotherapy, including tDCS. *The Journal of Neuroscience Methods*, 190(2):188–197.

Montgomery, A.S., 1994. *Excitability of somatic afferent pathways to the motor cortex during locomotion in the cat*. University of Bristol.

Morehead, J.R., Qasim, S.E., Crossley, M.J., and Ivry, R., 2015. Savings upon Re-Aiming in Visuomotor Adaptation. *The Journal of Neuroscience*, 35(42):14386–14396.

Morton, S.M. and Bastian, A.J., 2006. Cerebellar contributions to locomotor adaptations during splitbelt treadmill walking. *The Journal of Neuroscience*, 26(36):9107–16.

Mukhopadhyay, S. and Ray, G.C., 1998. A new interpretation of nonlinear energy operator and its efficacy in spike detection. *IEEE Transactions on Biomedical Engineering*, 45(2):180–187.

Nacher, V., Ledberg, A., Deco, G., and Romo, R., 2013. Coherent delta-band oscillations between cortical areas correlate with decision making. *Proceedings of the National Academy of Sciences*, 110(37):15085–15090.

Newport, R., Brown, L., Husain, M., Mort, D., and Jackson, S.R., 2006. The role of the posterior parietal lobe in prism adaptation: Failure to adapt to optical prisms in a patient with bilateral damage to posterior parietal cortex. *Cortex*, 42(5):720–729.

Niedermeyer, E., 2004. *Electroencephalography : Basic Principles, Clinical Applications, and Related Fields*. Lippincott Williams & Wilkins.

Nieratschker, V., Kiefer, C., Giel, K., Krüger, R., and Plewnia, C., 2015. The COMT Val/Met polymorphism modulates effects of tDCS on response inhibition. *Brain Stimulation*, 8(2):283–288.

Nitsche, M.A. and Paulus, W., 2000. Excitability changes induced in the human motor cortex by weak transcranial direct current stimulation. *The Journal of Physiology*, 527(3):633–639.

Noda, T. and Yamamoto, T., 1984. Response properties and morphological identification of neurons in the cat motor cortex. *Brain Research*, 306(1–2):197–206.

Norris, S.A., Hathaway, E.N., Taylor, J.A., and Thach, W.T., 2011. Cerebellar inactivation impairs memory of learned prism gaze-reach calibrations. *The Journal of neurophysiology*, 105(5):2248–2259.

Nowak, M., Zich, C., and Stagg, C.J., 2018. Motor Cortical Gamma Oscillations: What Have We Learnt and Where Are We Headed? *Current Behavioral Neuroscience Reports*, 5:136–142.

Nozari, N., Woodard, K., and Thompson-Schill, S.L., 2014. Consequences of cathodal stimulation for behavior: When does it help and when does it hurt performance? *PLoS ONE*, 9(1).

O'Reilly, J.X., Mesulam, M.M., and Nobre, A.C., 2008. The Cerebellum Predicts the Timing of Perceptual Events. *The Journal of Neuroscience*, 28(9):2252–2260.

Oldrati, V. and Schutter, D.J.L.G., 2018. Targeting the Human Cerebellum with Transcranial Direct Current Stimulation to Modulate Behavior: a Meta-Analysis. *The Cerebellum*, 17(2):228–236.

Oscarsson, O., 1979. Functional units of the cerebellum - sagittal zones and microzones. *Trends in Neurosciences*, 2:143–145.

Oscarsson, O., 1980. Functional organisation of Olivary projection to cerebellar antrior lobe. In: J. Courville, C. De Montigny, & Y. Lamarre, eds. *The Inferior Oliveary Nucleus: Anatomy and*

Physiology. Raven Press, pp.279–289.

Özdenizci, O., Yalçın, M., Erdoğan, A., Patoğlu, V., Grosse-Wentrup, M., and Çetin, M., 2017. Electroencephalographic identifiers of motor adaptation learning. *The Journal of Neural Engineering*, 14(4):046027.

Pakaprot, N., Kim, S., and Thompson, R.F., 2009. The role of the cerebellar interpositus nucleus in short and long term memory for trace eyeblink conditioning. *Behavioral Neuroscience*, 123(1):54–61.

Palmer, E.M., Horowitz, T.S., Torralba, A., and Wolfe, J.M., 2011. What are the shapes of response time distributions in visual search? *The Journal of Experimental Psychology: Human Perception and Performance*, 37(1):58–71.

Panouillères, M.T.N., Miall, R.C., and Jenkinson, N., 2015. The role of the posterior cerebellum in saccadic adaptation: a transcranial direct current stimulation study. *The Journal of Neuroscience*, 35(14):5471–9.

Parazzini, M., Rossi, E., Ferrucci, R., Liorni, I., Priori, A., and Ravazzani, P., 2014. Modelling the electric field and the current density generated by cerebellar transcranial DC stimulation in humans. *Clinical Neurophysiology*, 125(3):577–584.

Pasalar, S., Roitman, a V, Durfee, W.K., and Ebner, T.J., 2006. Force field effects on cerebellar Purkinje cell discharge with implications for internal models. *Nature Neuroscience*, 9(11):1404–1411.

Paz, R., Boraud, T., Natan, C., Bergman, H., and Vaadia, E., 2003. Preparatory activity in motor cortex reflects learning of local visuomotor skills. *Nature Neuroscience*, 6(8):882–890.

Pellerin, J.P. and Lamarre, Y., 1997. Local field potential oscillations in primate cerebellar cortex during voluntary movement. *The Journal of Neurophysiology*, 78(6):3502–3507.

Penfield, W. and Boldrey, E., 1937. Somatic motor and sensory representation in the cerebral cortex of man as studied by electrical stimulation. *Brain*, 60(4):389–443.

Pereda, E., Quiroga, R.Q., and Bhattacharya, J., 2005. Nonlinear multivariate analysis of neurophysiological signals. *Progress in Neurobiology*, 77(1–2):1–37.

Pfurtscheller, G., 2001. Functional brain imaging based on ERD/ERS. *Vision Research*, 41(10–11):1257–1260.

Pfurtscheller, G., Stancák, A., and Neuper, C., 1996. Post-movement beta synchronization. A correlate of an idling motor area? *Electroencephalography and Clinical Neurophysiology*, 98(4):281–293.

Pierrot-Deseilligny, C., Müri, R.M., Ploner, C.J., Gaymard, B., Demeret, S., and Rivaud-Pechoux, S., 2003. Decisional role of the dorsolateral prefrontal cortex in ocular motor behaviour. *Brain*, 126(6):1460–1473.

Pochon, J.-B.B., Levy, R., Poline, J.B., Crozier, S., Lehéricy, S., Pillon, B., Deweer, B., Le Bihan, D., and Dubois, B., 2001. The Role of Dorsolateral Prefrontal Cortex in the Preparation of Forthcoming Actions: an fMRI Study. *Cerebral Cortex*, 11(3):260–266.

Polikov, V.S., Tresco, P.A., and Reichert, W.M., 2005. Response of brain tissue to chronically implanted neural electrodes. *The Journal of Neuroscience Methods*, 148(1):1–18.

Popa, D., Spolidoro, M., Proville, R.D., Guyon, N., Belliveau, L., and Lena, C., 2013. Functional Role of the Cerebellum in Gamma-Band Synchronization of the Sensory and Motor Cortices. *The Journal of Neuroscience*, 33(15):6552–6556.

Popa, L.S., Hewitt, a. L., and Ebner, T.J., 2012. Predictive and Feedback Performance Errors Are

Signaled in the Simple Spike Discharge of Individual Purkinje Cells. *The Journal of Neuroscience*, 32(44):15345–15358.

Popa, L.S., Streng, M.L., Hewitt, A.L., and Ebner, T.J., 2016. The Errors of Our Ways: Understanding Error Representations in Cerebellar-Dependent Motor Learning. *Cerebellum*, 15(2):93–103.

Priori, A., 2003. Brain polarization in humans: A reappraisal of an old tool for prolonged non-invasive modulation of brain excitability. *Clinical Neurophysiology*, 114(4):589–595.

Richardson, A.G., Borghi, T., and Bizzi, E., 2012. Activity of the same motor cortex neurons during repeated experience with perturbed movement dynamics. *The Journal of Neurophysiology*, 107(11):3144–3154.

Richardson, A.G., Overduin, S.A., Valero-Cabre, A., Padoa-Schioppa, C., Pascual-Leone, A., Bizzi, E., and Press, D.Z., 2006. Disruption of Primary Motor Cortex before Learning Impairs Memory of Movement Dynamics. *The Journal of Neuroscience*, 26(48):12466–12470.

Rispal-Padel, L., Cicirata, F., and Pons, C., 1982. Cerebellar nuclear topography of simple and synergistic movements in the alert baboon (Papio papio). *Experimental Brain Research*, 47(3):365–80.

Rodenbeck, A., Binder, R., Geisler, P., Danker-Hopfe, H., Lund, R., Raschke, F., Weeß, H.-G., and Schulz, H., 2006. A Review of Sleep EEG Patterns. Part I: A Compilation of Amended Rules for Their Visual Recognition according to Rechtschaffen and Kales. *Somnologie*, 10(4):159–175.

Roemmich, R.T., Long, A.W., and Bastian, A.J., 2016. Seeing the Errors You Feel Enhances Locomotor Performance but Not Learning. *Current Biology*, 26(20):2707–2716.

Russell, M., Goodman, T., Wang, Q., Groshong, B., and Lyeth, B.G., 2014. Gender Differences in Current Received during Transcranial Electrical Stimulation. *Frontiers in Psychiatry*, 5:104.

Sakai, K., Hikosaka, O., Miyauchi, S., Takino, R., Sasaki, Y., and Pütz, B., 1998. Transition of brain activation from frontal to parietal areas in visuomotor sequence learning. *The Journal of Neuroscience*, 18(5):1827–40.

Saleh, M., Reimer, J., Penn, R., Ojakangas, C.L., and Hatsopoulos, N.G., 2010. Fast and Slow Oscillations in Human Primary Motor Cortex Predict Oncoming Behaviorally Relevant Cues. *Neuron*, 65(4):461–471.

Salman, M.S., 2002. Topical Review : The Cerebellum: It's About Time! But Timing Is Not Everything-New Insights Into the Role of the Cerebellum in Timing Motor and Cognitive Tasks. *The The Journal of Child Neurology*, 17(1):1–9.

Samar, V.J., Bopardikar, A., Rao, R., and Swartz, K., 1999. Wavelet Analysis of Neuroelectric Waveforms: A Conceptual Tutorial. *Brain and Language*, 66(1):7–60.

Santarnecchi, E., Biasella, A., Tatti, E., Rossi, A., Prattichizzo, D., and Rossi, S., 2017. High-gamma oscillations in the motor cortex during visuo-motor coordination: A tACS interferential study. *Brain Research Bulletin*, 131:47–54.

Schepens, B. and Drew, T., 2003. Strategies for the integration of posture and movement during reaching in the cat. *The Journal of Neurophysiology*, 90(5):3066–3086.

Schlaug, G., Renga, V., and Nair, D., 2009. Transcranial Direct Current Stimulation in Stroke Recovery. *Stroke*, 65(12):1571–1576.

Schmahmann, J.D. and Sherman, J.C., 1998. The cerebellar cognitive affective syndrome. *Brain*, 121(4):561–579.

Schmitzer-Torbert, N., 2004. Neuronal Activity in the Rodent Dorsal Striatum in Sequential Navigation: Separation of Spatial and Reward Responses on the Multiple T Task. *The Journal of Neurophysiology*, 91(5):2259–2272.

Schmitzer-Torbert, N., Jackson, J., Henze, D., Harris, K., and Redish, A.D., 2005. Quantitative measures of cluster quality for use in extracellular recordings. *Neuroscience*, 131(1):1–11.

Schutter, E. De and Maex, R., 1996. The cerebellum: cortical processing and theory. *Current Opinion in Neurobiology*, 6(6):759–764.

Seidler, R.D., Gluskin, B.S., and Greeley, B., 2017. Right prefrontal cortex transcranial direct current stimulation enhances multi-day savings in sensorimotor adaptation. *The Journal of Neurophysiology*, 117(1):429–435.

Seidler, R.D., Kwak, Y., Fling, B.W., and Bernard, J.A., 2013. Neurocognitive mechanisms of error-based motor learning. Advances in Experimental Medicine and Biology. M. J. Richardson, M. A. Riley, & K. Shockley, eds. *Advances in Experimental Medicine and Biology*, 782:39–60.

Seidler, R.D. and Noll, D.C., 2008. Neuroanatomical Correlates of Motor Acquisition and Motor Transfer. *The Journal of Neurophysiology*, 99(4):1836–1845.

Sellers, K.K., Yu, C., Zhou, Z.C., Stitt, I., Li, Y., Radtke-Schuller, S., Alagapan, S., and Fröhlich, F., 2016. Oscillatory Dynamics in the Frontoparietal Attention Network during Sustained Attention in the Ferret. *Cell Reports*, 16(11):2864–2874.

Shadmehr, R. and Holcomb, H.H., 1997. Neural correlates of motor memory consolidation. *Science*, 277:821–825.

Shadmehr, R. and Mussa-Ivaldi, F. a, 1994. Adaptive representation of dynamics during learning of a motor task. *The Journal of Neuroscience*, 14(5):3208–3224.

Shadmehr, R., Smith, M. a, and Krakauer, J.W., 2010. Error correction, sensory prediction, and adaptation in motor control. *Annual Review of Neuroscience*, 33:89–108.

Shidara, M., Kawano, K., Gomi, H., and Kawato, M., 1993. Inverse-dynamics model eye movement control by Purkinje cells in the cerebellum. *Nature*, 365(6441):50–52.

Sing, G.C. and Smith, M.A., 2010. Reduction in learning rates associated with anterograde interference results from interactions between different timescales in motor adaptation. *PLoS Computational Biology*, 6(8):1000893.

Smith, M.A., Ghazizadeh, A., and Shadmehr, R., 2006. Interacting Adaptive Processes with Different Timescales Underlie Short-Term Motor Learning The Harvard community has made this article openly Interacting Adaptive Processes with Different Timescales Underlie Short-Term Motor Learning. *PLoS Biology*, 4(6):1035–1043.

Sokolov, A.A., Miall, R.C., and Ivry, R.B., 2017. The Cerebellum: Adaptive Prediction for Movement and Cognition. *Trends in Cognitive Sciences*, 21(5):313–332.

Stagg, C.J. and Nitsche, M.A., 2011. Physiological Basis of Transcranial Direct Current Stimulation. *The Neuroscientist*, 17(1):37–53.

Stockinger, C., Focke, A., and Stein, T., 2014. Catch trials in force field learning influence adaptation and consolidation of human motor memory. *Frontiers in Human Neuroscience*, 8:231.

Stolyarova, A., 2018. Solving the credit assignment problem with the prefrontal cortex. *Frontiers in Neuroscience*, 12:182.

Strata, P., 2009. David Marr's theory of cerebellar learning: 40 years later. *The Journal of*

Physiology, 587(23):5519–5520.

Streng, M.L., Popa, L.S., and Ebner, T.J., 2017. Climbing fibers predict movement kinematics and performance errors. *The Journal of Neurophysiology*, 118(3):1888–1902.

Strick, P.L., Dum, R.P., and Fiez, J.A., 2009. Cerebellum and Nonmotor Function. *Annual Review of Neuroscience*, 32(1):413–434.

Striemer, C.L. and Borza, C.A., 2017. Prism adaptation speeds reach initiation in the direction of the prism after-effect. *Experimental Brain Research*, :1–14.

Tan, H., Jenkinson, N., and Brown, P., 2014. Dynamic Neural Correlates of Motor Error Monitoring and Adaptation during Trial-to-Trial Learning. *The Journal of Neuroscience*, 34(16):5678–5688.

Tan, H., Wade, C., and Brown, P., 2016. Post-Movement Beta Activity in Sensorimotor Cortex Indexes Confidence in the Estimations from Internal Models. *The Journal of Neuroscience*, 36(5):1516–1528.

Tanaka, H., Krakauer, J.W., and Sejnowski, T.J., 2012. Generalization and Multirate Models of Motor Adaptation. *Neural Computation*, 24(4):939–966.

Tanaka, H., Sejnowski, T.J., and Krakauer, J.W., 2009. Adaptation to visuomotor rotation through interaction between posterior parietal and motor cortical areas. *The Journal of Neurophysiology*, 102(5):2921–32.

Taubert, M., Stein, T., Kreutzberg, T., Stockinger, C., Hecker, L., Focke, A., Ragert, P., Villringer, A., and Pleger, B., 2016. Remote Effects of Non-Invasive Cerebellar Stimulation on Error Processing in Motor Re-Learning. *Brain Stimulation*, 9(5):692–699.

Taylor, J.A. and Ivry, R.B., 2014. Cerebellar and Prefrontal Cortex Contributions to Adaptation, Strategies, and Reinforcement Learning. *Progress in Brain Research*, 210:217–253.

Taylor, J.A., Krakauer, J.W., and Ivry, R.B., 2014. Explicit and Implicit Contributions to Learning in a Sensorimotor Adaptation Task. *The Journal of Neuroscience*, 34(8):3023–3032.

Thair, H., Holloway, A.L., Newport, R., and Smith, A.D., 2017. Transcranial direct current stimulation (tDCS): A Beginner's guide for design and implementation. *Frontiers in Neuroscience*, 11:641.

Thier, P., Dicke, P.W., Haas, R., Thielert, C.D., and Catz, N., 2002. The role of the oculomotor vermis in the control of saccadic eye movements. *Annals of the New York Academy of Sciences*, 978:50–62.

Timmann, D. and Daum, I., 2007. Cerebellar contributions to cognitive functions: A progress report after two decades of research. *The Cerebellum*, 6(3):159–162.

Toni, I., Ramnani, N., Josephs, O., Ashburner, J., and Passingham, R.E., 2001. Learning arbitrary visuomotor associations: Temporal dynamic of brain activity. *NeuroImage*, 14(5):1048–1057.

Torrecillos, F., Alayrangues, J., Kilavik, B.E., and Malfait, N., 2015. Distinct Modulations in Sensorimotor Postmovement and Foreperiod -Band Activities Related to Error Salience Processing and Sensorimotor Adaptation. *The Journal of Neuroscience*, 35(37):12753–12765.

Torrence, C. and Compo, G.P., 1998. A Practical Guide to Wavelet Analysis. *Bulletin of the American Meteorological Society*, 79(1):61–78.

Trott, J.R. and Apps, R., 1991. Lateral and medial sub-divisions within the olivocerebellar zones of the paravermal cortex in lobule Vb/c of the cat anterior lobe. *Experimental Brain*

Research, 87(1):126–140.

Trott, R. and Armstrong, D.M., 1987. The Cerebellar Corticonuclear Projection from lobule Vb/c of the cat anterior lobe: a combined electrophysiological and autoradiographic study. *Experimental Brain Research*, 66(2):318–338.

Tseng, Y.-W., Diedrichsen, J., Krakauer, J.W., Shadmehr, R., and Bastian, A.J., 2007. Sensory prediction errors drive cerebellum-dependent adaptation of reaching. *The Journal of Neurophysiology*, 98(1):54–62.

Tzagarakis, C., Ince, N.F., Leuthold, A.C., and Pellizzer, G., 2010. Beta-Band Activity during Motor Planning Reflects Response Uncertainty. *Journal of Neuroscience*, 30(34):11270–11277.

Tzagarakis, C., West, S., and Pellizzer, G., 2015. Brain oscillatory activity during motor preparation: Effect of directional uncertainty on beta, but not alpha, frequency band. *Frontiers in Neuroscience*, 9(JUN):246.

Ugawa, Y., Genba-Shimizu, K., Rothwell, J.C., Iwata, M., and Kanazawa, I., 1994. Suppression of motor cortical excitability by electrical stimulation over the cerebellum in ataxia. *Annals of Neurology*, 36(1):90–96.

Urigüen, J.A. and Garcia-Zapirain, B., 2015. EEG artifact removal—state-of-the-art and guidelines. *The Journal of Neural Engineering*, 12(3):031001.

Utz, K.S., Dimova, V., Oppenländer, K., and Kerkhoff, G., 2010. Electrified minds: Transcranial direct current stimulation (tDCS) and Galvanic Vestibular Stimulation (GVS) as methods of non-invasive brain stimulation in neuropsychology—A review of current data and future implications. *Neuropsychologia*, 48(10):2789–2810.

Vahdat, S., Darainy, M., Milner, T.E., and Ostry, D.J., 2011. Functionally Specific Changes in Resting-State Sensorimotor Networks after Motor Learning. *The Journal of Neuroscience*, 31(47):16907–16915.

Le Van Quyen, M., Foucher, J., Lachaux, J.-P., Rodriguez, E., Lutz, A., Martinerie, J., and Varela, F.J., 2001. Comparison of Hilbert transform and wavelet methods for the analysis of neuronal synchrony. *The Journal of Neuroscience Methods*, 111(2):83–98.

Vasant, D.H., Michou, E., Mistry, S., Rothwell, J.C., and Hamdy, S., 2015. High-frequency focal repetitive cerebellar stimulation induces prolonged increases in human pharyngeal motor cortex excitability. *The Journal of Physiology*, 593(22):4963–4977.

Vaswani, P.A., Shmuelof, L., Haith, A.M., Delnicki, R.J., Huang, V.S., Mazzoni, P., Shadmehr, R., and Krakauer, J.W., 2015. Persistent Residual Errors in Motor Adaptation Tasks: Reversion to Baseline and Exploratory Escape. *The Journal of Neuroscience*, 35(17):6969–6977.

Wada, Y., Kawabata, Y., Kotosaka, S., Yamamoto, K., Kitazawa, S., and Kawato, M., 2003. Acquisition and contextual switching of multiple internal models for different viscous force fields. *Neuroscience Research*, 46(3):319–331.

Watson, T.C., Becker, N., Apps, R., and Jones, M.W., 2014. Back to front: cerebellar connections and interactions with the prefrontal cortex. *Frontiers in Systems Neuroscience*, 8:4.

Watson, T.C., Jones, M.W., and Apps, R., 2009. Electrophysiological mapping of novel prefrontal - cerebellar pathways. *Frontiers in Integrative Neuroscience*, 3:18.

Weible, A.P., Weiss, C., and Disterhoft, J.F., 2007. Connections of the caudal anterior cingulate cortex in rabbit: Neural circuitry participating in the acquisition of trace eyeblink conditioning. *Neuroscience*, 145(1):288–302.

Whelan, R., 2008. Effective Analysis of Reaction Time Data. *The Psychological Record*, 58(3):475–

482.

White, O. and Diedrichsen, J., 2013. Flexible Switching of Feedback Control Mechanisms Allows for Learning of Different Task Dynamics. P. L. Gribble, ed. *PLoS ONE*, 8(2):e54771.

Wiegand, A., Nieratschker, V., and Plewnia, C., 2016. Genetic Modulation of Transcranial Direct Current Stimulation Effects on Cognition. *Frontiers in Human Neuroscience*, 10:651.

Wiese, H., Stude, P., Nebel, K., Forsting, M., and De Greiff, A., 2005. Prefrontal cortex activity in self-initiated movements is condition-specific, but not movement-related. *NeuroImage*, 28(3):691–697.

Wiethoff, S., Hamada, M., and Rothwell, J.C., 2014. Variability in Response to Transcranial Direct Current Stimulation of the Motor Cortex. *Brain Stimulation*, 7(3):468–475.

Wise, S.P. and Murray, E.A., 2000. Arbitrary associations between antecedents and actions. *Trends in Neurosciences*, 23(6):271–276.

Wolpert, D.M., Diedrichsen, J., and Flanagan, 2011. Principles of sensorimotor learning. *Nature Reviews Neuroscience*, 12:739–51.

Wolpert, D.M. and Kawato, M., 1998. Multiple Paried Forward and Inverse Models for Motor Control. *Neural Networks*, 11:1317–1329.

Wolpert, D.M., Miall, R.C., and Kawato, M., 1998. Internal models in the cerebellum. *Trends in Cognitive Sciences*, 2(9):338–347.

Woods, A.J., Antal, A., Bikson, M., Boggio, P.S., Brunoni, A.R., Celnik, P., Cohen, L.G., Fregni, F., Herrmann, C.S., Kappenman, E.S., Knotkova, H., Liebetanz, D., Miniussi, C., Miranda, P.C., Paulus, W., Priori, A., Reato, D., Stagg, C., Wenderoth, N., and Nitsche, M.A., 2016. A technical guide to tDCS, and related non-invasive brain stimulation tools. *Clinical Neurophysiology*, 127(2):1031–1048.

Yavari, F., Mahdavi, S., Towhidkhah, F., Ahmadi-Pajouh, M.A., Ekhtiari, H., and Darainy, M., 2015. Cerebellum as a forward but not inverse model in visuomotor adaptation task: a tDCS-based and modeling study. *Experimental Brain Research*, 234(4):1–16.

Yavari, F., Towhidkhah, F., and Ahmadi-Pajouh, M.A., 2013. Are fast/slow process in motor adaptation and forward/inverse internal model two sides of the same coin? *Medical Hypotheses*, 81(4):592–600.

De Zeeuw, C.I., Hoebeek, F.E., and Schonewille, M., 2008. Causes and Consequences of Oscillations in the Cerebellar Cortex. *Neuron*, 58(5):655–658.

Zhan, Y., Halliday, D., Jiang, P., Liu, X., and Feng, J., 2006. Detecting time-dependent coherence between non-stationary electrophysiological signals-A combined statistical and time-frequency approach. *The Journal of Neuroscience Methods*, 156(1–2):322–332.

Zhang, X.-Y., Wang, J.-J., and Zhu, J.-N., 2016. Cerebellar fastigial nucleus: from anatomic construction to physiological functions. *Cerebellum & ataxias*, 3:9.

Appendix – Supplementary Animal Electrophysiology

7.1 Introduction

Contained within this appendix are additional methodological details, and results of several analyses of the cat electrophysiological data not contained within the main body of the thesis.

7.2 Arrangement of implant connectors

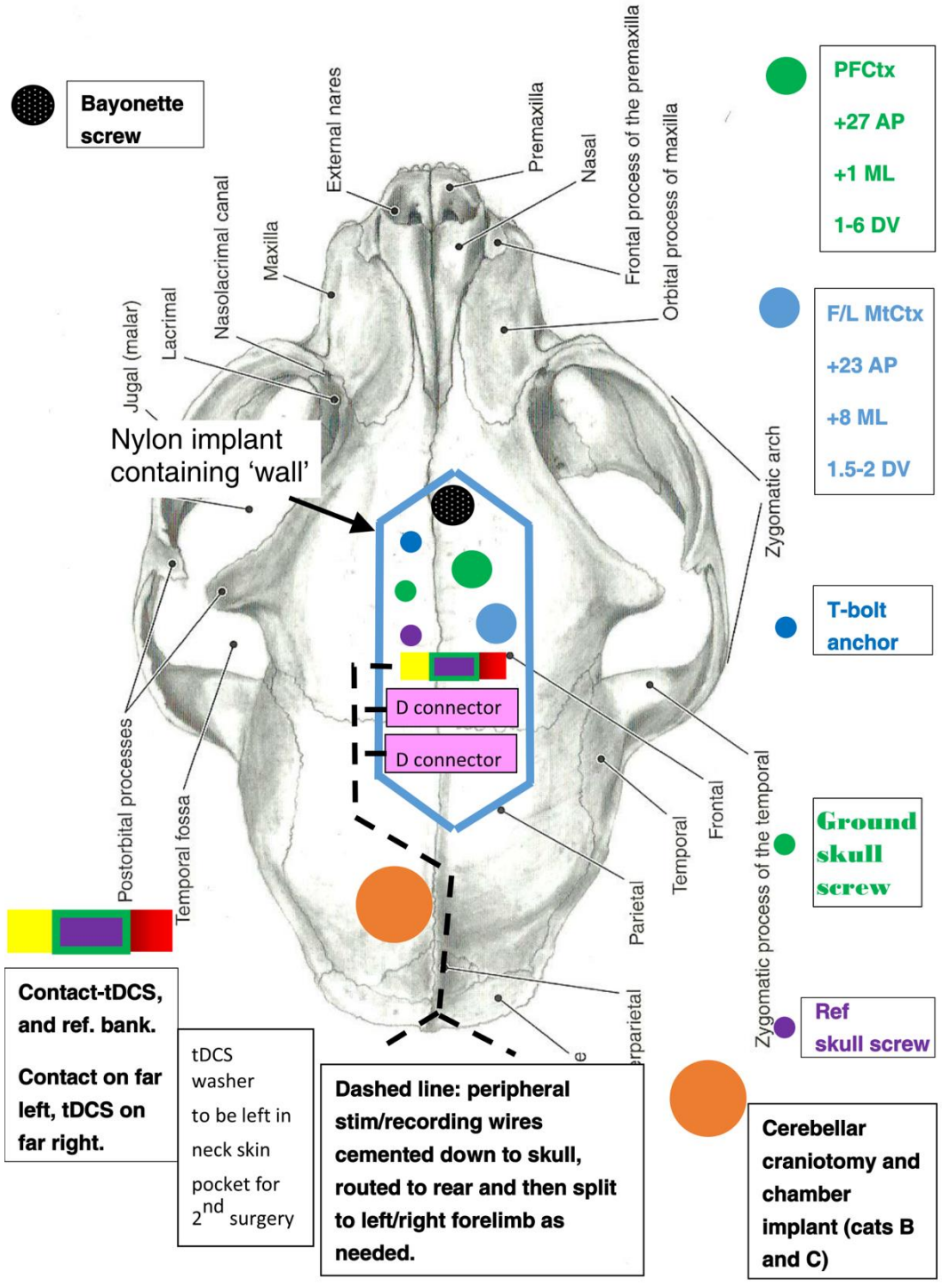

Figure 7.1 Surgical plan of headpiece connectors.
Planned arrangement of the implant hardware on the skull as used during surgery of cat C. Rostral D-connector held peripheral stimulator electrode wires, caudal D-connector held Peripheral EMG electrode and peripheral ground wires.

7.3 Gamma oscillations during motor adaptation

7.3.1 Motor cortex

In line with the notion that motor cortical high gamma oscillations are related to active control of motor processes, the high gamma components of the motor cortical signal were tested at both the movement initiation, and post-movement time periods.

During the pre-movement period, cat A showed a statistically significant decrease in power specifically during early adaptation (Wald $\chi^2(3)=12.126$, $p=0.007$. Bonferroni corrected comparisons; baseline- early adapt. $p=0.037$, baseline-late adapt and late after $p>0.05$) in contrast, neither cat B (Wald $\chi^2(3)=6.656$, $p=0.084$) nor cat C (Wald $\chi^2(3)=2.511$, $p=0.473$) exhibited statistically significant effects. Further, cats B and C showed a trend for an increased power during early adaptation, opposite to that of cat A (**Figure 7.2**).

This continued into the post-movement period (**Figure 7.3**), in which the early adaptation decrease in power remained in cat A (Wald $\chi^2(3)=26.537$, $p<0.0005$. Bonferroni corrected comparisons; baseline- early adapt. $p<0.0005$, baseline-late adapt and late after $p>0.05$). Comparisons for cat B now showed a significant increase during early adaptation (Wald $\chi^2(3)=14.373$, $p=0.002$. Bonferroni corrected comparisons; baseline- early adapt. $p=0.004$, baseline-late adapt and late after $p>0.05$). Whilst cat C's data remained not statistically significant (Wald $\chi^2(3)=2.128$, $p=0.546$),

The present data does not show a clear relationship between high gamma power in the motor cortex and the stages of adaption either pre-movement or post-movement, with cats A and B exhibiting opposing effects of adaptation on motor cortical high gamma power.

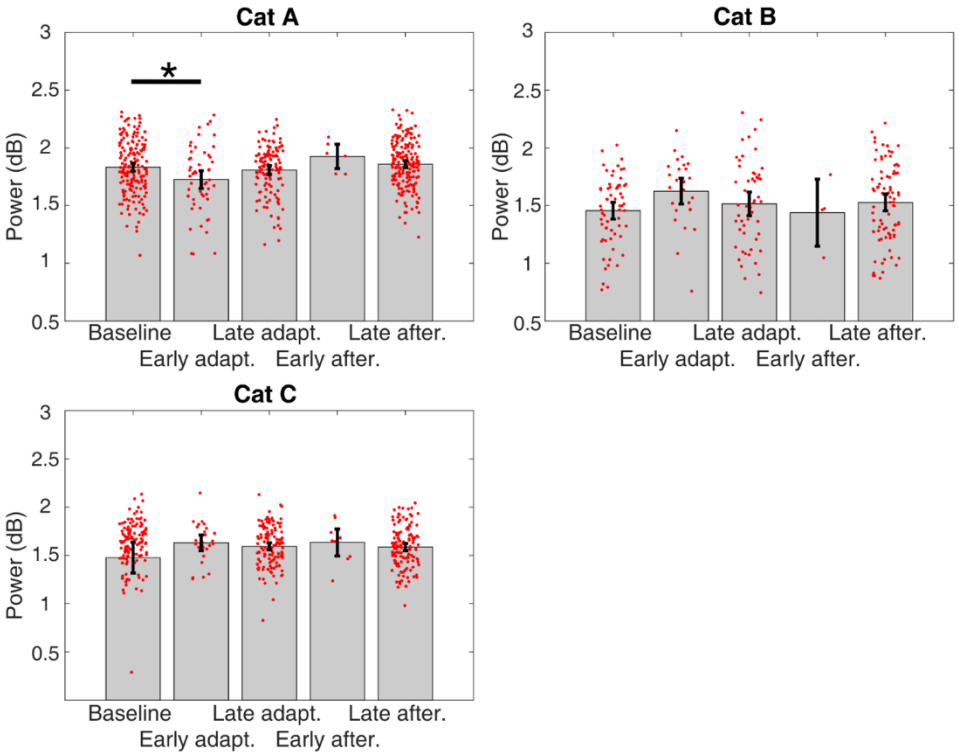

Figure 7.2 Forelimb motor cortical high gamma power pre-movement.
Bar charts showing trial averaged high gamma power (55-80Hz) during different stages of adaptation. Error bars indicate 95% confidence of the mean. Asterisks and bars indicate Bonferroni corrected comparisons (p<0.05). Red points indicate individual trial data.

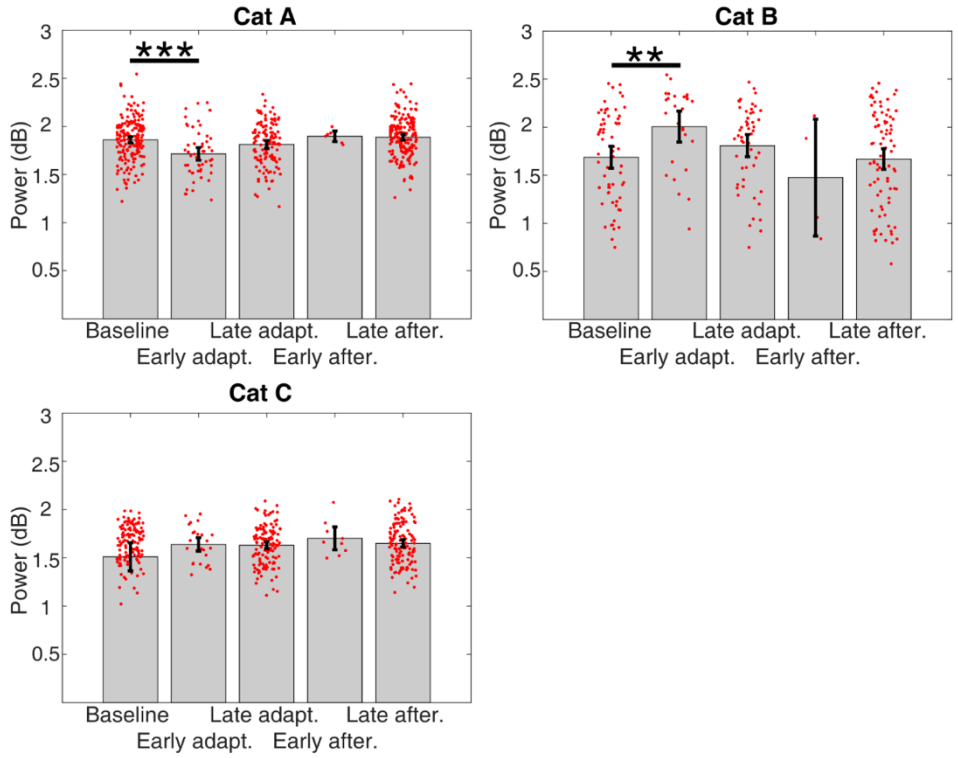

Figure 7.3 Forelimb motor cortical high gamma power post-movement.
Bar charts showing trial averaged high gamma power (55-80Hz) during different stages of adaptation. Error bars indicate 95% confidence of the mean. Asterisks and bars indicate Bonferroni corrected comparisons (triple asterisks p<0.0005, double asterisks p<0.01). Red points indicate individual trial data.

7.3.2 Cerebellar cortex

Being driven in part by the activity of the principle output neuron of the cerebellar cortex indicates that cerebellar gamma rhythms might be particularly useful as a measurement of changes in neuronal processing in the cerebellar cortex.

Considering data in the pre-movement time window (**Figure 7.4**), a generalised linear model found no significant effect of adaptation in either cat A or cat B (Cat A $_{(C2\ zone)}$: Wald $\chi^2(3)=6.933$, $p=0.074$. Cat A $_{(C1\ zone)}$: Wald $\chi^2(3)=2.234$, $p=0.525$. Cat B: Wald $\chi^2(3)=0.176$, $p=0.981$), but did indicate a significant effect in cat C (Wald $\chi^2(3)=26.643$, $p<0.0005$). Bonferroni corrected comparisons showed that all adaptation and after-effect phases had significantly higher power than baseline (baseline-early and late adapt. $p<0.0005$, baseline-late after. $p=0.001$).

From this it appears that pre-movement high gamma oscillations are not modulated by adaptation.

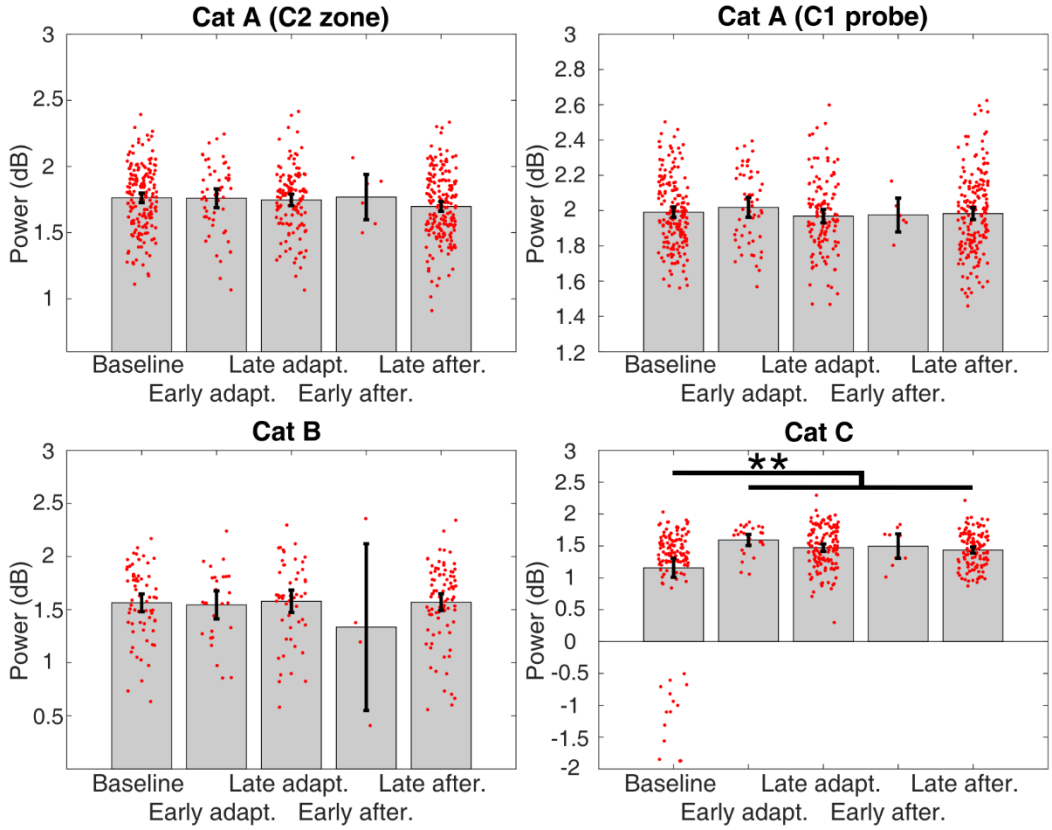

Figure 7.4 Cerebellar cortex high gamma power pre-movement.
Bar charts showing trial averaged high gamma power (55-80Hz) during different stages of adaptation. Error bars indicate 95% confidence of the mean. Asterisks and bars indicate Bonferroni corrected comparisons (double asterisks $p<0.01$). Red points indicate individual trial data.

Similarly, there was no robust effect of adaptation on high gamma frequencies during the post movement time window (**Figure 7.5**). Here, a generalised linear model found no effect of adaptation in data from cat B (Wald $\chi^2(3)=1.207$, $p=0.751$). Whilst both C1 and C2 signals in cat

A were shown to have a significant main effect of adaption condition (C1 Wald $\chi^2(3)=14.045$, p=0.003, C2 Wald $\chi^2(3)=16.259$, p=0.001), only the comparison between baseline and late after-effect trials was significant after Bonferroni correction (p=0.002, all other Bonferroni corrected comparison p values >0.05). Cat C also exhibited a significant effect of adaptation (Wald $\chi^2(3)=18.919$, p<0.0005). After Bonferroni correction, all comparisons to the baseline trials were seen to be significantly higher than baseline trials (all comparisons p<0.0005).

Overall then, in both the pre and post-movement periods, there does not appear to be an adaptation specific modulation of high gamma oscillations in the cerebellar cortex.

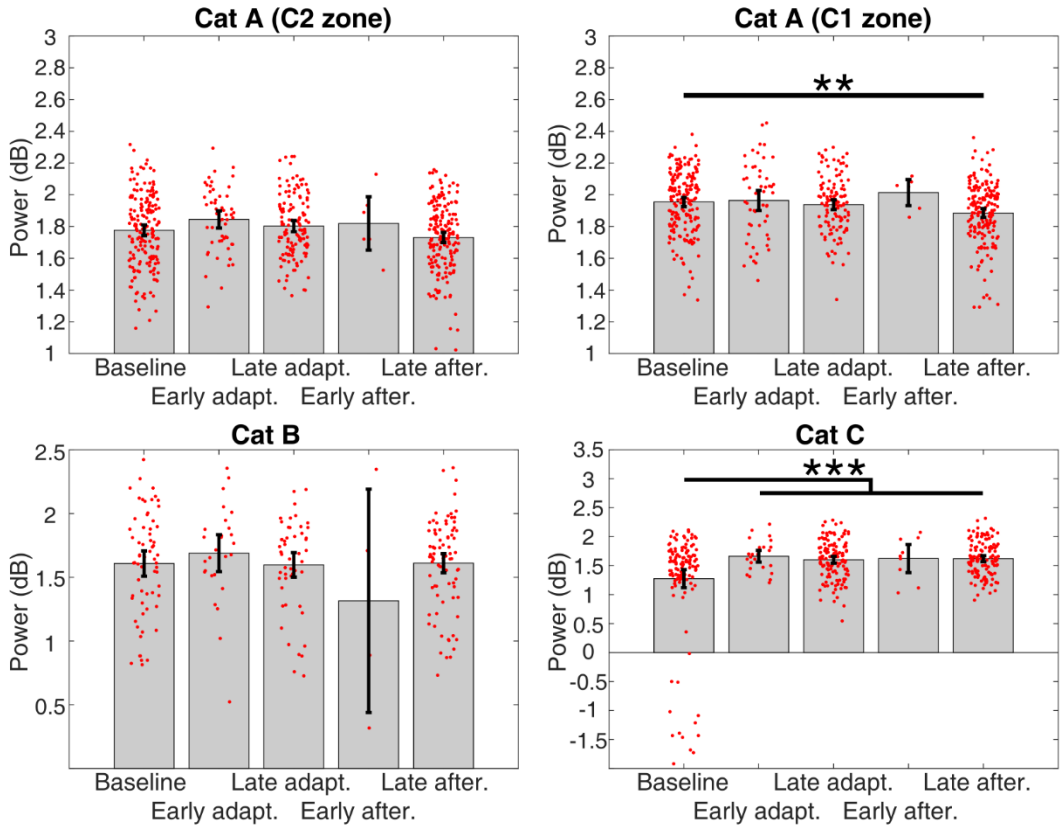

Figure 7.5 Cerebellar cortex high gamma power post-movement.
Bar charts showing trial averaged high gamma power (55-80Hz) during different stages of adaptation. Error bars indicate 95% confidence of the mean. Asterisks and bars indicate Bonferroni corrected comparisons (double asterisks p<0.01, triple asterisks p<0.0005). Red points indicate individual trial data.

7.4 Inhibitory/excitatory single unit pairings

While most of the putative Purkinje cell displayed a reduction in firing around the time of paw lift, many of the unclassified units displayed an increase. In two instances putative Purkinje cell units and un-classified units were recorded simultaneously (**Figure 7.6**). The distances between the electrode sites with the largest average waveform were 300µm (**Figure 7.6A**) and 600µm (**Figure 7.6B**). The tightly coupled, almost antagonistic nature of this activity is interesting, as it suggests that the two examples may be synaptically linked, possibly an inhibitory interneuron supressing the associated Purkinje cell activity during the reaching movement. This active

suppression of the Purkinje cell activity will lead to disinhibition of the deep cerebellar nuclei (the nucleus interpositus for the C1-3 zone recordings made here), perhaps 'ungating' its role in providing online control of coordinated limb movement through spinocerebellar pathways (Armstrong and Edgley 1984; Ekerot et al. 1995). If this pattern of active suppression of movement related Purkinje cell activity, it is possible that it is the inhibitory interneurons of the cerebellar cortex that have a principle role in governing cerebellar output.

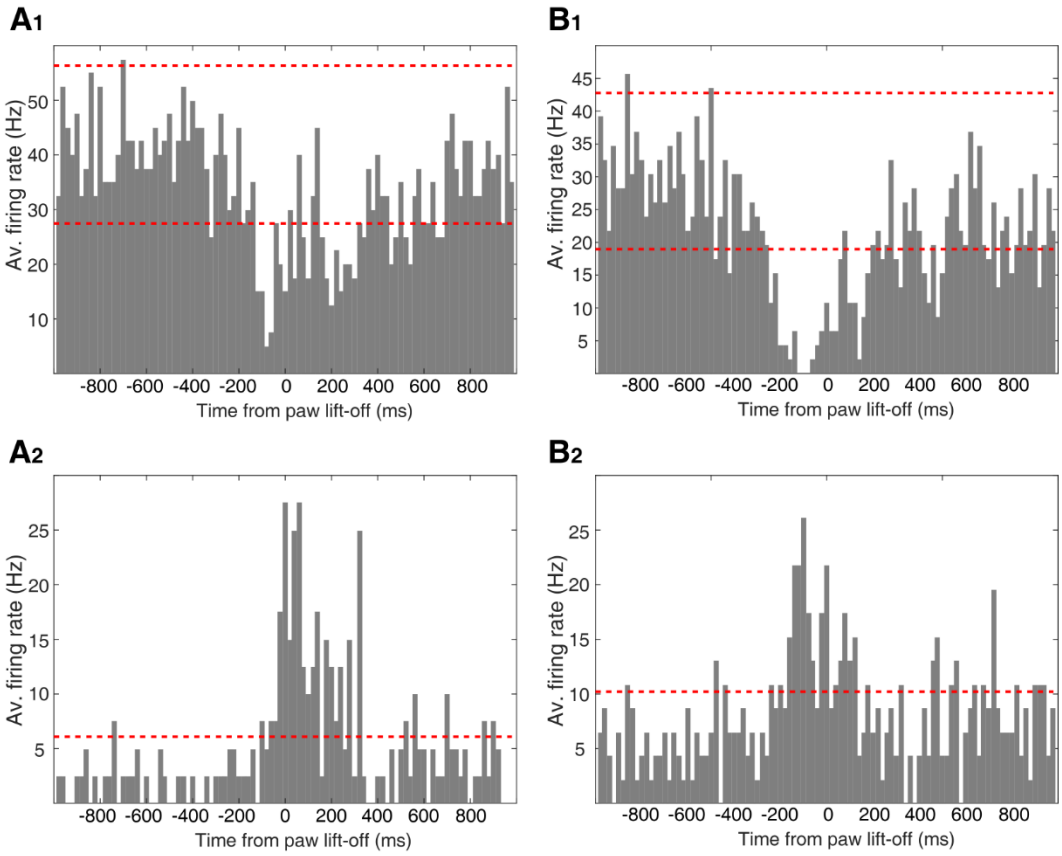

Figure 7.6 Putative Purkinje cell – inhibitory cell pairs.
Two simultaneously recorded units exhibiting reciprocal firing rate modulation. Peri-stimulus time histograms showing average spike rate, aligned to paw lift-off, 10ms bins. ***A_1****: putative Purkinje cell activity simultaneously recorded with* ***A_2****, an unclassified single unit.* ***B_1****: putative Purkinje cell activity simultaneously recorded with* ***B_2****, an unclassified single unit. Red dashed lines indicate 2 standard deviations away from -1000 to -500ms mean period (only upper bounds shown if lower bound falls below zero). Note that the decreases in putative Purkinje unit activity aligns to increases in the unclassified units.*